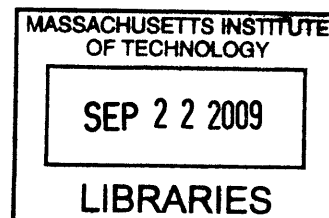


**Investigations of the Inhibition Mechanisms of Human Ribonucleotide Reductase by
Gemcitabine-5'-diphosphate and *Saccharomyces cerevisiae* Ribonucleotide
Reductase by Sml1**

by

Jun Wang

B.S. Chemistry
Peking University, 1997



Submitted to the Department of Chemistry
In Partial Fulfillment of the Requirements for the Degree of
Doctor of Philosophy in Biological Chemistry

at the

MASSACHUSETTS INSTITUTE OF TECHNOLOGY

September 2009

ARCHIVES

© 2009 Massachusetts Institute of Technology
All rights reserved

Signature of Author _____ Department of Chemistry
Aug 20, 2009

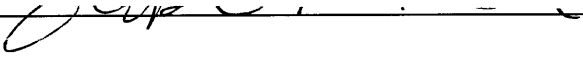
Certified by: _____ JoAnne Stubbe
Novartis Professor of Chemistry and Professor of Biology
Thesis Supervisor

Accepted by: _____ Robert W. Field
Haslam and Dewey Professor of Chemistry
Chairman, Departmental committee on Graduate Students

This Doctoral Thesis has been examined by a committee of the Department of Chemistry as follows:

Catherine L. Drennan
Professor of Chemistry and Professor of Biology
Investigator and Professor, Howard Hughes Medical Institute
Chair

JoAnne Stubbe
Novartis Professor of Chemistry and Professor of Biology
Thesis Supervisor


Stephen P. Bell
Professor of Biology
Investigator of Howard Hughes Medical Institute

TO MY FAMILY

Acknowledgements

First, I would like to acknowledge my advisor, Professor JoAnne Stubbe first. Thanks JoAnne for taking me as her student and offering me the best training. Thanks JoAnne for always giving me very constructive suggestions to guide me through all the difficulties in my projects. JoAnne's passion and dedication to science will serve as my standard. I feel I own too much to JoAnne. Without her help, this thesis would not have been possible.

Second, I want to thank Professor Catherine Drennan and Professor Stephen Bell for serving on my thesis committee and giving me helpful feedbacks. Thanks Cathy for being my co-advisor for three and half years. I have learnt quite a lot by attending to Cathy's group meetings and discussing my projects with Cathy. I also want to thank Professor Stuart Licht for being my chair for four years.

I thank Yang (David) Lee from Professor Stephen Elledge lab for the help on the Dif1 project. I thank Professor Mingxia Huang for the help on the Sml1 project. I thank Brad Evans from Professor Neil Kelleher lab for the help on Mass spectrometry analysis. Thanks Christina Stock and Nozomi Ando from Cathy's lab for working on the gemcitabine project. Thanks Danny Yun and Hector Hernandez for teaching me how to solve the structures. Thanks Nelson Olivier for the help on AUC and Pymol.

I want to thank all my labmates in Stubbe lab. Thanks Greg and Erin for helping me start on the gemcitabine project. Thanks Ally for the help on the Sml1 project. Thanks Daniela for the friendship and being supportive. I thank Mo for being a good mentor. Thanks Aaron for the help on SEC and the encouraging messages. I thank Chia for being a great friend and bringing a lot fun. Thanks Joey, Ellen Mimi, Rachael, Crystal for proof reading my chapters and giving me very helpful suggestions. Thanks for them to organize lab activities. I will miss Joey's new models and Ellen's jokes. Thanks Mimi and Rachael for being my best deskmates and sharing the happiness and sadness. Thanks Kan for the help on kinetics. Thanks Yan, Ping Luke, Rick and Daniel for friendship. Thanks Yimon for taking over my projects and proofreading my manuscripts. Thanks Mac and Andrew for the support. Thanks Betty Lou for the help.

Finally I want to thank my husband and my family for the support and being with me through tough times. Thanks God for guiding my path.

Investigations of the Inhibition Mechanisms of Human Ribonucleotide Reductase by Gemcitabine-5'-diphosphate and *Saccharomyces cerevisiae* Ribonucleotide Reductase by Sml1

by

Jun Wang

Submitted to the Department of Chemistry
In Partial Fulfillment of the Requirements for the Degree of

Doctor of Philosophy in Biochemistry

ABSTRACT

Ribonucleotide reductases (RNRs) catalyze the conversion of nucleotides to deoxynucleotides supplying the dNTPs required for DNA replication and DNA repair. Class I RNRs require two subunits (α and β) for activity. The α subunit binds the substrates and the allosteric effectors that govern specificity and turnover. The β subunit houses the diferric Y• cofactor required to initiate nucleotide reduction. Human cells possess two type of β subunits of RNR: one (β) is involved in DNA replication and the second (p53 β') is required for mitochondrial DNA replication and likely plays some role in DNA repair. Gemcitabine (2',2'-difluoro-2'-deoxycytidine, F₂C) is used clinically in a variety of cancer treatments and the phosphorylated F₂C targets many enzymes involved in nucleotide metabolism, including RNR. The studies presented here with [1'-³H]- and [5-³H]-F₂CDP have established that F₂CDP is a sub-stoichiometric mechanism based inhibitor (0.5 equivalents F₂CDP/ α) of both the *E. coli* and the human RNRs in the presence of a reductant. Inactivation is caused by covalent labeling of RNR by the sugar of F₂CDP (0.5 equivalents/ α) and is accompanied by the release of 0.5 equivalent cytosine/ α . Studies using size exclusion chromatography reveal that in the *E. coli* RNR, an α 2 β 2 tight complex is generated subsequent to enzyme inactivation by F₂CDP, while in the human RNR, an α 6 β 6 or α 6 β' 6 tight complex is generated.

The second part of this thesis focuses on the Sml1 inhibition mechanism in *S. cerevisiae*. Sml1 is a 12 kDa small protein RNR inhibitor. It regulates RNR activity by binding directly to α to repress RNR activity. The binding of Sml1 to α has been proposed to block the reduction of the active site disulfide formed concomitantly with dNTP production, leaving α in the oxidized form. A fluorescence titration method was employed to measure the K_d of Sml1 with different forms of α . Our data suggest that Sml1 binds to α by a mechanism that involves its C-terminal helix (likely the hydrophobic face) and a region of α that includes W688. The kinetics studies suggest that Sml1 behaves as an uncompetitive inhibitor relative to the substrate, and binds to the oxidized form of α in preference to the reduced form.

Thesis Supervisor: JoAnne Stubbe
Title: Novartis Professor of Chemistry

Table of Contents

Acknowledgments	4
Abstract	5
Table of Contents	6
List of Figures	12
List of Tables	16
List of Schemes	18
Abbreviation	19

Chapter 1

Introduction to the Human and *Saccharomyces cerevisiae* Ribonucleotide Reductase

1.1 Overview	21
1.2 Structure and Mechanism of Class Ia RNR	24
1.2.1 Structure of class I RNR	24
1.2.2 Mechanism of nucleotide reduction class I RNR	30
1.2.3 Mechanism of 2'-monohalo-2'-deoxynucleotide inhibition	31
1.2.4 Regulation of <i>E. coli</i> RNR	33
1.3 Yeast RNR	35
1.3.1 Structure of yeast RNR	35
1.3.2 Mechanism of yeast RNR	38
1.3.3 Regulation of yeast RNR	39
1.4 Human RNR	49
1.4.1 Introduction to human RNR	49
1.4.2 Regulation of human RNR	51
1.5 RNR as target for anti-cancer therapy	57
1.5.1 Gemcitabine	58
1.5.2 Hydroxyurea	63
1.6 References	64

Chapter 2

Characterization of Human Ribonucleotide Reductase

2.1 Introduction.....	79
2.2 Materials and Methods.....	83
2.2.1 Materials.....	83
2.2.2 General Procedures.....	84
2.2.3 Construction of plasmids for expression of His- α , His- β and His- β' in <i>E. coli</i>	85
2.2.4 Expression and purification of α	86
2.2.5 Expression and purification of β	88
2.2.6 Expression and purification of β'	89
2.2.7 Conversion of human apo β 2 to holo β 2.....	91
2.2.8 Conversion of human apo β' 2 to holo β' 2.....	91
2.2.9 Construction of the genes for Y124F- β' , Y138F- β' , and Y162F- β , Y176- β , expression and isolation of the mutant proteins.....	92
2.2.10 Human RNR Activity assays.....	93
2.2.11 Stability test of the wt β and β' and Y124F- β' mutant.....	94
2.3 Results and Discussion.....	94
2.3.1 Purification of the His- α of human RNR.....	94
2.3.2 Purification of the His- β	97
2.3.3 Purification of β' subunit of human RNR.....	97
2.3.4 Characterization of β subunit of human RNR.....	98
2.3.5 Reconstitution and characterization of human β'	101
2.3.6 Characterization of human α	103
2.3.7 Investigation of the proposed role for a second tyrosine required for RNR activity.....	103
2.4 Discussion.....	106
2.5 Reference.....	109

Chapter 3

Inactivation studies of Human Ribonucleotide Reductase by Gemcitabine

3.1 Introduction	113
3.2 Materials and Methods	117
3.2.1 Materials	117
3.2.2 Expression and purification of human α , α mutants and β	117
3.2.3 Activity assays	119
3.2.4 Time dependent inactivation studies	119
3.2.5 Quantitation of covalent labeling of <i>E. coli</i> RNR and human RNR with [1'- ³ H]-F ₂ CDP and [5- ³ H]-F ₂ CDP	119
3.2.6 Quantification of cytosine released during the inactivation of <i>E. coli</i> and human RNR by [5- ³ H]-F ₂ CDP	120
3.2.7 SEC to examine the quaternary structure of RNRs subsequent to inactivation by F ₂ CDP	121
3.2.8 Quantitative analysis of the subunits of <i>E. coli</i> and human RNRs by SDS PAGE	121
3.2.9 Trypsin digestion of human RNR inactivated with [1'- ³ H]-F ₂ CDP	122
3.2.10 In gel Trypsin digestion and Mass spectrometry	123
3.3 Results	124
3.3.1 Time Dependent Inactivation of Human RNRs	124
3.3.2 Quantitation of covalent labeling of human and <i>E. coli</i> RNR inactivated by [1'- ³ H] and [5- ³ H]-F ₂ CDP	126
3.3.3 Cytosine release by human RNR	127
3.3.4 Subunit interactions of <i>E. coli</i> RNR in the presence of F ₂ CDP	128
3.3.5 Subunit Interactions of Human RNR in the presence of F ₂ CDP	133
3.3.6 Identification of the covalent labeling site of human RNR inactivated by F ₂ CDP	136
3.3.7 Time-dependent inactivation in the absence of reductants	141
3.4 Discussion	144
3.5 Reference	147

Chapter 4

Inactivation studies of Human p53R2 and H1 RNR complex by Gemcitabine

4.1 Introduction	151
4.2 Materials and Methods.....	154
4.2.1 Material	154
4.2.2 Expression and purification of human β'	155
4.2.3 Construction of Y124F- and Y138F- β' , growth, and isolation	156
4.2.3 Conversion of apo β' to holo β'	158
4.2.4 Mutants of α : construction of mutant genes, growth, and purification.....	159
4.2.5 Purification of α and α mutants by Ni NTA and dATP affinity chromatography	
159	
4.2.6 Activity assays.....	161
4.2.7 Time dependent inactivation studies.....	161
4.2.8 Quantitation of covalent labeling of human $\alpha_n(\beta'2)_m$ with $[1'-^3\text{H}]\text{-F}_2\text{CDP}$ and $[5\text{-}^3\text{H}]\text{-F}_2\text{CDP}$	162
4.2.9 Quantitation of cytosine released during the inactivation of human $\alpha_n(\beta'2)_m$ by $[5\text{-}^3\text{H}]\text{-F}_2\text{CDP}$	162
4.2.10 SDS PAGE of Inactivation mixture without boiling.....	163
4.2.11 Incubation of $[1'-^3\text{H}]\text{F}_2\text{CDP}$ and C218S/A-, C429S/A-, C444S/A-, C787S/A-, C790S/A-, E431Q/D- α and β' and analysis for covalent labeling by Sephadex chromatography.....	163
4.2.12 SEC to examine the quaternary structure of $\alpha_n(\beta'2)_m$ subsequent to inactivation by F_2CDP	164
4.2.13 Quantitative analysis of the subunits of $\alpha_n(\beta'2)_m$ by SDS PAGE	165
4.3 Results	165
4.3.1 Purification and reconstitution of the $\beta'2$	165
4.3.2 Time dependent inactivation studies of α , $\beta'2$ by $\text{F}_2\text{CDP}/\text{ATP}$	166
4.3.3 Quantitation of labeled RNR and small molecules generated by inactivation with $[1'-^3\text{H}]$ and $[5\text{-}^3\text{H}]\text{-F}_2\text{CDP}$	168

4.3.4 Analysis of the inactivation mixture of wt and C218S- α by SDS PAGE without boiling.....	170
4.3.5 Identification of potential sites of covalent modification of human RNR inactivated by [$1\text{-}^3\text{H}$] F ₂ CDP using site directed mutants of important residues in α involved in catalysis.....	172
4.3.6 SEC to examine the quaternary structure of hRNR (with β') inactivated by F ₂ CDP	156
4.3.7 An additional control: SEC to examine the quaternary structure of hRNRs with Y138F- β' in the presence of F ₂ CDP and ATP.....	180
4.4 Discussion.....	181
4.5 Reference.....	184

Chapter 5

Efforts to Understand Sml1 Inhibition of *S. cerevisiae* RNR

5.1 Introduction.....	189
5.2 Methods.....	193
5.2.1 Materials.....	193
5.2.2 Expression and purification of wt α , W688A- α , E689D- α single mutants, and W688A E689D- α double mutants.....	194
5.2.3 Expression and purification of Sml1 and Sml1-E71C, W65C, S61C, M80C mutants.....	196
5.2.4 Labeling of Sml1 mutants by BADAN.....	198
5.2.5 Activity assays.....	199
5.2.6 Inactivation assay of wt α and α -C883S C886S by Sml1.....	200
5.2.7 Determination of K _d for DAN-Sml1 to α	200
5.2.8 Preparation of oxidized α	202
5.2.9 Surface plasmon resonance by BIAcore to determine K _d for Sml1 to α	203
5.2.10 Inhibition on studies with Sml1 using CDP as the variable substrate.....	204
5.3 Results.....	204
5.3.1 Alkylation of Sml1, site specifically, with BADAN.....	204
5.3.2 Labeling Sml1 mutants with BADAN.....	206

5.3.3 Inactivation of RNR activity by mutants and DAN-Sml1 mutants.....	207
5.3.4 Measurement of the K_d for DAN-Sml1 relative to α	208
5.3.5 Purification and activity assays of W688A- α , E689D- α , W688A, E689D- α	216
5.3.6 Measurement of the affinity of Sml1 for W688A, E689D- α	221
5.3.7 Purification and activity assays of C883S C886S- α	223
5.3.8 Measurement of the affinity of Sml1 to oxidized α	224
5.3.9 Mechanism of inhibition of Sml1 relative to CDP.....	226
5.4 Discussion.....	228
5.5 Reference.....	234
Curriculum Vitae.....	237
Appendix I. Plasmid Maps.....	239
Appendix II. Published Works.....	243

List of Figures

Figure 1.1	The ribonucleotide reduction reaction.....	21
Figure 1.2	Docking model of <i>E. coli</i> $\alpha_2\beta_2$ complex.....	26
Figure 1.3	Proposed PCET pathway between β and α	27
Figure 1.4	Model showing the asymmetry of the radical propagation pathway.....	27
Figure 1.5	Structure of class Ib nrDEF complex from <i>Salmonella typhimurium</i>	30
Figure 1.6	The proposed mechanism of class Ia RNR.....	31
Figure 1.7	The mechanism of inactivation of RNR by 2'-monohalo-2'-deoxy-nucleotides.....	33
Figure 1.8	Structure of <i>E. coli</i> α_2 highlighting the allosteric effector binding sites.....	35
Figure 1.9	Structure of <i>S. cerevisiae</i> α at 2.2 Å.....	37
Figure 1.10	Specificity cross-talk of <i>S. cerevisiae</i> α for different effector/substrate pair.....	37
Figure 1.11	Model depicting the C-terminal tail of one α regenerating the active site of its neighbor α	39
Figure 1.12	RNR regulation in <i>S. cerevisiae</i> during (A) DNA replication and (B) in response to DNA damage.....	41
Figure 1.13	Sequence alignment of Dif1, Sml1, Hug1, Spd1 and Aer122c.....	45
Figure 1.14	Model of the nuclear import facilitator and anchor of $\beta\beta'$ in response to DNA damage.....	46
Figure 1.15	The current model for Sml1 regulation in <i>S. cerevisiae</i>	47
Figure 1.16	Overview of the regulation of human RNR in S-phase and in response to DNA damage.....	52
Figure 1.17	The modulation of mouse α oligomerization state and the activity by ATP and dATP effectors.....	54
Figure 1.18	Gemcitabine metabolism.....	59
Figure 1.19	Proposed mechanism of inactivation of RNR by F_2 CDP in the absence and the presence of reductant.....	62
Figure 1.20	Yeast RNR active site structures with F_2 CTP (left) or CDP (right) bound.....	63

Figure 2.1	Purification of human RNR subunits	96
Figure 2.2	Purification of α subunit by dATP-affinity chromatography	96
Figure 2.3	Analysis of fractions from Q-Sepharose column for β'	98
Figure 2.4	EPR spectra at 9 GHz of tyrosyl radical in human β and β' at 77 K.....	99
Figure 2.5	Activity assays of α , β and β'	100
Figure 2.6	EPR Spectra at 9 GHz of human β' and β mutants.....	105
Figure 2.7	Activity assays of Y162F- β and Y124F- β'	105
Figure 2.8	Stability test of Y124F- β' , wt- β' , wt- β at 37 °C.....	106
Figure 2.9	Comparison of the positions of Y176, Y162 of human β , Y138, Y124 of human β' to Y122, V108 of <i>E. coli</i> β in the active site structures.....	108
Figure 3.1	Products accompanying <i>E. coli</i> RNR inactivation	114
Figure 3.2	Time-dependent inactivation of human RNR by F ₂ CDP.....	125
Figure 3.3	Time-dependent inactivation of human RNR by F ₂ CDP.....	125
Figure 3.4	Analysis by HPLC of products generated during inactivation of human RNR and <i>E. coli</i> RNR by [5- ³ H]-F ₂ CDP.....	128
Figure 3.5	SEC on a Superose 12 column to detect complex formation (α 2 β 2) in <i>E. coli</i> RNR incubated with ATP in the presence or absence of [1'- ³ H] F ₂ CDP.....	130
Figure 3.6	Control experiment, α and β inactivated with N ₃ UDP.....	131
Figure 3.7	SEC on Superose 12 column to determine the molecular weight of the α , α 2, β 2 and α 2 β 2 in <i>E. coli</i> RNR.....	133
Figure 3.8	SEC on a Superdex 200 column to detect the complex formation in human RNR upon inactivation by F ₂ CDP/ATP.....	134
Figure 3.9	Standards on SDS PAGE to determine the ratio of α and β in human RNR	134
Figure 3.10	SEC on a Superdex 200 column to determine the molecular weight of the α , α 2, β 2 and α 6 β 6 in human RNR.....	136
Figure 3.11	Trypsin digestion under the conditions of 100 mM NH ₄ HCO ₃ , 2M urea, pH 8 for 5 h at 37°C. 4:1 (w/w) protein to trypsin was used. The protein concentration was 0.5 μ M.....	138

Figure 3.12	Rechromatography of peptides from human RNR inactivated with [1'- ³ H]-F ₂ CDP	140
Figure 3.13	Mass spectrometry analysis of the in gel trypsin digested peptides isolated subsequent to alkylation with iodoacetamide	141
Figure 3.14	Time-dependent inactivation of human RNR by F ₂ CDP in the absence of reductant	142
Figure 3.15	EPR Spectrum at 9 GHz of human RNR inactivated by F ₂ CDP in the absence of reductant	143
Figure 4.1	A Time dependent inactivation assay of human β'2 and α by F ₂ CDP	167
Figure 4.2	Time dependent inactivation assay of human β'2 and α by F ₂ CDP in the presence of an excess of the other subunit	168
Figure 4.3	Analysis by HPLC of products generated during inactivation of α _n (β'2) _m by [5- ³ H]-F ₂ CDP	170
Figure 4.4	SDS-PAGE analysis of the inactivation mixture	171
Figure 4.5	The yeast RNR active site structures with F ₂ CDP (left) or CDP (right) bound	174
Figure 4.6	SEC on a S200 column to detect complex formation after human p53R2 α is inactivated by [1'- ³ H] F ₂ CDP	177
Figure 4.7	Gel filtration molecular weight standards (GE healthcare)	178
Figure 4.8	SEC of a control with β'2, α and α2 with TTP	179
Figure 4.9	<i>E. coli</i> α and β standards	179
Figure 4.10	SEC on a S200 column to detect complex formation with human Y138F-β'/α incubated with [1'- ³ H] F ₂ CDP	180
Figure 5.1	A molecular model of yeast Sml1	191
Figure 5.2	A model for the role of the α C-terminal tail in regeneration of the reduced form of α and inhibition by Sml1	192
Figure 5.3	Model for the Sml1-Y1 binding	205

Figure 5.4	Structure of BADAN	205
Figure 5.5	Mass spectrum of DAN-Sml1-S61	207
Figure 5.6	α inactivation by the Sml1 cysteine mutants	208
Figure 5.7	SEC spectra of α in the presence of TTP	210
Figure 5.8	Titration of DAN-Sml1-S61C with α_n	213
Figure 5.9	Titration of DAN- Sml1-M80C by α	214
Figure 5.10	Determine the K_d of wtSml1 with α with surface plasmon resonance method using a Biacore	216
Figure 5.11	SDS-PAGE gel (10%) of purified W688A- α , E689D- α single mutants, and W688A E689D- α double mutants	217
Figure 5.12	Activity assay of W688A- α , E689D- α , W688A E689D - α mutants	219
Figure 5.13	FACS analysis by Huang's group	220
Figure 5.14	Western blot showing the protein levels of wt- α , W688A E689D- α , W688A- α , E689D- α , W688G- α mutants	221
Figure 5.15	Titration of DAN- Sml1-S61C with W688A E689D- α double mutant	222
Figure 5.16	SEC spectra of W688A E689D- α in the presence of TTP	222
Figure 5.17	Inactivation assay of wt- α and C883SC886S- α by Sml1	224
Figure 5.18	Titration of DAN-S61C-Sml1 with oxidized α (100 μ M TTP)	225
Figure 5.19	CDP vs Sml1 competition assay	228
Figure 5.20	Structure of <i>S. cerevisiae</i> α showing the position of W688	230

List of Tables

Table 1.1 Overview of the different classes of RNRs.....	23
Table 1.2 Important catalytic residues on RNR in <i>E. coli</i> , human and <i>S. cerevisiae</i>	24
Table 2.1 Conserved key residues in PCET pathway of <i>E. coli</i> , mouse and human small subunits.....	81
Table 2.2 Primers for making the new constructs His-H1, His-H2, His-p53R2 and correcting sequence errors.....	86
Table 2.3 Primers for generation of Y124F-, Y138F- β' , and Y162F-, Y176- β	93
Table 2.4 Comparison of the human RNR activities obtained from different groups....	100
Table 3.1 Covalent labeling of <i>E. coli</i> and human RNR with [1'- ³ H]-F ₂ CDP and [5- ³ H]-F ₂ CDP analyzed by SEC.....	117
Table 3.2 Molecular Weight Determination of <i>E. coli</i> and human RNR and their subunits by SEC.....	131
Table 3.3 Quantitation of the [³ H]-label associated of human RNR mutants inactivated by [1'- ³ H] F ₂ CDP	137
Table 4.1 Primers for mutants of β' and α	157
Table 4.2 Covalent labeling of human $\alpha_n(\beta'2)_m$ with [1'- ³ H]-F ₂ CDP and [5- ³ H]-F ₂ CDP analyzed by SEC.....	169
Table 4.3 Quantitation of sugar label covalently attached to human RNR mutants incubated with [1'- ³ H]-F ₂ CDP.....	173
Table 4.4 Molecular weight determination of inactivated hRNR by SEC.....	178
Table 5.1 Sml1 mutants primers.....	197
Table 5.2 Determine the amount of DAN labeling with mass spectrometry.....	206

Table 5.3 Molecular Weight Determination of <i>S. cerevisiae</i> α in the presence of effectors by SEC	211
Table 5.4 Summary of W688A, E689D α single mutants and W688A E689D α double mutant	219
Table 5.5 Fitting v vs [CDP] data to distinguish competitive and uncompetitive inhibition model	227

List of Schemes

Scheme 5.1	Substitution and deletions constructs of <i>S. cerevisiae</i> <i>RNR1</i>	191
Scheme 5.2	The kinetic model of Sml1 binding to different forms of α	226

Abbreviations

RNR	ribonucleotide reductases
α	ribonucleotide reductase large subunit
β	ribonucleotide reductase small subunit
β'	the second ribonucleotide reductase small subunit,
h	human
hRNR	human RNRs
h β	human β
dNTP	deoxynucleoside 5'-triphosphate
dNDP	deoxynucleoside 5'-diphosphate
eq.	equivalent
DTT	dithiothreitol
β -ME	β -mercaptoethanol
IPTG	isopropyl- β -D-thiogalactopyranoside
wt	wild type
Y•	tyrosyl radical
SEC	size exclusion chromatography
Amp	ampicillin
CM	chloramphenicol
PMSF	phenylmethanesulphonylfluoride
F ₂ C	2', 2'-dideoxy-difluorocytidine, gemcitabine
F ₂ CDP	5'-diphosphate of F ₂ C
F ₂ CTP	5'-triphosphate of F ₂ C
TR	thioredoxin
TRR	thioredoxin reductase
SDS-PAGE	sodium dodecylsulfate polyacrylamide gel electrophoresis

Chapter 1

Introduction to the Human and *Saccharomyces cerevisiae*

Ribonucleotide Reductase

1.1 Overview

In all organisms, ribonucleotide reductases (RNRs) uniquely catalyze the reduction of the four ribonucleotides to their corresponding 2'-deoxyribonucleotides, and consequently are essential in DNA biosynthesis and repair (Figure 1.1) (1-3). A continuous and balanced deoxynucleoside triphosphate (dNTP) pool, which is critical for the fidelity of DNA replication, is maintained through controlling RNR's activity by an exquisite regulatory network including transcriptional and translational regulation, controlled protein degradation, subunit localization, post-translational modification, and protein-protein interactions.

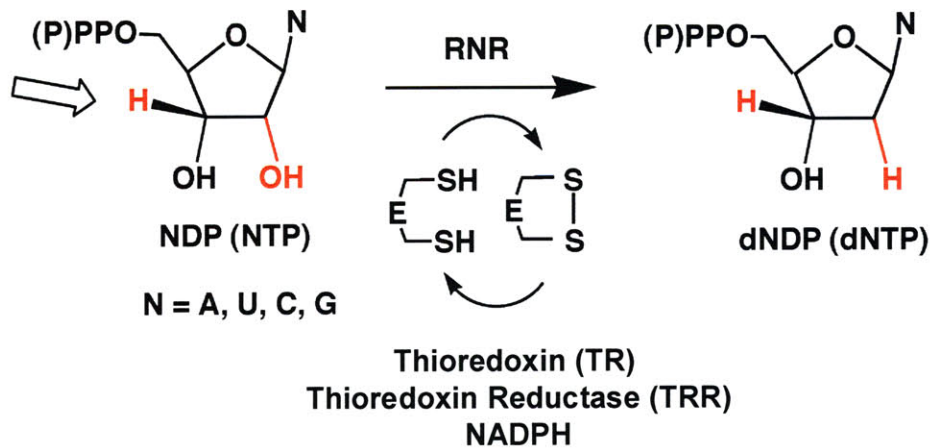


Figure 1.1: The ribonucleotide reduction reaction. The arrow indicates that the 3' hydrogen is abstracted by the thiyl radical in the active site. At the end of the reaction, the active site disulfide is re-reduced by two cysteines from the C-terminal tail of R1, which are then reduced by thioredoxin. Thioredoxin is reduced by thioredoxin reductase, and NADPH serves as the terminal e^- donor.

RNRs have been divided into three classes based on their metal cofactors (Table 1.1). Two or more classes of RNR can coexist in one organism and can be expressed under different growth conditions. The class Ia RNRs, which are found in aerobic

organisms, are composed of two homodimeric subunits: a large subunit R1 (α 2) and a small subunit R2 (β 2). β 2 contains a diferric tyrosyl radical ($Y\bullet$) cofactor, essential for catalysis, that initiates formation of a transient thiyl radical ($S\bullet$) 35 Å away in α 2, where nucleotide reduction occurs (4-7). α 2 contains the active site and the allosteric regulation sites that control substrate specificity and turnover rate. Five conserved cysteine residues in α are involved in the reduction process (Table 1.2), three of which are located in the active site and two of which are in the C-terminus (Table 1.2). The $Y\bullet$ in β generates $S\bullet$ on one of the active site cysteines to initiate nucleotide reduction and the two other cysteines in the active site supply the reducing equivalents to directly reduce the substrate. The active enzyme is regenerated by re-reducing the resulting disulfide bond with the pair of C-terminal cysteines on α (4).

Class I RNRs are divided into class Ia, Ib, Ic. Class Ib is distinct from class Ia, lacking the N-terminal allosteric regulation domain in α (8). In most prokaryotic cells, the class Ib RNR is the enzyme involved in aerobic conditions. Recently, a class Ic RNR that utilizes a manganese(IV)/iron(III) cofactor in place of the $Y\bullet$ was discovered in *Chlamydia trachomatis*, a human intracellular parasite (9-12). Class II RNRs (α or α 2) are found in organisms living under aerobic or anaerobic conditions. Unlike the $Y\bullet$ cofactor in class I RNRs, the adenosylcobalamin cofactor in class II RNRs can directly interact with the active site cysteine and initiate transient thiyl radical formation (13-18). Class III RNRs are found in bacteria growing under strict anaerobic conditions and in bacteriophages. A smaller subunit (β 2), which is also called the activase, carries a 4Fe-4S cluster coupled to S-adenosylmethionine (SAM) and generates a glycy radical ($G\bullet$) in α 2 (19-24).

Table 1.1: Overview of the different classes of RNRs (adapted from Ref.(3))

	Class Ia	Class Ib	Class Ic	Class II	Class III
Metallocofactor	Fe(III)-O-Fe(III)	Mn(III)-O-Mn(III) ? Fe(III)-O-Fe(III)?	Mn(IV)-O-Fe(III)	Adenosyl Cobalamin	Fe ₄ S ₄ , SAM
Radical initiator	Y•	Y•	Mn(IV)-O-Fe(III)	deoxyadenosyl radical	G•
Catalytic radical	S•	S•	S•	S•	S•
Complex structure	$\alpha 2\beta 2$, $\alpha 6\beta 6$ $\alpha 4\beta 4?$ $\alpha 6\beta 2?$	$\alpha 2\beta 2$	$\alpha 2\beta 2?$	$\alpha 2$, α	$\alpha 2$ or $\alpha 2\beta 2$ ($\beta 2$ for initiation)
Oxygen dependence	aerobic	aerobic	aerobic	aerobic or anaerobic	anaerobic
Substrate	NDP	NDP	NDP	NDP, NTP	NTP
Allosteric sites	A-, S- and H-sites ^a	S-site	S-site	S-site	S- and A-site (purine site)
Reductants	Thioredoxin, Glutaredoxin	NrdH Glutaredoxin	Thioredoxin?	Thioredoxin	Formate
Occurrence	Eukaryotes Eubacteria bacteriophages viruses	Eubacteria	Archebacteria Eubacteria	Archebacteria Eukaryotes algae	Archebacteria Eubacteria bacteriophages
Prototype for class, gene names	<i>E. coli nrdA</i> , <i>nrdB</i>	<i>S. typhimurium nrdE</i> , <i>nrdF</i>	<i>Chlamydia trachomatis</i> , <i>nrdA</i> , <i>nrdB</i>	<i>L. leichmannii nrdJ</i>	<i>E. coli nrdD</i> , <i>nrdG</i>

^a: S-site, specificity site; A-site, activity site, H-site, a proposed third allosteric site, called hexamerization site,

Table 1.2: Important catalytic residues on RNR in *E. coli*, human and *S. cerevisiae*

	<i>E. coli</i> RNR	Human RNR	<i>S. cerevisiae</i> RNR
α	C439	C429	C428
	C225	C218	C218
	C462	C444	C443
	C754	C787	C883
	C759	C790	C886
	E441	E431	E430
β	Y122 (Y•)	Y176 (β), Y138 (β')	Y183(β)

Despite the differences in sequences, structures, metal cofactors, and reductants among the three classes of RNRs, their active site structures are similar and the chemistry of nucleotide reduction is believed to be largely conserved (4, 25). Only class Ia RNRs are found in nearly all eukaryotic organisms. The following sections will focus on studies of the class Ia RNRs, especially the mammalian and *S. cerevisiae* enzymes.

1.2 Structure and Mechanism of Class Ia RNR

1.2.1 Structure of class I RNR

The *E. coli* class Ia enzyme is a prototype for class I RNRs. The active form of *E. coli* RNR is a 1:1 complex of α_2 and β_2 . Although structures of α_2 (26-28) and β_2 (29-31) have been solved, only recently has a structure of the *S. typhimurium* class Ib enzyme

with both α and β present been solved at 4.5 Å resolution (32). As discussed later, it is not likely to be the active complex, but may be indicative of interactions leading to an active complex. The docking model of the *E. coli* $\alpha_2\beta_2$ class Ia holoenzyme, generated based on shape complementarities between α_2 and β_2 , and on the co-crystal structure of α_2 with a β_2 C-terminal peptide, is shown in figure 1.2 (26).

The interactions between *E. coli* α_2 and β_2 are weak ($K_d \sim 0.4 \mu\text{M}$ in the absence of nucleotide), and are largely governed by the C-terminal tail of β_2 (33, 34). A peptide of the C-terminal tail of β behaves as a competitive inhibitor of $\alpha:\beta$ interactions (33-38). The β_2 C-terminal tail is structurally flexible and cannot be resolved in any of the reported X-ray crystal structures (26, 29-31, 39). In the *E. coli* β_2 structures, the last 35 residues (from 341 to 375) are not visible. In the structure of α_2 with a 20 residue peptide (355-375) corresponding to the β_2 C-terminal tail, only residues 360-375 are visible. Thus the locations of residues 341 to 359 in β , including Y356, a key residue in the electron transfer pathway between α and β , cannot be defined in the $\alpha_2\beta_2$ docking model.

The 35 Å distance between the Y^\bullet site of β (Y122) and the S^\bullet site of α (C439) is too long for transient tunneling of the radical, given the turnover of *E. coli* RNR ($2\text{-}10 \text{ s}^{-1}$). As a result, radical propagation from Y122 to C439 has been proposed to occur by long range proton-coupled electron transfer (PCET) via a network of aromatic amino acid radical intermediates (40-44). As shown in Figure 1.3, the radical is proposed to be propagated in β from Y122 to W48, and to Y356 on the C-terminal tail, and then across the β/α interface to Y731 and Y730, which oxidizes C439. The radical transfer is reversible, and the reverse reaction occurs on each turnover (45, 46).

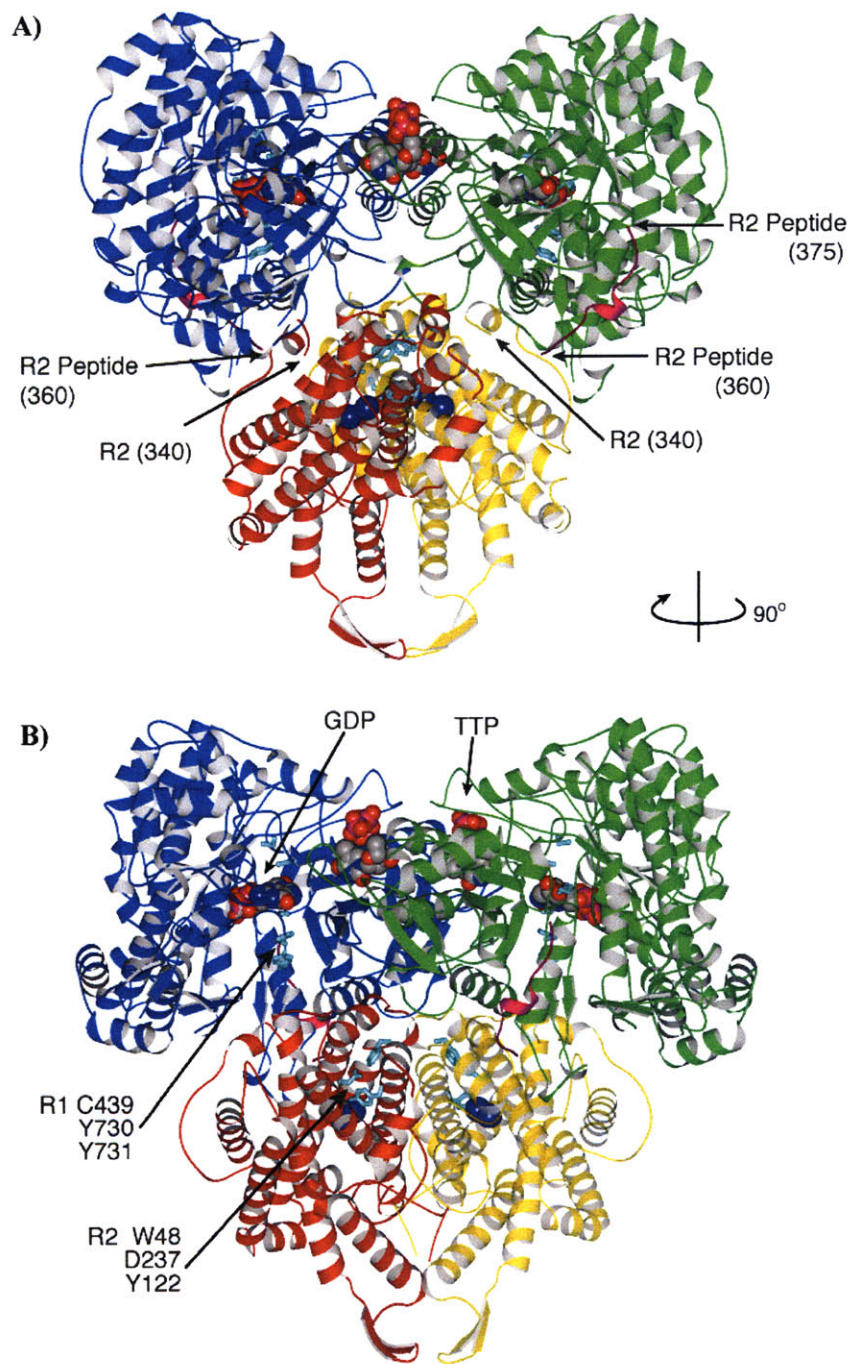


Figure 1.2: Docking model of *E. coli* $\alpha_2\beta_2$ complex (26).

α_2 (blue and green) and β_2 (red and yellow) are shown. The iron atoms are in blue. The β_2 C-terminal peptide is shown in magenta. GDP (substrate) and TTP (allosteric effector) are rendered as space filling models. The key residues in PCET (cyan) are shown using a stick model.

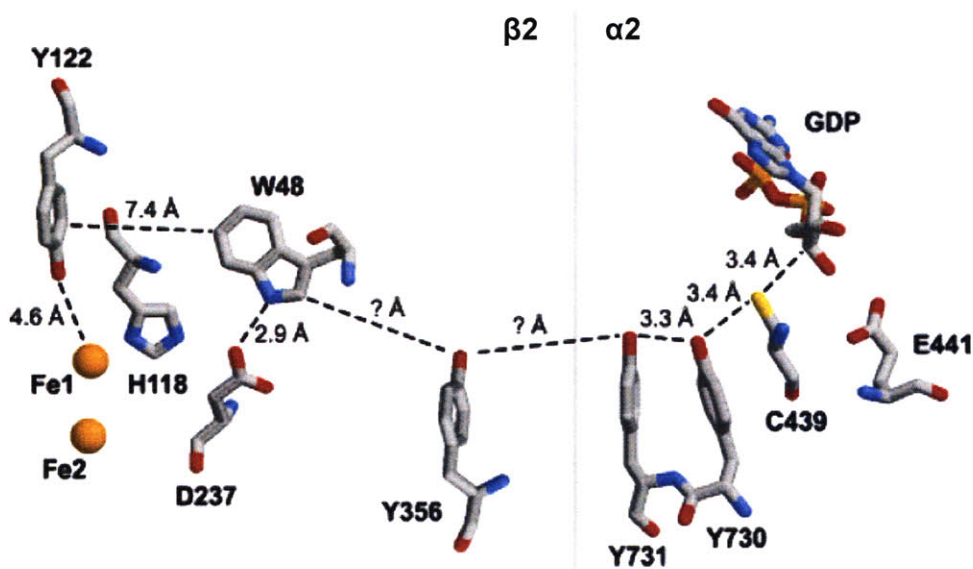


Figure 1.3: Proposed PCET pathway between β and α .

The amino acids proposed to be involved in the PCET pathway between $\beta 2$ (left) and $\alpha 2$ (right) are shown. The distances between each residue are shown and Y356 is disordered in the structure.

Although the docking model predicts a symmetric RNR subunit organization, increasing experimental data now suggest an asymmetry in the structure of the RNR complex. Recent pulsed electron-electron double resonance (PELDOR) studies suggest that firing of the radical occurs on one side first and second firing may occur subsequent to formation of the first dNDP (47, 48). In studies carried out using wt $\beta 2$ (1.2 Y \bullet / $\beta 2$) and Y731NH₂Y- $\alpha 2$ (unnatural amino acid acting as radical trap), the Y122 \bullet in one β gave rise to a NH₂Y \bullet at Y731 in α , while the Y122 \bullet in the second β subunit remain unchanged (48). In another set of experiments using wt $\alpha 2$, $\beta 2$ (Figure 1.4), inactivation of RNR with the mechanism based inhibitor, N₃UDP (2'-azido-2'-deoxyuridine-5'-diphosphate), which labels the active site with a nitrogen-centered radical (N \bullet), did not result in N \bullet -N \bullet species in both active sites (Figure 1.4, c), but instead led to Y \bullet -N \bullet interaction in only one of the two active

sites (Figure 1.4, b) (47, 48). This and other PELDOR data has shown a distance across the β_2 and α_2 pair between Y122• and Y356 in β as 30.6 Å, 38 Å between Y731 and Y122•, and 48 Å between Y122• and C225 in the symmetry-related α active site. All those distances agree well with the docking model and indicate that the distance between Y122 and C439 is long (48). The docking model indicates a distance of 25 Å between the W48 on β_2 and Y731 on α_2 .

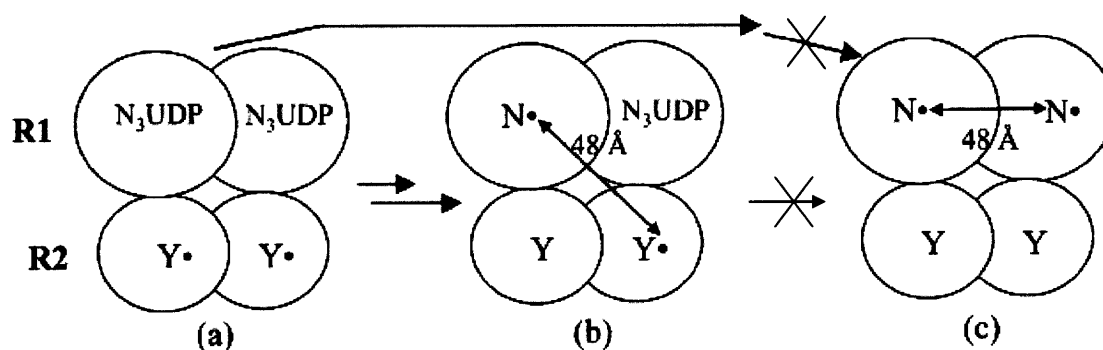


Figure 1.4: Model showing the asymmetry of the radical propagation pathway (47). (a) N₃UDP binds to both active sites of α_2 . (b) The Y₁₂₂• in one β transfers the radical to N• on the different side of α . (c) Y•s on both β s transfer the radical to both active sites of α_2 . The experimental data support model (b) instead of (c).

The unnatural tyrosine analogue 3,4-dihydroxyphenylalanine (DOPA) incorporated into position 356 of β_2 , has been employed as a probe to detect the conformational gating between α_2 and β_2 (49). As DOPA behaves as a radical trap during radical propagation, loss of Y122• is kinetically correlated with the appearance of DOPA•. Only in the presence of substrate and/or effector and α_2 , the conditions that generate active RNR complex, is DOPA• generated, with only 50% of total Y122• being converted to DOPA•. This indicates asymmetry in the active RNR complex (41). In addition, incubation of α_2 , effector, and substrate with a heterodimer DOPA- $\beta\beta'$ in which β' is missing the C-terminal 22 residues, only ~25% of Y• was converted into DOPA• (45). This study

emphasizes the essential role of the β C-terminal tail in the PCET pathway, as well as the asymmetry of the α - β or $\alpha\beta$ interaction.

The first structure of a class I $\alpha_2\beta_2$ complex was solved recently for the class Ib enzyme from *Salmonella typhimurium* (32). The structure suggests an asymmetry of α_2 and β_2 interaction: or one β interacts with α , whereas the other β only contacts its partner in the dimer (Figure 1.5 (a)). The crystallization was successfully induced at pH 7.5 in the presence of both the substrate ADP and the effector dGTP. Strong electron density, likely associated with a substrate, was seen in the active site of one α of the dimer. No extra density was identified in the other α , although the effector dGTP was bound to both α subunits, suggesting an asymmetry of substrate binding to RNR. The structure may report on an intermediate step in catalysis, i.e., binding of substrate triggers a conformational change that puts one β in an optimal position for radical transfer, while the second β moves away, perhaps to allow re-reduction of the active site cysteines [Figure 1.5 (a)], and then moves back into contact with α to resume the reaction [Figure 1.5 (b)].

This X-ray structure, agrees well with the half-site reactivity consistently observed in the studies using mechanism-based inhibitors. Further discussion on this subject will be presented in Chapters 3 and 4.

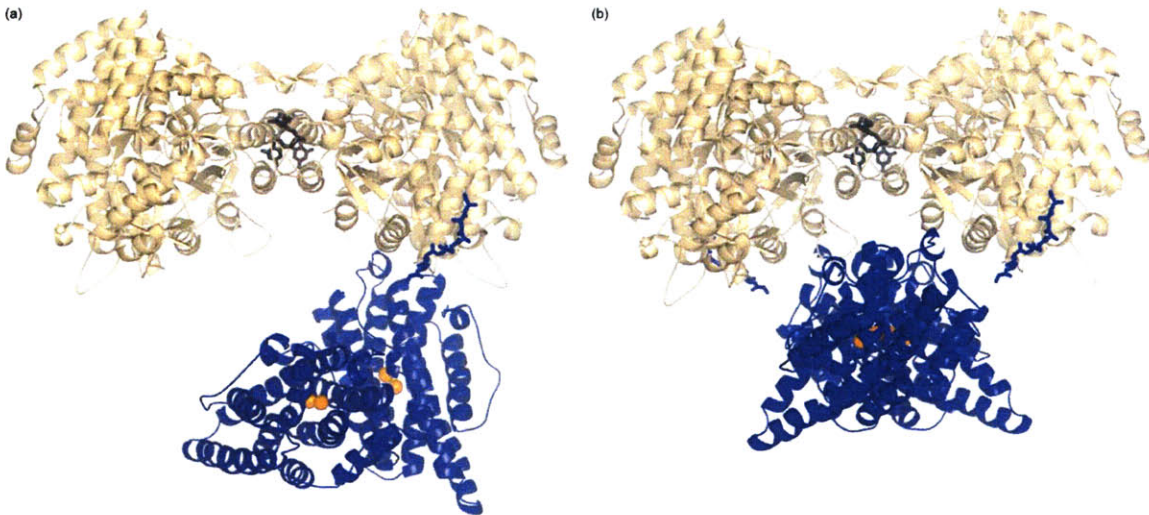


Figure 1.5: Structure of class Ib nrdEF complex from *Salmonella typhimurium* (32). The dGTP effectors (grey sticks) are located at the α_2 dimer interface. The irons are in orange spheres. The β binding site in α is a hydrophobic cleft. The tail of β is shown as a peptide in blue sticks. (a) nrdEF complex, as crystallized (b) Proposed movement of β_2 to form a symmetric complex.

1.2.2 Mechanism of nucleotide reduction class I RNR

The nucleotide reduction mechanism in *E. coli* RNR has been well established by the Stubbe group (1, 4, 50-54). As shown in Figure 1.6, the initiation step of the reaction is the abstraction of an H atom from the C3' position of the substrate by a thiyl radical generated via long-range oxidation from the Y122• on β_2 (Figure 1.6 a). The cleavage of the 2' carbon-hydroxyl bond is facilitated by deprotonation of the 3'-hydroxyl by a carboxylate (E441 in *E. coli* RNR) in the active site (b). Loss of H₂O generates an α -keto radical (c) which is then reduced by oxidation of two cysteines in the active site to generate a disulfide radical anion and the 3'-keto deoxynucleotide (d). This intermediate is reduced by PCET to generate the 3'-deoxynucleotide radical (e) (55-57). Finally the H atom which was originally removed by thiyl radical is used to reduce the 3' radical, regenerating the thiyl radical and yielding the 2'-deoxynucleotide (f).

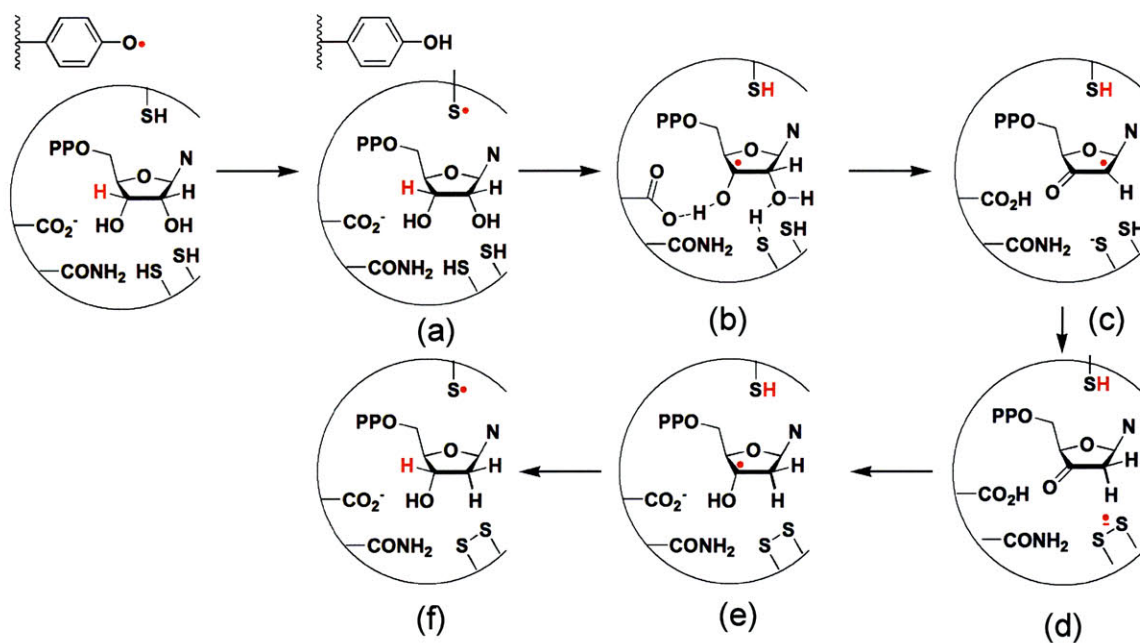


Figure 1.6: The proposed mechanism of class Ia RNR.

To complete the turnover, the active site disulfide is re-reduced by two cysteines located on the C-terminal tail of $\alpha 2$, and the resulting disulfide is then reduced by thioredoxin/thioredoxin reductase or by glutaredoxin/glutaredoxin reductase *in vivo* (55, 57, 58). In *E. coli*, pre-steady-state and steady-state kinetic experiments have revealed that the rate-limiting step in RNR is a physical step prior to rapid nucleotide reduction (46). This physical step is likely a conformational change triggered by ternary or quaternary complex formation, prior to long-range PCET.

1.2.3 Mechanism of 2'-monohalo-2'-deoxynucleotide inhibition

The class of 2'-monohalo-2'-deoxynucleotide inhibitors (2'-XNDP, X=F, Cl) has been studied since 1976 (59). The targets of these compounds are the α and β subunits of *E. coli* or mammalian RNRs (60, 61), with multiple turnovers occurring before RNR is completely inactivated. The inactivation occurs with release of Cl^- or F^- , pyrophosphate, and elimination

of the base, concomitant with the formation of a new chromophore, with maximum absorption at 320 nm. A furanone (Figure 1.7g) is found to be covalently attached to the inactivated α .

The proposed mechanism of RNR inhibition by 2'-monohalo-2'-deoxynucleotides is shown in Figure 1.7. The reaction is initiated as in the normal RNR mechanism by abstraction of a hydrogen atom from the C3' position (a). The next step (b) is different from the mechanism involving normal substrate, since the 2'-halides can leave without protonation from C225 (bottom face cysteine) because they are better leaving groups with lower pK_a values. An α -keto radical is formed and the reaction proceeds by abstraction of a hydrogen atom from either the top face cysteine (C439, *E. coli*) to regenerate the thiyl radical (c) or from the bottom face cysteine (C225, *E. coli*) (d). In the latter scenario (d), the thiyl radical cannot be reformed and inactivation results in loss of $Y\cdot$ on β . In both pathways (c, d), no disulfide radical anion is formed and the 3'-ketonucleotide is released into solution (e, f). The 3'-ketonucleotide decomposes into an electrophilic furanone upon elimination of pyrophosphate and base (g). This furanone derivative is alkylated by cysteines of α (h) or by the thiols of DTT *in vitro*. Alkylation of the furanone by the C-terminal tail cysteines of α , followed by reaction with K760 is thought to produce the chromophore that absorbs at 320-330 nm.

Addition of DTT protects RNR against inactivation by quenching the reactive furanone. A substantially different number of turnovers per inactivation is observed with different bases and/or effectors, reflecting a change in the partitioning of the intermediate between inactivation and normal reduction (62). Compared to the 2'-chloro-2'-deoxy analogs, 2'-fluoro-2'-deoxy analogs behave more similarly to the normal substrate, resulting in

production of more dNDPs or dNTPs relative to inactivation (63, 64). The reduction with normal substrate requires protonation of the leaving group and the difference in partitions between Cl^- and F^- is likely due to differences in acidity with $\text{Cl}^- > \text{F}^- > \text{OH}^-$.

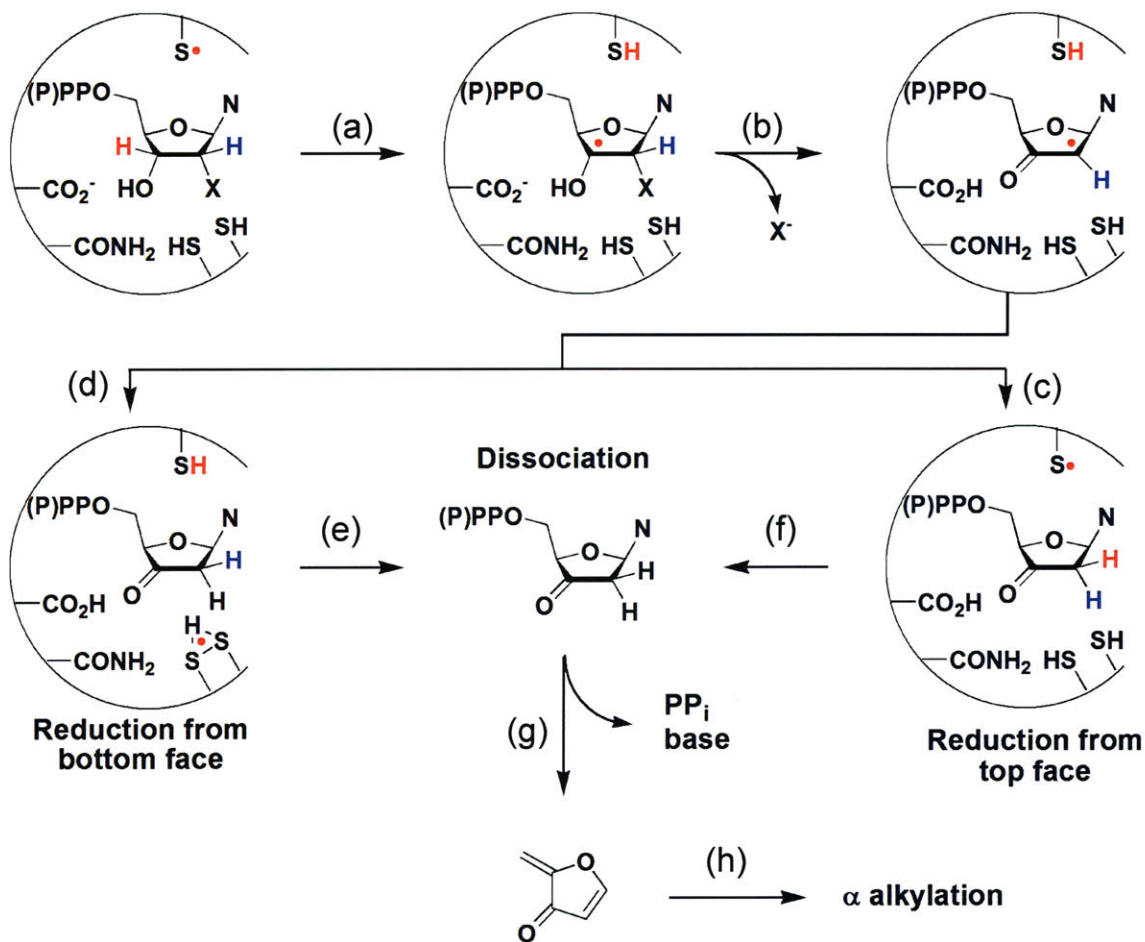


Figure 1.7: The mechanism of inactivation of RNR by 2'-monohalo-2'-deoxy-nucleotides (X = F, Cl).

1.2.4 Regulation of *E. coli* RNR

RNR is tightly regulated in cells to keep balanced dNTP pools for DNA replication and repair. Insufficient RNR activity causes mis-incorporation of dNTPs into DNA, growth defects and increased sensitivity to DNA damaging agents, whereas excess RNR activity decreases fidelity of DNA replication and affects RNA synthesis.

One method of regulation of RNR's nucleotide reduction utilizes ATP and dNTPs as allosteric effectors. In class Ia RNRs, the α subunit contains at least two allosteric sites. The specificity site (S site) binds ATP, dATP, dGTP, or TTP and regulates substrate specificity. The activity site (A site) binds ATP or dATP and controls the overall enzyme activity (65). As shown in the *E. coli* $\alpha 2$ structure in Figure 1.8, the S site (red) is a four helix bundle generated from two helices from each α (28). Binding of effectors to the S site controls which substrate is reduced. Binding of ATP or dATP prepares RNR for the reduction of UDP or CDP; TTP is the effector for GDP reduction and dGTP for ADP reduction.

The A site (magenta) binds either ATP, to stimulate activity, or dATP, to inhibit reaction. The A site is located at the N-terminus of α , adjacent to the α/β interface (Figure 1.2, 1.8) (28). Moreover, it has been observed that the type of effector (ATP, dGTP, TTP, dATP) bound to the S site affects the affinity of dATP for the A site, suggesting the existence of communication between the S site and A site (65, 66).

Above all is the general mechanism of class Ia RNR. The *S. cerevisiae* RNR and human RNR will be the focus of this thesis.

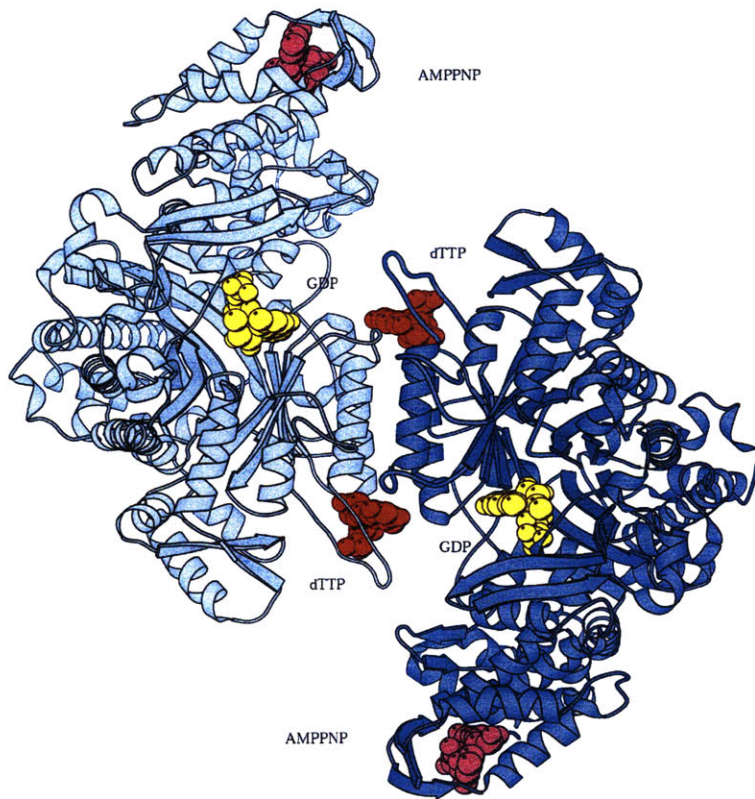


Figure 1.8: Structure of *E. coli* α_2 highlighting the allosteric effector binding sites (67).

Allosteric activity sites are at the N-terminus of α , with ATP analog AMPNP (magenta) bound. Specificity sites are at the α_2 dimer interface, shown with TTP (red) bound. GDP (yellow) is bound in catalytic sites at a distance of 15 Å from the specificity site.

1.3 Yeast RNR

1.3.1 Structure of yeast RNR

In *Saccharomyces cerevisiae*, four genes encode RNR subunits. *RNR1* and *RNR3* encode the large subunits Y1 (α) and Y3 (α'), which share 80% and ~60% identity with the mammalian α respectively (68, 69). The physiological role of *RNR3* is not clear.

Although overproducing *RNR3* can complement the deletion of *RNR1*, deletion of *RNR3* exhibits no obvious phenotype, and does not change the cells' sensitivity to DNA damaging agents. *RNR2* and *RNR4* encode the small subunits Y2 (β) and Y4 (β'), which

are essential for mitotic viability in *S. cerevisiae*. β and β' share 56% sequence identity. Besides lacking 50 residues at the N-terminus of β , β' lacks three of the six residues involved in iron binding, and exhibits a Y to F substitution at the position of the essential Y• (70-72). A large body of data suggests that the active form of the small subunit is the Y2Y4 ($\beta\beta'$) heterodimer, in which β' facilitates iron delivery to β (73, 74).

Structures of *S. cerevisiae* α with different effector/substrate pairs have been solved (75). These structures are the first of a α subunit to show ordering of certain loops upon substrate and effector binding. The overall structure of the *S. cerevisiae* α is very similar to that of the *E. coli* protein. The primary difference is a C-terminal insert and three helix insert (Figure 1.9 blue and red). In the active site of the structure, the pair of cysteines that provide the reducing equivalent for NDP reduction (C218, C443) is reduced and the 2' and 3' OH of the ribose are close to the catalytic residues C428, C218, C443, E430. Two loops are important for the allosteric regulation. Loop 1 only interacts with the effector region (S site), and loop 2 contacts both the specificity and active sites. Binding of different effectors and substrates twists the position of loop 2 into a specific conformation for each effector/substrate pair (Figure 1.10). The structure presented here shows α as a dimer. However, the oligomerization state of the *S. cerevisiae* α in solution is more complicated than it appears from the structure. In Chapter 5, we present our studies on the oligomerization state of *S. cerevisiae* α with different substrate/effector pairs.

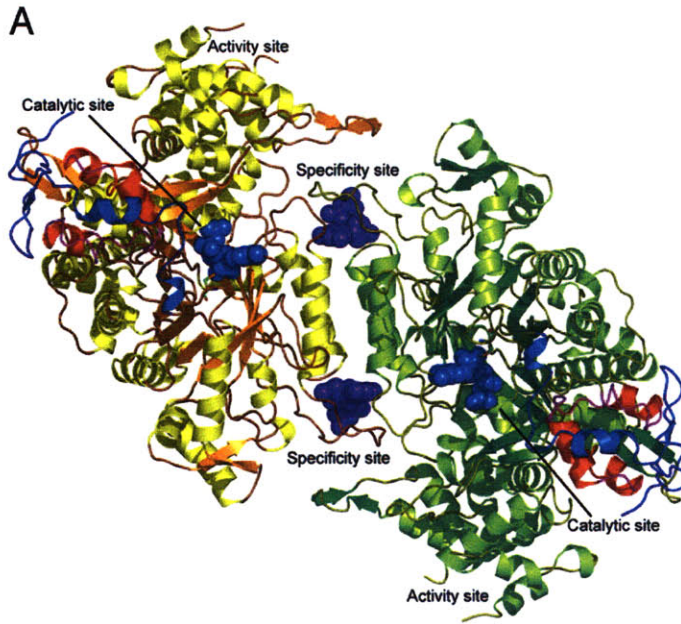


Figure 1.9: Structure of *S. cerevisiae* α at 2.2 Å (75).

The structure is very similar to that of *E. coli* α with dGTP (violet) and ADP (blue) binding at the catalytic site and S site. A major difference between the *S. cerevisiae* and *E. coli* α structures is that the former contains a three-helix insert (red) and C-terminal insert (blue).

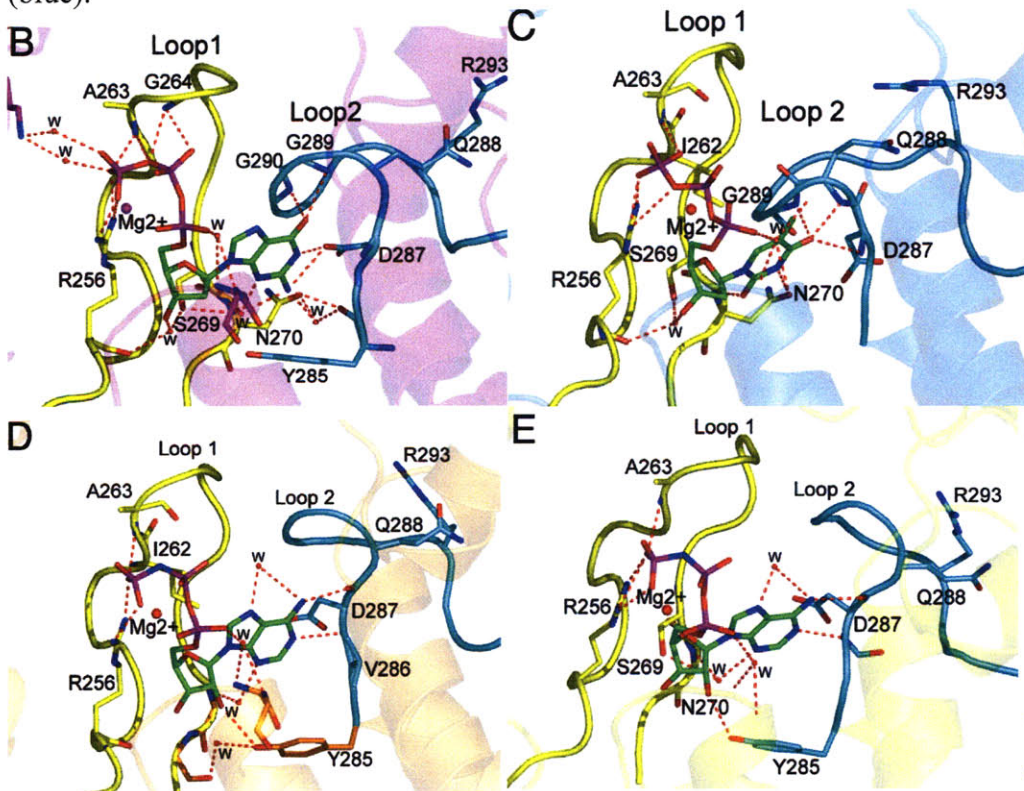


Figure 1.10: Specificity cross-talk of *S. cerevisiae* α for different effector/substrate pairs (75).

Loop 1 (yellow) folds on the effector, and loop 2 (cyan) spans over both the effector (green) site and catalytic site. (B) with dGTP/ADP, (C) with TTP-GDP, (D) with AMPPNP/CDP, and (E) AMPPNP/UDP. The position of loop 2 adapt to a specific conformation for each effector/substrate pair

In vivo, close to 1 Y•/ββ' is observed with whole cell EPR method (76). However, generation of stoichiometric amounts of diferric-Y• cofactor (1 Y•/ ββ') *in vitro* has been difficult with the *S. cerevisiae* ββ'. Stoichiometries of only 0.2-0.4 Y•/ββ' are routinely obtained using *in vitro* reconstitution methods developed by the Stubbe lab. Co-expression of His-ββ' in *E. coli*, followed by purification and *in vitro* reconstitution, was carried out in an attempt to achieve higher Y• content without success. Rapid isolation of Flag-ββ' directly from yeast strains yielded a maximum of 0.5 Y•.

1.3.2 Mechanism of yeast RNR

The mechanism of nucleotide reduction by yeast RNR is very similar to that of the *E. coli* RNR. On each turnover in *E. coli*, the pair of bottom-face cysteines in the active site is oxidized and is re-reduced by the pair cysteines (CX₂C motif) on the C-terminal tail of α for subsequent reactions (55, 77, 78). Recent work on RNR in *S. cerevisiae* has supported this model *in vivo* (79). Δ *RNR3* strains carrying an *RNR1* gene in which the C-terminal tail has been mutated (CX₂C to SX₂S) are not viable. Mutation of C428, the essential S•-forming cysteine (equivalent to C439 in *E. coli*) is also lethal. However, a yeast strain harboring both a C428S *RNR1* with a wt CX₂C at the tail and an *RNR1* gene with no C428 mutation but a SX₂S C-terminal tail is viable albeit with severely retarded growth (79). This suggests that via interallelic complementation, the C-

terminal tail of one α is able to regenerate the active site of its neighboring α (Figure 1.11), although this may not be true of wt *RNR1*.

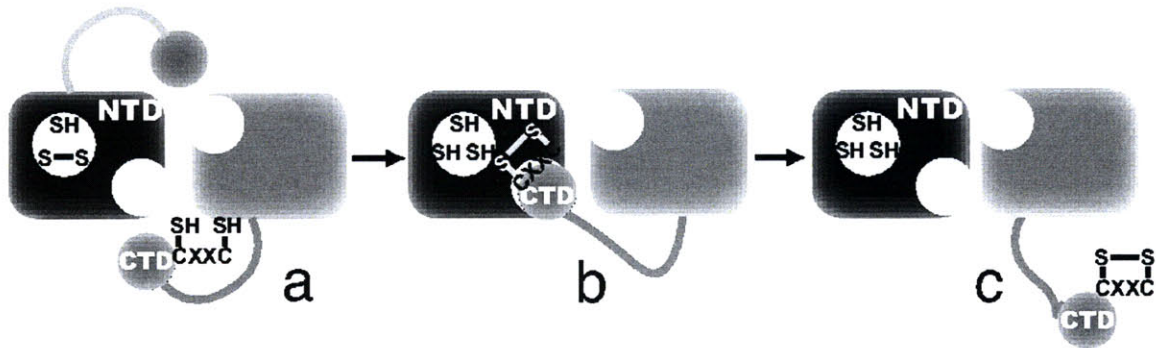


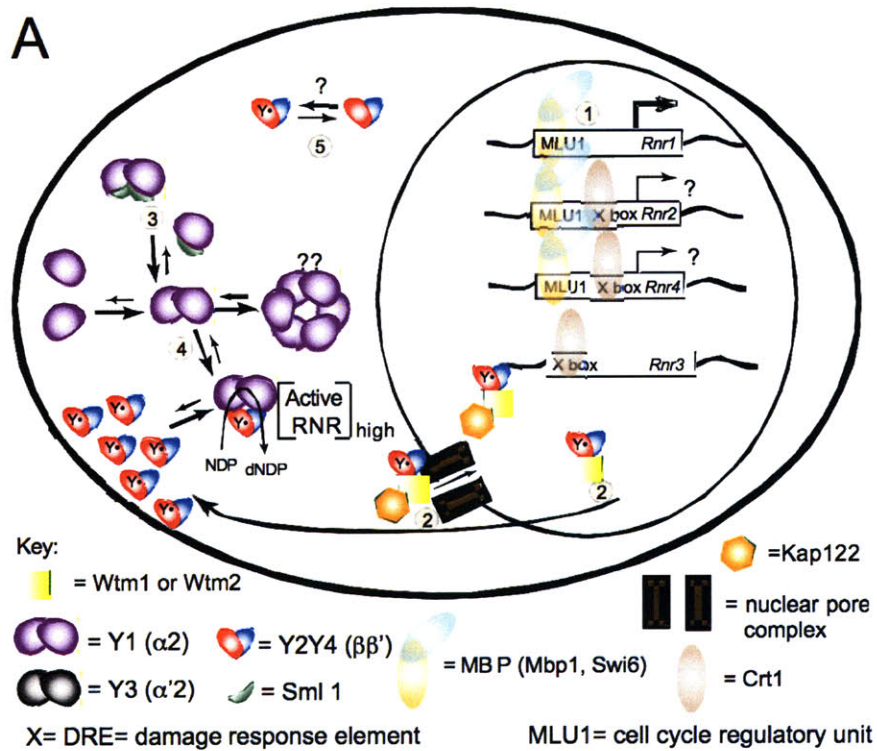
Figure 1.11: Model depicting the C-terminal tail of one α regenerating the active site of its neighbor α (79).

(a) α is oxidized at the end of each turnover cycle with a disulfide bond formed between the redox active cysteine pair in the active site. (b-c) The C-terminal tail of one α accesses to the active site of the neighbor α and reduces its active site cysteines via disulfide exchange.

1.3.3 Regulation of yeast RNR

In yeast cells, RNR is controlled at the level of substrate specificity (80), transcription (81, 82), subunit localization (83-86), and Sml1 (small protein RNR inhibitor) regulation during S-phase of the cell cycle or in DNA repair. The overall regulation of *S. cerevisiae* is shown in Fig 1.12. As with the *E. coli* RNR, the activity and substrate specificity of *S. cerevisiae* RNR are regulated by ATP and dNTPs. The cell-cycle dependent expression of *RNR1*, *RNR2*, and *RNR4* are regulated at the transcription level through the Mbp1/Swi6 (transcription factors) binding to MCB (Mlu1 cell cycle box) (Fig 1.12A). In resting cells, $\beta\beta'$ is localized in nucleus by an anchor protein Wtm1, while α stays in cytosol. The RNR activity is also regulated by a 12 kDa protein inhibitor, Sml1, in S phase and in DNA damage. As suggested by yeast two hybrid assays,

immunoprecipitation, and biochemical studies (87-90), Sml1 inhibits RNR activity by directly binding to α . In response to DNA damage or replication blocks, the Mec1 (signal transducers) and Rad53/Dun1 (effector S/T kinases) checkpoint pathway is triggered (91-93), resulting in release of Sml1 inhibition, translocation of $\beta\beta'$ from the nucleus to the cytoplasm, and stimulation of RNR transcription via removal of Crt1, which binds a conserved cis element (X-box) of *RNR2*, *RNR3*, and *RNR4* to repress their transcription (Fig 1.12B).



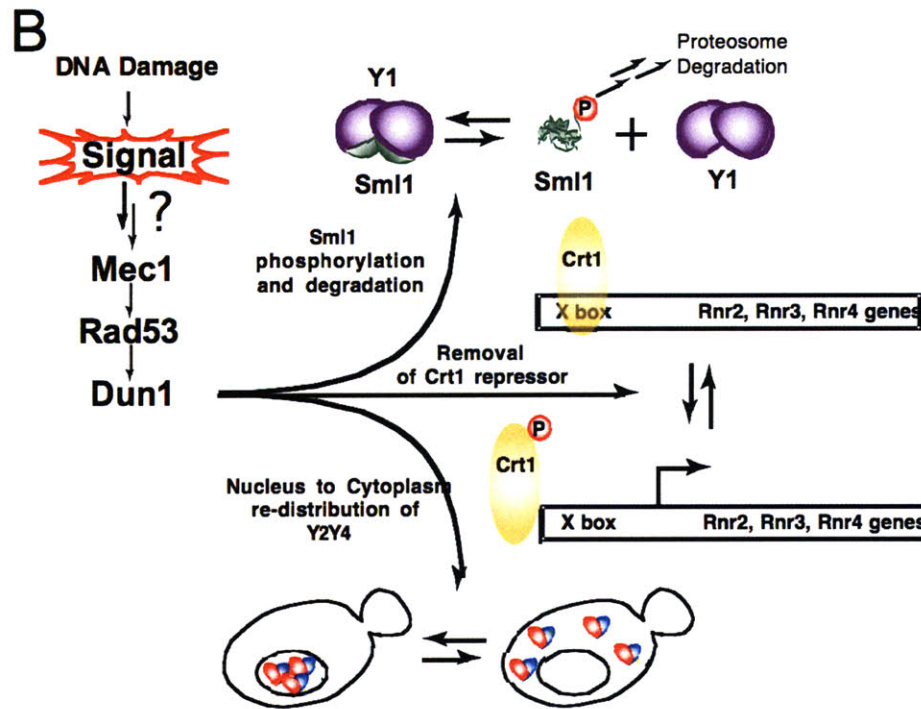


Figure 1.12: RNR regulation in *S. cerevisiae* during (A) DNA replication and (B) in response to DNA damage.

1.3.3.1 Allosteric regulation

In contrast to the *E. coli* and mammalian RNRs, the *S. cerevisiae* RNR shows a relaxed dATP feedback inhibition (80). While 50% of the activity of the mammalian RNR is inhibited at 5-10 μM dATP, the inhibition of the *S. cerevisiae* RNR requires at least 50 μM dATP (66, 94, 95). In addition, the activity of the *S. cerevisiae* RNR is regulated by Sml1, the expression levels of which correlate inversely with the amount of dATP. Sml1 will be described in more detail in section 1.3.3.5 and Chapter 5. The interplay between levels of dATP and Sml1 in the cell is important in controlling RNR activity and balancing the dNTP pools in *S. cerevisiae* (80). Moreover, dNTP levels in yeast cells are about four fold higher after DNA damage than in undamaged cells in S phase. Therefore, it appears that yeast cells require more dNTPs for DNA repair than for

DNA replication, a different scenario from what is observed in mammalian cells. One of the explanations for the high dNTP requirement in yeast cells is that the yeast translesion DNA synthesis (TLS) protein used in DNA repair has K_m for dNTPs at least 10-fold higher than the polymerase used in normal DNA synthesis (80, 96). Therefore, the concentration of dNTPs has to be at least above the K_m for efficient DNA repair even at the expense of higher mutation rates.

1.3.3.2 Cell cycle-dependent regulation

Transcription of *RNR1*, *RNR2* and *RNR4* in yeast is cell cycle-dependent, and is regulated through Mbp1/Swi6 binding to Mlul cell cycle box (MCB). Swi6 is a regulatory protein, and Mbp1 is a DNA binding protein that recognizes the MCB promoter elements (97-99). *RNR1*, which is essential for mitotic viability, is tightly cell-cycle regulated. The mRNA level of *RNR1* reaches a maximal level in the late G₁/S phases and a minimal level in G₁ phase. The half life of *RNR1* mRNA is short relative to *RNR2* and seems to be rate-limiting. *RNR3*, which is not an essential gene, expresses at very low levels under normal conditions, but is induced over a hundred-fold in response to cell cycle arrest, or in response to DNA damage, compared to 3 to 5 fold induction level of *RNR1* under same conditions (69, 100, 101). The expression of both *RNR2* and *RNR4* remain constant throughout the cell cycle but increase 2-20 fold after DNA damage (71, 72).

1.3.3.3 Transcriptional regulation during DNA damage and at replication

checkpoints

RNR is transcriptionally induced through Mec1/Rad53/Dun1 kinase pathway in budding yeast, or through rad3/cds1/chk1 checkpoint pathways in fission yeast, in response to both transcription and cell cycle arrest. *MEC1* Δ and *RAD53* Δ mutants show failure to activate RNR, decreased dNTP pools, incomplete chromosome replication, and eventually cell death (102).

Three genes, *CRT1*, *TIP1*, and *SSN6*, are downstream targets of *DUN1* (DNA damage responsive kinase). Crt1 binds a 13-bp cis-regulatory element (X-box) in the 5'-untranslated region (5'-UTR) of the *RNR2*, *RNR3*, and *RNR4* genes and represses their transcription by recruitment of the co-repressor complex Tup6-Ssn6 (81, 103). Upon activation of the Mec1-Rad53-Dun1 kinase cascade, Crt1 is inactivated by phosphorylation and loses its ability to bind X-box elements present on RNR promoters. After DNA damage is repaired, *CRT1* is induced and the increased amount of Crt1 rapidly restores RNR repression. Furthermore, it has been found that *RNR2* and *RNR4* are partially induced in response to DNA damage in a *DUN1* deletion strain, indicating the existence of a *DUN1*-independent pathway for the transcription of RNR in response to DNA damage.

1.3.3.4 Regulation by subcellular localization

In contrast to human and mouse RNRs, the small RNR subunits in *S. cerevisiae* are anchored in the nucleus and the large RNR subunits remain in the cytoplasm when dNTPs are not needed (86). In *S. cerevisiae*, Wtm (WD40-containing transcriptional

modulator) proteins and the importin β homolog Kap122 are regulators of $\beta\beta'$ localization (83, 104). Wtm1 and Wtm2, which are nuclear proteins, have been observed to be physically interacting with $\beta\beta'$. Deletion of Wtm1 or Kap122 causes $\beta\beta'$ to lose its nuclear localization, but increases the viability of *MEC* Δ cells in hydroxyurea (HU), an anti-cancer drug which inhibits RNR by scavenging $Y\bullet$. The role of Wtm2 is unclear, although high levels of Wtm2 can suppress the sensitivity of *MEC* Δ *SML1* Δ mutant cells to HU, suggesting that it may play a supportive role to Wtm1. The Mec1/Rad53/Dun1 checkpoint kinase pathway has been proposed to control the redistribution of $\beta\beta'$ through regulating Wtm1 in response to cell replication or DNA damage.

In addition, Dif1 (Damage regulated import facilitator 1) was discovered recently to mediate the localization of $\beta\beta'$ in *S. cerevisiae* (105). It is a sequence homolog of Sml1 and Hug1 in *S. cerevisiae*, and Spd1 (S phase delayed protein) in *S. pombe* (Fig 1.13A). Three conserved domains have been identified. *HUG1* is located directly upstream of *SML1* in the genome (Fig 1.13B). Dif1, Hug1 and Sml1 are paralogs from an ancestral gene duplication. Hug1 is highly induced after DNA repair via the Mec1 pathway, but its function still remains unclear. The details of the function of Spd1 and Sml1 will be described in the next section.

Although deletion of Dif1 does not affect the *in vivo* RNR levels, its phenotype is the same as that of Δ *WTM1*, i.e., loss of $\beta\beta'$ nuclear localization. However, Dif1 functions through a pathway distinct from Wtm1. Blocking nuclear export in Δ *Wtm1* causes accumulation of nuclear $\beta\beta'$, whereas this is prevented in the Δ *Wtm1* Δ *Dif1* mutant. Based on this and other data, Dif1 has been proposed to facilitate the nuclear import of $\beta\beta'$ rather than serving as an anchor in the nucleus (figure 1.14). In addition, the level of Dif1

expression is regulated in a cell-cycle dependent fashion by Dun1 phosphorylation, reaching a maximum at the end of S phase for transport of $\beta\beta'$ back to the nucleus.

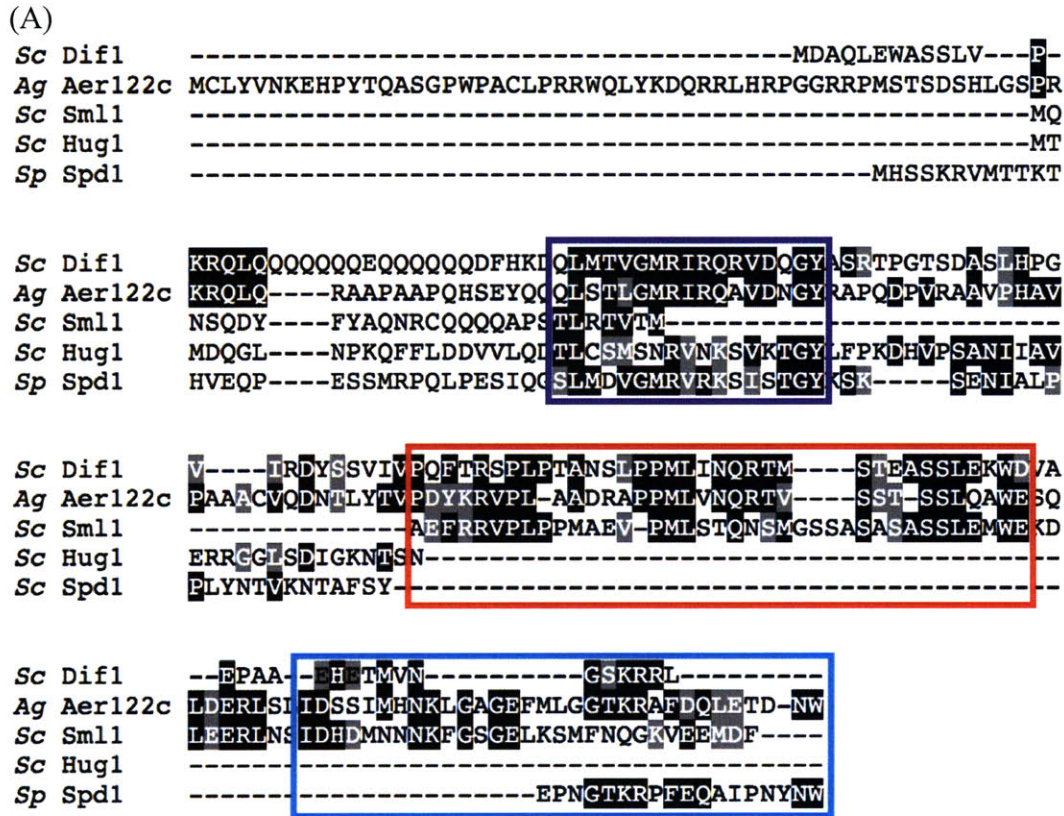


Figure 1.13: Sequence alignment of Dif1, Sml1, Hug1, Spd1 and Aer122c.
 (A) Dif1, Sml1, and Hug1 are *S. cerevisiae* proteins, Spd1 is in *S. pombe*, and Aer122c is a Dif1/Sml1 ortholog in *Ashbya gossypii*. Three conserved domains have been identified.
 (B) Synteny in the proximity of the HUG1/SML1 loci on chromosome XIII and the DIF1 locus in *S. cerevisiae*.

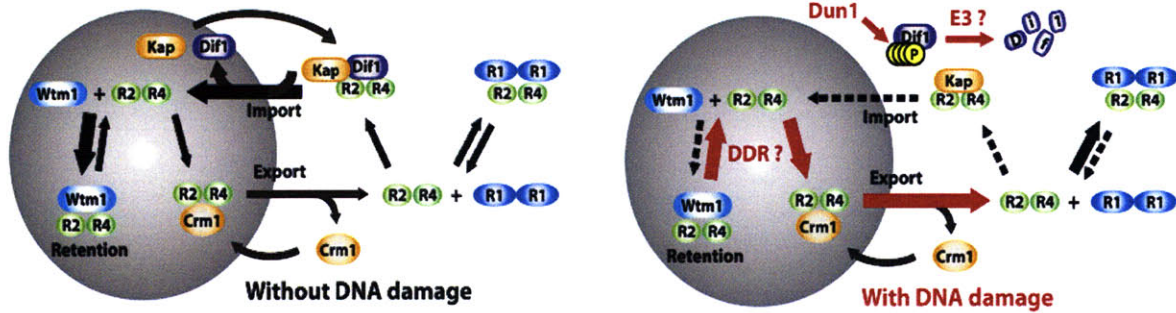


Figure 1.14: Model of the nuclear import facilitator and anchor of $\beta\beta'$ in response to DNA damage (106).

Dif1 facilitates the nuclear import of $\beta\beta'$ (R2R4), while Wtm1 aids in retention of $\beta\beta'$. At left, the cell in the absence of DNA damage. At right, Dif1 is phosphorylated, and degraded, resulting in the release of $\beta\beta'$ in response to DNA damage (DDR). The affinity between Wtm1 and $\beta\beta'$ is also decreased. Kap is Kap122, which facilitates $\beta\beta'$ import. Crm1 is an exportin that mediates $\beta\beta'$ nuclear export. E3 stands for E3 ubiquitin ligase. Dashed arrows indicate pathways that are blocked during DNA damage.

1.3.3.5 Regulation of RNR by protein-protein interaction

In *S. cerevisiae*, DNA damage or S-phase activates the Mec1/Rad53 kinases, which subsequently activate Dun1 and regulate RNR activity by controlling the phosphorylation state of Sml1 (Figure 1.15) (107). Sml1 was originally identified as an RNR inhibitor as Sml1 deletion suppresses the lethality of $\Delta MEC1$ or $\Delta RAD53$ (108). The expression level of Sml1 depends on both the cell cycle and DNA damage; it is lowest during S phase, and is almost undetectable after DNA damage. However, the dNTP levels in $\Delta SML1$ cells do not differ significantly from those in wild-type cells after DNA damage, indicating rapid degradation of Sml1 after DNA damage (96). This rapid change in RNR activity indicates post-translational regulation rather than transcriptional regulation. Cells lacking Sml1 showed 2.5 times higher dNTP levels than in the wild-type cells in normal growth and increased resistance to DNA-damaging agents.

Relief of Sml1 inhibition is proposed to be associated with its phosphorylation, which targets it for degradation. The current model proposed by Rothstein's group is that the Mec1/Rad53 kinases activate Dun1 to control the induction of RNR genes by relieving Crt1 repression and targeting the degradation of Sml1 by phosphorylation in response to DNA damage or in S phase (Figure 1.15) (107, 108).

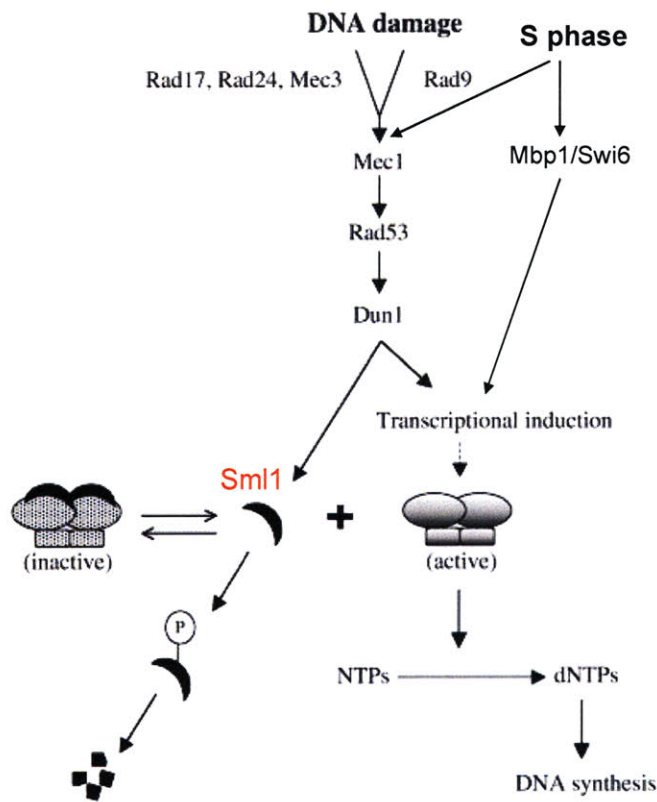


Figure 1.15: The current model for Sml1 regulation in *S. cerevisiae* (96, 107, 109). Mec1/Rad53 pathway causes phosphorylation and degradation of the unbound form of Sml1, which drives the equilibrium from Sml1-bound RNR to the free RNR at S phase and after DNA damage. RNR is also controlled at a transcriptional level by Mbp1-Swi6 at S phase and Mec1/Rad53/Dun1 after DNA damage.

Studies from the yeast two-hybrid assay and co-immunoprecipitation experiments have revealed that Sml1 regulates RNR by binding directly to α rather than by controlling

the RNR transcription (90, 108). Further support for this proposal is the observation that the mRNA levels of *RNR1* in wild type and $\Delta sm11$ cells remain unchanged during normal growth and after DNA damage (108). A 2D NMR structure of Sml1 suggests it is loosely folded with two α helices, one at the N-terminus and the other at C-terminus oriented in an anti-parallel fashion. The residues (8-20) at the N-terminus have been proposed to be important for Sml1 dimerization, whereas the last 33 amino acid residues on the C-terminal alpha helix have been mapped as the site of interaction with α (89). A K_d of 0.4 μ M for Sml1- α binding in the absence of effectors was measured by surface plasmon resonance (SPR) spectrometry (90). Finally, recent two-hybrid assays have shown that deletion of the C-terminal tail of α (778-880) increases interaction between Sml1 and α , suggesting that Sml1 inhibits α by competing with the C-terminal tail's accessing the active site to re-reduce the disulfide formed by turnover (110). The assays also suggested that W688 of α plays a key role in Sml1- α interaction.

Spd1 in *S. pombe* is a homolog of Dif1 and Sml1. It is a 14 kDa protein and was initially found as a cell cycle-regulated protein, with the lowest level in S phase (111). Over-expression of Spd1 blocks S-phase and mitosis progression (112). It was initially proposed that Spd1 served to anchor β inside the nucleus on the bases of indirect immunofluorescence microscopy showing the nuclear co-localization of Spd1 and β (84). Although no direct interaction between β and Spd1 has been observed, deletion of *SPD1* causes β mis-localization (83, 104, 113). However, biochemical studies from Thelander's group have suggested that Spd1 plays a similar role to Sml1 as an inhibitor of α and does not interact with β (113). A K_d value of 2.4 μ M was obtained for Spd1 and *S. pombe* α using a biosensor method. Recent studies from Borgne *et al* (114) have suggested, in

contrast to earlier reports, that Spd1 localized in the cytosol, where it can bind α . Above all, more and more data supports that Spd 1 functions as a RNR inhibitor rather than a β anchor .

1.4 Human RNR

1.4.1 Introduction to human RNR

Most studies to date on mammalian RNRs have been carried out on calf thymus and mouse RNRs, with few reports on human RNR. The calf thymus RNR was the first mammalian RNR to be purified in 1979 (115). The mouse RNR was first purified in 1985 and has since been studied extensively. The most striking difference between the mouse, calf thymus, and *E. coli* β s is the stabilities of their Y• and diferric clusters. In the case of *E. coli* β , the Y• is stable for four days at 4 °C. In the case of the calf thymus enzyme, however, both the Y• and iron cluster are labile, with a half life of 10 min for Y• at 37 °C (116). Assays on calf thymus β were carried out at 37 °C requiring the presence of FeCl₃, DTT and a continuous supply of oxygen for *in vitro* regeneration of Y• to maintain activity (115). In the mouse β , 50% of the iron is lost after 30 min at 37 °C (117). EPR spectroscopy showed stronger interactions between the diferric cluster and the Y• in mouse β than in *E. coli* β (118). Despite these differences, the interaction between the subunits in mammalian RNRs is similar to that in *E. coli* RNR with a K_d of 0.5 μ M for mouse RNR in the absence of effectors (119). Unlike *E. coli* RNR, however, the presence of effector is required for enzyme activity (95).

Human cells contain three RNR subunits: H1 (α), H2 (β), and p53R2 (β'). The quaternary structure of human RNR has not been studied extensively. However,

Cooperman's lab has provided convincing evidence that mouse α which exhibits 80% sequence identity with human α , can be a monomer, dimer, tetramer or hexamer, depending on the presence and concentration of dNTPs and ATP (120). β and β' are always homodimers.

Both human β and β' contain tyrosyl radical, iron ligands, key residues in the PCET pathway, and C-terminal tail that binds α . The p53R2 (β') gene was first isolated from a colon cancer cell line by Tanaka and co-workers in 2000 (121). The gene contains a p53 binding motif in intron 1 and its expression is inducible by p53, a transcription factor which is regulated by ATM/ATR and CHK2 kinase signal transduction pathway and has a tumor-suppressing function through regulation of cell-cycle arrest or induction of apoptosis (122). β' is essential for mammalian cell survival and two models have been proposed for its role. β' 's induction by p53 suggests that it might be involved in DNA repair (123), but recent data suggests the role of β' is likely much more complex. Studies by three independent methods have demonstrated that the localization of ribonucleotide reduction in human cells is in the cytosol instead of the nucleus (124). The data also suggest that β' is localized to the cytosol (124) and is not shuttled to the nucleus as previously suggested (121, 125). In addition, low constitutive levels of β' are expressed in all stages of the cell cycle, regardless of p53 status (126), allowing the cell to provide basal levels of dNTPs for mitochondrial DNA synthesis in G₀/G₁ phases (126). Mutations of β' cause severe depletion of mitochondrial DNA in both mouse, and human cells, leading to the proposal that β' plays a primary role in mitochondrial DNA replication (127). However, most recent data has shown that β' interacts with ATM kinase (ataxia telangiectasia mutated) and is found in the MRE11 complex involved in DNA double

strand break repair, suggesting a role for β' in DNA repair, and a possible translocation to nucleus (128, 129).

1.4.2 Regulation of human RNR

In eukaryotic cells, nuclear DNA synthesis, requiring large dNTPs pools, occurs in S phase, whereas the replication of mitochondrial DNA, needs a much lower supply of dNTPs and occurs in all stages of the cell cycle. In S phase, the majority of dNTP/dNDPs are produced by an α/β RNR complex, the formation of which is mediated by allosteric regulation, S-phase transcription and G_0/G_1 phase degradation of β (Figure 1.16). β' is regulated by p53 at both transcriptional and protein levels. In resting cells devoid of β , β' is at a level of 30 fold lower than β in cycling cells (126). The rate of DNA synthesis is only 2-3% of that in cycling cell (130). Recent data suggest that β' is also regulated by the p53 family members p21 in a p53-mediated way (131) and p73 in a p53-independent way (123). Unlike in yeast, all the RNR subunits in human cells stay in cytosol (124).

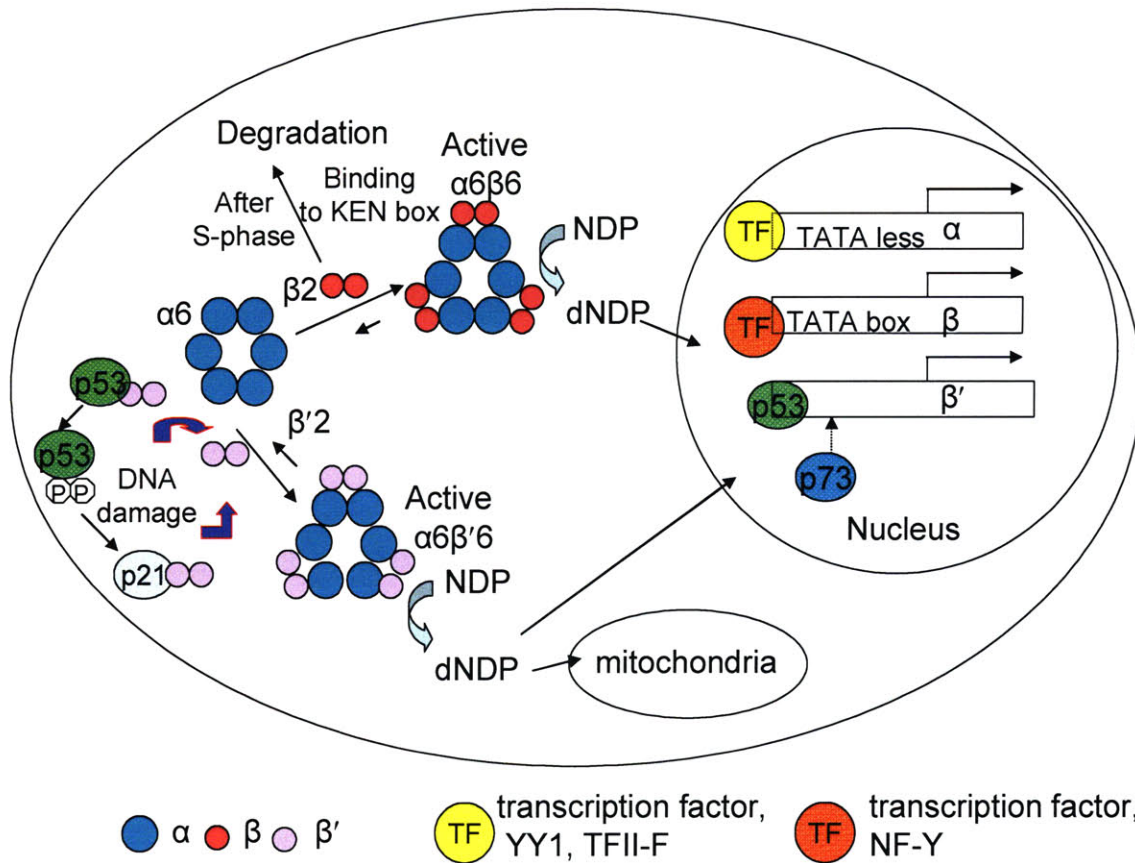


Figure 1.16: Overview of the regulation of human RNR in S-phase and in response to DNA damage.

YY-1, TFII-F and NF-Y are transcription factors which bind the promoter of α and β respectively. The transcription of β' is controlled in a p53 dependent pathway or p53 non-dependent way when p53 is absent. α , β and β' locate in the cytosol and provide DNA precursors for DNA replication and mitochondria DNA synthesis. β' is also regulated at protein level by p53 or p21.

1.4.2.1 Allosteric regulation

Unlike *E. coli* RNR, the mammalian RNR has a stringent requirement for bound effector binding to be active. Binding of the effectors to α at the dimer interface facilitates dimerization and is key for α binding to β . Compared to the K_d ($0.52 \mu\text{M}$) for mouse α and β in the absence of effectors, the affinity of them was increased in the

presence of TTP ($K_d = 0.46 \mu\text{M}$), dGTP ($K_d = 0.4 \mu\text{M}$), dATP ($K_d = 0.05 \mu\text{M}$), and ATP ($K_d = 0.12 \mu\text{M}$) (119).

For mouse RNR, Cooperman's group has proposed a third allosteric binding site, the hexamerization site (H site), which binds ATP and drives formation of the α hexamer, α_6 (132, 133). Based on glycerol gradients analytic centrifugation and dynamic light scattering studies, a model was proposed in which effector binding to the S site drives formation of the active form α_2 , and ATP or dATP binding to the A site drives formation of α_4 , in which the inactive form $(\alpha_4)_b$ predominates over an active $(\alpha_4)_a$ form (Figure 1.17). It was proposed that the interaction of α_4 and β_2 might distort the electron transfer distance and pathway and result in a decrease in the electron transfer rate. Higher concentrations of ATP leads to ATP binding at the H site, driving the formation of the α_6 form (133, 134). The required ATP concentration for α_6 formation is about the same as the *in vivo* ATP concentration in mouse cells. Therefore, the $\alpha_6(\beta_2)_j$ ($j = 1, 2, 3$) is proposed to be the major active form of RNR in mammalian cells.

Recent studies on mouse RNR using gas-phase electrophoretic-mobility macromolecule analysis (GEMMA) and mass spectrometry methods have demonstrated that in the presence of ATP/dATP, α stays in α_6 form, which can interact with β_2 and form an $\alpha_6\beta_2$ complex (135), whereas other allosteric effectors can only induce α to dimerize. In contrast to Cooperman's model, this study did not observe the tetramer and did not support the existence of H-site.

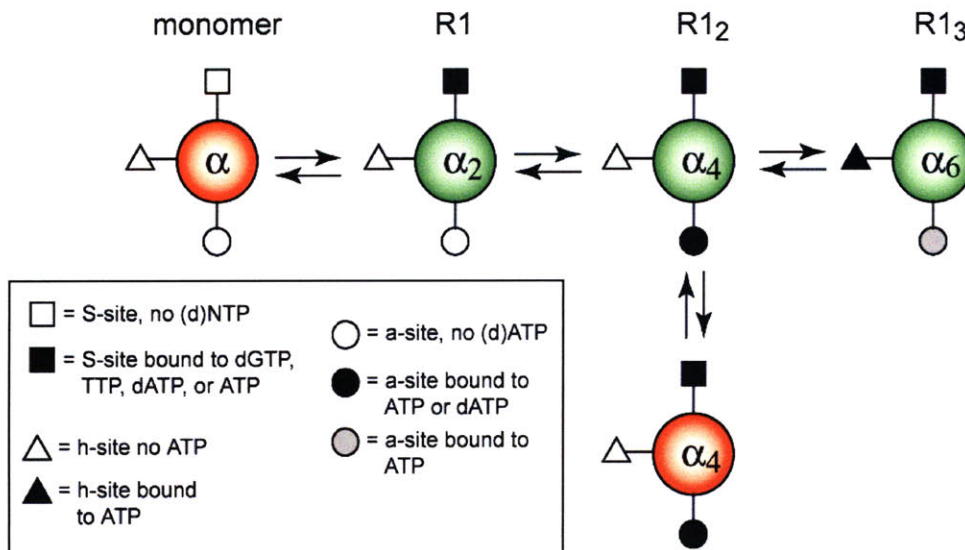


Figure 1.17: The modulation of mouse α oligomerization state and the activity by ATP and dATP effectors (132).

The equilibrium between different forms is regulated by three allosteric sites, S-site, A-site and H-site. The three forms in green are active forms, and the two forms in red are inactive.

1.4.2.2 Cell cycle-dependent regulation

The transcription of genes encoding α and β is exclusively cell cycle-dependent, reaching a maximum level during S-phase (66, 136). The half-life of α is about 15 h, long enough that the concentration of α is virtually constant throughout the cell cycle (136). β has a short half life (3 h) and is degraded in the G₀/G₁ phases. The maximal level of β' is reached at G₁/S transition. Therefore, S phase RNR activity is limited by the expression and degradation of β . Although the transcription of the genes encoding α and β reaches the maximum levels during S-phase, the genes' promoters do not show sequence homologies to explain the coordination of transcription. On the promoter of the mammalian α gene, a TATA-less region that contains four protein-binding DNA elements have been found to regulate the promoter activity (137, 138). Of the four elements, two are essential for cell cycle-regulated transcription of α ; and the other two

control the α promoter strength. Transcription factor YY-1 and TFII-F bind to the α promoter. In contrast to the α promoter, the mammalian β promoter contains a TATA-box. The S-phase specific transcription of β is mainly regulated by an upstream activating region and an element repressing the promoter activity in G_1 phase by binding to E2F4 element (139). At the beginning of S phase, repression of the β promoter is released by the recruitment of the NF-Y transcription factor to disrupt E2F4 binding; meanwhile, the upstream activating region is allowed to activate the promoter region.

The major sequence difference between β and β' is that β' lacks 33 amino acids at its N-terminus, which includes the KEN box in β . In G_0/G_1 phase, Cdh1-APC binds the KEN box of β to facilitate its polyubiquitination and subsequent degradation by the proteasome. Thus β is completely absent in postmitotic cells. The lack of KEN box in the p53R2 gene prevents the degradation of β' during the cell cycle. In the absence of DNA damage in quiescent cells, the expression level of β' is about 30-fold lower than β in S phase (126), and the nucleotide reduction rate is about 2 to 3% that in proliferating cells based on isotope incorporation experiments (130).

1.4.2.3 Transcriptional regulation through DNA damage and replication checkpoints

In human and mouse cells, β' is transcriptionally induced by p53 through ATM-ATR/CHK2 signal transduction pathway in response to DNA damage. It has been shown that homeodomain-interacting protein kinase 2 (HIPK2), which phosphorylates Ser46 of p53, is involved in p53 binding to the β' promoter in activating the transcription of β' (140). The level of activated β' and the efficiency of DNA repair were significantly

reduced as a result of HIPK2 deletion. It has been found that in the absence of p53, p73, another member of the p53 family that regulates factors involved in mitochondrial DNA synthesis, can induce β' in a p53-independent pathway (Figure 1.16) (123).

In contrast to yeast cells, no significant increase in the size of dNTP pools has been observed in mouse cells in G_0/G_1 and S phase after DNA damage (126), even though the basal level of β' is increased. One explanation might be that the activation of β' only increases the local concentration of dNTPs close to the DNA damage site. Since DNA repair requires much smaller amounts of dNTPs than DNA replication, mammalian cells might have evolved mechanisms to produce an optimal level of dNTPs in response to DNA damage while maintaining high fidelity in DNA replication. By contrast, it has been reported that the expression of β during S phase is not affected by DNA damage or cell cycle arrest (141).

1.4.2.4 Regulation of RNR subcellular localization

In human cells, α , β , β' are normally located in cytosol. However, the localization of the ribonucleotide reduction has become a debatable question. Tanaka *et al* reported that β' could undergo relocation from the cytosol to the nucleus in response to DNA damage (121, 125). During S phase, β and α are transported to the nucleus to produce dNTPs (142). Thus controlling the subcellular localization of α , β and β' was proposed as another RNR regulation mechanism. Nevertheless, the current model proposed by Pontarin *et al* (124) suggests that the ribonucleotide reduction occurs only in the cytoplasm and the produced dNTPs are imported into the nucleus or mitochondria for DNA replication or repair. Their data has demonstrated that even in S-phase and after

DNA damage, all three RNR subunits only locate to the cytoplasm (124). The translocation of β' was not observed. These results agree with earlier studies that suggested the RNR subunits exclusively localize to the cytoplasm (143).

1.4.2.6 Regulation by protein-protein interaction

Besides regulation at the transcriptional level, p53 also binds β' , but this binding is inhibited upon DNA damage. Moreover, it has been reported that the N-terminus (residues 1-113) of β' interacts with the N-terminus (residues 1-93) of p21 and the p21/ β' complex stays in the cytosol. p21, which is a downstream target of p53, is a cyclin-dependent kinase (Cdk) inhibitor that causes G₁ arrest (131, 144). After DNA damage, p21 dissociates from β' and inhibits Cdk2 in the nucleus to arrest cells in G₁ phase (131).

More recently, data has shown that ATM kinase can directly phosphorylates S72 of β' and forms a complex with β' (145). This modification has been found to be important for maintaining the stability of β' by inhibiting its polyubiquitination and degradation.

1.5 RNR as target for anti-cancer therapy

The discovery of β' has provided a connection between RNR activity and the p53 checkpoint pathways for DNA repair in an effort to maintain genome stability.

Inactivation of p53 directly interferes with the transcription of β' , causing insufficient RNR activity to provide dNTPs required for DNA repair, thereby increasing cell sensitivity to DNA-damaging agents (121). In addition, the expression level of β' has been found to be significantly correlated to the degree of tumor invasion (146). β' has

been shown to interact with ERK1/ERK2 (extracellular signal-regulated kinase) and to inhibit MEK-ERK kinase signaling and prevent cancer invasion (128, 129).

The key role of RNR in DNA replication and repair has made it an important target for anti-tumor agents. Increased RNR mRNA levels and activity have been found to be associated with tumor cell growth, and thus inactivation of RNR could inhibit cancer cell proliferation. Tumor cells are more sensitive to RNR inhibition than the normal cells due to their increased demands for dNTPs for their replication. In recent years, RNR inhibitors such as Gemzar®, Hydroxyurea, and Triapine® have been used for cancer treatment or have advanced to various phases of clinical trials. Inhibitors can target either the regulation of RNR gene expression or the RNR protein. The inhibitors targeting RNR proteins can attack either RNR subunit, or disrupt subunit interactions. The α inhibitors are usually nucleoside analogs that are either substrate analogs, such as Gemcitabine (2', 2'-difluorodeoxycytidine, F₂C) (147-149), Tezacitabine (2'-fluoromethylene cytidine, FMC)(150-152), or allosteric effector analogs, such as clofarabine, or those that inactivate α by alkylation. The β inhibitors are either iron chelators, such as thiosemicarbazones (153, 154), or radical scavengers, such as hydroxyurea (155-158). Drugs that are designed to prevent α , β complex formation are small peptides corresponding to the C-terminal tail of β .

1.5.1 Gemcitabine

Gemcitabine (F₂C) is taken up into cells via CNT type or ENT type nucleoside transporters, and is phosphorylated by deoxycytidine kinase (dC kinase) to F₂CMP and subsequently to the corresponding 5'-diphosphate (F₂CDP) and triphosphate (F₂CTP) forms.

Gemcitabine has multiple targets in the cell including RNR, dC kinase, and DNA polymerase (Figure 1.18). F₂CDP inhibits RNR, reducing the dNDP and consequently dNTP pools. The decrease in the dCTP pools activates dC kinase. The activated dC kinase produces more F₂CMP and consequently more F₂CDP which further inhibits RNR activity. The reduced dNTP pools allow F₂CTP to be more efficiently incorporated into DNA, resulting in chain termination and leads to cell death (159). Gemcitabine resistance has been observed to be associated with overexpression of α in some cell lines and β in other cell lines (160, 161).

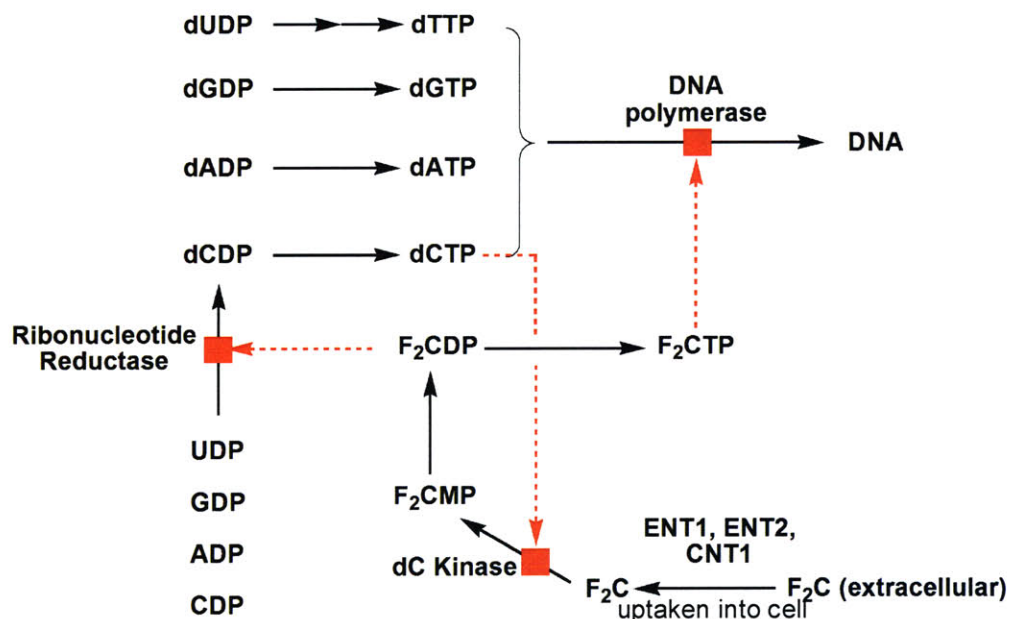


Figure 1.18: Gemcitabine metabolism.

Only unphosphorylated nucleosides can be taken into the cell. Once inside the cell, they must be phosphorylated to the di- and triphosphate states to be active. The diphosphate state targets RNR and reduces dNDP and consequently dNTP pools. The decrease in the dCTP pools activates dC kinase. The activated dC kinase produces more F₂CMP and consequently more F₂CDP which further inhibits RNR activity. The reduced dNTP pools allow F₂CTP to be more efficiently incorporated into DNA, which results in chain termination.

Gemcitabine has been widely used in anti-cancer treatment and has shown significant clinical activity. It is the first line treatment for non-small cell lung cancer and pancreatic

cancer (162-166). It has also been used in combination with other chemotherapies for the treatment of various carcinomas: bladder cancer, breast cancer, ovarian cancer and lymphomas (167-170). Patients with pancreatic cancer treated show significantly reduced rate of recurrence and improved longer disease-free survival with F₂C treatment after tumor resections (171, 172).

Gemcitabine has multiple intracellular targets including RNR, DNA and RNA chains, deoxycytidine kinase (dCK), CTP synthase, nucleoside transporters hENT1, hENT2. Over-production or decrease of any of those targets may cause resistance to the drug (75). Patients with higher levels of hENT1 transporters have shown longer survival and sensitivity after gemcitabine treatment, suggesting the amount and the type of nucleoside transporters on cells are related to the efficacy and toxicity of gemcitabine (173). Deoxycytidine kinase (dCK) which catalyzes the rate-limiting step in F₂C phosphorylation, has been found to be a pivotal factor for the cytotoxicity of F₂C. A lack of dCK causes resistance to F₂C in several leukemic cell lines (174-176). The efficacy of F₂C is significantly reduced with addition of 2'-deoxycytidine, which down-regulates dCK activity. In addition, over-expression of RNR α subunit or β subunit has been observed in several F₂C resistant cell lines, suggesting that both subunits are the targets of F₂C (177-180). The expression ratio of RNR and dCK closely correlates with efficacy of F₂C.

The deamination product F₂U is the major inactive metabolite of F₂C at low F₂CTP concentration, whereas most F₂C is secreted at high injection concentration (181). Cytidine deaminase (CDA) and cytosolic 5'-nucleotidase (cN-II) play major roles in inactivation of active metabolites. Over expression of CDA or cN-II has resulted in drug resistance and is associated with shorter survival (182).

Previous studies in our lab on the inactivation of *E. coli* RNR by gemcitabine have established that F₂CDP is a potent irreversible mechanism-based inhibitor of RNR (149, 183, 184). The inhibition mechanism of F₂CDP is unique. While the 2'-monohalo-2'-deoxy-nucleotides lead to partitioning between turnover and inactivation, 0.5 eq. F₂CDP can completely eliminate RNR activity accompanied with 1 cytosine and 2 F⁻ released, and 1 ribose ring covalently attached to the inactivated enzyme.

Based on our past and current studies on *E. coli* and *L. leichmannii* RNRs, a model to account for the pathway of inactivation has been proposed (Figure 1.19) (185). The first step is 3'-hydrogen atom abstraction followed by loss of F⁻ (1 to 3, Figure 5), as in the mechanism of 2'-fluoro-2'-deoxynucleoside 5'-diphosphate (Figure 1.7). The partitioning of the next step depended on the presence of reductant (4, 61). In the presence of reductant, one of the bottom phase cysteine attacks the 2' carbon to generate 5 with forming covalent linked product. In the absence of reductant, water attacks the 2' carbon to generate 4 concomitant with loss of the second F⁻. Intermediates 4, 6 are proposed to be the new nucleotide radical detected by EPR spectroscopy. The conversion of 3 to 4 has no chemical precedent. This step is the reverse of water loss in the normal reduction process and requires that there is a water in the active site in the vicinity of the C2' carbon.

A computational method has also been used recently in an attempt to unravel the F₂CDP inhibition mechanism (186, 187), leading to the proposal of a similar mechanism. In their work, C225, one of the redox cysteines in the active site has been proposed as the conjugation site. However, the charges on the intermediate proposed in their model appear to be incorrect, which require the kinetics to be reexamined.

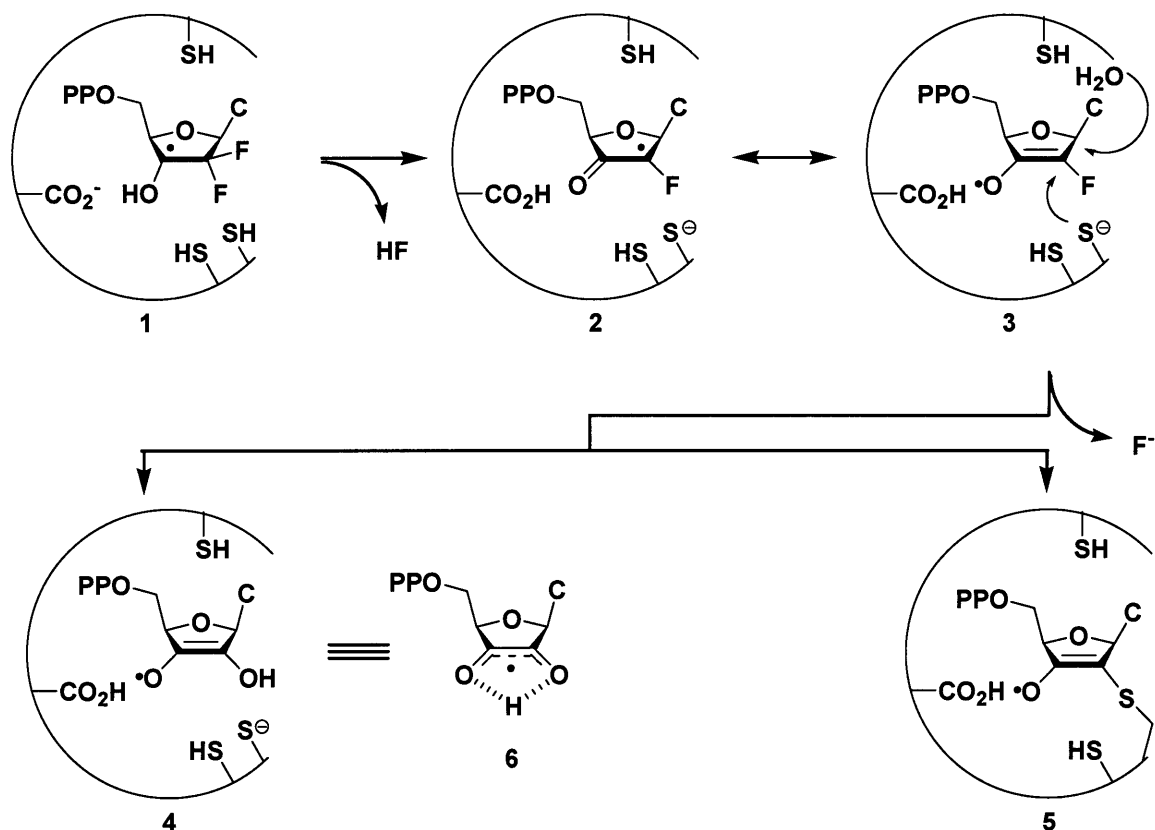


Figure 1.19: Proposed mechanism of inactivation of RNR by F_2CDP in the absence (4) and the presence (5) of reductant.

The recently solved crystal structures of yeast RNR with $F_2CDP/AMPPNP$ (effector analogue) bound, and $CDP/AMPPNP$ bound display different binding modes (Figure 1.20) (75, 188). The crystals were grown under following conditions: 0.1 M sodium acetate, pH 6.5, 20-25% PEG 3350, and 0.2 M ammonium sulfate, followed by soaking with 20 mM $AMPNP-F_2CDP$ pair or $AMPNP-CDP$ in a mother liquor containing 20 mM DTT and 10 mM $MgCl_2$. As shown in the $AMPPNP-CDP$ structure in figure 1.20 (right), the 2' and 3' OH of the ribose are close to the catalytically relevant residues, N426 and E430, the thiyl radical residue C428, and the active site cysteine C218. In the $AMPPNP-F_2CDP$ structure (Figure 1.20 left), however, the cytosine and ribose ring bind higher and away from N426 and E430. C218 remains close to the 2' carbon of F_2CDP . In

addition, two additional water molecules close to the ribose of F₂CDP have been identified. Overall, these structures provide support for our proposed mechanism (Figure 1.19).

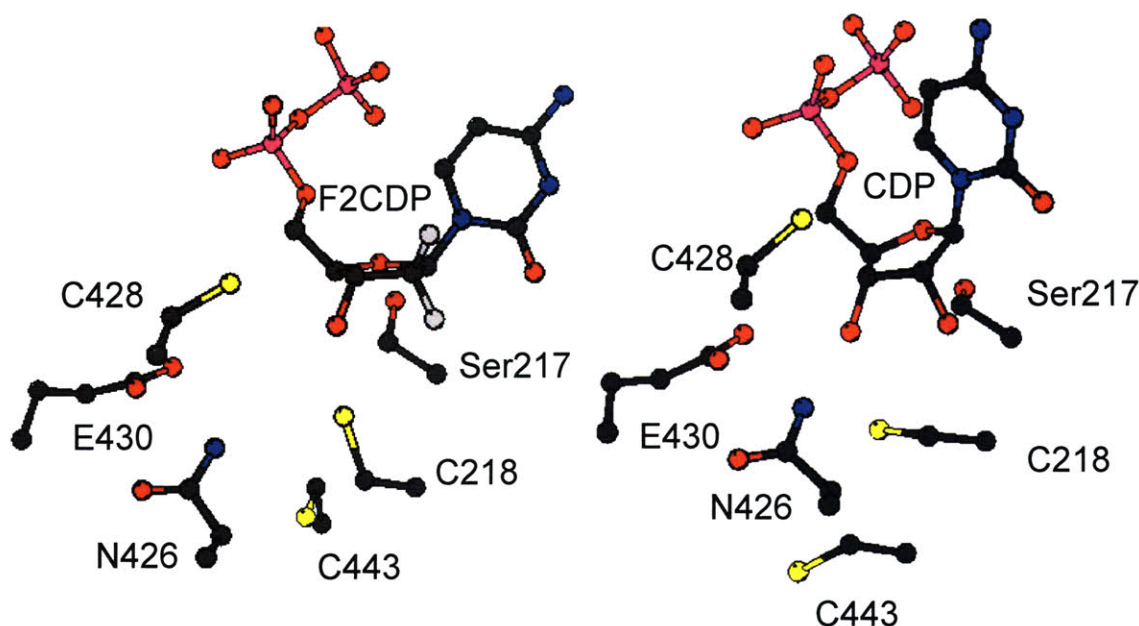


Figure 1.20: Yeast RNR active site structures with F₂CTP (left) or CDP (right) bound.

1.5.2 Hydroxyurea

Hydroxyurea is another important anti-tumour drug used in combination with other chemotherapies targeting RNR. It causes decreased dNTP pools to inhibit DNA synthesis by starving the DNA polymerase at the replication fork (189). Hydroxyurea inactivates RNR by reducing the Y• in β via a one-electron transfer mechanism (190). The Y• in mammalian RNR is more sensitive to hydroxyurea inhibition than the *E. coli* analog, perhaps because the iron center is more solvent exposed in mammalian β (191). However, the activation energies of the reactions are quite similar for both the *E. coli* (67 kJ mol⁻¹) and mouse RNRs (66 kJ mol⁻¹), suggesting a common reaction pathway (192). The presence of α reduces RNR

susceptibility to hydroxyurea, whereas the addition of positive effector and substrate makes the radical in RNR complex more susceptible to hydroxyurea inactivation and accelerates the inhibition significantly. The control experiment with addition of substrate to β alone did not change the radical susceptibility to hydroxyurea by a large extent (192). It might be that addition of α to β blocks the radical site, but addition of positive allosteric effectors changes the RNR complex conformation drastically from apo to holo form and opens up the active site. The data thus far suggest that there is no particular binding site for hydroxyurea inhibition.

1.6 References

- (1) Stubbe, J. (1990) Ribonucleotide reductases. *Adv Enzymol Relat Areas Mol Biol.* 63, 349-419.
- (2) Jordan, A., and Reichard, P. (1998) Ribonucleotide reductases. *Annu Rev Biochem.* 67, 71-98.
- (3) Kolberg, M., Strand, K. R., Graff, P., and Andersson, K. K. (2004) Structure, function, and mechanism of ribonucleotide reductases. *Biochim. Biophys. Acta.* 1699, 1-34.
- (4) Stubbe, J., and van der Donk, W. A. (1998) Protein radicals in enzyme catalysis. *Chemical Reviews* 98, 705-762.
- (5) Larsson, A., and Sjöberg, B. M. (1986) Identification of the stable free-radical tyrosine residue in ribonucleotide reductase. *EMBO J.* 5, 2037-2040.
- (6) Sjöberg, B. M., Reichard, P. (1977) Nature of Free-Radical in Ribonucleotide Reductase from *Escherichia-Coli*. *J. Biol. Chem.* 252, 536-541.
- (7) Atkin, C. L., Thelander, L., Reichard, P., and Lang, G. (1973) Iron and Free-Radical in Ribonucleotide Reductase - Exchange of Iron and Mossbauer-Spectroscopy of Protein-B2 Subunit of *Escherichia-Coli* Enzyme. *J. Biol. Chem.* 248, 7464-7472.
- (8) Jordan, A., Aragall, E., Gibert, I., and Barbe, J. (1996) Promoter identification and expression analysis of *Salmonella typhimurium* and *Escherichia coli* nrdEF operons encoding one of two class I ribonucleotide reductases present in both bacteria. *Mol. Microbiol.* 19, 777-790.
- (9) Jiang, W., Yun, D., Saleh, L., Barr, EW., Xing, G., Hoffart, LM., Maslak, MA., Krebs, C., Bollinger, JM Jr. . (2007) A manganese(IV)/iron(III) cofactor in *Chlamydia trachomatis* ribonucleotide reductase. *Science* 316, 1188-1191.
- (10) Jiang, W., Saleh, L., Barr, EW., Xie, J., Gardner, MM., Krebs, C., Bollinger, JM Jr. (2008) Branched activation- and catalysis-specific pathways for electron relay

- to the manganese/iron cofactor in ribonucleotide reductase from *Chlamydia trachomatis*. *Biochemistry* 47, 8477-8484.
- (11) Jiang, W., Hoffart, L.M., Krebs, C., Bollinger, J.M. Jr. (2007) A manganese(IV)/iron(IV) intermediate in assembly of the manganese(IV)/iron(III) cofactor of *Chlamydia trachomatis* ribonucleotide reductase. *Biochemistry*, 8709-8716.
 - (12) Jiang, W., Bollinger, J.M. Jr., and Krebs, C., (2007) The active form of *Chlamydia trachomatis* ribonucleotide reductase R2 protein contains a heterodinuclear Mn(IV)/Fe(III) cluster with S=1 ground state. *J. Am. Chem. Soc.* 129, 7504-7505.
 - (13) Eliasson, R., Pontis, E., Jordan, A., and Reichard, P. (1999) Allosteric control of three B12-dependent (class II) ribonucleotide reductases. Implications for the evolution of ribonucleotide reduction. *J. Biol. Chem.* 274, 7182-7189.
 - (14) Jordan, A., Torrents, E., Jeanthon, C., Eliasson, R., Hellman, U., Wernstedt, C., Barbe, J., Gibert, I., and Reichard, P. (1997) B12-dependent ribonucleotide reductases from deeply rooted eubacteria are structurally related to the aerobic enzyme from *Escherichia coli*. *Proc. Natl. Acad. Sci. U.S.A.* 94, 13487-13492.
 - (15) Tauer, A., and Benner, S.A. (1997) The B12-dependent ribonucleotide reductase from the archaeobacterium *Thermoplasma acidophila*: An evolutionary solution to the ribonucleotide reductase conundrum. *Proc. Natl. Acad. Sci. U.S.A.* 94, 53-58.
 - (16) Riera, J., Robb, F.T., Weiss, R., and Fontecave, M. (1997) Ribonucleotide reductase in the archaeon *Pyrococcus furiosus*: A critical enzyme in the evolution of DNA genomes? *Proc. Natl. Acad. Sci. U.S.A.* 94, 475-478.
 - (17) Booker, S., Licht, S., Broderick, J., and Stubbe, J. (1994) Coenzyme B12-dependent ribonucleotide reductase: Evidence for the participation of five cysteine residues in ribonucleotide reduction. *Biochemistry* 33, 12676-12685.
 - (18) Panagou, D., Orr, M.D., Dunstone, J.R., and Blakley, R.L. (1972) A monomeric, allosteric enzyme with a single polypeptide chain. Ribonucleotide reductase of *Lactobacillus leichmannii*. *Biochemistry* 11, 2378-2388.
 - (19) Sun, X., Ollagnier, S., Schmidt, P.P., Atta, M., Mulliez, E., Lepape, L., Eliasson, R., Gräslund, A., Fontecave, M., Reichard, P., *et al.* (1996) The free radical of the anaerobic ribonucleotide reductase from *Escherichia coli* is at glycine 681. *J. Biol. Chem.* 271, 6827-6831.
 - (20) Young, P., Andersson, J., Sahlin, M., and Sjöberg, B.M. (1996) Bacteriophage T4 anaerobic ribonucleotide reductase contains a stable glycy radical at position 580. *J. Biol. Chem.* 271, 20770-20775.
 - (21) Sun, X., Harder, J., Krook, M., Jörnvall, H., Sjöberg, B. M., and Reichard, P. (1993) A possible glycine radical in anaerobic ribonucleotide reductase from *Escherichia coli*: Nucleotide sequence of the cloned nrdD gene. *Proc. Natl. Acad. Sci. U.S.A.* 90, 577-581.
 - (22) Reichard, P. (1993) The anaerobic ribonucleotide reductase from *Escherichia coli*. *J. Biol. Chem.* 268, 8383-8386.
 - (23) Mulliez, E., Fontecave, M., Gaillard, J., and Reichard, P. (1993) An iron-sulfur center and a free radical in the active anaerobic ribonucleotide reductase of *Escherichia coli*. *J. Biol. Chem.* 268.

- (24) Torrents, E., Eliasson, R., Wolpher, H., Gräslund, A., and Reichard, P. (2001) The anaerobic ribonucleotide reductase from *Lactococcus lactis*. Interactions between the two proteins NrdD and NrdG. *J. Biol. Chem.* 276, 33488-33494.
- (25) Stubbe, J., Ge, J., and Yee, C. S. (2001) The evolution of ribonucleotide reduction revisited. *Trends Biochem. Sci.* 26, 93-99.
- (26) Nordlund, P., Sjöberg, B.M., and Eklund, H. (1990) 3-dimensional structure of the free-radical protein of ribonucleotide reductase. *Nature (London)* 345, 593-598.
- (27) Uhlin, U. a. E., H. (1994) Structure of ribonucleotide reductase protein R1. *Nature* 370, 533-539.
- (28) Eriksson, M., Uhlin, U., Ramaswamy, S., Ekberg, M., Regnstrom, K., Sjöberg, BM, and Eklund, H. (1997) Binding of allosteric effectors to ribonucleotide reductase protein R1: reduction of active-site cysteines promotes substrate binding. *Structure* 5, 1077-1092.
- (29) Kauppi, B., Nielsen, B. B., Ramaswamy, S., Larsen, I. K., Thelander, M., Thelander, L. & Eklund, H. (1996) The three-dimensional structure of mammalian ribonucleotide reductase protein R2 reveals a more accessible iron-radical site than *Escherichia coli* R2. *J. Mol. Biol.* 262, 706-720.
- (30) Voegtli, W. C., Ge, J., Perlstein, D. L., Stubbe, J. & Rosenzweig, A. C. (2001) Structure of the yeast ribnucleotide reductase Y2Y4 heterodimer. *Proc. Natl. Acad. Sci. U.S.A.* 98, 10073-10078.
- (31) Xu H, F., C., Uchiki, T., Fairman, JW., Racca, J., & Dealwis, C. (2006) Structures of eukaryotic ribonucleotide reductase I provide insights into dNTP regulation. *Proc. Natl. Acad. Sci. U.S.A.* 103, 4022-4027.
- (32) Uppsten, M., Färnegårdh, M., Domkin, V., and Uhlin, U. (2006) The first holocomplex structure of ribonucleotide reductase gives new insight into its mechanism of action. *J. Mol. Biol.* 359, 365-377.
- (33) Climent, I., Sjöberg, B.M., and Huang, C.Y. (1991) Carboxyl-terminal peptides as probes for *Escherichia-coli* ribonucleotide reductase subunit interaction-kinetic analysis of inhibition studies. *Biochemistry* 30, 5164-5171.
- (34) Climent, I., Sjöberg, B. M., and Huang, C. Y. (1992) Site-Directed Mutagenesis and Deletion of the Carboxyl Terminus of *Escherichia-Coli* Ribonucleotide Reductase Protein R2 - Effects on Catalytic Activity and Subunit Interaction. *Biochemistry* 31, 4801-4807.
- (35) Sjöberg, B. M., Karlsson, M., and Jornvall, H. (1987) Half-site reactivity of the tyrosyl radical of ribonucleotide reductase from *Escherichia-Coli*. *J. Biol. Chem.* 262, 9736-9743.
- (36) Fisher, A., Yang, F. D., Rubin, H., and Cooperman, B. S. (1993) R2 C-terminal peptide inhibition of mammalian and yeast ribonucleotide reductase. *J. Med. Chem.* 36, 3859-3862.
- (37) Fisher, A., Laub, P. B., and Cooperman, B. S. (1995) Nmr structure of an inhibitory R2 C-terminal peptide bound to mouse ribonucleotide reductase R1 subunit. *Nat. Struct. Biol.* 2, 951-955.
- (38) Gao, Y., Kashlan, O. B., Kaur, J., Tan, C., and Cooperman, B. S. (2005) Mechanisms of action of peptide inhibitors of mammalian ribonucleotide reductase targeting quaternary structure. *Biopolymers* 80, 9-17.

- (39) Nordlund, P., and Eklund, H. (1993) Structure and function of the *Escherichia coli* ribonucleotide reductase protein R2. *J. Mol. Biol.* 232, 123-164.
- (40) Seyedsayamdost, M., Xie, J., Chan, C.T., Schultz, P.G. and Stubbe J. (2007) Site-specific insertion of 3-aminotyrosine into subunit alpha2 of E. coli ribonucleotide reductase: direct evidence for involvement of Y730 and Y731 in radical propagation. *J. Am. Chem. Soc.* 129, 15060-15071.
- (41) Seyedsayamdost, M. R., and Stubbe, J. (2006) Site-specific replacement of Y-356 with 3,4-dihydroxyphenylalanine in the beta 2 subunit of E. coli ribonucleotide reductase. *J. Am. Chem. Soc.* 128, 2522-2523.
- (42) Seyedsayamdost, M., Yee, C.S., Reece, S.Y., Nocera, D.G., and Stubbe J. (2006) pH rate profiles of FnY356-R2s (n = 2, 3, 4) in *Escherichia coli* ribonucleotide reductase: evidence that Y356 is a redox-active amino acid along the radical propagation pathway. *J. Am. Chem. Soc.* 128, 1562-1568.
- (43) Stubbe, J., Nocera, D. G., Yee, C. S., and Chang, M. C. Y. . (2003) Radical initiation in the class I ribonucleotide reductase: long-range proton-coupled electron transfer? *Chem. Rev.* 103, 2167-2201.
- (44) Uhlin, U., Eklund, H. (1994) Structure of ribonucleotide reductase protein R1. *Nature* 370, 533-539.
- (45) Seyedsayamdost, M., and Stubbe J. (2007) Forward and reverse electron transfer with the Y356DOPA-beta2 heterodimer of E. coli ribonucleotide reductase. *J. Am. Chem. Soc.* 129, 2226-2227.
- (46) Ge, J., Yu, G. X., Ator, M.A., and Stubbe, J. (2003) Pre-steady-state and steady-state kinetic analysis of E-coli class I ribonucleotide reductase. *Biochemistry* 42, 10071-10083.
- (47) Bennati, M., Robblee, J. H., Mugnaini, V., Stubbe, J., Freed, J. H., and Borbat, P. (2005) EPR distance measurements support a model for long-range radical initiation in E. coli ribonucleotide reductase. *J. Am. Chem. Soc.* 127, 15014-15015.
- (48) Seyedsayamdost, M., Chan, C. T.Y., Mugnaini, V., Stubbe J., & Bennati, M. (2007) PELDOR spectroscopy with DOPA-β2 and NH2Y-α2s: distance measurements between residues involved in the radical propagation pathway of E. coli ribonucleotide reductase. *J. Am. Chem. Soc.* 129, 15748-15749.
- (49) Zlateva, T., Quaroni, L., Que, L., & Stankovich, M. T. (2004) Here, conformational changes in the E. coli RNR complex were investigated by measuring the reduction potential of Y122. in the presence of different substrates and effectors. *J. Biol. Chem.* 279, 18742-18747.
- (50) Licht, S., Stubbe, J. (1999) *Comprehensive Natural Products Chemistry*, Vol. 5, Elsevier.
- (51) Licht, S., Gerfen, G. J., and Stubbe, J. (1996) Thiyl radicals in ribonucleotide reductases. *Science* 271, 477-481.
- (52) Ator, M. A., and Stubbe, J. (1985) Mechanism of Inactivation of *Escherichia-Coli* Ribonucleotide Reductase by 2'-Chloro-2'-Deoxyuridine 5'-Diphosphate - Evidence for Generation of a 2'-Deoxy-3'-Ketonucleotide Via a Net 1,2 Hydrogen Shift. *Biochemistry* 24, 7214-7221.
- (53) Mao, S. S., Johnston, M. I., Bollinger, J. M., and Stubbe, J. (1989) Mechanism-based inhibition of a mutant *escherichia-coli* ribonucleotide reductase (cysteine-225-serine) by its substrate CDP. *Proc. Natl. Acad. Sci. U.S.A.* 86, 1485-1489.

- (54) Stubbe, J., Ackles, D., Segal, R., and Blakley, R. L. (1981) On the mechanism of ribonucleoside triphosphate reductase from lactobacillus-leichmannii-evidence for 3' C-H bond-cleavage. *J. Biol. Chem.* 256, 4843-4846.
- (55) Mao, S. S., Holler, T. P., Yu, G. X., Bollinger, J. M., Booker, S., Johnston, M. I., and Stubbe, J. (1992) A Model for the role of multiple cysteine residues involved in ribonucleotide reduction - amazing and still confusing. *Biochemistry* 31, 9733-9743.
- (56) Lin, A. N. I., Ashley, G. W., and Stubbe, J. (1987) Location of the redox-active thiols of ribonucleotide reductase - sequence similarity between the escherichia-coli and lactobacillus-leichmannii enzymes. *Biochemistry* 26, 6905-6909.
- (57) Thelander, L. (1974) Reaction-Mechanism of Ribonucleoside Diphosphate Reductase from Escherichia-Coli - Oxidation-Reduction Active Disulfides in B1 Subunit. *Journal of Biological Chemistry* 249, 4858-4862.
- (58) Gon, S., Faulkner, M.J., and Beckwith J. (2006) In vivo requirement for glutaredoxins and thioredoxins in the reduction of the ribonucleotide reductases of Escherichia coli. *Antioxid Redox Signal* 8, 735-742.
- (59) Thelander, L., and Larsson, B. (1976) Active-Site of Ribonucleoside Diphosphate Reductase from Escherichia-Coli - Inactivation of Enzyme by 2'-Substituted Ribonucleoside Diphosphates. *Journal of Biological Chemistry* 251, 1398-1405.
- (60) Stubbe, J., and Kozarich, J. W. (1980) Inorganic pyrophosphate is released from 2'-chloro-2'-deoxyuridine 5'-diphosphate by ribonucleoside diphosphate reductase. *J. Am. Chem. Soc.* 102, 2505-2507.
- (61) Stubbe, J., and Kozarich, J. W. (1980) Fluoride, pyrophosphate, and base release from 2'-deoxy-2'-fluoronucleoside 5'-diphosphates by ribonucleoside-diphosphate reductase. *J. Biol. Chem.* 255, 5511-5513.
- (62) Stubbe, J., Kozarich, J.W. (1980) Fluoride, pyrophosphate, and base release from 2'-deoxy-2'-fluoronucleoside-diphosphate reductase. *J. Biol. Chem.* 255, 5511-5513.
- (63) Harris, G., Ashley, G. W., Robins, M. J., Tolman, R. L., and Stubbe, J. (1987) 2'-Deoxy-2'-Halonucleotides as Alternate Substrates and Mechanism-Based Inactivators of Lactobacillus-Leichmannii Ribonucleotide Reductase. *Biochemistry* 26, 1895-1902.
- (64) Harris, G., Ator, M., and Stubbe, J. (1984) Mechanism of inactivation of *Escherichia coli* and *Lactobacillus leichmannii* ribonucleotide reductases by 2'-chloro-2'-deoxynucleotides: evidence for generation of 2-methylene-3(2H)-furanone. *Biochemistry* 23, 5214-5225.
- (65) Brown, N. C., Reichard, P. (1969) Role of Effector Binding in Allosteric Control of Ribonucleoside Diphosphate Reductase. *J. Mol. Biol.* 46, 39-55.
- (66) Reichard, P., Eliasson, R., Ingemarson, R., and Thelander, L. (2000) Cross-talk between the allosteric effector-binding sites in mouse ribonucleotide reductase. *J. Biol. Chem.* 275, 33021-33026.
- (67) Reichard, P. (2002) Ribonucleotide reductases: The evolution of allosteric regulation. *Arch. Biochem. Biophys.* 397, 149-155.
- (68) Yagle, K., and McEntee, K. (1990) The DNA damage-inducible Gene-Din1 of *Saccharomyces-cerevisiae* encodes a regulatory subunit of ribonucleotide reductase and is identical to Rnr3. *Mol. Cell. Biol.* 10, 5553-5557.

- (69) Elledge, S. J., and Davis, R.W. (1990) Two genes differentially regulated in the cell-cycle and by DNA-damaging agents encode alternative regulatory subunits of ribonucleotide reductase. *Genes Dev* 4, 740-751.
- (70) Elledge, S. J., and Davis, R.W. (1987) Identification and isolation of the gene encoding the small subunit of ribonucleotide reductase from *Saccharomyces cerevisiae*-DNA damage-inducible gene required for mitotic viability. *Mol. Cell. Biol.* 7, 2783-2793.
- (71) Huang, M. X., and Elledge, S. J. (1997) Identification of RNR4, encoding a second essential small subunit of ribonucleotide reductase in *Saccharomyces cerevisiae*. *Mol. Cell. Biol.* 17, 6105-6113.
- (72) Wang, P. J., Chabes, A., Casagrande, R., Tian, X. C., Thelander, L., and Huffaker, T. C. (1997) Rnr4p, a novel ribonucleotide reductase small-subunit protein. *Mol. Cell. Biol.* 17, 6114-6121.
- (73) Perlstein, D. L., Ge, J., Ortigosa, A. D., Robblee, J. H., Zhang, Z., Huang, M., and Stubbe, J. (2005) The active form of the *S. cerevisiae* ribonucleotide reductase small subunit is a heterodimer in vitro and in vivo. *Biochemistry* 44, 15366-15377.
- (74) Chabes, A., Domkin, V., Larsson, G., Liu, A. M., Graslund, A., Wijmenga, S., and Thelander, L. (2000) Yeast ribonucleotide reductase has a heterodimeric iron-radical-containing subunit. *Proc. Natl. Acad. Sci. U.S.A.* 97, 2474-2479.
- (75) Xu H, F., C., Uchiki, T., Racca, J., & Dealwis, C. (2006) Structures of eukaryotic ribonucleotide reductase I define gemcitabine diphosphate binding and subunit assembly. *Proc. Natl. Acad. Sci. U.S.A.* 103, 4028-4033.
- (76) Ortigosa, A. D., Hristova, D., Perlstein, D. L., Zhang, Z., Huang, M. X., and Stubbe, J. (2006) Determination of the in vivo stoichiometry of tyrosyl radical per beta beta ' in *Saccharomyces cerevisiae* ribonucleotide reductase. *Biochemistry* 45, 12282-12294.
- (77) Sjöberg, B. M., and Sahlin, M. (2002) Thiols in redox mechanism of ribonucleotide reductase. *Methods in Enzymology* 348, 1-21.
- (78) Aberg, A., Hahne, S., Karlsson, M., Larsson, A., Ormo, M., Ahgren, A., and Sjoberg, B.M. (1989) *J. Biol. Chem.* 264, 12249-12252.
- (79) Zhang, Z., Yang, K., Chen, C., Feser, J., and Huang, M. (2007) Role of the C terminus of the ribonucleotide reductase large subunit in enzyme regeneration and its inhibition by Sml1. *Proc. Natl. Acad. Sci. U.S.A.* 104, 2217-2222.
- (80) Chabes, A., Georgieva, B., Domkin, V., Zhao, X, Rothstein, R., and Thelander, L.,. (2003) Survival of DNA damage in yeast directly depends on increased dNTP levels allowed by relaxed feedback inhibition of ribonucleotide reductase. *Cell* 112, 391-401.
- (81) Huang, M., Zhou, Z., and Elledge, S.J. (1998) The DNA replication and damage checkpoint pathways induce transcription by inhibition of the Crt1 repressor. *Cell* 94, 595-605.
- (82) Zhou, Z., and Elledge, S.J. (1992) Isolation of *crt* mutants constitutive for transcription of the DNA damage inducible gene *rnr2* in *Saccharomyces cerevisiae*. *Genetics* 131, 851-866.
- (83) Lee, Y., and Elledge, S.J. (2006) Control of ribonucleotide reductase localization through an anchoring mechanism involving Wtm1. *Genes Dev* 20, 334-344.

- (84) Liu, C., Powell, K.A., Mundt, K., Wu, L., Carr, A.M., and Caspari, T. (2003) Cop9/signalosome subunits and Pcu4 regulate ribonucleotide reductase by both checkpoint-dependent and -independent mechanisms. *Genes Dev* 17, 1130-1140.
- (85) Liu, X. Y., Zhou, B. S., Xue, L. J., Shih, J., Tye, K., Qi, C., and Yen, Y. (2005) The ribonucleotide reductase subunit M2B subcellular localization and functional importance for DNA replication in physiological growth of KB cells. *BIOCHEMICAL PHARMACOLOGY* 70, 1288-1297.
- (86) Yao, R. J., Zhang, Z., An, X. X., Bucci, B., Perlstein, D. L., Stubbe, J., and Huang, M. X. (2003) Subcellular localization of yeast ribonucleotide reductase regulated by the DNA replication and damage checkpoint pathways. *PNAS* 100, 6628-6633.
- (87) Zhao, X., Georgieva, B., Chabes, A., Domkin, V., Ippel, J. H., Schleucher, J., Wijmenga, S., Thelander, L., and Rothstein, R. (2000) Mutational and structural analyses of the ribonucleotide reductase inhibitor Sml1 define its Rnr1 interaction domain whose inactivation allows suppression of mec1 and rad53 lethality. *Mol. Cell. Biol.* 20, 9076-9083.
- (88) Zhao, X., Chabes, A., Domkin, V., Thelander, L., and Rothstein, R. (2001) The ribonucleotide reductase inhibitor Sml1 is a new target of the Mec1/Rad53 kinase cascade during growth and in response to DNA damage. *EMBO J* 20, 3544-3553.
- (89) Georgieva, B., Zhao, X., and Rothstein, R. (2000) Damage response and dNTP regulation: the interaction between ribonucleotide reductase and its inhibitor, Sml1. *Cold Spring Harb Symp Quant Biol.* 65, 343-346.
- (90) Chabes, A., V. Domkin and Thelander, L.,. (1999) Yeast Sml1, a protein inhibitor of ribonucleotide reductase. *J. Biol. Chem.* 274, 36679-36683.
- (91) Sanchez, Y., Desany, B.A., Jones, W.J., Liu, Q., Wang, B., and Elledge, S.J. (1996) Regulation of RAD53 by the ATM-like kinase MEC1 and TEL1 in yeast cell cycle checkpoint pathways. *Science* 271, 357-360.
- (92) Sun, Z., Fay, D.S., Marini, F., and Stern, D.F. (1996) Spk1/Rad53 is regulated by Mec1-dependent protein phosphorylation in DNA replication and damage checkpoint. *Genes Dev* 10, 395-406.
- (93) Zhou, Z., and Elledge, S.J. (1993) DUN1 encodes a protein kinase that controls the DNA damage response in yeast. *Cell* 75, 1119-1127.
- (94) Domkin, V., Thelander, L., and Chabes, A. (2002) Yeast DNA damage-inducible Rnr3 has a very low catalytic activity strongly stimulated after the formation of a cross-talking Rnr1/Rnr3 complex. *J. Biol. Chem.* 277, 18574-18578.
- (95) Eriksson, S., Thelander, L., and Akerman, M. (1979) Allosteric regulation of calf thymus ribonucleoside diphosphate reductase. *Biochemistry* 18, 2948-2952.
- (96) Zhao, X., and Rothstein, R. (2002) The Dun1 checkpoint kinase phosphorylates and regulates the ribonucleotide reductase inhibitor Sml1. *Proc. Natl. Acad. Sci. U.S.A.* 99, 3746-3751.
- (97) McIntosh, E. M. (1993) Mcb elements and the regulation of DNA-replication genes in yeast. *Curr. Genet.* 24, 185-192.
- (98) McIntosh, E. M., Atkinson, T., Storms, R. K., and Smith, M. (1991) Characterization of a short, cis-acting DNA-sequence which conveys cell-cycle stage-dependent transcription in *Saccharomyces-cerevisiae*. *Mol. Cell. Biol.* 11, 329-337.

- (99) Primig, M., Sockanathan, S., Auer, H., and Nasmyth, K. (1992) Anatomy of a transcription factor important for the start of the cell-cycle in *Saccharomyces cerevisiae*. *Nature* 358, 593-597.
- (100) Elledge, S. J., Zhou, Z., Allen, J. B., and Navas, T. A. . (1993) DNA-damage and cell-cycle regulation of ribonucleotide reductase. *BioEssays* 15, 333-339.
- (101) Gasch, A. P., Huang, M. X., Metzner, S., Botstein, D., Elledge, S. J., and Brown, P. O. (2001) Genomic expression responses to DNA-damaging agents and the regulatory role of the yeast ATR homolog Mec1p. *Mol. Cell. Biol.* 21, 2987-3003.
- (102) Desany, B. A., Alcasabas, A. A., Bachant, J. B., and Elledge, S. J. (1998) Recovery from DNA replicational stress is the essential function of the S-phase checkpoint pathway. *Genes Dev* 12, 2956-2970.
- (103) Zaim, J., Speina, E., and Kierzek, AM., . (2005) Identification of new genes regulated by the Crt1 transcription factor, an effector of the DNA damage checkpoint pathway in *Saccharomyces cerevisiae*. *J. Biol. Chem.* 280, 28-37.
- (104) Zhang, A., An, X., Yang, K., Perlstein, DL., Hicks, L., et al. (2006) Nuclear localization of the *saccharomyces cerevisiae* ribonucleotide reductase small subunit requires a kayopherin and a WD40 repeat protein. *Proc. Natl. Acad. Sci. U.S.A.* 103, 1422-1427.
- (105) Lee, Y., Wang, J., Stubbe, J., and Elledge, SJ. (2008) Dif1 is a DNA-damage-regulated facilitator of nuclear import for ribonucleotide reductase. *Mol. Cell.* 32, 70-80.
- (106) Lee, Y., Wang, J., Stubbe, J., and Elledge, SJ. (2008) Dif1 is a DNA-damage-regulated facilitator of nuclear import for ribonucleotide reductase. *Mol Cell* 32, 70-80.
- (107) Zhao, X., Chabes, A., Domkin, V., Thealander, L., and Rothstein, R. (2001) The ribonucleotide reductase inhibitor Sml1 is a new target of the Mec1/Rad53 kinase cascade during growth and in response to DNA damage. *EMBO J.* 20, 3544-3553.
- (108) Zhao, X., Muller, E. G. and Rothstein, R. . (1998) A suppressor of two essential checkpoint genes identifies a novel protein that negatively affects dNTP pools. *Mol. Cell.* 2, 329-340.
- (109) Gupta, V., Peterson, C. B., Dice, L. T., Uchiki, T., Racca, J., Guo, J. T., Ying, X., Hettich, R., Zhao, X. L., Rothstein, R., and Dealwis, C. G. (2004) Sml1 1p is a dimer in solution: Characterization of denaturation and of recombinant Sml1 1p. *Biochemistry* 43, 8568-8578.
- (110) Zhang, Z., Yang, K., Chen, C., Feser, J., and Huang, M. (2007) Role of the C terminus of the ribonucleotide reductase large subunit in enzyme regeneration and its inhibition by Sml1. *Proc. Natl. Acad. Sci. U S A.* 104, 2217-2222.
- (111) Woollard, A., Basi, G., and Nurse, P. (1996) A novel S phase inhibitor in fission yeast. *EMBO J.* 15, 4603-4612.
- (112) Borqne, A., and Nurse, P. (2000) The Spd1p S phase inhibitor can activate the DNA replication checkpoint pathway in fission yeast. *J. Cell. Sci.* 23, 4341-4350.
- (113) Hakansson, P., Dahl, L., Chilkova, O., Domkin, V., and Thelander, L.,. (2006) The schizosaccharomyces pombe replication inhibitor Spd1 regulates rebonucleotide reductase activity and dNTPs by binding to the large Cdc22 subunit. *J. Biol. Chem.* 281, 1778-1783.

- (114) Borgne, A., Nurse, P. (2000) The Spd1p S phase inhibitor can activate the DNA replication checkpoint pathway in fission yeast. *J. Cell Sci.* 113, 4341-4350.
- (115) Engström, Y., Eriksson, S., Thelander, L., and Akerman, M. (1979) Ribonucleotide reductase from calf thymus. Purification and properties. *Biochemistry* 18, 2941-2948.
- (116) Thelander, L., Graslund, A. and Thelander, M. (1983) Continual presence of oxygen and iron required for mammalian ribonucleotide reduction: possible regulation mechanism. *Biochem Biophys Res Commun* 110, 859-865.
- (117) Mann, G., Gräslund, A., Ochiai, E.-I., Ingemarson, R., and Thelander, L. (1991) Purification and characterization of recombinant mouse and herpes simplex virus ribonucleotide reductase R2 subunit. *Biochemistry* 30, 1939-1947.
- (118) Mann, G., Gräslund, A., Ochiai, E.-I., Ingemarson, R., and Thelander, L. (1991) Purification and characterization of recombinant mouse and herpes simplex virus ribonucleotide reductase R2 subunit. *Biochemistry* 30, 1939-1947.
- (119) Ingemarson, R., and Thelander, L. (1996) A kinetic study on the influence of nucleoside triphosphate effectors on subunit interaction in mouse ribonucleotide reductase. *Biochemistry* 35, 8603-8609.
- (120) Thelander, L. (1973) Physicochemical Characterization of Ribonucleoside Diphosphate Reductase from Escherichia-Coli. *Journal of Biological Chemistry* 248, 4591-4601.
- (121) Tanaka, H., Arakawa, H., Yamaguchi, T., Shiraishi, K., Fukuda, S., Matsui, K., Takei, Y. and Nakamura, Y. (2000) A ribonucleotide reductase gene involved in a p53-dependent cell-cycle checkpoint for DNA damage. *Nature* 404, 42-49.
- (122) el-Deiry, W. S., Kern, S.E., Pietenpol, J. A., Kinzler, K. W., and Vogelsterin, B., (1992) Definition of a consensus binding site for p53. *Nature Genet.* 1, 45-49.
- (123) Nakano, K., Balint, E., Ashcroft, M., and Vousden, K.H. (2000) A ribonucleotide reductase gene is a transcriptional target of p53 and p73. *Oncogene* 19, 4283-4289.
- (124) Pontarin, G., Fijolek, A., Pizzo, P., Ferraro, P., Rampazzo, C., Pozzan, T., Thelander, L., Reichard, P. A., and Bianchi, V. (2008) Ribonucleotide reduction is a cytosolic process in mammalian cells independently of DNA damage. *Proc. Natl. Acad. Sci. U.S.A.* 105, 17801-17806.
- (125) Yamaguchi, T., Matsuda, K., Saqiya, Y., Iwadate, M., Fujino, M. A., Nakamura, Y., Arakawa, H. (2001) p53R2-dependent pathway for DNA synthesis in a p53-regulated cell cycle checkpoint. *Cancer Res.* 61, 8256-8262.
- (126) Hakansson, P., Hofer, A., and Thelander, L., (2006) Regulation of mammalian ribonucleotide reduction and dNTP pools after DNA damage and in resting cells. *J. Biol. Chem.* 281, 7834-7841.
- (127) Bourdon, A., Minai, L., Serre, V., Jais, J., Sarzi, E., Aubert, S., Chretien, D., Lonlay, P., Paquis-fluckinger, V., Arakawa, H., Nakamura, Y., Munnich, A. and Rötig, A. (2007) Mutation of RRM2B, encoding p53-controlled ribonucleotide reductase (p53R2), causes severe mitochondrial DNA depletion. *Nat. Genet.* 39, 776-780.
- (128) Chang, L., Zhou, B., Hu, S., Guo, R., Liu, X., Jones, SN., and Yen, Y. (2008) ATM-mediated serine 72 phosphorylation stabilizes ribonucleotide reductase small subunit p53R2 protein against MDM2 to DNA damage. *Proc. Natl. Acad. Sci. U.S.A.* 105, 18519-18524.

- (129) Piao, C., Jin, M., Kim, H.B., Lee, S.M., Amatya, P.N., Hyun, J.W., Chang, I.Y., and You, H.J. (2009) Ribonucleotide reductase small subunit p53R2 suppresses MEK-ERK activity by binding to ERK kinase 2. *Oncogene* 28, 2173-2184.
- (130) Pontarin, G. e. a. (2007) p53R2-dependent ribonucleotide reduction provides deoxy-ribonucleotides in quiescent human fibroblasts in the absence of induced DNA damage. *J. Biol. Chem.* 282, 16820-16828.
- (131) Xue, L., Zhou, B., Liu, X., Heung, Y., Chau, J., Chu, E., Li, S., Jiang, C., Un, F., and Yen, Y.,. (2007) Ribonucleotide reductase small subunit p53R2 facilitates p21 induction of G1 arrest under UV irradiation. *Cancer Res.* 67, 16-21.
- (132) Scott, C. P., Kashlan, O. B., Lear, J. D., and Cooperman, B. S. (2001) A quantitative model for allosteric control of purine reduction by murine ribonucleotide reductase. *Biochemistry* 40, 1651-1661.
- (133) Kashlan, O. B., Scott, C. P., Lear, J. D., and Cooperman, B. S. (2002) A comprehensive model for the allosteric regulation of mammalian ribonucleotide reductase. Functional consequences of ATP- and dATP-induced oligomerization of the large subunit. *Biochemistry* 41, 462-474.
- (134) Cooperman, B. S., and Kashlan, O. B. (2003) A comprehensive model for the allosteric regulation of Class Ia ribonucleotide reductases, in *Advances in Enzyme Regulation, Vol 43* pp 167-182.
- (135) Rofougaran, R., Vodnala, M., and Hofer, A. (2006) Enzymatically active mammalian ribonucleotide reductase exists primarily as an alpha(6)beta(2) octamer. *Journal of Biological Chemistry* 281, 27705-27711.
- (136) Engström, Y., Eriksson, S., Jildevik, I., Skog, S., Thelander, L., and Tribukait, B. (1985) Cell cycle-dependent expression of mammalian ribonucleotide reductase. Differential regulation of the two subunits. *J. Biol. Chem.* 260, 9114-9116.
- (137) Johansson, E., Hjortsberg, K., and Thelander, L. (1998) Two YY-1-binding proximal elements regulate the promoter strength of the TATA-less mouse ribonucleotide reductase R1 gene. *J. Biol. Chem.* 273, 29816-29821.
- (138) Johansson, E., Skogman, E. and Thelander, L. (1995) The TATA-less promoter of mouse ribonucleotide reductase R1 gene contains a TFII-I binding initiator element essential for cell cycle-regulated transcription. *J. Biol. Chem.* 270, 30162-30167.
- (139) Chabes, A., Bjorklund, S. and Thelander, L. (2004) S phase-specific transcription of the mouse ribonucleotide reductase R2 gene requires both a proximal repressive E2F-binding site and an upstream promoter activating region. *J. Biol. Chem.* 279, 10796-10807.
- (140) Nardinocchi, L., Puca, R., Sacchi, A., and D'Orazi, G. (2007) HIPK2 knock-down compromises tumor cell efficiency to repair damaged DNA. *Biochem Biophys Res Commun* 361, 249-255.
- (141) Chabes, A., and Thelander, L. (2000) Controlled protein degradation regulates ribonucleotide reductase activity in proliferating mammalian cells during the normal cell cycle and in response to DNA damage and replication blocks. *J. Biol. Chem.* 275, 17747-17753.
- (142) Xue, L., Zhou, B., Liu, X., Qiu, W., Jin, Z., and Yen, Y.,. (2003) Wild-type p53 regulates human ribonucleotide reductase by protein-protein interaction with p53R2 as well as hRRM2 subunits. *Cancer Res.* 63, 980-986.

- (143) Engström, Y., and Rozell, B. (1988) Immunocytochemical evidence for the cytoplasmic localization and differential expression during the cell cycle of the M1 and M2 subunits of mammalian ribonucleotide reductase. *EMBO J.* 3, 863-867.
- (144) Wang, X., Zhenchuk, A., Wiman, KG., and Albertioni, F. . (2008) Regulation of p53R2 and its role as potential target for cancer therapy. *Cancer Lett.*
- (145) Chang, L., Zhou, B., Hu, S., Guo, R., Liu, X., Jones, S. N., and Yen, Y. (2008) ATM-mediated serine 72 phosphorylation stabilizes ribonucleotide reductase small subunit p53R2 protein against MDM2 to DNA damage. *Proc. Natl. Acad. Sci. U S A.* 105, 18519-18524.
- (146) Okumura, H., Natsugoe, S., Yokomakura, N., Kita, Y., Matsumoto, M., Uchikado, Y., Setoyama, T., Owaki, T., Ishigami, S., and Aikou, T. (2006) Expression of p53R2 is related to prognosis in patients with esophageal squamous cell carcinoma. *Clin. Cancer. Res.* 12, 3740-3745.
- (147) Plunkett, W., Huang, P., and Gandhi, V. (1997) Gemcitabine: actions and interactions. *Nucleosides & Nucleotides* 16, 1261-1270.
- (148) Silva, D. J., Stubbe, J., Samano, V., and Robins, M. J. (1998) Gemcitabine 5'-triphosphate is a stoichiometric mechanism-based inhibitor of *Lactobacillus leichmannii* ribonucleoside triphosphate reductase: Evidence for thiyl radical-mediated nucleotide radical formation. *Biochemistry* 37, 5528-5535.
- (149) van der Donk, W. A., Yu, G. X., Perez, L., Sanchez, R. J., Stubbe, J., Samano, V., and Robins, M. J. (1998) Detection of a new substrate-derived radical during inactivation of ribonucleotide reductase from *Escherichia coli* by gemcitabine 5'-diphosphate. *Biochemistry* 37, 6419-6426.
- (150) van der Donk, W. A., Yu, G., Silva, D. J., and Stubbe, J. (1996) Inactivation of ribonucleotide reductase by (E)-2'-fluoromethylene-2'-deoxycytidine 5'-diphosphate: a paradigm for nucleotide mechanism based inhibitors. *Biochemistry* 35, 8381-8391.
- (151) van der Donk, W. A., Gerfen, G. G., and Stubbe, J. (1998) Direct EPR spectroscopic evidence for an allylic radical generated from (E)-2'-fluoromethylene-2'-deoxycytidine 5'-diphosphate by *E. coli* ribonucleotide reductase. *J. Am. Chem. Soc.* 120, 4252-4253.
- (152) Kanazawa, J., Takahashi, T., Akinaga, S., Tamaoki, T., and Okabe, M. (1998) The relationship between the antitumor activity and the ribonucleotide reductase inhibitory activity of (E)-2'-deoxy-2'-(fluoromethylene) cytidine. *Anti-Cancer Drugs* 9, 653-657.
- (153) Finch, R. A., Liu, M. C., Cory, A. H., Cory, J. G., and Sartorelli, A. C.,. (1999) Triapine (3-aminopyridine-2-carboxaldehyde thiosemicarbazone; 3-AP): an inhibitor of ribonucleotide reductase with antineoplastic activity. *Adv. Enzyme Regul.* 39, 3-12.
- (154) Finch, R. A., Liu, M. C., Grill, S. P., Rose, W. C., Loomis, R., Vasquez, K. M., Cheng, Y. C., and Sartorelli, A. C.,. (2000) Triapine (3-aminopyridine-2-carboxaldehydethiosemicarbazone): a potent inhibitor of ribonucleotide reductase activity with broad spectrum antitumor activity. *Biochem. Pharmacol.* 59, 983-991.
- (155) Mayhew, C. N., Sumpter, R., Inayat, M., Cibull, M., Phillips, J. D., Elford, H. L., and Gallicchio, V. S. (2005) Combination of inhibitors of lymphocyte activation

- (hydroxyurea, trimidox, and didox) and reverse transcriptase (didanosine) suppresses development of murine retrovirus-induced lymphoproliferative disease. *Antiviral Res.* 65, 13-22.
- (156) Sumpter, L. R., Inayat, M. S., Yost, E. E., Duvall, W., Hagan, E., Mayhew, C. N., Elford, H. L., and Gallicchio, V. S. (2004) In vivo examination of hydroxyurea and the novel ribonucleotide reductase inhibitors trimidox and didox in combination with the reverse transcriptase inhibitor abacavir: suppression of retrovirus-induced immunodeficiency disease. *Antiviral Res.* 62, 111-120.
- (157) Hendricks, S. P., and Mathews, C. K. (1998) Differential effects of hydroxyurea upon deoxyribonucleoside triphosphate pools, analyzed with vaccinia virus ribonucleotide reductase. *J. Biol. Chem.* 273, 29519-29523.
- (158) Gwilt, P. R., and Tracewell, W. G. (1998) Pharmacokinetics and pharmacodynamics of hydroxyurea. *Clin. Pharmacokinet.* 34, 347-358.
- (159) Huang, P., Chubb, S., Hertel, L. W., Grindey, G. B., and Plunkett, W. (1991) Action of 2',2'-difluorodeoxycytidine on DNA-synthesis. *Cancer res.* 51, 6110-6117.
- (160) Davidson, J. D., Ma, L. D., Flagella, M., Geeganage, S., Gelbert, L. M., and Slapak, C. A. (2004) An increase in the expression of ribonucleotide reductase large subunit 1 is associated with gemcitabine resistance in non-small cell lung cancer cell lines. *Cancer research* 64, 3761-3766.
- (161) Duxbury, M., Ito, H., Zinner, MJ., Ashley, SW., and Whang, EE. (2004) RNA interference targeting the M2 subunit of ribonucleotide reductase enhances pancreatic adenocarcinoma chemosensitivity to gemcitabine. *Oncogene* 23, 1539-1548.
- (162) Barlesi, F., Jacot, W., Astoul, P., and Pujol, J.-L. (2006) Second-line treatment for advanced non-small cell lung cancer: a systematic review. *Lung Cancer* 51, 159-172.
- (163) Rosti, G. (2006) Small cell lung cancer. *Annal. Oncol.* 17, 5-10.
- (164) Sebastiani, V., Ricci, F., Rubio-Viquiera, B., Kulesza, P., Yeo, C. J., Hidalgo, M., Klein, A., Laheru, D., and Lacobuzio-Donahue, C. A. (2006) Immunohistochemical and genetic evaluation of deoxycytidine kinase in pancreatic cancer: relationship to molecular mechanisms of gemcitabine resistance and survival. *Clin. Cancer Res.* 12, 2492-2497.
- (165) Shore, S., Raraty, M. G. T., Ghaneh, P., and Neoptolemos, J. P. (2003) Chemotherapy for pancreatic cancer. *Aliment Pharmacol. Ther.* 18, 1049-1069.
- (166) Akerele, C. E., Rybalova, I., Kaufman, H. L., and Mani, S. (2003) Current approaches to novel therapeutics in pancreatic cancer. *Invest. New Drugs* 21, 113-129.
- (167) Juffs, H. G., Moore, M. J., and Tannock, I. F. (2002) The role of systemic chemotherapy in the management of muscle-invasive bladder cancer. *Lancet Oncol.* 3, 738-747.
- (168) Witjes, J. A., Vriesema, J. L. J., van der Heijden, A. G., Peters, G. J., and Schalken, J. A. (2003) Pharmacokinetics of intravesical gemcitabine: a preclinical study in pigs. *Eur. Urol.* 44, 615-619.
- (169) Barniaas, A. (2006) Systemic chemotherapy in inoperable or metastatic bladder cancer. *Annal. Oncol.* 17, 553-561.

- (170) Colomer, R. (2005) Gemcitabine plus taxane combination in metastatic breast cancer: a comprehensive review. *EJC Suppl.* 3, 9-16.
- (171) Oettle, H., Post, S., Neuhaus, P., et al. (2007) Adjuvant chemotherapy with gemcitabine vs observation in patients undergoing curative-intent resection of pancreatic cancer. *JAMA* 297, 266-277.
- (172) Ueno, H., Kosuge, T. (2008) Adjuvant treatments for resectable pancreatic cancer. *J Hepatobiliary Pancreat Surg.* 15, 468-472.
- (173) Spratlin, J., Sangha, R., Glubrecht, D., Dabbagh, L., Young, J. D., Dumontet, C., Cass, C., Lai, R., and Mackey, J. R. (2004) The absence of human equilibrative nucleoside transporter 1 is associated with reduced survival in patients with gemcitabine-treated pancreas adenocarcinoma. *Clin. Cancer Res.* 10, 6956-6961.
- (174) Giovannetti, E., Mey, V., Loni, L., Nannizzi, S., Barsanti, G., Savarino, G., Ricciardi, S., Tacca, M. D., and Danesi, R. (2007) Cytotoxic activity of gemcitabine and correlation with expression profile of drug-related genes in human lymphoid cells. *Pharmacological research* 55, 343-349.
- (175) Richel, D., Colly, LP., Arkesteijn, GJ., Arentsen-Honders, MW., Kerster, MG., ter Riet, PM., et al. (1990) Substrate-specific deoxycytidine kinase deficiency in 1-beta-D-arabinofuranosylcytosine-resistant leukemic cells. *Cancer Res.* 50, 6515-6519.
- (176) Bergman, A., Pinedo, HM., Jongsma, AP., Brouwer, M., Ruiz van Haperen, VW., Veerman, G., et al. (1999) Decreased resistance to gemcitabine (2', 2'-difluorodeoxycytidine) of cytosine arabinoside-resistant myeloblastic murine and rat leukemia cell line: role of altered activity and substrate specificity of deoxycytidine kinase. *Biochem Pharmacol* 57, 397-406.
- (177) Dumontet, C., Fabianowska-Majewska, K., Mantincic, D., Callet, Bauchu, E., Tigaud, I., Gandhi, V., et al. (1999) Common resistance mechanisms to deoxynucleosid analogues in variants of the human erythroleukaemic line K562. *Br J Haematol* 106, 78-85.
- (178) Mansson, E., Spasokoukotskaja, T., Sallstrom, J., Eriksson, S., Albertioni, F. (1999) Molecular and biochemical mechanisms of fludarabine and cladribine resistance in a human promyelocytic cell line. *Cancer Res.* 59, 5956-5963.
- (179) Bergman, A., Pinedo, HM., Peters, GJ. (2002) Determinants of resistance to 2', 2'-difluorodeoxycytidine (gemcitabine). *Drug Resist Updat* 5, 19-33.
- (180) Mnsso, E., Flordal, E., Liliemark, J., Spasokoukotskaja, T., Elford, H., Lagercrantz S., et al. (2003) Down-regulation of deoxycytidine kinase in human leukemic cell lines resistant to cladribine and clofarabine and increased ribonucleotide reductase activity contributes to fludarabine resistance. *Biochem Pharmacol* 65, 237-247.
- (181) Heinemann, V., Xu, Y., Chubb, S., Sen, A., Hertel, L. W., Grindey, G. B., and Plunkett, W. (1992) Cellular elimination of 2',2'-difluorodeoxycytidine 5'-triphosphate: a mechanism of self-potential. *Cancer Res.* 52, 533-539.
- (182) Galmarini, C., Graham, K., Thomas, X., Calvo, F., Rousselot, P., El Jafaari, A., et al. (1998) Expression of high Km 5'-nucleotidase in leukemic blasts is an independent prognostic factor in adults with acute myeloid leukaemia. *Blood* 44, 1922-1926.

- (183) Wang, J., Lohman, G.J., and Stubbe, J. (2007) Enhanced subunit interactions with gemcitabine-5'-diphosphate inhibit ribonucleotide reductases. *Proc. Natl. Acad. Sci. U.S.A.* 104, 14324-14329.
- (184) Baker, C. H., Banzon, J., Bollinger, J. M., Stubbe, J., Samano, V., Robins, M. J., Lippert, B., Jarvi, E., and Resvick, R. (1991) 2'-deoxy-2'-methylencytidine and 2'-deoxy-2',2'-difluorocytidine 5'-diphosphates - potent mechanism-based inhibitors of ribonucleotide reductase. *J. Med. Chem.* 34, 1879-1884.
- (185) Artin, E., Wang, J., Lohman, G., Yu, G., Griffin, G., Barr, G., and Stubbe, J. (2009) Insight into the mechanism of inactivation of ribonucleotide reductase by Gemcitabine 5'-diphosphate in the presence and absence of reductant. *manuscript submitted*.
- (186) Cerqueira, N. M. F. S. A., Fernandes, P. A., and Ramos, M. J. (2007) Understanding ribonucleotide reductase inactivation by gemcitabine. *Chem. Eur. J.* 13, 8507-8515.
- (187) Pereira, S., Fernandes, P. A., and Ramos, M. J. (2004) Mechanism for ribonucleotide reductase inactivation by the anticancer drug gemcitabine. *J. Comput. Chem.*, 1286-1294.
- (188) Xu H, F., C., Uchiki, T., Fairman, J.W., Racca, J., and Dealwis, C. (2006) Structures of eukaryotic ribonucleotide reductase I provide insights into dNTP regulation. *Proc. Natl. Acad. Sci. U S A.* 103, 4022-4027.
- (189) Koc, A., Wheeler, L. J., Mathews, C. K., and Merrill, G. F., . (2004) Hydroxyurea arrests DNA replication by a mechanism that preserves basal dNTP pools. *J. Biol. Chem.* 279, 223-230.
- (190) Lassmann, G., Thelander, L., Graslund, A. (1992) EPR stopped-flow studies of the reaction of the tyrosyl radical of protein R2 from ribonucleotide reductase with hydroxyurea. *Biochem Biophys Res Commun* 188, 879-887.
- (191) S. Nyholm, L. T., a. Graeslund. (1993) Reduction and loss of the iron center in the reaction of the small subunit of mouse ribonucleotide reductase with hydroxyurea. *Biochemistry* 32, 11569-11574.
- (192) Karlsson, M., Sahlin, M., and Sjöberg, B-M. (1992) *Escherichia coli* ribonucleotide reductase: radical susceptibility to hydroxyurea is dependent on the regulatory state of the enzyme. *J. Biol. Chem.* 267, 12622-12626.

Chapter 2

Characterization of Human Ribonucleotide Reductase

2.1 Introduction

Ribonucleotide reductases (RNRs) catalyze the reduction of all four ribonucleotides to the corresponding deoxyribonucleotides and consequently are essential in DNA biosynthesis and repair. Human RNR (hRNR), a class Ia enzyme, is composed of one large subunit H1 (α) and two small subunits, H2 (β) and p53R2 (β'), which share 80% sequence identity (1). As with other class Ia enzymes, β contains a diferric-tyrosyl radical ($Y\bullet$) cluster, which is essential for catalysis. Current evidence suggests that there is one $Y\bullet$ and 2 diferric clusters/ β 2 (2, 3). α contains the active site and effector binding sites that control substrate specificity and turnover rate (4-7). The quaternary structure of human α has yet to be investigated, but based on analogy with mouse RNR (90% homolog), it can be a monomer, dimer, tetramer or hexamer depending on the type of nucleotide present (8, 9).

In mammalian cells, RNR is regulated at the level of allosteric regulation(10), transcription during S-phase or DNA repair (11), proteolysis of β in late mitosis (12), and subunit localization. Transcription of α and β genes are exclusively cell cycle dependent, reaching their maximum levels during S-phase (13, 14). However, the half-life of α is about 15 h, so its levels remain constant throughout the cell cycle (14). β has a short half life of only 3 h, and is degraded during G_0/G_1 phases, thus RNR activity in the S phase is controlled by the expression and degradation of β . In the G_0/G_1 phase active RNR is required for mitochondrial DNA replication and DNA repair. Because β is degraded during these phases, β' must be capable of forming a complex with α to generate active RNR.

Both human β (h β) and β' (h β') contain the essential Y• and the diferric cluster, as well as the conserved PCET pathway residues D265/D227, W102/W64, Y369/Y332 (*E. coli* D237, W48, Y356 equivalents) (Table 2.1). The major sequence differences between β and β' are in their N-termini. β' lacks 33 N-terminal amino acids which correspond to a KEN box in β , the site for polyubiquitination when β is targeted for degradation during the G₀/G₁ phase. Because β' lacks this domain, its levels remain constant throughout the cell cycle (15, 16).

The function of β' is not well understood. Recent studies (17) suggest that β' is localized to the cytosol and is not transported to the nucleus as previously thought (1, 18). The authors proposed that β' plays a primary role in mitochondrial DNA replication. Another report has suggested that β' can be phosphorylated directly by the kinase ATM, and that phosphorylated β' has been detected in the MRE11 complex involved in DNA double strand break repair (19). β' has also been proposed to have catalase activity to protect the mitochondrial membrane from oxidative stress, an activity that has not been attributed to β (20). β' shows less susceptibility to hydroxyurea and more susceptibility to the iron chelator deferoxamine mesylate compared to β , but both of the β' and β are inhibited with similar potency by Triapine (20, 21).

Table 2.1: Conserved key residues in PCET pathway of *E. coli*, mouse and human small subunits.

	<i>E. coli</i> β	Mouse β	Mouse β'	Human β	Human β'
In PCET pathway	Y122	Y177	Y138	Y176	Y138
	W48	W103	W64	W102	W64
	D237	D266	D227	D265	D227
	Y356	Y370	Y332	Y369	Y332
Iron ligands	D84	D139	D100	D138	D100
	E115	E170	E131	E169	E131
	H118	H173	H134	H172	H134
	E204	E233	E194	E232	E194
	E238	E267	E228	E266	E228
	H241	H270	H231	H269	H231

The prototype for the class Ia RNR is the *E. coli* enzyme. The human small subunit β is 90% identical to mouse β , but only 27% homologous to *E. coli* β . Despite the low sequence homology, the overall structure of mouse and human β are very similar to that of *E. coli* β , with a root mean squared deviation of only 1.6 Å for 262 C $^{\alpha}$ atoms (22). All of the key residues in the PCET pathway and the iron ligands are conserved (Table 2.1), and the major differences is that the mammalian β and β' lack the β -hairpins on the tip of the heart shape structure of *E. coli* β . In both the mouse and *E. coli* β , the essential Y• is closely coupled with the iron cluster, with the former displaying a stronger magnetic interaction (23). In addition, the X-ray structures reveal that a 15 Å wide, 10 Å long

hydrophobic channel connects the surface of the protein to a proposed oxygen binding site near Y177• in the mouse β , making the radical diiron center more accessible to the solvent (22). Furthermore, the mouse β and *E. coli* β have different reduction properties: the Y• and iron center of mouse β can be reduced simultaneously, whereas in the *E. coli* β , the Y• is reduced before the iron center (24, 25).

The cloning, expression and purification of human α , β , and β' have been reported by the Thelander and Yen groups (16, 21). Yen's group reported 1.2 Y•/ β 2 and 0.8 Y•/ β' 2 based on EPR experiments at 20 K for the His-tagged proteins. However, their constructs of β and β' contain long (24 amino acid) linker regions between the His-tag and the start of the protein. In these studies, the protein concentration was determined by Bradford assay, which might account for the difference in the quantitation of Y• content, compared to the method using extinction coefficients. In addition, Yen's lab reported activities of 75 nmol/min/mg and 52 nmol/min/mg for h β and h β' respectively (21). Thelander's lab reported values of 158 and 95 nmol/min/mg for the activities of non-tagged h β and h β' , and 140, and 60 nmol/min/mg for mouse β and β' respectively (16). Mouse β isolated by Thelander's lab contains 0.8 Y• per β 2 (26). The radical content of mouse and human β' has not been reported by Thelander's lab.

Furthermore, from site-directed mutagenesis and EPR studies, Yen's group proposed that an additional tyrosine residue, Y162 in h β and Y124 in h β' , is essential for radical formation and enzymatic activity. The evidence for their dityrosyl-diiron cluster model in β' was that both the Y124F- β' and Y138F- β' (Y122 equivalent) were EPR silent, suggesting that both Y124 and Y138 are essential to β' . The evidence for a dityrosyl center in β is contradictory to that of β' . Both the Y162F- β and Y176F- β (Y122

equivalent) still contains radicals and were active, only the double mutants Y176F Y162F- β lost all activity (27). Therefore, they proposed that human β and β' contain a unique dityrosyl-diiron center.

Here we report that using the *in vitro* reconstitution methods developed in the Stubbe group, 1.2 Y•/ β 2 and 0.63 Y•/ β' 2 have been obtained with the his-tagged β and non-tagged β' . The highest activities obtained for these constructs are 1089 nmol/mg/min for β and 420 nmol/mg/min for β' . The stability of the Y• in β and β' have been measured, revealing similar half-lives in the two subunits. The mutants Y176F- β , Y162F- β , Y138F- β' and Y124F- β' have been constructed to examine Yen's proposal that, in contrast to *E. coli* RNR, human β and β' contain a dityrosyl-diiron cofactor, essential in catalysis. Our results do not support their findings, rather we have found that the essential tyrosine mutant Y176F- β and Y138F- β' are EPR silent, while the second tyrosine mutants Y162- β and Y124- β' contain 0.1 Y• and 0.2-0.3 Y• per dimer respectively. However, our stability test revealed that the Y• in those mutants are very unstable compared to wt. Overall, our data are inconsistent with Yen's dityrosyl-diiron model, and instead we believe that h β and h β' contain a single essential Y• as with the other class Ia RNR.

2.2 Materials and Methods

2.2.1 Materials

Luria Bertani (LB) broth powder and agar were purchased from Difco (Sparks, MD). Competent *E. coli* BL21 (DE3) cells were purchased from Stratagene. The pET28a vector was obtained from Novagen (part of EMD Biosciences, Inc, San Diego, CA). Complete EDTA-free protease inhibitor tablets, DNaseI, and calf alkaline phosphatase

(20 U/ μ L) were purchased from Roche Biochemicals (Indianapolis, IN). Restriction enzymes were obtained from New England Biolabs (Beverly, MA). [3 H]-CDP (17 Ci/ μ mol) was obtained from Moravsek Biochemicals, Inc (Brea, CA). Ni-NTA resin was purchased from Qiagen (Valencia, CA). Isopropyl β -D-thiogalactoside (IPTG) and 1,4-dithiothreitol (DTT) were obtained from Mallinckrodt Chemicals (Paris, KY). DEAE Sepharose Fast Flow, Q Sepharose Fast Flow and Sephadex G-25 column were obtained from Amersham Biosciences (part of GE Healthcare, Piscataway, NJ). Ultrafiltration membranes (YM30), Centricons, and Amicon Ultra centrifugal devices were obtained from Millipore (Bedford, MA). All other chemicals were purchased from Sigma-Aldrich (St. Louis, MO).

2.2.2 General Procedures

E. coli thioredoxin (TR, specific activity of 40 U/mg) and thioredoxin reductase (TRR, specific activity of 1320 U/mg) were isolated as previously described (28, 29). Plasmids containing the genes for α (formerly called H1) and β (formerly called H2), phRRM1 and phRRM2, were generous gifts from Yun Yen (City of Hope National Medical Center). p53R2 containing the gene for β' was a gift from Prof. Lars Thelander (Department of Medical Biosciences, Medical Biochemistry, Umeå University, SE-901 87 Umeå, Sweden). Protein concentrations were determined using the extinction coefficients ($\epsilon_{280\text{ nm}}$) of the monomer [45,900 M $^{-1}$ cm $^{-1}$ for (His) $_6$ - β , 119,160 M $^{-1}$ cm $^{-1}$ for α , 62,000 M $^{-1}$ cm $^{-1}$ for β'].

2.2.3 Construction of plasmids for expression of His- α , His- β and His- β' in *E. coli*.

Sequencing of the α and β genes in phRRM1 and phRRM2, respectively, obtained from Yen's lab, revealed a number of mutations relative to the sequences reported in the NCBI data base (30, 31). In the α gene, nucleotide C521 was mutated to a T resulting in a Val to Ala substitution. At nucleotide 1763, C was changed to T resulting in an Ile to Thr substitution. In the gene for β , A650 was changed to G resulting in the conversion of a Lys to Arg. These mutations were corrected by site directed mutagenesis using the Quick Change Kit by Stratagene with primers shown in table 2.2. In addition the N-terminal tags of each protein were re-engineered to minimize the number of additional residues. The NdeI digestion site in α was silenced. All α , β and β' genes were PCR amplified with primers listed in table 2.2, digested with NdeI and NotI and ligated into the NdeI - NotI sites of pET28a (Novagen) to produce (His)₆- α , (His)₆- β , (His)₆- β' containing a "MGSSHHHHHSSGLVPRGSH"- N-terminus. We name them as pHis-H1, pHis-H2 and pHis-p53R2 plasmid. The construct of Yen's (His)₆- α (phRRM1) contains the N-terminal sequence "MGSSHHHHHSSGLVPRGSHMASMTGGQQMGRDPNSSSVDKLA" and (His)₆- β (phRRM2) and (His)₆- β' (php53R2) contains the N-terminal sequence "MGSSHHHHHSSGLVPRGSHMASMTGGQQMGRGT".

The non-tagged p53R2 in pET3a construct from Thelander's lab is not modified. The plasmid maps are attached in the appendix. All constructs were verified by sequencing at the MIT biopolymers laboratory.

Table 2.2 Primers for making the new constructs His-H1, His-H2, His-p53R2 and correcting sequence errors.

Primer name	Sequence of the primer (from 5'-3')
H1-5' primer (NdeI site)	CTTGCGGCC CATATG CATGTGATCAAGCGAGATGG
H1-3' primer (NotI site)	CGAGT GCGGCCG CTCAGGATCCACACATCAGACATTC
H2-5' primer (NdeI site)	CGCGGATCC CATATG CTCTCCCTCCGTGTCCCGC
H2-3' primer (NotI site)	GCTT GCGGCCG CTTAGAAGTCAGCATCCAAGGTA AAAAG
His-p53R2 5' primer (NdeI site)	GGGTCGCGGAC CATATG GGGCGACCCGGAAAGGCCGG
His-p53R2 3' primer (NotI site)	CGAGT GCGGCCG CTTAAAAATCTGCATCCAAGGTGAAGAC
H1-521 forward	CC ACAACATATG TTGATGAGAG TATCTGTTGG GATCCAC
H1-521 reverse	GTGGATC CCAACAGATA CTCTCATCAA CATATGTTGT GG
H1-1763 forward	GGGAC TGAAGGTTTCAAGGAGAA GATTGCAAAG TGTGG
H1-1763 reverse	CCATA CTTTGCAATC TTCTCCTTGA GAACCTTCCA GTCCC
H2-650 forward	GCGCTGGA TTGGGGACAA AGAGGCTACC TATGG
H2-650 reverse	CCATA GGTAGCCTCT TTGTCCCAA TCCAGCGC

The restriction sites and mutation sites are highlighted.

2.2.4 Expression and purification of α

The expression and purification procedures of human α and β were based on the reported procedures described by Yen's group (21). Additional steps were included to remove DNA to increase the purity of the isolated protein.

pHis-H1 was transformed into *E. coli* BL21 Codon Plus (DE3) (Stratagene), plated on LB agar plates with 50 µg /mL kanamycin (kan) and a single colony chosen for growth. For growth of α , an overnight culture (40 mL) was grown from a single colony at 37 °C and transferred to 2L of LB and grown at 37 °C. IPTG (1 mM) was added at an OD_{600nm} 0.7- 0.9 and the cells were grown overnight (16 h) at 25 °C. The cells were harvested and growths typically yielded 4 g/L.

The isolation of α was carried out at 4 °C by the following general procedure. The cell pellets (15 g) were suspended (5 vol/g) in 50 mM NaH₂PO₄, pH 7.0, 0.1% Triton X-100 and 10 mM 2-mercaptoethanol with the complete protease inhibitor (Roche). The suspension was passed through the French press at 14,000 psi. The cell lysate was centrifuged at 20,000 x g for 30 min. The supernatant was treated with streptomycin sulfate to a final concentration of 1% (w/v) (determined by streptomycin titration) and the pellet was removed by centrifugation. The supernatant was incubated with Ni-NTA agarose resin (1 mL/g of cells, Qiagen) at 4 °C for 1 h and then loaded into a column (2.5 x 10 cm). The column was subsequently washed with 40 column volumes of 50 mM NaH₂PO₄, 800 mM NaCl, 50 mM imidazole, pH 7.0, 0.1% Triton X-100 and 10 mM 2-mercaptoethanol. The protein was eluted with 50 mM NaH₂PO₄, 300 mM NaCl, 125 mM imidazole, pH 7.0. Fractions containing protein were identified using the Bradford assay. The fractions were pooled and concentrated to < 10 mL, and then the imidazole was removed by Sephadex G-25 chromatography (200 mL, 2.5 x 50 cm). α was stored in 50 mM Tris, 100 mM KCl, 15 mM MgCl₂, 5 mM DTT, pH 7.6, 5% glycerol. Protein yields of α were typically about 1-2 mg per g of cell pellet.

α purified using the method above (15 mg) in buffer of 50 mM Tris, pH 7.6, 5% glycerol, 1 mM DTT was added to a dATP resin (30 mL, 2.5 x 10 cm, pre-equilibrated with 50 mM Tris, pH 7.6, 5% glycerol, 1 mM DTT) and stirred gently for 2 h at 4 °C. The resin was then placed in a column (2.5 x 10 cm), and the column was washed with 300 mL 50 mM Tris, pH 7.6, 5% glycerol, 300 mM KCl, 1mM DTT. The protein was eluted with 50 mM Tris, pH 7.6, 5% glycerol, 100 mM KCl, 5mM DTT, 10 mM ATP. Fractions containing protein were identified using the Bradford assay. The fractions were pooled and concentrated to < 0.5 mL, and the ATP was removed by Sephadex G-25 chromatography (40 mL, 2.5 x 30 cm). α was stored in 50 mM Tris, 100 mM KCl, 15 mM MgCl₂, 5 mM DTT, pH 7.6, 5% glycerol. The typical yield of α was about 0.2 mg per g of cell pellet after the dATP column.

2.2.5 Expression and purification of β

pHis-H2 was transformed into *E. coli* BL21 Codon Plus (DE3) (Stratagene), plated on LB agar plates with 50 μ g /mL kanamycin (kan) and a single colony chosen for growth. For isolation of β , an overnight culture (40 mL) in 250 mL flask grown to saturation was diluted into 2 L of LB in 6 L flask containing 50 μ g/mL kan and grown at 37 °C to OD_{600nm} 0.7- 0.9. Isopropyl-1-thio- β -D-galactopyranoside (IPTG, 1mM) was then added and the cells were grown for an additional 6 h at 30 °C.

The isolation of β 2 was carried out by the following general procedure. The cell pellets (15 g) were suspended (5 mL/g) in 50 mM NaH₂PO₄, pH 7.0, 0.1% Triton X-100 and 10 mM 2-mercaptoethanol with the complete protease inhibitor (Roche). The suspension was passed through the French press at 14,000 psi. The cell lysate was

centrifuged at 20,000 x g for 30 min. The supernatant was treated with streptomycin sulfate to a final concentration of 1% (w/v) (determined by streptomycin titration) and the pellet was removed by centrifugation. The supernatant was incubated with Ni-NTA agarose resin (1 mL/g of cells, Qiagen) at 4 °C for 1 h and then loaded into a column (2.5 x 10 cm). The column was subsequently washed with 40 column volumes of 50 mM NaH₂PO₄, 800 mM NaCl, 50 mM imidazole, pH 7.0, 0.1% Triton X-100 and 10 mM 2-mercaptoethanol. The protein was eluted with 50 mM NaH₂PO₄, 300 mM NaCl, 125 mM imidazole, pH 7.0. Fractions containing protein were identified using the Bradford assay. The fractions were pooled and concentrated to < 10 mL, and the imidazole was removed by Sephadex G-25 chromatography (200 mL, 2.5 x 50 cm). β was stored in 50 mM Tris, 100 mM KCl, pH 7.6, 5% glycerol. Protein yields of β were about 5 mg per g of culture.

2.2.6 Expression and purification of β'

The expression and purification procedures of β' were based on the reported procedures described by Thelander's groups (16).

The plasmid of p53R2 (non-tagged, from the Thelander lab) was transformed to BL21 Codon Plus (DE3)-RIL cells (Stratagene), plated on LB agar plates with 100 μ g/mL Amp and 34 μ g/mL Chloramphenicol (CM). For the expression of β' , an overnight culture (20 mL LB in 150 mL flask) was grown to saturation, diluted into 2 L of LB in 6L flask containing 100 μ g/mL Amp, 34 μ g/mL CM and grown at 37 °C to OD_{600nm} 0.7. 1,10-Phenanthroline (100 μ M) was added and the cells were grown for an additional 15 min. IPTG (400 μ M) was added and the cells were induced and grown at 37 °C for 5 h. The cells were harvested and typically yielded 2 g/L.

For the isolation of the apo β' , around 16 g of cell pellet were suspended (4 mL/g) in extraction buffer (50mM Tris-HCl, pH7.6, 1mM PMSF, 1mM EDTA at 4 °C). The suspension was passed through the French press at 14,000 psi. The cell lysate was centrifuged at 27, 000 x g for 30 min at 4 °C. A 10% (w/v) solution of streptomycin sulfate, in extraction buffer, was added to the supernatant over 10 min while stirring at 4 °C, to a final concentration of 2.5 % (w/v, from Thelander's protocol). After an additional 10 min of stirring, the pellet was removed by centrifugation (27, 000 x g for 30 min, 4 °C). Solid ammonium sulfate (0.243 g/mL, 40% saturation) was added to the supernatant over 10 min at 4 °C. After an additional 30 min of stirring, the protein pellet was recovered by centrifugation (27, 000 x g for 30 min, 4 °C).

The pellet was dissolved into 4 mL of extraction buffer and loaded directly onto a Phenyl Sepharose 6 Fast flow column (20 mL, 2.5 x 10 cm) which was pre-equilibrated with buffer A (200 mL, 25 mM Tris pH 7.6, 10% glycerol, 30% w/v $(\text{NH}_4)_2\text{SO}_4$). The column was washed with buffer A (100 mL) followed by buffer B (300 mL, 25 mM Tris pH 7.6, 10% glycerol, 5% w/v $(\text{NH}_4)_2\text{SO}_4$). Finally β' was eluted with 50 mM Tris pH7.6, 5% glycerol, 1 mM EDTA, 1 mM PMSF. Fractions (2 mL) containing p53R2 (based on Bradford assay) were collected.

The pooled protein elution fractions were loaded onto a Q-sepharose column (20 mL, 2.5 x 10 cm), which was pre-equilibrated with 100 mL 50 mM Tris, 5% glycerol, 1 mM EDTA, 1 mM PMSF, pH 7.6 at 4 °C. The column was washed with 200 mL of 50 mM Tris, 150 mM KCl, 5% glycerol, pH 7.6 at 4 °C. The protein was eluted with a 70 mL x 70 mL linear gradient from 150 – 400 mM KCl in 50 mM Tris, 5% glycerol, pH 7.6. Fractions (2 mL) containing β' (based on Bradford assay and 10% SDS-PAGE) were

collected. Apo β' eluted around 220 mM KCl. The impurities around 50 kDa eluted around 280 mM KCl. At typical yield of 0.4 mg of apo β' was obtained per g of cells.

2.2.7 Conversion of human apo β 2 to holo β 2.

Stock solutions of (His)₆- β 2 (2 mL, 2.5 mg/mL) were deoxygenated by 6 cycles of evacuation (for 3x 5 s) followed by argon flushing (2 min) on a Schlenk line. The deoxygenated β 2 solution was brought into the glove box (M. Braun, Stratham, NH) and 5 eq of Fe(II) per β 2 was added from a degassed Fe(NH₄)₂(SO₄) solution in buffer A (50 mM Tris, 100 mM KCl, pH 7.6, 5% glycerol). The resulting mixture was incubated at 4 °C for 15 min. The protein was then removed from the glove box and 1 mL of O₂ saturated buffer A (50 mM Tris, 100 mM KCl, pH 7.6, 5% glycerol) was added. Excess iron was removed by Sephadex G-25 chromatography (40 mL, 2.5 x 20 cm). The typical recovery of β 2 is about 65%. With this method, 0.8-1.2 Y• is routinely generated with a specific activity of about 800-1100 nmol/min/mg.

2.2.8 Conversion of human apo β' 2 to holo β' 2

A solution of β' 2 (60 μ M) in 500 μ L in 50 mM Hepes, 100 mM KCl, 10% glycerol, pH 7.6, ascorbic acid (2.5 mM) was deoxygenated by 6 cycles of evacuation (3x 5 s) followed by argon flushing (2 min) on a Schlenk line. The deoxygenated β' 2 solution was brought into the glove box (M. Braun, Stratham, NH) and 6 eq. of Fe (II) (ferrous ammonium sulfate solution in 50 mM Hepes, 100 mM KCl, pH 7.6) per β' 2 was added. The resulting mixture was incubated at 4 °C for 30 min. The protein was then removed from the glove box and 100 μ L of O₂ saturated buffer of 50 mM Tris, 100 mM KCl, pH

7.6 was added. O₂ (g) was blown over the surface of the protein solution for 1 min. Excess iron was removed by Sephadex G-25 chromatography (40 mL, 2.5 x 30 cm). The activity assay was carried out immediately and 250 μL protein solution was packed and frozen into EPR tube for Y• measurement. With this method, 0.5-0.6 Y• is routinely generated with a specific activity of about 300-400 nmol/min/mg.

2.2.9 Construction of the genes for Y124F-β', Y138F-β', and Y162F-β, Y176-β, expression and isolation of the mutant proteins.

The Y124F-β', Y138F-β', and Y162F-β, Y176F-β were generated by site directed mutagenesis using the Quick Change Kit (Stratagene). The β gene in pET28a (pHis-H2 plasmid) or β' gene in pET3a (non-tagged p53R2 plasmid) was amplified by PCR using PfuUltra II polymerase (Stratagene) with primers for Y176F, Y162F, or Y138F, Y124F (Table 1). Success obtain mutagenesis reaction was confirmed by sequencing at the MIT biopolymers laboratory. Y124F-β', Y138F-β', and Y162F-β, Y176F-β were expressed, purified, and reconstituted as described for β' or β with similar yields.

Table 2.3: Primers for generation of Y124F- β' , Y138F- β' , and Y162F- β , Y176- β

Name of the mutant	Sequence of the primer (from 5'-3')
Y138F- β' forward	GAATGTTCACTCAGAGATG TT CAGTTTGCTGATAGACAC
Y138- β' reverse	GTGTCTATCAGCAA ACTG AACATCTCTGAGTGAACATTC
Y124F- β' forward	CCAGAGGCTCGCTGTTT CTTT GGCTTCAAATTCTCATCG
Y124F- β' reverse	CGATGAGAATTTGAAAGCCAA AGAA CAGCGAGCCTCTGG
Y176F- β forward	CAGAAGCCCGCTGTTT CTTT GGCTTCAAATTGCCATGG
Y176- β reverse	CCATGGCAATTTGGAAGCCAA AGAA ACAGCGGGCTTCTG
Y162F- β forward	CATGGAAAACATACATTCTGAAATG TTT AGTCTTCTTATTGACAC
Y162- β reverse	GTGTCAATAAGAAGACTAA AC ATTTCAGAATGTATGTTTTCCATG

The mutation sites are highlighted.

2.2.10 Human RNR Activity assays

The reaction mixture contained in a final volume of 350 μ L: 50 mM Hepes (pH 7.6), 15 mM $MgCl_2$, 1 mM EDTA, 0.3 μ M (or 2.1 μ M) α , 2.1 μ M (or 0.3 μ M) β or β' , 3 mM ATP, 1 mM [3H]-CDP (specific activity 3400 cpm /nmol), 100 μ M *E.coli* TR, 1.0 μ M TRR, 2 mM NADPH. The assay mixture was pre-incubated at 37 $^{\circ}$ C for 2 min and the reaction was initiated by the addition of CDP. Aliquots of 50 μ L were removed over a 15 min time period and quenched in a boiling water bath. dCDP production was analyzed by the method of Steeper and Stuart (32) subsequently to dephosphorylation with alkaline phosphatase. The activities of Y124F- β' and Y162F- β were measured at 1 μ M in the presence of 7 μ M α .

2.2.11 Stability test of the wt β and β' and Y124F- β' mutant

Stock solutions (15 μ L, 30 μ M) of wt β , β' or Y124F- β' were incubated at 37 °C. Aliquots of 0.5 μ L from each of them was removed at several time points from 30 s to 30 min and diluted into 50 μ L of assay mixture with a final concentration 0.3 μ M. The assay mixture contained the following: 3 μ M α , 3 mM ATP, 1mM [³H]-CDP (specific activity 4800 cpm /nmol), 100 μ M *E.coli* TR, 1.0 μ M TRR, 2 mM NADPH, and assay buffer. The reaction mixture was incubated for 3 min at 37°C and quenched in a boiling water bath. dCDP production was measured as described above.

2.3 Results and Discussion

2.3.1 Purification of the His- α of human RNR

We obtained the plasmid phRRM1 from the Yen group. However, sequencing of the clone revealed a number of mutations relative to the sequences reported in the NCBI database. In addition the N-terminal His-tag region of α was re-engineered to minimize the number of additional residues in the linker region between the His-tag and α .

Mutations in the genes were corrected and the N-terminus of α was re-engineered to maintain the (His)₆ tag and to reduce the length of the intervening linker prior to the start of the gene to 10 amino acids. The detailed changes are described in the method section.

Based on Yen's growth protocol in which overexpression of α is induced at 30°C for 3 h, we tested various conditions of induction time, and temperature and found that higher amounts of soluble α can be obtained when IPTG is added after the cell culture was cooled to 25 °C or 20 °C for overnight induction. The final optimized condition is described in the method section. The purification protocol for His- α was based on the

protocol reported by Yen and uses only Ni-NTA affinity chromatography (16, 21). In our hands, the resulting proteins were contaminated with a large amount of DNA. Therefore, a streptomycin sulfate precipitation step was added to the protocol. The final streptomycin sulfate concentration used was chosen based on streptomycin titration and activity assays. The proteins were then chromatographed on a Ni affinity column yielding about 90% homogeneity based on SDS-PAGE (Figure 2.1), which co-purified with a protein of 74 kDa. Initially we thought that this 74 kDa protein was proteolytically clipped α . However, N-terminal sequencing revealed that it was Arna (bifunctional polymyxin resistance protein), a hexameric *E. coli* protein.

α purified using the Ni affinity column always contains ~ 10% contamination of Arna, which is a hexamer and has a huge extinction monomer coefficient of $89895 \text{ M}^{-1} \text{ cm}^{-1}$ at 280 nm, with monomer MW of 74 kDa and hexamer MW of 444 kDa. Because Arna interferes with SEC analysis to determine the MW of α_6 (540 kDa), $\alpha_6\beta_6$ (872 kDa) and $\alpha_6\beta'_6$ (794 kDa), dATP-affinity chromatography was explored as a method to remove the Arna impurity and to obtain highly pure α . However, the binding affinity of α to dATP resin is relatively weak, leading to only 25% recovery of the total loaded α . The purification gel (Figure 2.2, lane 3) with 8 μL of wash through buffer (from 300 mL total volume without concentration) shows the loss of α during the wash (50 mM Tris, pH 7.6, 5% glycerol, 300 mM KCl, 1mM DTT). Highly pure and active α (specific activity of 232 nmol/min/mg) could be obtained at the end but with low recovery (Figure 2.2).

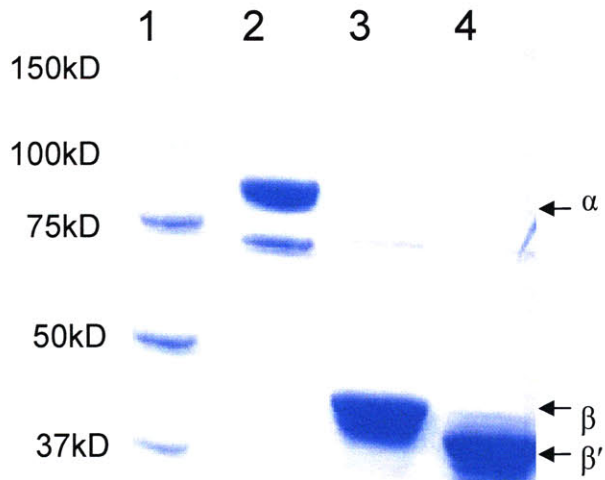


Figure 2.1: Purification of human RNR subunits.

10% SDS-PAGE gel. Lane 1, molecular mass markers. Lane 2, His- α (5 ug); Lane 3, His- β (5 ug); Lane 4, His- β' (5 ug).

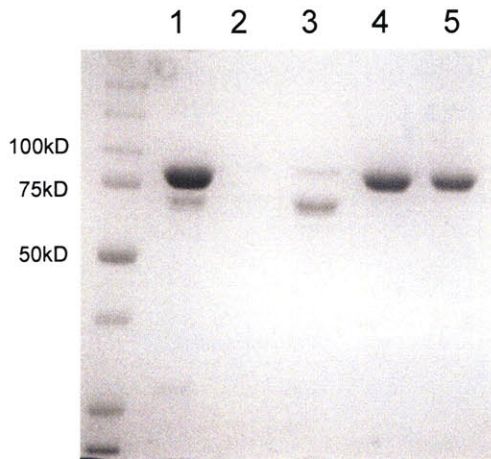


Figure 2.2: Purification of α subunit by dATP-affinity chromatography.

1. α purified from Ni column, 2, dATP column flow through, 3, wash, 4, 5, α elution from dATP column. 10% SDS-PAGE was used.

2.3.2 Purification of the His- β

The plasmid phRRM2 from the Yen group revealed one mutation relative to the sequences reported in NCBI data base. It was corrected by Quick Change site directed mutagenesis, and the N-terminal His tag was re-engineered to minimize the number of additional residues in the linker region.

Based on Yen's growth protocol in which β expression is induced at 30°C for 3 h, we optimized the induction temperature and time. To obtain a higher amount of soluble β , induction at 30°C for 6 h was selected. The purification protocol for His- β uses only Ni-NTA affinity chromatography, which is similar as that for His- α optimized as described above.

2.3.3 Purification of β' subunit of human RNR

p53R2 obtained from Thelander's lab does not contain an affinity tag or any extra amino acids in its sequence. The purification protocol of holo β' developed by Thelander lab includes precipitation of nucleic acids with streptomycin, ammonium sulfate fractionation, and DEAE chromatography (16). We applied the same procedure for apo β' purification but did not obtain protein of the same purity. Therefore, additional purification steps including Phenyl Sepharose 6 Fast and Q-sepharose Fast Flow anion exchange chromatography (Figure 2.3) were investigated. Although the purity of apo β' could be improved by each additional chromatography step, purifying apo β' with Phenyl Sepharose 6 Fast and Q-sepharose chromatography omitting the DEAE chromatography gave about the same purity (80%). Elution from the Q-Sepharose column with a 150-400 mM KCl gradient resulted in separation of two distinct peaks. The first peak centered at

220 mM KCl is apo β' as judged by SDS-PAGE (Figure 2.3). The second peak eluting at 280 mM KCl is a 50 kDa impurity.

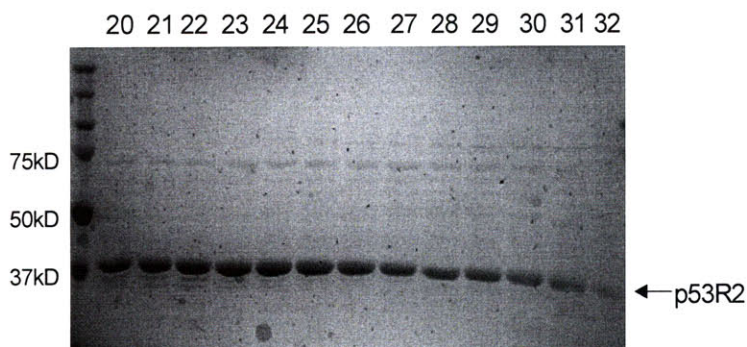


Figure 2.3: Analysis of fractions from Q-Sepharose column for β' . 10% SDS/PAGE shows the eluted apo β' fractions after Q-sepharose chromatography. The numbers above each lane are the fraction #.

2.3.4 Characterization of β subunit of human RNR

The growth of apo β in the presence of 1, 10-phenanthroline resulted in failure of expression, thus β has to be induced under conditions without phenanthroline. β as isolated is in the apo form and was reconstituted based on the protocol we have developed for reconstitution of the *E. coli* β_2 (33). Unfortunately, apo β is very unstable, and addition of ferrous solution to the protein caused β precipitation. pH measurement revealed that the ferrous water solution was acidic. Thus the reconstitution condition was improved by dissolving ferrous into Tris buffer (pH 7.6) in the glove box and gentle addition to apo β protein in the presence of glycerol. Various amounts of ferrous (1 eq. to 8 eq./ β_2) were titrated and demonstrated that titration in 6 eq. of ferrous which results in maximum β activity. With our optimized protocol, the resulting protein yielded 0.8- 1.2 Y•/ β_2 (Figure 2.4) and a specific activity of 800-1089 nmol/min/mg in the presence of a

seven fold excess of α (Figure 2.5). These results contrast with previous reports in the literature of 75 nmol/min/mg and 158 nmol/min/mg for β (Table 2.4) (16, 21). The difference in the activities might be related to the method of protein purification, reconstitution and assaying. Both of these two groups use DTT as reductants while we use *E. coli* TR, TRR and NADPH. Thelander's lab also has large excess of Fe(II) in the assay. Unlike the assay method of Yen's group in which β or β' (0.625–10 μ g) is incubated with 30 μ g α in the presence of 0.05 mM CDP (21), we assayed with 1 mM CDP to saturate the enzyme active site. Given the low affinity between α 2 and β 2, the activity of an individual RNR subunit is generally assayed in the presence of a large excess the other subunit. We titrated the activity of one subunit with increasing amount of the other subunit to obtain optimum activity. We have established that in the presence of seven fold excess of α , the highest activity is achieved.

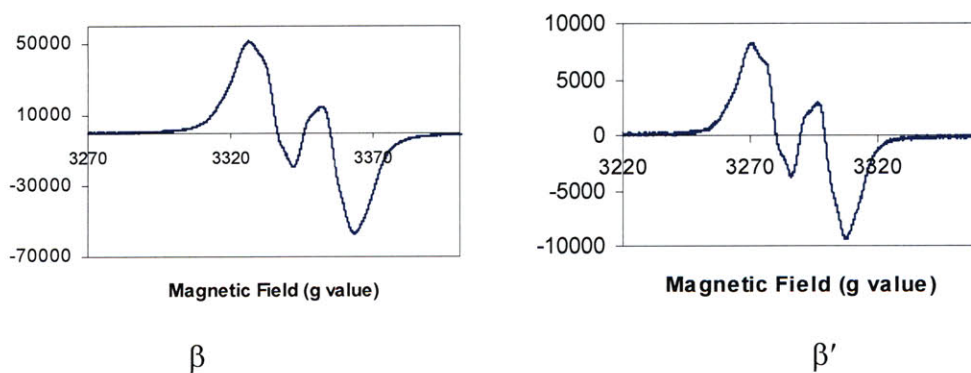


Figure 2.4: EPR spectra at 9 GHz of tyrosyl radical in human β and β' at 77 K. Power is at 1.006 mW; modulation amplitude is 1.00 G, and the frequency is 9.386 GHz. [β] = 76 μ M in 50 mM Tris, 100 mM KCl, pH 7.6, 5% glycerol, and [β'] = 25 μ M in 50 mM Hepes, 100 mM KCl, 10% glycerol. 0.8-1.2 Y•/ β 2 and 0.5-0.63 Y•/ β' 2 are routinely obtained.

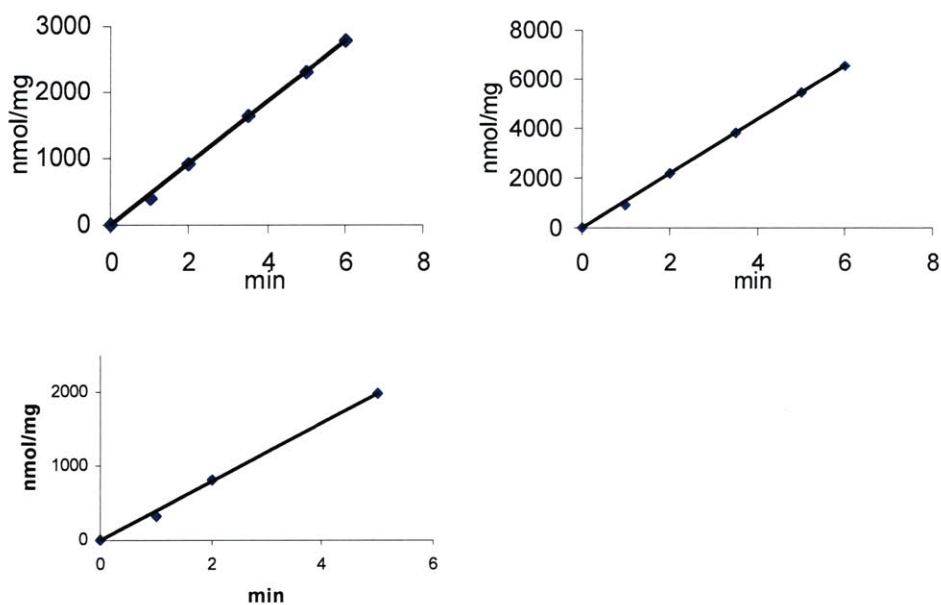


Figure 2.5: Activity assays of α (top left), β (top right) and β' (bottom)

The specific activity of α is 462 nmol/min/mg when assayed with 7 fold excess of β . The activity of β is 1089 nmol/min/mg, and that of β' is 420 nmol/min/mg, when assayed with 7 fold excess of α .

Table 2.4 Comparison of the human RNR activities obtained from different groups (16, 21, 26)

	α (nmol/min/mg)	β (nmol/min/mg)	β' (nmol/min/mg)
Stubbe	462	1089	420
Yen	6.8	75	52
Thelander	ND	158	95
Thelander	ND	140 (mouse)	63 (mouse)
Cooperman	201 (mouse)	ND	ND

2.3.5 Reconstitution and characterization of human β'

Expression of β' was carried out in the presence of 1,10-phenanthroline, which results in apo protein, as this procedure gave higher recovery of $Y\bullet$ and activity than growth in the absence of phenanthroline. A variety of methods to assemble the essential diferric-tyrosyl radical ($Y\bullet$) cluster of $\beta'2$ including anaerobic, or aerobic reconstitution on the purified apo- β' , addition of Fe(II) to crude cell extracts, or addition during purification, were examined. Both the His-tagged and non-tagged β' constructs and various ratios of Fe(II)/ β' have been titrated. The procedure described in Methods section gave 0.63 $Y\bullet$ per $\beta'2$ with an activity of 420 nmol/min/mg in the presence of 7 fold excess of α (Figure 2.5, Table 2.4). The His- β' construct gave 0.5 $Y\bullet/\beta'2$ as the best when reconstituted by the same method. The β' isolated by Thelander group gave activity of 95 nmol/min/mg (16), but the radical amount was not reported. Yen's group reported that their His tagged- $\beta'2$ contain 0.8 $Y\bullet/\beta'2$ and a specific activity of 50 nmol/min/mg (21). The low activity and high $Y\bullet$ content reported by these groups are at odds with activity being directly proportional to $Y\bullet$ (34, 35). In our hands we have been unable, after many attempts with identical constructs to those used by Thelander, to obtain higher levels of $Y\bullet/\beta'2$, although our reconstitution of β did obtain higher amount of radical (1.2 $Y\bullet/\beta2$).

An aerobic reconstitution method was also carried out. An Fe(II) solution was prepared by dissolving ferrous ammonium sulfate in water and the pH was adjusted to 2.3 by addition of concentrated nitric acid. The protein solution was not degassed or put into the glove box. Seven equivalents of Fe(II) (2-10 μ L) per $\beta'2$ were added aerobically to the protein solution very slowly with mixing. A few sec after the final addition of Fe (II),

O₂ (g) was blown over the surface of the protein solution for 5 min. An activity of 356 nmol/min/mg and 0.6 Y•/β'2 was obtained with this method.

A third assembly method we used was described by Anderson and Solomon (36), which involved reducing β' with methyl viologen and dithionite, adding 7 eq./β'2 of ferrous solution anaerobically, and incubating for 15 min at 4 °C. The protein solution was removed from the glove box and an O₂ saturated solution was added immediately. Only 0.4 Y•/β'2 with activity of 163 nmol/min/mg was obtained from this method.

An additional method of cofactor assembly used was to add ferrous ammonium sulfate to the partially purified apo-β'. After purification by streptomycin sulfate precipitation, ammonium sulfate fractionation, and Phenyl sepharose chromatography steps, ferrous ammonium sulfate (5 mg/g of cell) and sodium ascorbate (5 mg/g of cell) were dissolved in 50 mM Tris, pH 7.6, 5% glycerol and added over 10 min to the partially purified apo-β' at 4 °C with stirring. After stirring for an additional 15 min at 4 °C, the protein solution was loaded onto a Q-Sepharose column and purification continued as described in methods section. The rest of the procedure is the same as it described in the purification method. β' with a specific activity of 396 nmol/min/mg was obtained (the Y• content was not measured). An alternative method with addition of ferrous to the crude cell extracts before purification gave a specific activity of 272 nmol/min/mg. The last two reconstitution methods were repeated only once.

Overall, both the anaerobic and aerobic methods on the reconstitution of purified apo-β' can give the highest amount of Y• (0.6 Y•) and activity. It remains unknown why we can not achieve 1 Y•/β'2 remains unclear.

2.3.6 Characterization of human α

With titration of amount of β in the activity assay, we have obtained a specific activity of α as high as 462 nmol/min/mg (Figure 2.5) in the presence of a 7 fold excess of β . This result contrasts with the previous report in the literature of 6.8 nmol/min/mg (Table 2.4) (21). However, α was difficult to work with because of its low solubility. The highest concentration that can be obtained for His-tagged α is 3 mg/mL. The non-tagged α purified from Dealwis group can be concentrated to more than 10 mg/mL. We have measured the activity of their α , which gave a specific activity of 484 nmol/min/mg, a value similar to ours. Whether the His-tag makes a difference on the solubility of α is not clear. The difference might be related to the methods of purification used. Whereas we use Ni and dATP chromatography, a peptide affinity chromatography was employed by Dealwis lab (37).

2.3.7 Investigation of the proposed role for a second tyrosine required for RNR activity (38)

Recently Yen's group proposed that human β and β' contain a unique dityrosyl-diiron cofactor center. In addition to the essential tyrosines, Y176 of h β and Y138 of h β' (Y122 equivalent in *E. coli*), Yen's group suggest that Y162 of h β and Y124 of h β' , which correspond to V108 in *E. coli* β by structure alignment, are also essential for the RNR activities. The evidence for the di-tyrosine cofactor model in h β' proposed by Yen was that isolated Y138F- β' and Y124F- β' were both EPR silent and contained no activity. The evidence for the di-tyrosine cofactor model in h β was that both Y176F- β and Y162F- β contained 3% activity, 0.012 Y• per dimer, and only the double mutant Y176F/Y162F-

β were completely inactive (38). Yen's group also made additional tryptophan mutants, which gave the contradictory results that Y124W- β' contained 0.28 Y• per dimer, and Y138W- β' were EPR silent. For β mutants, neither Y176W- β , Y162W- β showed any activity. Unfortunately, Yen's group did not address those problems properly, and they interpreted these inconsistencies as a result from the radical harboring ability of phenylalanine and tryptophan, and structural differences between β and β' .

In order to investigate Yen's model, we did site directed mutagenesis on the His- β and non-tag β' plasmids, cloned and isolated Y176F- β , Y162F- β , Y138F- β' , and Y124F- β' following the protocol for wt β and β' . The Y• amounts in these mutants were quantified immediately after cluster assembly, compared to quantification after overnight dialysis performed by Yen's lab. In our studies, Y176F- β and Y138F- β' are EPR silent (Figure 2.6) and showed no activity, which agree well with their essential role in RNR activities. However, in contrast to results from Yen's lab, our EPR studies have demonstrated that Y124F- β' and Y162F- β contain 0.2-0.3 Y• and 0.1 Y• per dimer respectively (Figure 2.6). Both of the mutants have activity (Figure 2.7), although the linear range is short and shows time dependent loss of activity, likely associated with loss of Y• as a function of assay conditions. The activity of Y162F- β has been measured at 1 μ M and 1.5 μ M β concentration, which resulted in a proportional increase of the rate. The stability test of Y124F- β' has been carried out, which revealed that the Y• in the Y124F decays fast with a half life of about 5 min at 37 °C, compared to the half life of wt β' of 30 min. This might explain why Yen's group has observed these mutants to be EPR silent (Figure 2.8).

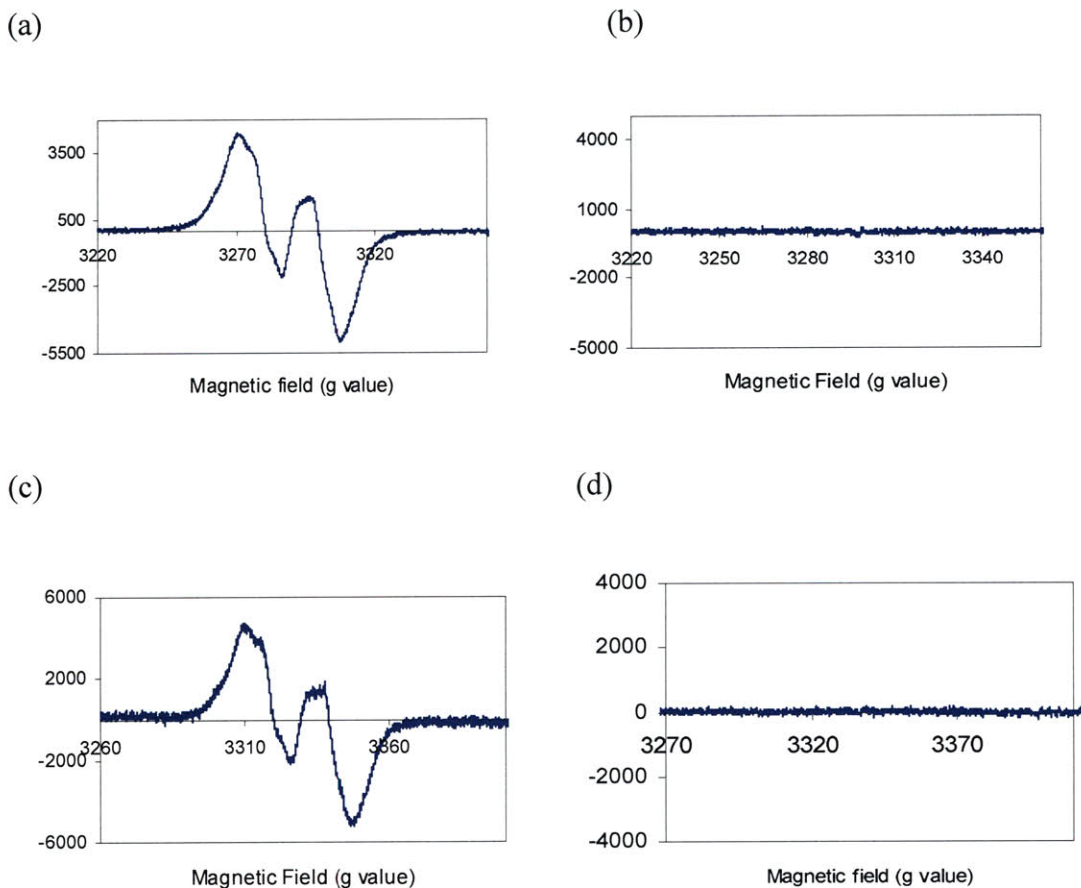


Figure 2.6: EPR Spectra at 9 GHz of human β' and β mutants.

(a) Y124F- β' (b) Y138F- β' (c) Y162F- β (d) Y176F- β are shown. Instrument settings for all spectra were as follows: frequency, 9.341 GHz, power 1.003 mW, modulation amplitude 1.00 G, number of scans (a) 5, (b) 5, (c) 20, (d) 5, and temperature 77 K.

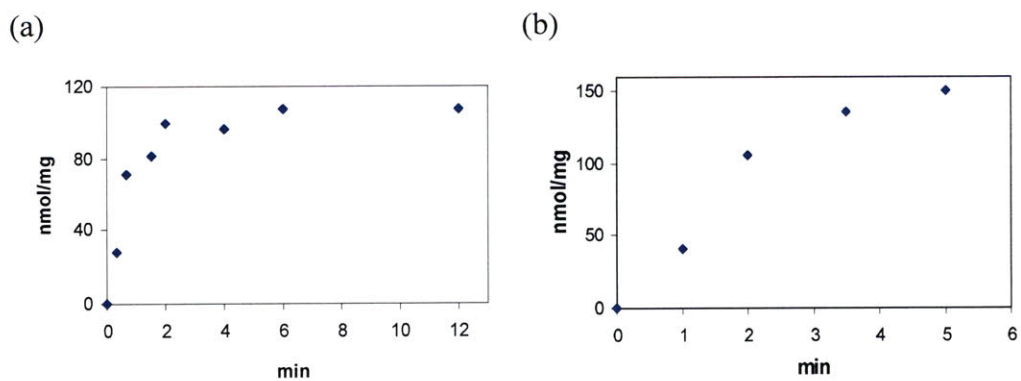


Figure 2.7: Activity assays of Y162F- β and Y124F- β' .

(a) Y162F- β (1.5 μ M) was assayed in the presence of 7 fold α (10.5 μ M); (b) Y124F- β' (0.3 μ M) was assayed in the presence of 10 fold α (2.1 μ M).

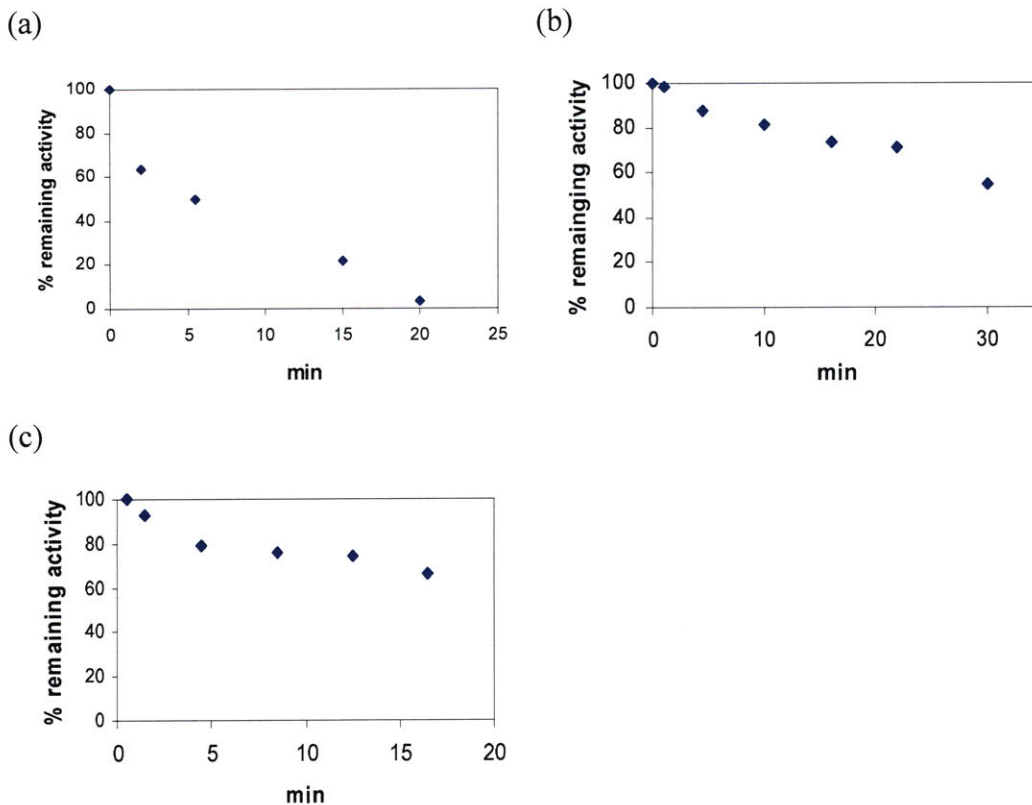


Figure 2.8: Stability test of Y124F- β' , wt- β' , wt- β at 37 °C.

Stock solutions of (a) Y124F- β' , (b) wt- β' , (c) wt- β (15 μ L each) were incubated at 37 °C. Aliquots were removed at various times and diluted into 0.3 μ M in assay mixture to measure the β' or β activity in the presence of 10 fold excess α .

2.4 Discussion

In our studies, the three human RNR subunits, α , β and β' , have been purified, characterized and found to have significantly higher activities than have been obtained in previous reports. The reason why we have achieved such high activities might be due to the way in which we assay for activity as discussed in section 2.3.4.

Using our *in vitro* reconstitution method, we have obtained β_2 containing 1.2 Y• and β'_2 containing 0.63 Y• as the highest radical content, compared to 1.2 Y• and 0.8 Y• for β_2 and β'_2 obtained by Yen's group. Multiple methods have been explored to attempt

to increase the Y• content in β'2, however, no significant improvement has been achieved. The problem of sub-stoichiometric amount of Y• is not unique to the human β'2. We have seen this with *S. cerevisiae* RNR and other proteins as well, indicating that another factor might be required for cluster assembly (39).

In addition, we have investigated whether human β2 and β'2 contain the unique diiron-dityrosyl radical cofactor as proposed by Yen. Mutagenesis studies have been carried out by making the essential tyrosine mutants, Y176F-β and Y138F-β', and mutants of proposed second essential tyrosines, Y162F-β and Y124F-β'. Our results from EPR quantitation and activity measurements have demonstrated that Y176 and Y138 are the only essential tyrosines in β and β'. β and β' mutants with Y162 and Y124 substituted with phenylalanine still have activity, although their Y• decay faster than in the wt proteins.

The structure of hβ (PDB ID 2UW2) and hβ' (PDB ID 2VUX) have recently been solved. Compared to the *E. coli* β structure (PDB ID 1AV8), the positions of Y176/Y138 relative to Y162/Y124 in human β and β' are very similar to that of Y122 relative to V108 in *E. coli* β (Figure 2.9). V108/Y162/Y124 are more deeply buried than Y122/Y176/Y138. Moreover, the distance between Y176/Y138 and the essential tryptophan radical in the PCET pathway, W102/W64 (W48 in *E. coli* β), is 7.8 Å compared to 15.9 Å from Y162/Y124 to W102/W64 in the human proteins. Y176/Y138 is 5.8 Å away from H172/H134 (H118 of *E. coli* β), whereas Y162/Y124 is 16.8 Å away from this residue. The second proposed tyrosine is clearly too far away from the current suggested PCET pathway to be directly involved in it. Thus far, no alternative route of PCET has been identified, suggesting that Y162 is unlikely involved in radical initiation and propagation.

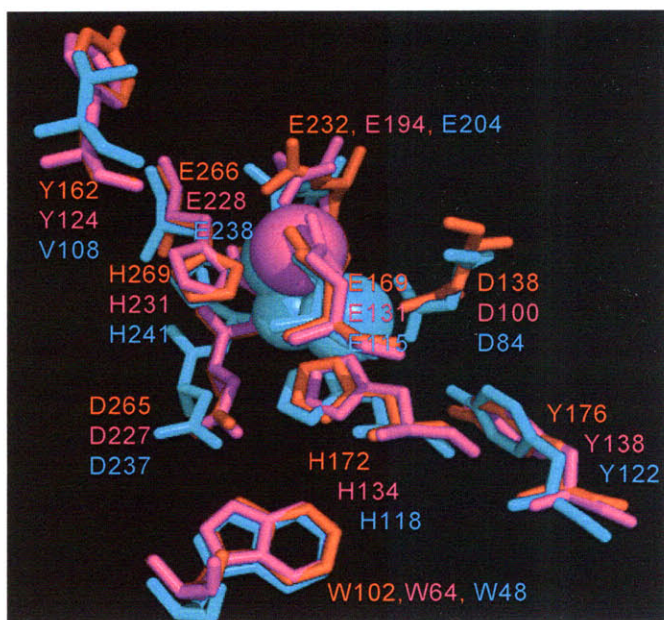


Figure 2.9: Comparison of the positions of Y176, Y162 of human β , Y138, Y124 of human β' to Y122, V108 of *E. coli* β in the active site structures.

The overlay structures of key residues in PCET pathway Y122, W48, D237, H118 of *E. coli* β (cyan), Y176, W102, D265, H172 of human β (red), Y138, W64, D227, H134 of human β' (magenta), and iron ligands, D84, E115, E204, E238, H241 of *E. coli* β (cyan), D138, E169, E232, E266, H269 of human β (red), D100, E131, E194, E228, H231 of human β' (magenta) are shown in stick. Irons are shown in spheres. The second proposed essential tyrosine Y162 of human β (red), Y124 of human β' (magenta) and the equivalent residue V108 of *E. coli* β (cyan) are shown.

Above all, the Y124 in $\beta'2$ and Y162 in $\beta2$ may play important roles in maintaining the activity and stability of the human RNR diiron cluster, but our data does not support the proposal that these residues are essential tyrosine radicals or that the cluster in human RNR is a diiron-dityrosyl radical cofactor. We believe that human RNR shares the same mechanism as other class Ia RNRs, which contains only one essential tyrosyl radical.

2.5 Reference

- (1) Tanaka, H., Arakawa, H., Yamaguchi, T., Shiraishi, K., Fukuda, S., Matsui, K., Takei, Y. and Nakamura, Y. (2000) A ribonucleotide reductase gene involved in a p53-dependent cell-cycle checkpoint for DNA damage. *Nature* 404, 42-49.
- (2) Fritscher, J., Artin, E., Wnuk, S., Bar, G., Robblee, J. H., Kacprzak, S., Kaupp, M., Griffin, R. G., Bennati, M., and Stubbe, J. (2005) Structure of the nitrogen-centered radical formed during inactivation of E-coli ribonucleotide reductase by 2'-azido-2'-deoxyuridine-5'-diphosphate: Trapping of the 3'-ketonucleotide. *JOURNAL OF THE AMERICAN CHEMICAL SOCIETY* 127, 7729-7738.
- (3) Seyedsayamdost, M. R., and Stubbe, J. (2006) Site-specific replacement of Y-356 with 3,4-dihydroxyphenylalanine in the beta 2 subunit of E. coli ribonucleotide reductase. *J. Am. Chem. Soc* 128, 2522-2523.
- (4) Stubbe, J., and van der Donk, W. A. (1998) Protein radicals in enzyme catalysis. *Chemical Reviews* 98, 705-762.
- (5) Larsson, A., and Sjöberg, B. M. (1986) Identification of the stable free-radical tyrosine residue in ribonucleotide reductase. *EMBO J.* 5, 2037-2040.
- (6) Sjöberg, B. M., Reichard, P. (1977) Nature of Free-Radical in Ribonucleotide Reductase from *Escherichia-Coli*. *J. Biol. Chem.* 252, 536-541.
- (7) Atkin, C. L., Thelander, L., Reichard, P., and Lang, G. (1973) Iron and Free-Radical in Ribonucleotide Reductase - Exchange of Iron and Mossbauer-Spectroscopy of Protein-B2 Subunit of *Escherichia-Coli* Enzyme. *J. Biol. Chem.* 248, 7464-7472.
- (8) Nordlund, N., and Reichard, P. (2006) Ribonucleotide reductases. *ANNUAL REVIEW OF BIOCHEMISTRY* 75, 681-706.
- (9) Kashlan, O. B., Scott, C. P., Lear, J. D., and Cooperman, B. S. (2002) A comprehensive model for the allosteric regulation of mammalian ribonucleotide reductase. Functional consequences of ATP- and dATP-induced oligomerization of the large subunit. *Biochemistry* 41, 462-474.
- (10) Chabes, A., Georgieva, B., Domkin, V., Zhao, X, Rothstein, R., and Thelander, L.,. (2003) Survival of DNA damage in yeast directly depends on increased dNTP levels allowed by relaxed feedback inhibition of ribonucleotide reductase. *Cell* 112, 391-401.
- (11) Huang, M., Zhou, Z., and Elledge, S.J. (1998) The DNA replication and damage checkpoint pathways induce transcription by inhibition of the Crt1 repressor. *Cell* 94, 595-605.
- (12) Chabes, A., and Thelander, L. (2000) Controlled protein degradation regulates ribonucleotide reductase activity in proliferating mammalian cells during the normal cell cycle and in response to DNA damage and replication blocks. *J. Biol. Chem.* 275, 17747-17753.
- (13) Reichard, P., Eliasson, R., Ingemarson, R., and Thelander, L. (2000) Cross-talk between the allosteric effector-binding sites in mouse ribonucleotide reductase. *J. Biol. Chem.* 275, 33021-33026.
- (14) Engström, Y., Eriksson, S., Jildevik, I., Skog, S., Thelander, L., and Tribukait, B. (1985) Cell cycle-dependent expression of mammalian ribonucleotide reductase. Differential regulation of the two subunits. *J. Biol. Chem.* 260, 9114-9116.

- (15) Chabes, A., Bjorklund, S. and Thelander, L.,. (2004) S phase-specific transcription of the mouse ribonucleotide reductase R2 gene requires both a proximal repressive E2F-binding site and an upstream promoter activating region. *J. Biol. Chem.* 279, 10796-10807.
- (16) Guittet, O., Håkansson, P., Voevodskaya, N., Fridd, S., Gräslund, A., Arakawa, H., Nakamura, Y., Thelander, L. (2001) Mammalian p53R2 protein forms an active ribonucleotide reductase in vitro with the R1 protein, which is expressed both in resting cells in response to DNA damage and in proliferating cells. *J Biol Chem* 276, 40647-40651.
- (17) Pontarin, G., Fijolek, A., Pizzo, P., Ferraro, P., Rampazzo, C., Pozzan, T., Thelander, L., Reichard, P. A., and Bianchi, V. (2008) Ribonucleotide reduction is a cytosolic process in mammalian cells independently of DNA damage. *Proc. Natl. Acad. Sci. U.S.A.* 105, 17801-17806.
- (18) Yamaguchi, T., Matsuda, K., Saqiya, Y., Iwadate, M., Fujino, M. A., Nakamura, Y., Arakawa, H. (2001) p53R2-dependent pathway for DNA synthesis in a p53-regulated cell cycle checkpoint. *Cancer Res.* 61, 8256-8262.
- (19) Chang, L., Zhou, B., Hu, S., Guo, R., Liu, X., Jones, S. N., and Yen, Y. (2008) ATM-mediated serine 72 phosphorylation stabilizes ribonucleotide reductase small subunit p53R2 protein against MDM2 to DNA damage. *Proc. Natl. Acad. Sci. U.S.A.* 105, 18519-18524.
- (20) Liu, X., Xue, L., and Yen, Y. (2008) Redox property of ribonucleotide reductase small subunit M2 and p53R2. *Methods Mol Biol.* 477, 195-206.
- (21) Shao, J. M., Zhou, B. S., Zhu, L. J., Qiu, W. H., Yuan, Y. C., Xi, B. X., and Yen, Y. (2004) In vitro characterization of enzymatic properties and inhibition of the p53R2 subunit of human ribonucleotide reductase. *Cancer Research* 64, 1-6.
- (22) Kauppi, B., Nielsen, B. B., Ramaswamy, S., Larsen, I. K., Thelander, M., Thelander, L. & Eklund, H. (1996) The three-dimensional structure of mammalian ribonucleotide reductase protein R2 reveals a more-accessible iron-radical site than *Escherichia coli* R2. *J Mol Biol* 262, 706-720.
- (23) Sahlin, M., Petersson, L., Gräslund, A., Ehrenberg, A., Sjöberg, B. M., Thelander, L. (1987) Magnetic interaction between the tyrosyl free radical and the antiferromagnetically coupled iron center in ribonucleotide reductase. *Biochemistry* 26, 5541-5548.
- (24) Nyholm, S., Mann, G.J., Johansson, A.G., Bergeron, R.J., Gräslund, A, and Thelander, L. (1993) Role of ribonucleotide reductase in inhibition of mammalian cell growth by potent iron chelators. *J Biol Chem* 268, 26200-26205.
- (25) Nyholm, S., Thelander, L., and Gräslund, A. (1993) Reduction and Loss of the Iron Center in the Reaction of the Small-Subunit of Mouse Ribonucleotide Reductase with Hydroxyurea. 32, 11569-11574.
- (26) Mann, G., Gräslund, A., Ochiai, E.-I., Ingemarson, R., and Thelander, L. (1991) Purification and characterization of recombinant mouse and herpes simplex virus ribonucleotide reductase R2 subunit. *Biochemistry* 30, 1939-1947.
- (27) Zhou, B., Su, L., Shao, J., Yuan, YC., Qi, C., Shih, J., Xi, B., Chu, B., and Yen, Y. (2005) A dityrosyl-diiron radical cofactor center is essential for human ribonucleotide reductases. *Mol. Cancer Ther.* 4, 1830-1836.

- (28) Lunn, C. A., Kathju, S., Wallace, B. J., Kushner, S. R., Pigiet, V. (1984) Amplification and purification of plasmid-encoded thioredoxin from *Escherichia-Coli*-K12. *J Biol Chem* 259, 469-474.
- (29) Russel, M., and Model, P. (1985) Direct Cloning of the Trxb Gene That Encodes Thioredoxin Reductase. *J. Bacteriol.* 163, 238-242.
- (30) Parker, N. J., Begley, C. G., and Fox, R. M. (1991) Human M1 Subunit of Ribonucleotide Reductase - Cdna Sequence and Expression in Stimulated Lymphocytes. *Nucleic Acids Research* 19, 3741-3741.
- (31) Pavloff, N., Rivard, D., Masson, S., Shen, SH., MesMasson, AM. (1992) Sequence analysis of the large and small subunits of human ribonucleotide reductase. *DNA sequence* 2, 227-234.
- (32) Steeper, J. R., Steuart, C.C. (1970) A rapid assay for CDP reductase activity in mammalian cell extracts. *Anal. Biochem.* 34, 123-130.
- (33) Bollinger, J. M., Tong, W. H., Ravi, N., Huynh, B. H., Edmondson, D. E., and Stubbe, J. (1995) Use of Rapid Kinetics Methods to Study the Assembly of the Diferric-Tyrosyl Radical Cofactor of Escherichia-Coli Ribonucleotide Reductase, in *Methods Enzymol.* pp 278-303.
- (34) Ortigosa, A. D., Hristova, D., Perlstein, D. L., Zhang, Z., Huang, M. X., and Stubbe, J. (2006) Determination of the in vivo stoichiometry of tyrosyl radical per beta beta ' in *Saccharomyces cerevisiae* ribonucleotide reductase. *Biochemistry* 45, 12282-12294.
- (35) Hristova, D., Wu, C. H., Jiang, W., Krebs, C., and Stubbe, J. (2008) Importance of the maintenance pathway in the regulation of the activity of Escherichia coli ribonucleotide reductase. *Biochemistry* 47, 3989-3999.
- (36) Wei, P., Tomter, AB., Rohr, AK, Andersson, KK., and Solomon, EI. (2006) Circular dichroism and magnetic circular dichroism studies of the active site of p53R2 from human and mouse: iron binding and nature of the biferrous site relative to other ribonucleotide reductases. *Biochemistry* 45, 14043-14051.
- (37) Xu H, F., C., Uchiki, T., Fairman, JW., Racca, J., and Dealwis, C. (2006) Structures of eukaryotic ribonucleotide reductase I provide insights into dNTP regulation. *Proc. Natl. Acad. Sci. U S A.* 103, 4022-4027.
- (38) Zhou, B. S., Shao, J., Su, L., Yuan, Y.C., Qi, c., Shih, J., Xi, B., Chu, B., and Yen, Y. (2005) A dityrosyl-diiron radical cofactor center is essential for human ribonucleotide reductases. *Mol Cancer Ther* 4, 1830-1836.
- (39) Wu, C. H., Jiang, W., Krebs, C., Stubbe, J. (2007) YfaE, a ferredoxin involved in diferric-tyrosyl radical maintenance in Escherichia coli ribonucleotide reductase. *Biochemistry* 46, 11577-11588.

Chapter 3

Inactivation studies of Human Ribonucleotide Reductase by Gemcitabine

Adapted from Wang J, Lohman GJ, Stubbe J. (2006) Enhanced subunit interactions with gemcitabine-5'-diphosphate inhibit ribonucleotide reductases. Proc Natl Acad Sci U S A. 104(36):14324-9

3.1 Introduction

2',2'-Difluoro-2'-deoxycytidine (gemcitabine, F₂C) is a drug that is used clinically in the first line treatment for advanced pancreatic cancer and non small cell lung carcinomas (1-3). As it is described in Chapter 1, the diphosphorylated F₂C is a potent mechanism based inhibitor of class I RNR. Studies on the inactivation of *E. coli* RNR by F₂CDP were carried out and reported by our group several years ago (4, 5). It was shown that one equivalent (eq.) of F₂CDP per *E. coli* RNR ($\alpha_2\beta_2$), in the presence of reductants, thioredoxin (TR) and TR reductase or dithiothreitol (DTT), is sufficient for enzyme inactivation. The inactivation was accompanied by release of 2 fluoride ions and one cytosine (Figure 3.1) (4).

The inhibition in the absence of reductants was also studied. A new and stable radical was formed concomitant with the loss of Y•. Carrying out the inhibition by F₂CDP in D₂O or with uniformly deuterated α did not change the EPR spectrum of the new radical, suggesting that the hyperfine interactions are not associated with solvent or α . Recently, Artin in the Stubbe lab showed that inactivation with 1'-[²H]-F₂CDP caused collapse of the triplet signal to a doublet, indicating that one of the couplings is associated with the nucleotide (6). The source of the 2nd hyperfine interaction has not been established, but is postulated to be associated with the 4'-H of F₂CDP. This postulation is based on the similarity of its EPR spectrum with that resulting from interaction of E441Q RNR with CDP. The proposed structure is shown in Figure 3.1.

Studies with several mutants of RNR have defined further the requirements for its formation. F₂CDP with C754S, C759S generate the same radical as did oxidized α , that

C225 and C462 in a disulfide form. Thus 4 of the 5 essential cysteines are not required for radical formation.

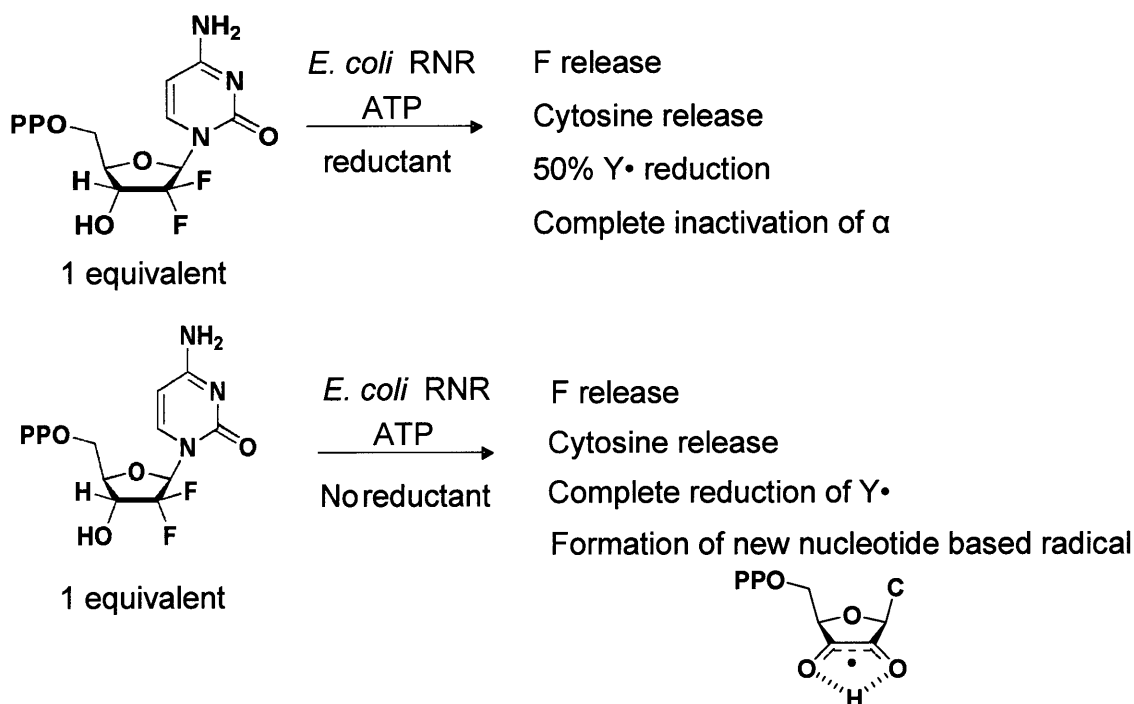


Figure 3.1: Products accompanying *E. coli* RNR inactivation (4).

While many parallels lie between inactivation by F₂CDP and 2'-substituted CDP analogs, subtle differences exist that are mechanistically important. The F₂CDP mechanism involves inactivation of both α and β subunits as do all 2'-substituted nucleotide inhibitors. However, unlike other 2'-substituted nucleotide inhibitors where DTT protects α from inactivation, DTT is required for α inhibition by F₂CDP. With 2'-deoxy-2'-halonucleotides, an electrophilic furanone derivative is generated resulting in RNR inactivation. This reactive sugar is alkylated by cysteines of α or by the thiols of DTT. Alkylation of furanone by the C-terminal tail cysteines of α followed by reaction with K760 produces a chromophore that absorbs between 320-330 nm. This chromophore has not been detected after RNR

inactivation by F₂CDP, indicating that the reaction might happen here in the active site where structure analysis reveals the absence of a lysine.

In addition, the inactivation of the *L. leichmannii* RTPR by F₂CTP has also been studied (7, 8). One eq. of F₂CTP can rapidly inactivate 90% of the activity in 15 s. The inactivation can happen in the presence and absence of external reductants. The synthesis of [1'-³H] and [5-³H]-F₂CTP has made it possible to quantitate the end products of the inactivation process. After inactivation, 0.47 eq. ribose ring from F₂CTP covalently labeled RTPR and 0.16 eq. of cytosine remained attached to the enzyme, while 0.7 eq. cytosine is released. Moreover, about 0.8 eq. of 5'-dA per RTPR was released and on a very slow time scale the protein was alkylated by an AdoCbl-derived species. Glu-C digestion of the covalent modified RTPR at pH 5.8 followed by HPLC separation identified a peptide containing a cobalamin chromophore. Further characterization of the peptide by N-terminal sequencing revealed that it contained residues 411-420 and an adduct attached to the active site residue C419, one of the bottom face reducing equivalents. A Co-S linkage was detected suggesting that the chemistry happened within the active site.

Rapid freeze quench EPR and stopped flow UV-vis spectroscopy were used to study the kinetics of the inactivation. A thiyl radical exchange coupled to cob(II)abamin species was first detected at 22 ms, followed by the formation of a new nucleotide-based radical, concomitant with disappearance of the initial thiyl radical over the subsequent 255 ms.

The details of the inhibition by F₂CDP have remained largely unexplored due to the unavailability of radiolabeled sugar and base F₂CDP. Dr. Greg Lohman in our group

has recently developed methods to synthesize [$1\text{'-}^3\text{H}$] and [$5\text{-}^3\text{H}$]- F_2CDP (7, 8), which has allowed us to re-investigate the mechanism of inhibition of the *E. coli* RNR and to study for the first time the details of the inhibition of the human RNR. Incubation of human and *E. coli* RNRs with [$1\text{'-}^3\text{H}$] or [$5\text{-}^3\text{H}$] F_2CDP in the presence of reductant results in one eq. of sugar covalently bound per α_2 , and one cytosine released per α_2 , agreeing well with our previous studies on *E. coli* RNRs.

To investigate how sub-stoichiometric labeling can prevent nucleotide reduction, size exclusion chromatography has been employed to study the effect of F_2CDP on the RNR subunits interaction. In prokaryotic systems α and β are both homodimers. The active *E. coli* RNR is thought to be an $\alpha_2\beta_2$ complex (9, 10). The α of eukaryotic RNR can be a monomer, dimer, tetramer or hexamer based on the presence of allosteric effectors (dATP, TTP, dGTP, ATP) (11, 12). In the absence of nucleotides α is a monomer. The millimolar levels of ATP found intracellularly cause α to oligomerize to a hexamer (α_6). β is a homodimer (β_2). The complex responsible for RNR activity has been proposed by Cooperman and coworkers to be $\alpha_2\beta_2$, $\alpha_6\beta_2$ or $\alpha_6\beta_6$ based on a variety of physical biochemical and kinetic studies (12). Recent Gas-Phase Electrophoretic-Mobility Macromolecule Analysis studies have suggested that the mouse quaternary structure is $\alpha_6\beta_2$ (13).

Studies using size exclusion chromatography of the inactivated RNRs reveal that sub-stoichiometric labeling of α dramatically alters α_n/β_n subunit interactions, forming a tight complex, which is ultimately responsible for complete RNR inhibition. In the *E. coli* RNR, a $\alpha_2\beta_2$ tight complex is generated subsequent to enzyme inactivation by F_2CDP , while in the human RNR, a $\alpha_6\beta_6$ tight complex is generated. This information, and the

proposed asymmetry between the interactions of $\alpha\eta\beta\eta$, provides an explanation for complete inactivation of RNR with sub-stoichiometric amounts of F_2CDP .

Furthermore, mutagenesis studies have been carried out replacing all the key residues in the active site and C-terminal tail of α to identify the site of labeling.

3.2 Materials and Methods

3.2.1 Materials

[5- 3H] F_2C and 2-deoxy-3,5-di-*O*-benzoyl-3,3-difluororibonolactone were kind gifts of Eli Lilly. Competent *E. coli* BL 21 (DE3) cells were purchased from Stratagene. Complete EDTA-free protease inhibitor tablets and calf alkaline phosphatase (20 U/ μ L) were purchased from Roche Biochemicals. Plasmids containing the genes for α (formerly called H1) and β (formerly called H2), phRRM1 and phRRM2, were generous gifts from Yun Yen (City of Hope National Medical Center). Protein concentrations were determined by using extinction coefficients ($\epsilon_{280\text{ nm}}$) per monomer [45,900 $M^{-1} \text{ cm}^{-1}$ for (His) $_6$ - β , 119,160 $M^{-1} \text{ cm}^{-1}$ for α]. *E. coli* TR (specific activity of 40 U/mg) (14) and TR reductase (specific activity of 1320 U/mg) (15) were isolated as previously described.

3.2.2 Expression and purification of human α , α mutants and β

phRRM1 and phRRM2 were transformed into *E. coli* BL21 (DE3) (Stratagene), plated on LB agar plates with 50 μ g /mL kanamycin (kan) and a single colony chosen for growth. For isolation of β , an overnight culture (40 mL) grown to saturation was diluted into 2 L of LB containing 50 μ g/mL kan and grown at 37°C to $OD_{600\text{ nm}}$ 0.7- 0.9.

Isopropyl-1-thio- β -D-galactopyranoside (IPTG, 1mM) was then added and the cells were

grown for an additional 6 h at 30°C. For growth of α , an overnight culture (40 mL) was grown from a single colony at 37°C and transferred to a 2L of LB and grown at 37°C. IPTG (1 mM) was added at an OD_{600nm} 0.7- 0.9 and the cells were grown overnight (16 h) at 25°C. The cells were harvested and typically yielded 4 g/L.

The isolation of $\beta 2$ and α were carried out by the following general procedure. The cell pellets were suspended (5 vol/g) in 50 mM NaH_2PO_4 , pH 7.0, 0.1% Triton X-100, 10 mM 2-mercaptoethanol, and cocktail protease inhibitor (1 tablet / 10 mL, Roche). The suspension was passed through the French press at 14,000 psi. The cell lysate was centrifuged at 20,000 x g for 30 min. The supernatant was treated with streptomycin sulfate to a final concentration of 1% (w/v) and the pellet was removed by centrifugation. The supernatant was incubated with Ni-NTA agarose resin (1 mL/g of cells, Qiagen) at 4°C for 1 h and then loaded into a column (2.5 x 10 cm). The column was subsequently washed with 40 column volumes of 50 mM NaH_2PO_4 , 800 mM NaCl, 50 mM imidazole, pH 7.0, 0.1% Triton X-100 and 10 mM 2-mercaptoethanol. The protein was eluted with 50 mM NaH_2PO_4 , 300 mM NaCl, 125 mM imidazole, pH 7.0. Fractions containing protein were identified using the Bradford assay. The fractions were pooled and concentrated to < 10 mL, and then the imidazole was removed by Sephadex G-25 chromatography (200 mL, 2.5 x 50 cm). $\beta 2$ was stored in 50 mM Tris, 100 mM KCl, pH 7.6, 5% glycerol. α was stored in 50 mM Tris, 100 mM KCl, 15 mM $MgCl_2$, 5 mM DTT, pH 7.6, 5% glycerol. Protein yields of α and β were about 2 mg and 15 mg per L of culture, respectively. The mutants of α were purified following the same protocol as described for wt α with similar yields.

3.2.3 Activity assays

A reaction mixture contained in a final volume of 350 μL : 50 mM Hepes (pH 7.6), 15 mM MgCl_2 , 1 mM EDTA, 0.3 μM (or 2.1 μM) α , 2.1 μM (or 0.3 μM) β , 3 mM ATP, 1mM [^3H]-CDP (specific activity 3400 cpm /nmol), 100 μM *E.coli* TR, 1.0 μM TR reductase, 2 mM NADPH. The assay mixture was preincubated at 37 $^\circ\text{C}$ for 3 min and the reaction was initiated by the addition of CDP. Aliquots of 50 μL were removed over a 15 min time period and quenched in a boiling water bath. dCDP production was analyzed by the method of Steeper and Steuart (16).

3.2.4 Time dependent inactivation studies.

The inactivation mixture contained in a final volume of 100 μL : 1.2 μM α , 1.2 μM β , 3 mM ATP, 1 mM [^3H]-CDP (specific activity 3400 cpm /nmol), in the presence or absence of 5 mM DTT, 50 mM Hepes (pH 7.6), 15 mM MgCl_2 , and 1mM EDTA. The reaction was initiated by addition of F_2CDP (0.6 μM , 1.2 μM and 6 μM , final concentrations) and incubated at 37 $^\circ\text{C}$. Aliquots (12.5 μL) were removed from 30 s to 17 min, and assayed for dCDP production as described above. Control experiments were carried out in which the F_2CDP was omitted.

3.2.5 Quantitation of covalent labeling of *E.coli* RNR and human RNR with [$1\text{'-}^3\text{H}$]- F_2CDP and [$5\text{-}^3\text{H}$]- F_2CDP

A typical reaction mixture (5.5 μM α , β in 300 μL) was identical to that described above except that F_2CDP was replaced by either [$1\text{'-}^3\text{H}$]- F_2CDP (5889 cpm /nmol) or [$5\text{-}^3\text{H}$]- F_2CDP (6643 cpm/nmol). After 10 min at 37 $^\circ\text{C}$, an aliquot of 270 μL was loaded

onto a Sephadex G-50 column (1 cm x 20 cm, 20 mL) that was pre-equilibrated with the assay buffer (50 mM Hepes, 15mM MgCl₂, 1mM EDTA, pH7.6) or made 6 M in guanidine-HCl and loaded onto a Sephadex G-50 column with assay buffer containing 2 M guanidine-HCl. Fractions (1 mL) were collected and assayed for A_{280nm} and A_{260nm} and 500 µL of each fraction was analyzed by scintillation counting.

3.2.6 Quantification of cytosine released during the inactivation of *E. coli* and human RNR by [5-³H]-F₂CDP

The reaction mixture was as described above (1.2 µM human RNR α, β in 500 µL). The reaction was initiated by addition of 1.2 µM [5-³H]-F₂CDP (6643 cpm/nmol). After 20 min, the inactivation mixture was filtered through an YM-30 Centricon device (Millipore) at 4°C. F₂C (120 nmol) and cytosine (120 nmol) were added as carriers before filtration. The flow-through was treated with 30 U of alkaline phosphatase (Roche) for 3 h at 37 °C and filtered through a second YM-30 Centricon device. The flow through was analyzed using a Waters 2480 HPLC with an Altech Adsorbosphere Nucleotide Nucleoside C-18 column (250 mm x 4.6 mm) at a flow rate of 1mL/min. The elution buffer contained: Buffer A, 10 mM NH₄OAc, pH 6.8; Buffer B: 100% methanol. A 10 min isocratic elution was followed by a linear gradient to 40% B over 30 min. A linear gradient was then run to 100% B over 5 min. Fractions (1 mL) were collected and 200 µL of each were analyzed by scintillation counting. Standards: retention times are: cytosine, 5.7 min; cytidine, 12.6 min; *ara*-C, 17.4 min; dC, 19.0 min and F₂C, 23.2 min. The recovery of cytosine and F₂C was calculated based on the UV spectrum (cytosine, λ_{267 nm},

$\epsilon = 6100 \text{ M}^{-1}\text{cm}^{-1}$, F_2C , $\lambda_{268 \text{ nm}}$, $\epsilon = 9360 \text{ M}^{-1}\text{cm}^{-1}$). The radioactivity recovered with cytosine and F_2C was analyzed by scintillation counting.

3.2.7 SEC to examine the quaternary structure of RNRs subsequent to inactivation by F_2CDP

SEC was performed using a Superose 12 column (10 x 300 mm, GE healthcare) for *E. coli* RNR or a Superdex 200 column (10 x 300 mm, GE healthcare) for human RNR attached to a Waters 2480 HPLC. Gel filtration molecular weight standards (GE healthcare) were ovalbumin, 43 kDa; conalbumin, 75 kDa; aldolase, 158 kDa; pyruvate kinase, 232 kDa or catalase 232 kDa; ferritin, 440 kDa; thyroglobulin, 669 kDa; and blue dextran, 2000 kDa. The elution buffer was 50 mM Hepes (pH 7.6), 15 mM MgCl_2 and 0.5 mM ATP. KCl (150 mM) was added in the running buffer to separate *E. coli* RNR \pm F_2CDP in the presence of ATP on the Superose 12 column. Molecular weight standards were run at the beginning of each experiment. The reaction mixture was prepared as described above (15 μM α , β in 300 μL or 30 μM α , β in 150 μL). After 10 min incubation, 150 μL or 300 μL was injected onto the column. The elution rate was 0.5 mL/min and 0.5 mL fractions were collected. If [$1\text{'-}^3\text{H}$]- F_2CDP was used in the inactivation, 100 μL aliquots of each fraction was analyzed by scintillation counting.

3.2.8 Quantitative analysis of the subunits of *E. coli* and human RNRs by SDS PAGE.

The fractions collected from the SEC analysis were analyzed by 10% SDS- PAGE and compared with concentrations of α and β from *E. coli* RNR (0.4 μM to 3.2 μM) or

human RNR (0.2 μ M to 1.6 μ M) as standards. The proteins were visualized with Coomassie blue staining. The band intensities were quantified using Bio-Rads Quantity One software. The concentrations of α and β in the complex were determined from the standard curves.

3.2.9 Trypsin digestion of human RNR inactivated with [1'-³H]-F₂CDP

The reaction contained a final volume of 500 μ L: 7.7 μ M α , β , 3 mM ATP, 5 mM DTT, in 50mM Hepes, pH 7.6, 15mM MgSO₄, 5% glycerol, 1mM EDTA. 19.5 μ M [1'-³H]-F₂CDP (2.5 fold, SA 7584 cpm / nmol,) was used to initiate the reaction, and incubated at 37 °C for 8 min. The reaction was quenched with 1500 μ L 8M guanidine, 40 mM DTT, 5.33 mM EDTA, 400 mM Tris (pH 8) and the reaction was incubated at 37°C for 30min. Iodoacetamide was added to a final concentration of 250 mM and the reaction was incubated at 37°C for additional 1 h. The small molecules were removed by a Sephadex G-50 column (1 cm x 40 cm, 40 mL) to equilibrate in 100 mM NH₄HCO₃, 2M urea, pH 8.0. Fractions containing protein were identified using the Bradford assay. A typical recovery is 70%. Trypsin (Worthington, lot # 35J8187, ~ 20 μ L) was added from a freshly prepared stock to a final concentration 4:1 (w/w) RNR: trypsin and incubated for 5 h at 37°C. The reaction was quenched by addition of 60 μ L TFA to pH < 2. The peptides were loaded immediately on a Phenomenex Jupiter C18 peptide column (150 x 4.6 mm, 5 micron, 300 A pore size) by a 5 mL loop, and separated on a Waters 2487 HPLC at a flow rate of 1 mL/min. The solvent system was: Buffer A, 0.1% TFA in H₂O, Buffer B, 0.1% TFA in acetonitrile. A linear gradient of 0-45% B over 90 min was used. Fractions (1 mL) were collected and analyzed for radioactivity by scintillation counter.

The recovery of injected radioactivity was 85%, and 20% of the radioactivity eluted in the void volume of the column. The recovery of each region of radioactivity is reported in the results section below.

3.2.10 In gel Trypsin digestion and Mass spectrometry

In gel trypsin digestion on the F₂CDP inactivated human RNR and mass spectrometry analysis was performed by Brad Evans in Prof. Neil Kelleher's lab in University of Illinois, Urbana-Champaign for mass spectrometry. The reaction contained a final volume of 250 μ L: 7.7 μ M α , β , 3 mM ATP, 5 mM DTT, in 50mM Hepes, pH 7.6, 15mM MgSO₄, 5% glycerol, 1mM EDTA, 19.5 μ M (2.5 fold) of 1:1 mixed [1'-³H]-F₂CDP and [1'-D]-F₂CDP was used to initiate the reaction, and incubated at 37 °C for 8 min. The reaction was quenched with 750 μ L 8M guanidine, 40 mM DTT, 5.33 mM EDTA, 400 mM Tris (pH 8) and the reaction was incubated at 37°C for 30min. Iodoacetamide was added to a final concentration of 250 mM and the reaction was incubated at 37°C for additional 1 h. 300 μ L reaction mixture was loaded onto a 10% SDS-PAGE. After stain and destain the gel, gel slices containing α and β were cut out individually and dried in a speed vacuum without heating. To the dried gel slices, a solution of 12.5 ng/mL trypsin in 100 mM ammonium carbonate pH 8 was added to enough cover the slices. Digestion was carried out overnight at 25 °C. To extract the digested peptides, a solution with 50 mM ammonium carbonate pH 8 was added and mixed for 5 min. After removing the supernatant, 50% ammonium carbonate and 50% acetonitrile were added, mixed for 5 min and the supernatant was removed again. This aqueous/organic wash was repeated 3 times. For each time, the volume of the solution

added was just enough to cover the slices. Then washes with 100% acetonitrile followed by 100% ammonium carbonate were repeated twice. At the end, the peptide containing solution was concentrated by a speed vacuum to near dryness and then brought up to 35 μL in 0.1% acetic acid before injection onto C18 reversed phase nano LC column (10 cm x 75 μm) and analyzed. The flow rate is 300 nL/min. The mass spectrometry method was 5th order double play using 12T-FT-ICR-MS detection for MS and MS/MS with CID fragmentation. Data was analyzed manually as well as with ProSight PC.

3.3 Results

3.3.1 Time Dependent Inactivation of Human RNRs

Time dependent inactivation studies on the human RNR were carried out in the presence of reductants. The inactivation mixture contained 0.5 or 5.0 eq. of $\text{F}_2\text{CDP}/\alpha$ and revealed that 0.5 eq. of $\text{F}_2\text{CDP}/\alpha$ results in complete loss of RNR activity (Figure 3.2). The instability of the β_2 radical requires that a control in the absence of F_2CDP be carried out and used to correct the data observed in its presence. The weak interaction between α and β of RNR allow assays of the subunit activity individually (17, 18). Thus, the inactivation mixture was assayed as a 1:1 mixture of subunits (Figure 3.3) for activity of α (β) in the presence of a seven-fold excess of β (α). Under the latter conditions, α is 100% inactivated. β , on the other hand retained 60% of its activity (Figure 3.3) suggesting that the excess α is capable of facilitating subunit dissociation. The results of these experiments have interesting implications in recovering RNR activity *in vivo* subsequent to its inactivation by F_2CDP .

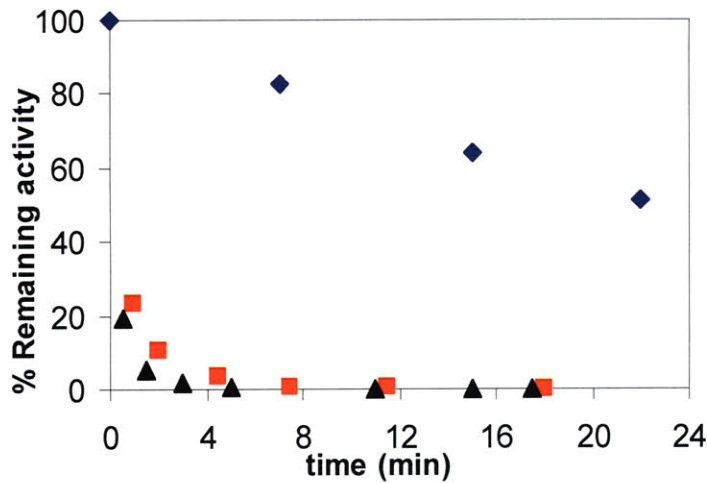


Figure 3.2. Time-dependent inactivation of human RNR by F₂CDP.

The inactivation mixture contained final concentrations of α , β , 1.2 μM ; F₂CDP, 0.6 μM (■) and 6 μM (▲); ATP, 3mM; DTT, 5mM. Aliquots were removed at various times and diluted 4 fold for determination of RNR activity. Control experiment (◆) is identical to the experiment except that F₂CDP was omitted.

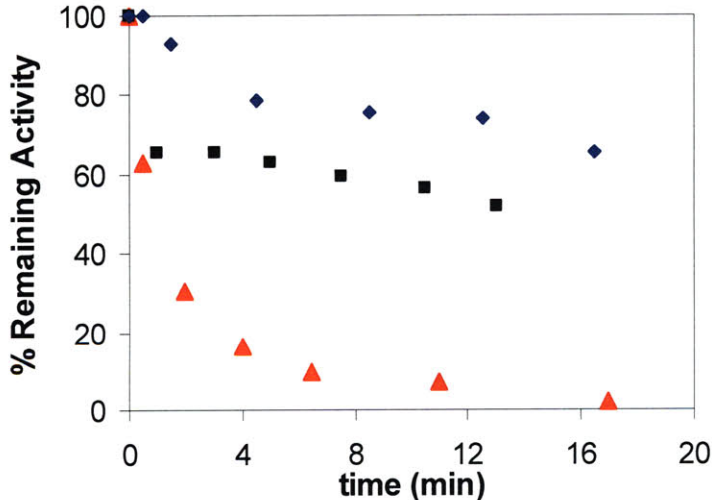


Figure 3.3. Time-dependent inactivation of human RNR by F₂CDP.

The inactivation mixture contained final concentrations of α , β , 1.2 μM ; F₂CDP, 0.6 μM ; ATP, 3mM; DTT, 5mM. Aliquots were removed at various times and diluted 4 fold for determination of α (▲) and β (■) activity in the presence of 7 fold excess of β or α . The activity of β (■) was adjusted using results from the control experiment (◆) for β activity, which is identical to the experiment except that F₂CDP was omitted.

3.3.2 Quantitation of covalent labeling of human and *E. coli* RNR inactivated by [1'-³H] and [5-³H]-F₂CDP

The previous studies of F₂CDP inactivation of *E. coli* RNR were carried out using unlabeled inhibitor. The results were provocative in that one mole of F₂CDP inactivated 1 mole of $\alpha_2\beta_2$ which has two active sites. The synthesis of [1'-³H]-F₂CDP and [5-³H]-F₂CDP allowed us to re-investigate the mechanism of RNR from *E. coli* and track the fate of the sugar ring and the base. Incubation of 15 μ M α_2 and 15 μ M β_2 with 15 or 30 μ M of [1'-³H]-F₂CDP in the presence of 5 mM DTT resulted in recovery of 0.9 (1.1) moles of radiolabel/RNR ($\alpha_2\beta_2$) from analysis of the reaction mixture that was passed through a Sephadex G50 column in the absence or presence of denaturant after 20 min incubation at 25 °C (Table 3.1). With the [5-³H]-F₂CDP, 0.19 and 0.08 eq. were detected in the absence or presence of denaturant, respectively. These results establish that there is one eq. of the sugar from F₂CDP covalently bound to the enzyme and that most of the cytosine has been released. In addition, under these conditions 40% of the tyrosyl radical is lost similar to our previous studies (4).

Incubation of [1'-³H] or [5-³H]-F₂CDP with human RNR followed by Sephadex G50 chromatography under native and denaturing conditions gave the results summarized in Table 3.1. With the [1'-³H] F₂CDP 0.8-0.85 labels were bound per α_2 , while with the [5-³H] only 0.1 labels were retained with the protein. The results are very similar to those observed with the *E. coli* RNR, with the unusual stoichiometry of 1 F₂CDP per α_2 observed. These results in conjunction with the time-dependent inactivation studies, establish that sub-stoichiometric amounts of F₂CDP completely inactivate the human and *E. coli* RNR.

Table 3.1. Covalent labeling of *E. coli* and human RNR with [1'-³H]-F₂CDP and [5-³H]-F₂CDP analyzed by SEC.

Protein	[³ H]-F ₂ CDP	Conditions	Reductants	[³ H]/α2
<i>E. coli</i> RNR	1'	native	Y	0.9
	1'	denaturing	Y	1.11
	5	native	Y	0.19
	5	denaturing	Y	0.08
human RNR	1'	native	Y	0.85
	1'	denaturing	Y	0.8
	1'	native	N	0.1
	5	native	Y	0.1
	5	native	N	0.1

3.3.3 Cytosine release by human RNR

The inactivation studies suggested that covalent modification is accompanied by cytosine release. To test this hypothesis, two eq. of [5-³H] F₂CDPs were incubated with α2β2. Subsequent to inactivation the nucleotides were recovered by ultrafiltration and analyzed by HPLC. The analysis revealed one eq. of cytosine and one eq. of F₂CDP (Figure 3.4). These results parallel those previously reported for inactivation of *E. coli* RNR (4) and support the model that inactivation can be achieved with sub-stoichiometric amounts of F₂CDP.

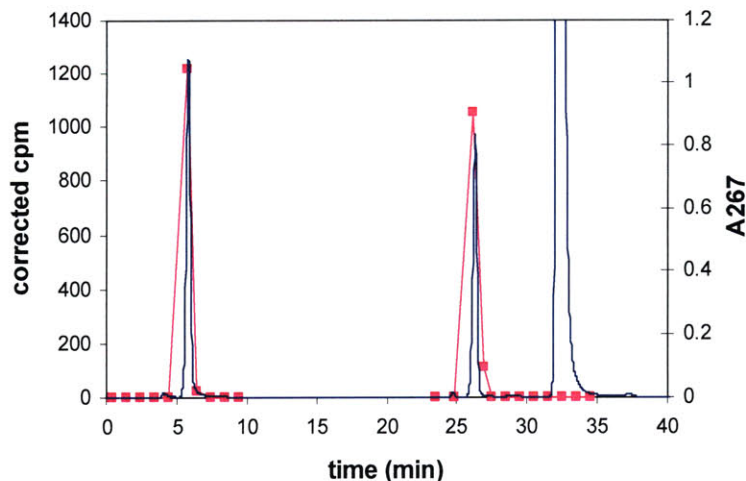


Figure 3.4. Analysis by HPLC of products generated during inactivation of human RNR and *E. coli* RNR by [5-³H]-F₂CDP.

The inactivation mixture contained final concentrations of α , β^1 , 1.2 μM ; [5-³H]-F₂CDP, 1.2 μM , 3mM ATP, 5mM DTT subsequent to removal of the protein from the small molecules by YM3 centricon, the filtrate was injected into Altech Adsorbosphere Nucleotide Nucleoside C-18 column at a flow rate of 1mL/min. The elution buffer contained: Buffer A, 10 mM NH₄OAc, pH 6.8; Buffer B: 100% methanol. A 10 min isocratic elution was followed by a linear gradient to 40% B over 30 min. The elution profile monitored by A_{280nm} (-) and scintillation counting (■). 1 cytosine / $\alpha_2\beta_2$ was released, 0.83 F₂C/ $\alpha_2\beta_2$ was recovered.

3.3.4 Subunit interactions of *E. coli* RNR in the presence of F₂CDP

The active form of *E. coli* RNR is thought to be a 1:1 mixture of α_2 and β_2 , although there is only one Y• per β_2 providing one piece of evidence that the active RNR complex is asymmetric. One way to achieve complete inactivation of $\alpha_2\beta_2$ with 1 F₂CDP is that once chemistry has occurred in the active site of the first α , it precludes chemistry from occurring in the active site of the second α . This chemistry further leads to a tight complex between the two subunits preventing recycling of the unmodified α . To test this model the inactivation mixture and a number of controls (including one with a mixture of α , β , and ATP) were examined using SEC on a Superose 12 FPLC column.

All elution buffers contained either 0.5 mM ATP or 100 μ M TTP previously shown to enhance α_2 formation (10, 19, 20) and more recently to enhance $\alpha_2\beta_2$ interactions (20).

The results of SEC analysis of RNR inactivated with F_2 CDP/ATP, with ATP in the elution buffer, are summarized in Figure 3.5 (A-C) and Table 3.2. Figure 3.5A reveals a single protein peak. Fractions collected through the protein peak were analyzed by scintillation counting and by SDS PAGE. The former revealed 0.9 labels per $\alpha_2\beta_2$ (Figure 3.5 A). The SDS PAGE analysis (Figure 3.5 B) revealed the presence of α and β . Their relative ratios were determined in each fraction by comparison with standard curves made with known concentrations of α and β (Figure 3.5 B) and found to be approximately 1:1 (Figure 3.5 C).

A control SEC analysis in the absence of F_2 CDP, with ATP in the elution buffer reveals separation of α_2 and β_2 (Figure 3.5 D and 3.5 E). Analysis of the ratio of α : β supports this conclusion (Figure 3.5 F). The analysis in Figure 3.5 suggests that a tight complex between subunits is unique to the presence of F_2 CDP.

Since the sub-stoichiometry inactivation is similar to another mechanism based inhibitor, 2'-azido-2'-deoxynucleotides (N_3 NDP) (21-23). With [5 '- 3 H] N_3 NDPs inactivation, >90% of RNR activity was lost in 2 min, 50% of $Y\cdot$ was reduced and 0.7 eq radiolabel are associated with RNR. Inactivation was carried out with equal molar α , β incubated with N_3 UDP, ATP, TR, TRR. A similar SEC experiment provides no evidence for an $\alpha_2\beta_2$ complex (Figure 3.6). It suggests that the chemistry associated with N_3 NDP is different that of F_2 CDP.

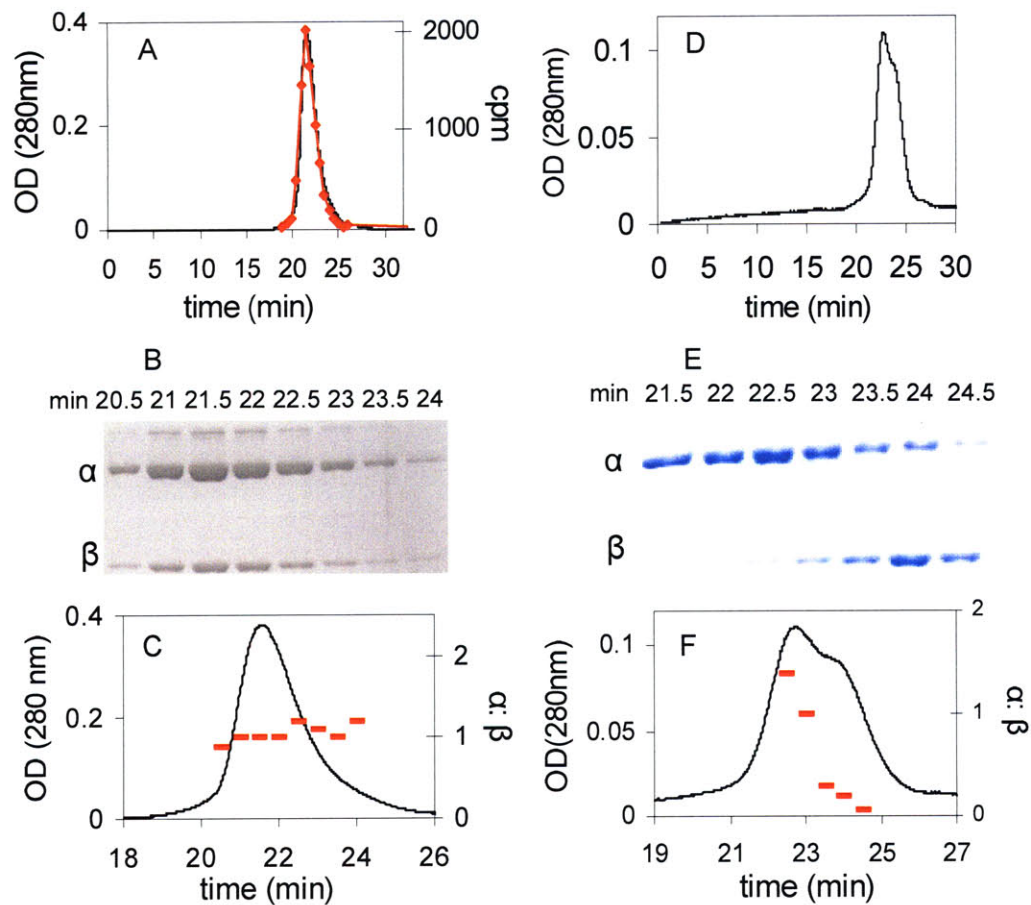


Figure 3.5. SEC on a Superose 12 column to detect complex formation ($\alpha_2\beta_2$) in *E. coli* RNR incubated with ATP in the presence or absence of $[1\text{'-}^3\text{H}] \text{F}_2\text{CDP}$. Elution buffer contains 0.5 mM ATP. A-C presence of F_2CDP : A, the elution profile monitored by $A_{280\text{nm}}$ and scintillation counting (\blacklozenge). B, fractions through the protein peak in A monitored by SDS PAGE. Note the slower migrating band (5% of the protein) is an altered conformation of α . C, analysis of the ratio of $\alpha:\beta$ (-), using standard curves generated from known amounts of α and β . D-F absence of F_2CDP : D, the elution profile; E, fractions through the protein peak in D monitored by SDS PAGE. F, analysis of the ratio of $\alpha:\beta$, using standard curves generated from known amounts of α and β .

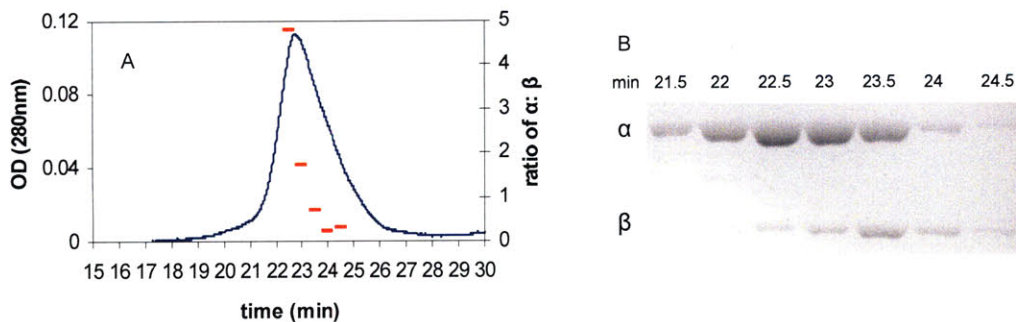


Figure 3.6. Control experiment, α and β inactivated with N_3 UDP.

(A) Equal molar *E. coli* [α] = [β] = $10\mu\text{M}$, $N_3\text{UDP}=5\mu\text{M}$, [ATP] = 1.6mM , [TR] = $20\mu\text{M}$, [TRR] = $0.5\mu\text{M}$. The mixture was loaded onto superose 12 column after 2 min inactivation at 25°C . The mobile phase contained 0.5mM ATP in the 50mM Hepes, 150mM KCl, 15mM MgCl_2 , pH7.6 running buffer. (–) ratio of α : β . (B) Fractions collected from 21.5min to 24.5min, show that α peak eluted first then overlap with β peak at the fraction eluted at 23min.

Table 3.2. Molecular Weight Determination of *E. coli* and human RNR and their subunits by SEC.

	Protein (effector)	Apparent mass (kDa)	Expected mass (kDa)	Retention Time (min)	Oligomeric state
<i>E. coli</i> RNR	β	96	87	25.4	β_2
	α^a	143, 105	172, 86	24.9	α_2, α
	α ($100\mu\text{M}$ TTP)	174	172	24	α_2
	α (0.5mM ATP)	174	172	24	α_2
	α, β^a	156, 108	172, 87	23	α_2, β_2
	α, β (ATP) ^b	167, 109	172, 87	22.5, 23.6	α_2, β_2
	α, β inactivated by F_2CDP^b	277	259	22	$\alpha_2\beta_2$ complex
human RNR	β	108	94	26.3	β_2
	α	88	92	25.6 ^d	α
	α ($100\mu\text{M}$ TTP)	189	184	24 ^d	α_2
	α, β (ATP)	589, 94	553, 94	21, 25.8	α_6, β_2
	α, β inactivated by $\text{F}_2\text{CDP}^{b,c}$	872	834	19.1	$\alpha_6\beta_6$ complex

a: The HPLC trace indicates multiple species. Gaussian fits to the peak shape using Origin 6.1 gave the peak retention times. b: Elution buffer contains 0.5mM ATP. Fractions were collected through the protein peak and were analyzed by 10% SDS-PAGE as summarized in Figure 3.5 (A-F) or Figure 3.9. c: apparent mass 872 kDa ($\alpha_6\beta_6$, 834 kDa) based on standard curve (Figure 3.7). d: Superose 12 column was used

Further experiments were carried out to assess the resolution of the SEC method and to obtain information about the relative molecular weights of the observed protein peaks. The behavior of the individual subunits and complex were examined. In the absence of nucleotides, α migrates as a mixture of monomer and dimer with apparent molecular weights of 105 and 143 KDa (Table 3.2), respectively. The apparent molecular weights are obtained by comparison of the retention times of the eluting proteins with retention times of known molecular weight standards. With ATP or TTP in the running buffer, α now migrates as a dimer (α_2) of 174 KDa (Table 3.2 and Figure 3.7). When RNR is inactivated by [$1'$ - 3 H] F₂CDP/ATP and chromatographed with ATP in the running buffer, the protein has an apparent molecular weight of 277 KDa (Figure 3.4 A and Figure 3.7). The SEC analysis presented in Figure 3.5 A-C, the stability of the complex during the inactivation reaction and the subsequent 25 min chromatography, and the apparent molecular weight suggests that the active form of RNR is $\alpha_2\beta_2$ and that the interaction between the subunits has dramatically increased relative to the non-nucleotide bound forms (Table 3.2).

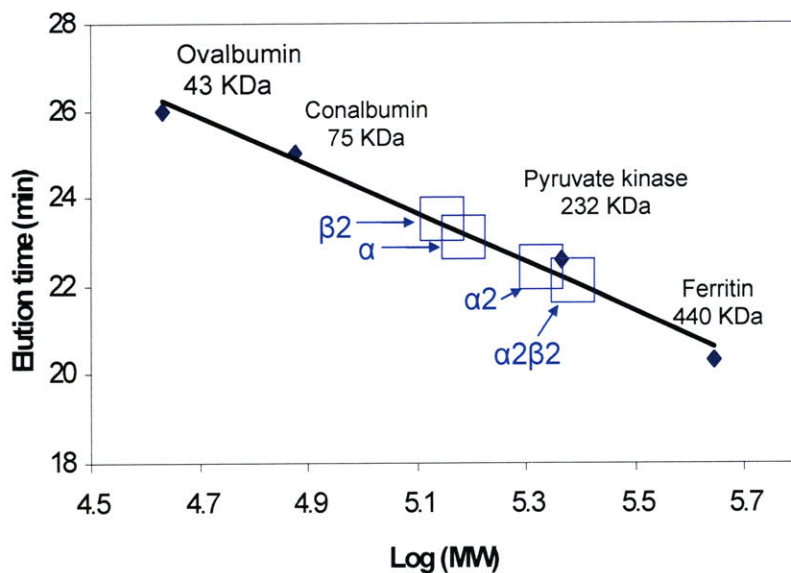


Figure 3.7. SEC on Superose 12 column to determine the molecular weight of the α , $\alpha 2$, $\beta 2$ and $\alpha 2\beta 2$ in *E. coli* RNR.

The mobile phase contained 0.5mM ATP in the 50 mM Hepes, 15 mM MgCl₂, pH7.6 running buffer. α was eluted with buffer containing 100 μ M TTP. α and β were eluted in buffer containing 0.5 mM ATP.

3.3.5 Subunit Interactions of Human RNR in the presence of F₂CDP

A similar set of experiments has been carried out with the human RNR. The Cooperman lab has demonstrated that in contrast with the prokaryotic RNRs, the active mouse RNR can be $\alpha 2\beta 2$, $\alpha 6\beta 2$ and $\alpha 6\beta 6$ depending on the concentration of ATP (12). Recent studies using Gas Phase Electrophoretic Mobility Macromolecule Analysis have suggested that the active form of human RNR is $\alpha 6\beta 2$ (13). Biacore studies and kinetic studies demonstrate that the interactions between α and β in the absence of nucleotides, as in the prokaryotic case, are weak ($K_d = 0.5 \mu$ M) (18, 24). Anticipated differences in the aggregation state of active RNR relative to the *E. coli* RNR caused us to switch to a Superdex 200 column for molecular weight analysis in the presence and absence of F₂CDP in addition to ATP. The results of incubation of either 0.5 or 1 eq. of [1'-³H]

F_2 CDP/ATP by SEC with ATP in the elution buffer are shown in Figure 3.7 A and B and are summarized in Table 3.2. Fractions were collected through the protein peak and analyzed by scintillation counting and by SDS PAGE (Figure 3.8 B). In the former case analysis gave 0.8 radiolabels/ α 2. SDS PAGE revealed the presence of both α and β . The relative ratio of α : β of 1:1 was established using standard curves made from human or *E. coli* α and β (Figure 3.9).

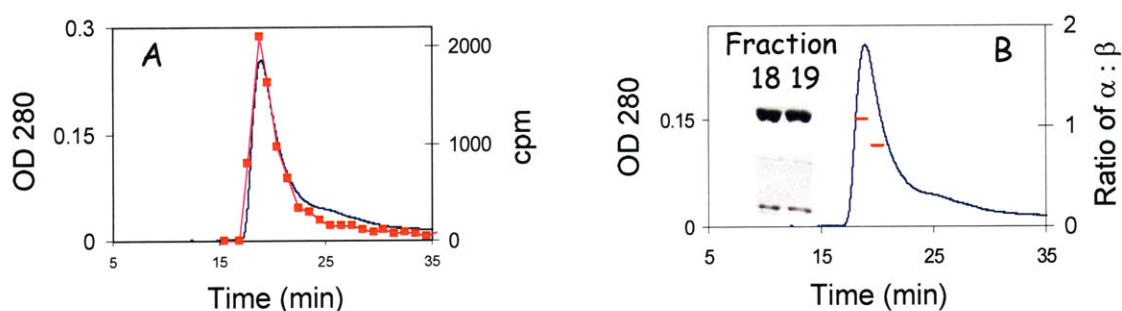


Figure 3.8. SEC on a Superdex 200 column to detect the complex formation ($\alpha\beta$) in human RNR upon inactivation by F_2 CDP/ATP.

A. The elution profile monitored by A_{214nm} and scintillation counting (■). B. Fractions through the protein peak in A monitored by SDS PAGE and analysis of the ratio of α : β using standard curves generated from known amounts of α and β .

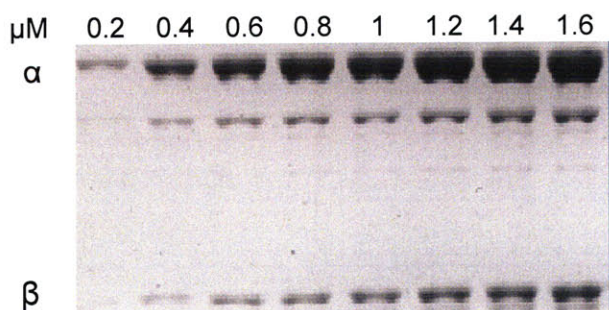


Figure 3.9. Standards on SDS PAGE to determine the ratio of α and β in human RNR.

α and β human RNR run on 10% SDS-PAGE with designated concentrations were used to generate standard curves to determine the amounts of α and β in each fraction in Fig. 3.7B.

Experiments were also carried out to assess the resolution of the SEC method and to obtain information about the relative molecular weights of the observed protein peaks. β_2 migrates with an apparent molecular weight of 108 KDa (calculated 94.1 KDa, Figure 3.10). α in the absence of nucleotides migrates as the expected monomer, while in the presence of TTP migrates as a dimer of 189 KDa (Figure 3.10). The retention time of the protein peak eluted from the RNR inactivated with F_2 CDP/ATP and with ATP in the elution buffer, relative to molecular weight standards reveals an apparent molecular weight of 872 KDa (Figure 3.10). The 1:1 ratio of α : β , the radiolabeling of the complex, and the apparent molecular weight in comparison with the expected mass of 834 KDa for $\alpha_6\beta_6$, 646 KDa for $\alpha_6\beta_2$, and 278 KDa for $\alpha_2\beta_2$, suggest that the active form of the human RNR is $\alpha_6\beta_6$ and that the subunits are tightly interacting. The results, as in the case of the *E. coli* RNR, provide an explanation for complete RNR inactivation with substoichiometric amounts of F_2 CDP. Inactivation of class I RNRs by F_2 CDP thus provides another paradigm for inhibitor design of this protein: increasing the subunit affinity.

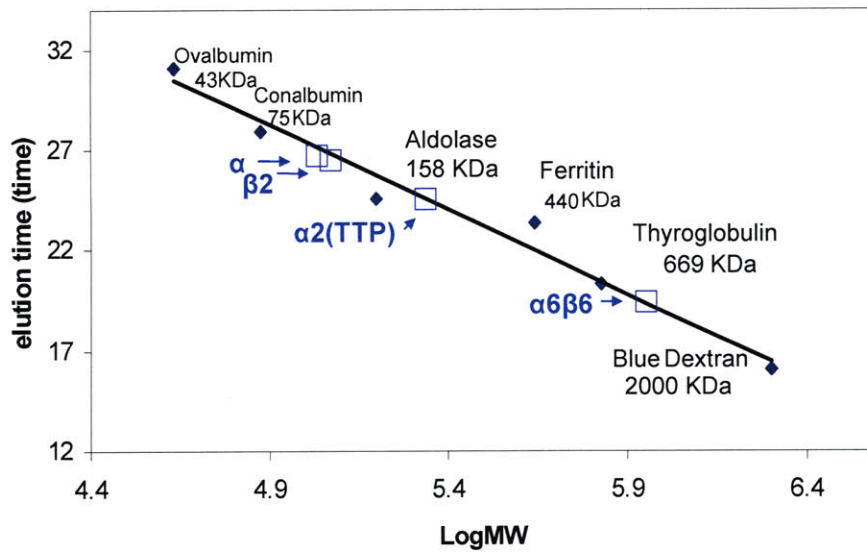


Figure 3.10. SEC on a Superdex 200 column to determine the molecular weight of the α , $\alpha 2$, $\beta 2$ and $\alpha 6\beta 6$ in human RNR.

The mobile phase contained 0.5 mM ATP in the 50 mM HEPES, 15 mM MgCl₂, pH 7.6 running buffer. α was eluted with buffer containing 100 μ M TTP. α and β were eluted in buffer containing 0.5 mM ATP.

3.3.6 Identification of the covalent labeling site of human RNR inactivated by

F₂CDP

To identify the site of covalent modification by the sugar, [1'-³H] F₂CDP, was incubated with active site mutants of the 5 essential cysteines, C429S/A, E431Q/D, C787S/A, C790S/A, C444S/A, C218S/A with β in the presence of DTT. Each mutant was purified as described for wt- α with similar recoveries. The extent of covalent labeling measured subsequent to Sephadex G50 chromatography in the absence of denaturant was determined by scintillation counting and compared to the labeling with wt-RNR. The results are summarized in Table 3.3.

Table 3.3 Quantitation of the [³H]-label associated of human RNR mutants inactivated by [1'-³H] F₂CDP

	labeling/ $\alpha 2\beta 2$
Wild type H1	0.8 to 0.9
C444S (C462) ^a	0.4
C444A (C462)	0.7
C218S (C225)	0.1
C218A (C225)	0.1
C429S (C439)	0.008
C429A (C439)	0.01
E431Q (E441)	0.01
E431D (E441)	0.08
C787S (C754)	0.8
C787A (C754)	0.3
C790S (C759)	0.6
C790A (C759)	0.1

a: In parenthesis are the corresponding residues in *E. coli* R1.

Comparison of the extent of labeling of mutants to wt hRNR suggests that C218 and E431 result in greatest loss of label and that either could be the site of covalent modification. However, both E431 and C218 mutants can carry out the first few steps in the normal reduction process. The E431Q however greatly reduces the rate of these steps and thus lack of α -modification is likely associated with the slow rate of the reaction. C218 on the other hand allow the first few steps to occur at a rate similar to wt RNR. Thus at present, and based on recent studies with the *E. coli* RNR inactivated by F₂CDP, we favor C218 as the site of covalent modification.

To try to identify a peptide alkylated by the sugar, trypsin digest was carried out on the [1'-³H]-F₂CDP inactivated human RNR of the protein subsequent to its alkylation with iodoacetamide. The [1'-³H] label associated protein was relatively stable under the conditions required for trypsin digestion, with 15% of the radioactivity being lost in 24 h. To minimize label loss, the digestion was carried out at 37 °C for 5 h with

high levels of digestion into RNR. The peptides were separated by reverse-phase HPLC in 0-45% CH₃CN, 0.1% TFA over 90 min as shown in Figure 3.11. Twenty % of the label was lost as it eluted in the void volume of the column. Four broad regions of radioactivity were identified indicating multiple sites of labeling. Radioactivity in region I from 65-67 min contain about 14% of total radioactivity, and the region II and III from 68-70 and 71-73 respectively accounted for 20% and 22% of the total radioactivity. Region IV from 74-76 min accounted for 10% of the radioactivity.

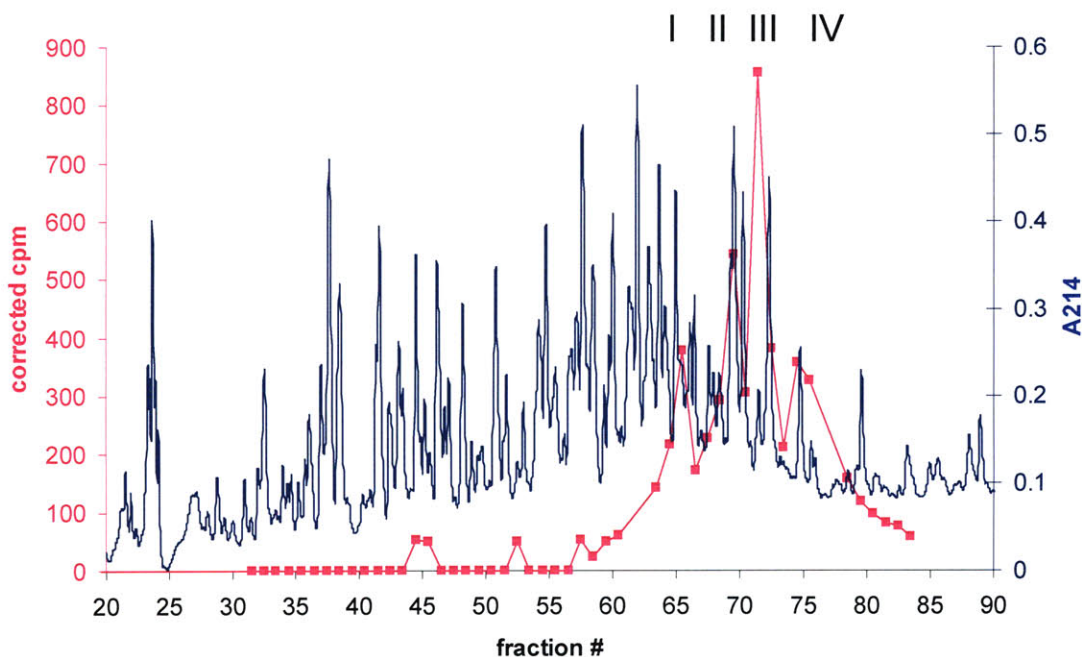


Figure 3.11: Trypsin digestion under the conditions of 100 mM NH₄HCO₃, 2M urea, pH 8 for 5 h at 37°C. 4:1 (w/w) protein to trypsin was used. The protein concentration was 0.5 μM.

Fractions from regions I, II, and III were combined, concentrated and re-injected onto the Jupiter C18 peptide column. The peptides were rechromatographed in 10 mM NH₄OAc (pH 6.4) (solvent A), CH₃CN (solvent B) from 0 to 70% in 90 min. An

additional 25% of the radioactivity was lost during concentration of each sample. The results from each rechromatography of region I showed 36% recovery (Figure 3.12 A), Region II showed no co-elution of radioactivity with any peptides in the rechromatograph (Figure 3.12 B). Region III showed a single peak associated with radiolabel with 30% recovery in rechromatograph (Figure 3.12 C). Substantial loss of the radiolabel was observed during the peptide purifications due to the instability of the sugar adduct formed and rearrangement of the label due to reverse Michael addition.

We collaborated with Prof. Neil Kelleher's lab in University of Illinois, Urbana-Champaign for mass spectrometry analysis of the purified peptides. Many peptides were found in each sample even though that they appeared as a single peak on HPLC analysis. Brad Evans in Kelleher's lab then carried out an in gel digestion on the F₂CDP inactivated human RNR. What he did was to separate α and β on 10% SDS-PAGE, cut the gel slices containing α and β individually, and treat them with trypsin for digestion overnight. The peptides were then extracted from gel slices with multiple ammonium carbonate and acetonitrile washes and separated on a nano C18 LC column followed by analyzing on a 12T-FT-ICR-MS with CID fragmentation. Whether the label is stable in this procedure has not been studied. The coverage of the peptides identified in the MS analysis is shown in Fig 3.13. Peptides containing the potential labeling site of C218 and the C-terminal tail Cys were missing. Crosslinking of the C218 with a second peptide might make the peptide difficult to be identified. All the other catalytic cysteines including C444 and C429 within their peptides were labeled with iodoacetamide that possibly rule them out as the site of label, because the protein was treated with

iodoacetamide after inactivation and cysteines which were not modified by F₂CDP would be labeled with iodoacetamide.

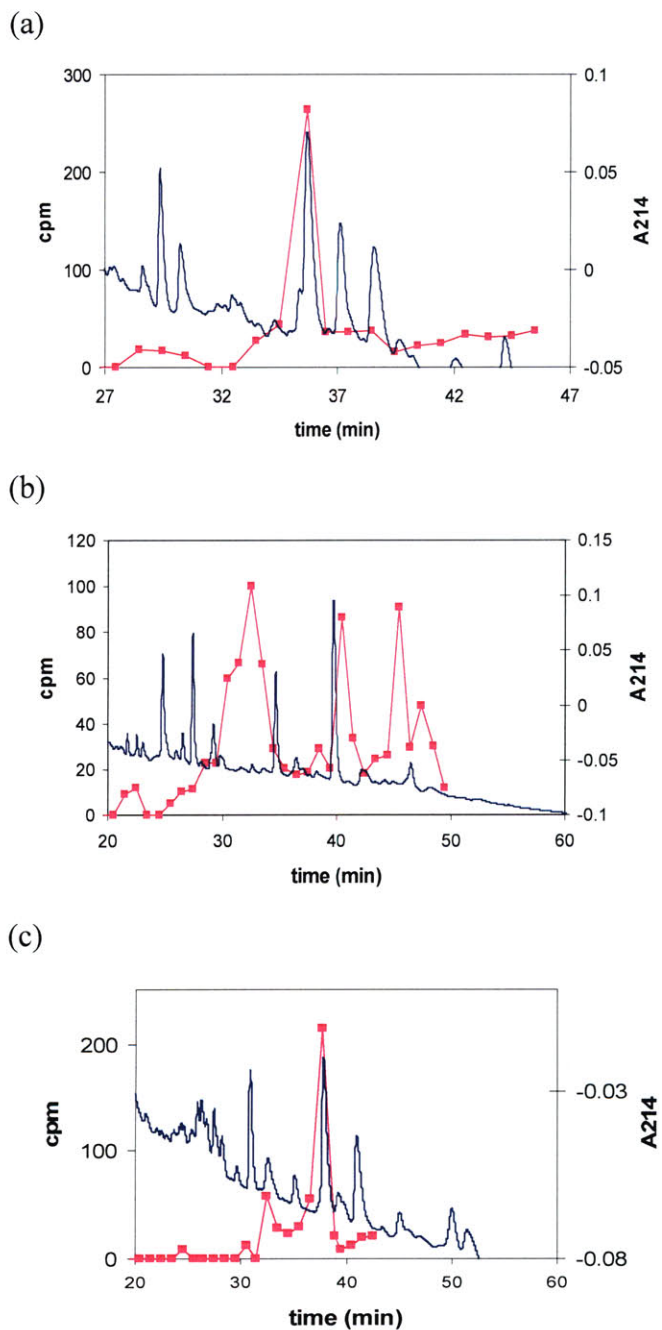


Figure 3.12: Rechromatography of peptides from human RNR inactivated with [1'-³H]-F₂CDP.

The gradient is 100% 10mM NH₄OAc (pH 6.4) for 5 min, increased to 20% CH₃CN over 7 min, then increased from 20% to 55% CH₃CN from 7 min to 90 min. A₂₁₄ (-), cpm (■) are shown. Rechromatography of the region I radioactive region (a) yielded a peak with

35.7% recovery, of region II (b) resulted in no radioactivity associated peptides, and of region III (c) yielded a peak with 63% recovery.

H1 sequence coverage map from 90 kDa band

```

MGSSHHHHHSSGLVPR GSHMHVIR DGR QER VMFDKITSR IQK LCYGLNMDFVDPAQITMK VIQGLYSGVTTVE
LDTLAAETAATLTTK HPDYAILAAR IAVSNLHKETK K VFSVDMEDLYNYINPHNGK HSPMVAK STLDIVLANK DR
LNSAIYDR DFSYNYFGFK TLER SYLLK IINGK VAERPQHMLMR VSVGIRK EDIDAAIETYNLLSER WFTHASPTLFN
AGTNRPQLSS CFLLSMK DDSIEGIYDTLK QCALISK SAGGIGVAVSCRATGSYIAGINGNSNGL VPMLR VYNNNTAR YV
DQGGNKRPGAFAIYLEPWHLDIFEFLLD K K NTGK EEQR AR DLFFALWIPDLFMK R VETNQDWSLMCPNECPGLDE
VWGEEFEK LYASYEKQGRVR K VVK AQQLWYAIIESQTETGTPYMLYK DSCNR K SNQQNLGTIK CSNLC TEIVEYT
SK DEVAVCNLASLALNMYVTSEHTYDFK K LAEVTK VVVRINLNK IIDINYYPVPEACLSNK R HRPIGIGVQGLADAF
ILMR YPFE SAEAQLLNK QIFETIYYGALEASCDLAK EQGPYETIEGSPVSK GILQYDMWNVTPDLWDWK VLKEK LA
KYGIR NSLLIAPMPTASTAOILGNNEIEPYTSNYTR R VLSGEFQIVNPHLLK DLTERGLWHEEMK NQIACNGSIQSIPE
IPDDLK QLYK TVWEISQK TVLK MAAR GAFIDQSQSLNIIHAEPNYGK LTMHFYGWK GLK TGMYYLR TRPAAN
PIQFTLNK EKLK DK EK VSKEEEEKER NTAAMVCSLENR DECLMCGS

```

H2 sequence coverage map from 40 kDa band

```

MGSSHHHHHSSGLVPR GSHMLSLR VPLAPITDPQQLQLSPLK GLSLVDK ENTTPALSGT VLASKTAR RIFQEPTPK
TK AAAPGVEDEPLLR ENPR R FVIFPIEYHDIWQMYK K AEASFWTAEVDLSKDIQHWESLKPEER YFISHVLAFFAAS
DGVNENLVER FSQEVQITEAR CFYGFQIAMENIHSEMYSLIDITYK DPKER EFLFNAIETMPCVK K K ADWALR WI
GDK EATYGER VVAFAAVEGIFFGSFSASIFWLK K R GLMPGLTFSNELISR DEGLH CDFACLMFK HLVHKPSEER VR
EIIINAVR IEQEFLTEALPVK LIGMNC TLMK QYIEFVADR LMLELGFSKVFR VENPFDMENISLEGK TNFFEK R VGE
YQR MGVMSSTENSFILDADF

```

Figure 3.13: Mass spectrometry analysis of the in gel trypsin digested peptides isolated subsequent to alkylation with iodoacetamide.

Those highlighted with red color are peptides identified. All of Cys are highlighted in yellow. The 1st residue in α is the 2nd Met on line 1 after His tag. C218 is the 1st C on the line 4 of α sequence. C429 is the last C on the line 6. C444 is the 1st C on the line 7 of α sequence. C787 and C790 are the last two C at the end of α sequence. The trypsin digest site is labeled with (■).

3.3.7 Time-dependent inactivation in the absence of reductants

Our previous studies on the *E. coli* RNR have shown that the mode of the inactivation by F₂CDP is reductant-dependent (4). In the presence of reductants, α is 100% inactivated, while in the absence of reductants, the Y• in β is completely lost, accompanied by a formation of a new stable radical, which recently shown to be nucleotide based (Figure 3.1)

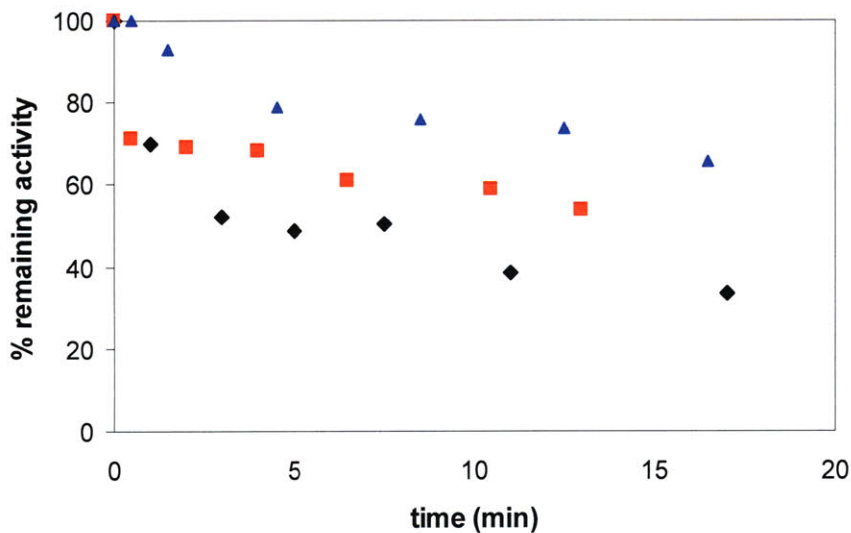


Figure 3.14: Time-dependent inactivation of human RNR by F₂CDP in the absence of reductant.

Inactivation mixtures contained final concentrations of α , β , 1.2 μM ; F₂CDP, 3 μM ; ATP, 3mM. Aliquots were removed at various times and diluted 4 fold for determination of α (\blacklozenge) and β (\blacksquare) activity in the 7 fold presence of excess of β or α . The activity of β (\blacksquare) was adjusted using results from the control experiment (\blacktriangle) for β activity, which is identical to the experiment except that F₂CDP was omitted.

The assays for inhibition on the human RNR were carried out in the absence of reductants. Small aliquots of the inactivated RNR complex were removed during a 20 min time course and tested for the activities in the presence of excess of the other subunit. The experiments revealed that about 50-60% of α activity was lost with 2.5 eq. of F₂CDP, and that 40% of the Y• was lost (Figure 3.14). These results differ from what we observed with *E. coli* RNR under similar conditions. In an effort to detect the generation of the new radical, a sample of 4.9 μM α , β (0.8 Y•), 49 μM F₂CDP, 3 mM ATP was incubated at 37 °C for 4.5 min in the absence of reductant before rapidly frozen in liquid N₂ and analyzed by EPR spectrometry at 30 K. As shown in Figure 3.15, no new radical has been identified besides the Y• after subtracting the spectrum of inactivation mixture

from the spectrum of the $Y\cdot$. At $t = 4.5$ min, 30% of $Y\cdot$ was lost. As limited by the concentration of α , the intensity of the subtraction spectrum has low signal to noise level.

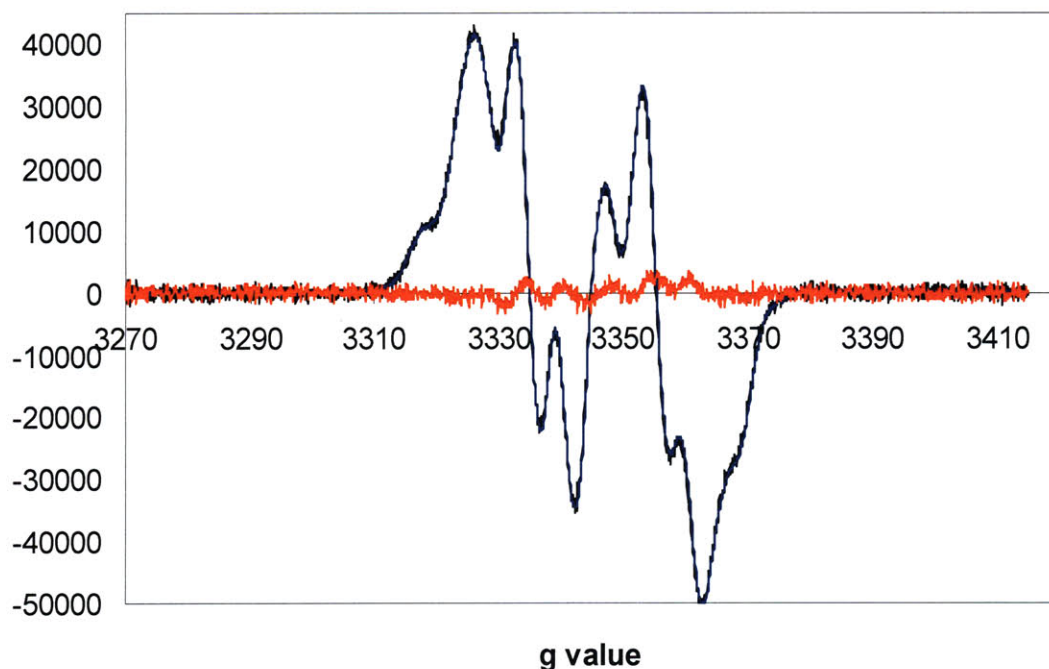


Figure 3.15: EPR Spectrum at 9 GHz of human RNR inactivated by F_2CDP in the absence of reductant.

The reaction mixture contained $4.9 \mu M \alpha, \beta$ ($0.8 Y\cdot$), $49 \mu M F_2CDP$, $3 mM ATP$, incubated at $37^\circ C$ for 4.5 min (-black, $0.56 Y\cdot$ remained) before frozen in liquid N_2 . The subtraction spectra (-red) was subtracted the intermediate spectra at 4.5 min (-black) from the spectra of $Y\cdot$ (- blue). Instrument settings for all spectra were as follows: frequency, $9.387 GHz$, power $0.201 mW$, modulation amplitude $2.00 G$, and temperature $30 K$.

The products were quantified after the human RNR was inactivated by the $[1\text{-}^3H]\text{-}F_2CDP$ or $[5\text{-}^3H]\text{-}F_2CDP$ in the absence of reductants (Table 3.1). Unlike the $0.8\text{-}0.9$ eq. of label per α_2 with $[1\text{-}^3H]\text{-}F_2CDP$ in the presence of reductants, only 0.1 eq. of label was associated per α_2 . Labeling with $[5\text{-}^3H]\text{-}F_2CDP$ resulted with 0.1 eq. per α_2 , showing the base is also gone after inactivation for 10 min.

3.4 Discussion

Many 2'-substituted-2'-deoxynucleotides have been shown to be potent mechanism based inhibitors of RNRs since the initial experiments in 1976 (25). The detailed studies on 2'-fluoro, 2'-chloro derivatives shown in chapter 1 have provided the basis for a general mechanism of inhibition by these substrate analogs (26, 27). Most 2'-substituted deoxynucleotides inhibit class I RNRs by a combination of pathways.

Studies presented in this chapter suggest an additional mechanism by which 2'-substituted nucleotides may inactivate RNR. F₂CDP has two fluorines at C2', both of which are lost during inactivation (4, 28). [1'-³H] F₂CDP inactivation is accompanied by 0.5 eq. of sugar labeling from F₂C/α and loss of cytosine, approximately 40% of tyrosyl radical loss and 100% loss of RNR activity. The mechanisms by which F₂CDP inactivate the *E. coli* and human RNRs, thus, must occur by multiple pathways as previously observed with other 2'-substituted nucleotides. The details of the inactivation mechanism are complex and are still not understood.

The observation of sub-stoichiometric amounts F₂CDP resulting in complete RNR inactivation is difficult to understand. An explanation for the unusual stoichiometry is provided by the analysis of the RNR quaternary structure. In the case of the *E. coli* RNR, SEC reveals a tight α₂β₂ complex when it is inactivated by F₂CDP (Figure 3.5). A control in the absence of F₂CDP reveals that α₂ partially separates from β₂ by the same chromatographic analysis (Fig.3.5). This sub-stoichiometry inactivation is similar to another mechanism based inhibitor, 2'-azido-2'-deoxynucleotides (N₃NDP) (21-23). With [5'-³H] N₃NDPs inactivation, >90% of RNR activity is lost in 2 min, 50% of Y• is reduced and 0.7 eq radiolabel are associated with RNR. However, the radiolabel is not

stable or it is non-covalently bound because denaturizing protein releases the radiolabel. In contrast with F_2CDP , activity of α with N_3UDP is recovered to 50% and complete inactivation over 30 min is associated with 100% loss of $Y\bullet$. Thus, while the subunits must be tightly associated initially to account for > 90% loss of activity with just 50% loss of $Y\bullet$, further chemistry associated with nucleotide allows subunit weakening and dissociation. A similar SEC experiment provides no evidence for an $\alpha_2\beta_2$ complex. (Figure 3.6) The unique chemistry associated with the different inhibitors thus can dramatically effect subunit interactions.

The inactivation of the human RNR shows some differences from that of the *E. coli* RNR in the absence of reductant, however, in the presence of reductant, it mirrors the observations made with the *E. coli* RNR. One major difference, however, involves the quaternary structure of the human RNR. Our SEC studies have provided direct evidence in support of an active $\alpha_6\beta_6$ complex based on standard curve made with globular proteins. This result contrasts with previous proposals of active $\alpha_2\beta_2$ and with the recent mass spectrometric studies suggesting that $\alpha_6\beta_2$ is the active form of RNR (13). Our results support the importance of the α_6 form of the large subunit, first proposed by Cooperman's lab (12). The SEC results also suggest that inactivation is the result of tight complex formation between the subunits which can occur even in the presence of sub-stoichiometric amounts of nucleotide. At odds with this interpretation is the activity assays for each subunit in the presence of an excess of the second subunit. If a tight complex were present subsequent to inactivation, one would have expected that α and β would be 100% inactive. While this was the case for α , β_2 retains 60% of its activity. These results are very intriguing and provide us with additional insight about

subunit interaction. The recovery of β_2 activity requires that excess α can form a transient ternary complex with $\alpha_6\beta_6$ and liberate β_2 which has retained some of its $Y\bullet$ and is thus active. This proposal is supported by a recent structure of a complex of the $\alpha_2\beta_2$ from *E. coli* where only one of the two β s interacts with α . Thus one could propose that binding of α to the unattached β of β_2 could facilitate α_2 release. In the case of the inactivated $\alpha\alpha^*\beta_2$ complex assayed with excess α (α^* = covalently labeled α), this mechanism would result in release of $\alpha\alpha^*$ and formation of active $\alpha_2\beta_2$. Since there is only one [^3H]-label per α_2 , one would have expected the unlabeled monomer to be also active in the presence of excess β , but this is not the case. Thus this result provides strong support for asymmetry within the α_2 (α_6), that is, modification of one α , precludes activity of the other. The results suggest that if the cell was able to increase the amount of α , that active RNR could be recovered. Interestingly resistance in a number of cell lines has identified elevated α levels (29-31). $F_2\text{CDP}$ is unique with respect to the well characterized 2' substituted nucleotide mechanism based inhibitors, in that in addition to labeling α and loss of $Y\bullet$ on β , inactivation is the result of tight subunit association.

3.5 Reference:

- (1) Hertel, L. W., Boder, G. B., Kroin, J. S., Rinzel, S. M., Poore, G. A., Todd, G. C., and Grindey, G. B. (1990) Evaluation of the Antitumor-Activity of Gemcitabine (2',2'-Difluoro-2'-Deoxycytidine). *Cancer Research* 50, 4417-4422.
- (2) Huang, P., Chubb, S., Hertel, L. W., Grindey, G. B., and Plunkett, W. (1991) Action of 2',2'-difluorodeoxycytidine on DNA-synthesis. *Cancer res.* 51, 6110-6117.
- (3) Plunkett, W., Huang, P., and Gandhi, V. (1997) Gemcitabine: actions and interactions. *Nucleosides & Nucleotides* 16, 1261-1270.
- (4) van der Donk, W. A., Yu, G. X., Perez, L., Sanchez, R. J., Stubbe, J., Samano, V., and Robins, M. J. (1998) Detection of a new substrate-derived radical during inactivation of ribonucleotide reductase from *Escherichia coli* by gemcitabine 5'-diphosphate. *Biochemistry* 37, 6419-6426.
- (5) Baker, C. H., Banzon, J., Bollinger, J. M., Stubbe, J., Samano, V., Robins, M. J., Lippert, B., Jarvi, E., and Resvick, R. (1991) 2'-deoxy-2'-methylenecytidine and 2'-deoxy-2',2'-difluorocytidine 5'-diphosphates - potent mechanism-based inhibitors of ribonucleotide reductase. *J. Med. Chem.* 34, 1879-1884.
- (6) Artin, E., Wang, J., Lohman, G., Yu, G., Griffin, G., Barr, G., and Stubbe, J. (2009) Insight into the mechanism of inactivation of ribonucleotide reductase by Gemcitabine 5'-diphosphate in the presence and absence of reductant. *manuscript submitted*.
- (7) Lohman, G. J. S., Stubbe, J. (2009) Inactivation of *L. leichmannii* ribonucleotide reductase by F₂CTP: covalent modification (part I). *manuscript preparation*.
- (8) Lohman, G. J. S., Gerfen, G. J., Stubbe, J. (2009) Inactivation of *L. leichmannii* ribonucleotide reductase by F₂CTP: adenosylcobalamin destruction and formation of a nucleotide based radical *manuscript preparation*.
- (9) Atkin, C. L., Thelander, L., Reichard, P., and Lang, G. (1973) Iron and Free-Radical in Ribonucleotide Reductase - Exchange of Iron and Mossbauer-Spectroscopy of Protein-B2 Subunit of *Escherichia-Coli* Enzyme. *J. Biol. Chem.* 248, 7464-7472.
- (10) Brown, N. C., Reichard, P. (1969) Role of Effector Binding in Allosteric Control of Ribonucleoside Diphosphate Reductase. *J. Mol. Biol.* 46, 39-55.
- (11) Nordlund, N., and Reichard, P. (2006) Ribonucleotide reductases. *ANNUAL REVIEW OF BIOCHEMISTRY* 75, 681-706.
- (12) Kashlan, O. B., Scott, C. P., Lear, J. D., and Cooperman, B. S. (2002) A comprehensive model for the allosteric regulation of mammalian ribonucleotide reductase. Functional consequences of ATP- and dATP-induced oligomerization of the large subunit. *Biochemistry* 41, 462-474.
- (13) Rofougaran, R., Vodnala, M., and Hofer, A. (2006) Enzymatically active mammalian ribonucleotide reductase exists primarily as an alpha(6)beta(2) octamer. *Journal of Biological Chemistry* 281, 27705-27711.
- (14) Russel, M., and Model, P. (1985) Direct Cloning of the Trxb Gene That Encodes Thioredoxin Reductase. *J. Bacteriol.* 163, 238-242.

- (15) Lunn, C. A., Kathju, S., Wallace, B. J., Kushner, S. R., Pigiet, V. (1984) Amplification and purification of plasmid-encoded thioredoxin from *Escherichia-Coli*-K12. *J Biol Chem* 259, 469-474.
- (16) Steeper, J. R., Steuart, C.C. (1970) A rapid assay for CDP reductase activity in mammalian cell extracts. *Anal. Biochem.* 34, 123-130.
- (17) Ortigosa, A. D., Hristova, D., Perlstein, D. L., Zhang, Z., Huang, M. X., and Stubbe, J. (2006) Determination of the in vivo stoichiometry of tyrosyl radical per beta beta ' in *Saccharomyces cerevisiae* ribonucleotide reductase. *Biochemistry* 45, 12282-12294.
- (18) Ingemarson, R., and Thelander, L. (1996) A kinetic study on the influence of nucleoside triphosphate effectors on subunit interaction in mouse ribonucleotide reductase. *Biochemistry* 35, 8603-8609.
- (19) Ormo, M. a. S., B. (1990) An ultrfiltration assay for nucleotide binding to ribonucleotide reductase. *Anal. Biochem.* 189, 138-141.
- (20) Kasrayan, A., Birgander, PL., Pappalardo, L., Regnstrom, K., Westman, M., Slaby, A., Gordon, E., and Sjoberg, BM.,. (2004) Enhancement by effectors and substrate nucleotides of R1-R2 interactions in *Escherichia coli* class Ia ribonucleotide reductase. *J. Biol. Chem.* 279, 31050-31057.
- (21) Salowe, S., Bollinger, J. M., Ator, M., Stubbe, J., McCracken, J., Peisach, J., Samano, M. C., and Robins, M. J. (1993) Alternative Model for Mechanism-Based Inhibition of *Escherichia-Coli* Ribonucleotide Reductase by 2'-Azido-2'-Deoxyuridine 5'-Diphosphate. *Biochemistry* 32, 12749-12760.
- (22) Salowe, S. P., Ator, M. A., and Stubbe, J. (1987) Products of the Inactivation of Ribonucleoside Diphosphate Reductase from *Escherichia-Coli* with 2'-Azido-2'-Deoxyuridine 5'-Diphosphate. *Biochemistry* 26, 3408-3416.
- (23) Fritscher, J., Artin, E., Wnuk, S., Bar, G., Robblee, J. H., Kacprzak, S., Kaupp, M., Griffin, R. G., Bennati, M., and Stubbe, J. (2005) Structure of the nitrogen-centered radical formed during inactivation of *E-coli* ribonucleotide reductase by 2'-azido-2'-deoxyuridine-5'-diphosphate: Trapping of the 3'-ketonucleotide. *JOURNAL OF THE AMERICAN CHEMICAL SOCIETY* 127, 7729-7738.
- (24) Hassan, Q., Wang, Y., Plate, L., and Stubbe, J. (2008) Methodology to probe subunit interactions in ribonucleotide reductases. *Biochemistry*.
- (25) Thelander, L., and Larsson, B. (1976) Active-Site of Ribonucleoside Diphosphate Reductase from *Escherichia-Coli* - Inactivation of Enzyme by 2'-Substituted Ribonucleoside Diphosphates. *Journal of Biological Chemistry* 251, 1398-1405.
- (26) Licht, S., Stubbe, J. (1999) *Comprehensive Natural Products Chemistry*, Vol. 5, Elsevier.
- (27) Stubbe, J. A., and van der Donk, W. A. (1995) Ribonucleotide reductases: Radical enzymes with suicidal tendencies. *CHEMISTRY & BIOLOGY* 2, 793-801.
- (28) Silva, D. J., Stubbe, J., Samano, V., and Robins, M. J. (1998) Gemcitabine 5'-triphosphate is a stoichiometric mechanism-based inhibitor of *Lactobacillus leichmannii* ribonucleoside triphosphate reductase: Evidence for thiyl radical-mediated nucleotide radical formation. *Biochemistry* 37, 5528-5535.
- (29) Davidson, J. D., Ma, L. D., Flagella, M., Geeganage, S., Gelbert, L. M., and Slapak, C. A. (2004) An increase in the expression of ribonucleotide reductase

- large subunit 1 is associated with gemcitabine resistance in non-small cell lung cancer cell lines. *Cancer research* 64, 3761-3766.
- (30) Bergman, A. M., Eijk, P. P., van Haperen, V., Smid, K., Veerman, G., Hubeek, I., van den Ijssel, P., Ylstra, B., and Peters, G. J. (2005) In vivo induction of resistance to gemcitabine results in increased expression of ribonucleotide reductase subunit M1 as the major determinant. *Cancer Res.* 65, 9510-9516.
- (31) Jordheim LP, G. O., Lepoivre M, Galmarini CM, Dumontet C. (2005) Increased expression of the large subunit of ribonucleotide reductase is involved in resistance to gemcitabine in human mammary adenocarcinoma cells. *Mol. Cancer Ther.* 4, 1268-1276.

Chapter 4

Inactivation studies of Human p53R2 and H1 RNR complex by Gemcitabine

Adapted from Wang J, Lohman GJ, Stubbe J. (2009) Mechanism of Inactivation of human Ribonucleotide Reductase with p53R2 by Gemcitabine-5'- diphosphate. Manuscript in preparation.

4.1 Introduction:

Gemcitabine (2, 2'-dideoxy-difluorocytidine, F₂C) is a drug that is used clinically in the treatment of non-small cell lung carcinomas and advanced pancreatic cancer (1-5). The mechanism of its cytotoxicity is multifactorial where its metabolites, the mono-, di- and tri-phosphates (F₂CMP, F₂CDP and F₂CTP) inhibit a variety of steps in nucleic acid metabolism (3, 6). The essential step in apoptosis of the cells is F₂CTP inhibition of DNA polymerase by its incorporation into the growing polymer chain, resulting in chain termination (2). Potentiation of the effects of F₂CTP results from the inhibition of ribonucleotide reductase(s) (RNR), the enzymes that make deoxynucleoside 5'-diphosphates (dNDPs) from nucleoside diphosphates (7-9). RNRs are stoichiometrically inhibited by F₂CDP (7-10). This inhibition leads to a reduction in dNDP pools and consequently reduction in dNTP pools. Reduced concentrations of dNTPs reduce the competition for F₂CTP to become incorporated into DNA.

Class I RNRs are composed of α (R1) and β (R2) subunits and the human RNRs (hRNR) have a complex quaternary structure $\alpha_n(\beta_2)_m$ ($n = 2, 4, 6$ and $m = 1, 3$) (7, 8). α houses the active site for nucleotide reduction and the binding sites for ATP/dNTP allosteric effectors that control the specificity and rate of nucleotide reduction. β houses the essential diferric-tyrosyl radical (Y•) cofactor (9-12). Recently, we have shown that hRNR involved in DNA replication, is substoichiometrically inactivated by F₂CDP (0.5 eq/ α) (13). Our studies unexpectedly revealed that the inhibition resulted from tight association of the two subunits and formation of a quaternary structure determined by size exclusion chromatography (SEC) where m is 3 and n is 6. Recently a second RNR small subunit was discovered in humans (14, 15). It was designated p53R2 as its levels

were induced by p53 (14). We will designate p53R2 as β' . In this chapter we report on the mechanism of inactivation of hRNR, $\alpha_n(\beta'2)_m$, by F_2CDP and compare the results with the replicative RNR $\alpha_n(\beta2)_m$.

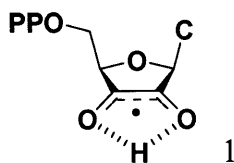
The biology and biochemistry of β' are actively being investigated. The biological function of β' is complex and appears to be different in quiescent cells and cells which have been subjected to DNA damage. Recent studies of Pontarin *et al* (16) suggest that β' is localized to the cytosol and is not shuttled to the nucleus as previously suggested (14, 17). They proposed that β' plays a primary role in mitochondrial DNA replication. This role is supported by identification of children with mutations in β' that experience severe mitochondrial DNA depletion (18).

While p53 mediates transcriptional induction of β' and as a consequence led to the proposal of its involvement in DNA repair, the induction process is not sufficiently rapid to supply dNTPs given the rate of damage repair (16, 19). Recent observations, however, have shown that β' interacts with and is phosphorylated by ATM and is found in the MRE11 complex involved in DNA double strand break repair. β' has also been shown to interact with ERK1(ERK2) and to inhibit MEK-ERK signaling and prevent cancer invasion, demonstrating an important role in genomic stability (19, 20).

β' is composed of 351 amino acids and is 80% homologous to h β (human β). Both proteins contain an essential diferric- $Y\bullet$ cofactor and are active in nucleotide reduction in the presence of α . h β' has been reported to have activity 1.4 fold lower than β and a $Y\bullet$ content of $0.8/\beta'2$, 67% of that of $\beta2$ (21). However, the activity of h β reported (21) is substantially lower (10 fold), than the activity recently reported from our lab (13) for

reasons unknown. β' has also been proposed to have catalase activity in contrast to $h\beta$ and to have a different susceptibility to inactivation by hydroxyurea (22).

As noted above F_2CDP is a potent inhibitor of RNRs and its demonstrated efficacy against a range of solid tumors warrants a detailed investigation of this process. Studies on the class Ia RNRs from *E. coli* and human $\alpha_n(\beta_2)_m$, and the class II RNR from *Lactobacillus leichmannii* have provided us with the following generalizations about the mechanism of inactivation. Using $[5-^3H]$ or $[1'-^3H]$ F_2CDP (F_2CTP) the stoichiometry of inhibition is 1 F_2CDP/α_2 for the class I RNRs (13) and 1 F_2CTP/α for the class II RNR (23, 24). The *L. leichmannii* RNR is a monomeric enzyme that uses adenosylcobalamin as a cofactor. Despite the stoichiometry, as with all mechanism based inhibitors of RNR, at least two pathways are responsible for inhibition (25). Covalent modification by a sugar moiety of F_2CDP is responsible for inactivation by one of these pathways. Destruction of the cofactor ($Y\cdot$ in the class Ia and adenosylcobalamin in the class II RNRs) (24) is responsible for the remaining inactivation. Subsequent to complete inactivation, stoichiometric amounts of cytosine are released, as are two fluoride ions. With the *E. coli* and *L. leichmannii* RNRs a new nucleotide radical has been recently identified **1** (10, 26, 27). This information has been used to formulate mechanisms of inactivation of the two pathways. Finally, with the class I RNRs we have recently made the unexpected observation that the basis for complete inactivation by 0.5 F_2CDP/α is that the α and β subunits form a tight complex: $\alpha_2\beta_2$ for *E. coli* RNR and $\alpha_6\beta_6$ for hRNR (13).



The prevalence of gemcitabine as a clinically useful drug and the wealth of literature evidence suggesting that controlling the levels of β' may increase potency of co-administered genotoxic therapeutics mandates a better understanding of the enzymology of β' to elucidate its function (26). In this chapter we report that F_2CDP is an inactivator of β' , although the binding of F_2CDP to the α/β' complex appears to be weaker (based on slower rates of inactivation at stoichiometric amounts) than that observed with the corresponding complex bearing $h\beta$. Studies with $[5-^3H]$ and $[1'-^3H]$ F_2CDP reveal the following: (i) >90% inactivation occurs with 0.5 eq. inhibitor/ α ; (ii) 0.5 sugars are attached covalently to α , and (iii) one cytosine is released per inactivation. SDS PAGE analysis of the inactivated RNR reveals that α has been covalently modified (40% of total α) migrates as a 120 kDa protein relative to unmodified α which migrates as a 90 kDa protein. Site directed mutagenesis studies of all of the residues involved in catalysis in α and studies of the effect of each mutation on the inactivation of RNR (comprising either $h\beta$ or β') suggest that C218 and a cysteine (C790 or C787) from the C-terminus of α are likely responsible for covalent modification of α and the unusual migratory properties of α by SDS PAGE analysis. Size exclusion chromatography suggests that subsequent to inactivation, RNR migrates as a $\alpha_6\beta'_6$ complex. β' thus could also be a target of gemcitabine and play a role in its cytotoxicity.

4.2 Materials and Methods

4.2.1 Material

Competent *E. coli* BL 21 (DE3) –RIL cells were purchased from Stratagene. Complete EDTA-free protease inhibitor tablets and calf alkaline phosphatase (20 U/ μ L) were purchased from Roche Biochemicals. [3 H]-CDP (17 Ci / μ mol) is from ViTrax radiochemicals (CA). p53R2 (27) containing the gene for β' was a gift from Lars Thelander (Department of Medical Biosciences, Medical Biochemistry, Umeå University, SE-901 87 Umeå, Sweden). phRRM1 containing the gene for α was from Dr. Yun Yen (City of Hope National Medical Center, Duarte, CA) (21). Protein concentrations were determined using extinction coefficients ($\epsilon_{280\text{ nm}}$) per monomer [62,000 $\text{M}^{-1}\text{ cm}^{-1}$ for β' , 119,160 $\text{M}^{-1}\text{ cm}^{-1}$ for α]. *E. coli* TR (specific activity of 40 U/mg) and TRR (specific activity of 1320 U/mg) were isolated as previously described (28, 29).

4.2.2 Expression and purification of human β' :

β' in pET3a, which does not contain a tag or extra amino acids, was transformed to BL21 Codon Plus (DE3)-RIL cells (Stratagene), plated on LB agar plates with 100 $\mu\text{g/mL}$ ampicillin (Amp) and 34 $\mu\text{g/mL}$ chloramphenicol (CM). A single colony was added to a culture (20 mL LB in 150 mL flask) and grown to saturation overnight. The culture was then diluted into 2 L of LB in a 6 L flask containing 100 $\mu\text{g/mL}$ Amp, 34 $\mu\text{g/mL}$ CM and grown at 37°C to $\text{OD}_{600\text{ nm}}$ 0.7. 1,10-Phenanthroline (100 μM) was then added to the media and the cells were grown for an additional 15min. IPTG (isopropyl-beta-D-thiogalactopyranoside, 400 μM) was then added and the cells were grown at 37°C for an additional 5 h. The cells were harvested and frozen in liquid N_2 and typically yielded 2 g/L.

For the isolation of the apo β' , 16 g cells were suspended (4 vol/g) in 50mM Tris-HCl, pH 7.6, 1mM PMSF (phenylmethanesulphonylfluoride), 1mM EDTA at 4 °C. The suspension was passed through the French press at 14,000 psi. The cell lysate was centrifuged at 27, 000 \times g for 30 min at 4 °C. Streptomycin sulfate of 10% (w/v) stock was added to the supernatant over 10 min while stirring at 4 °C, to a final concentration of 2.5 %. After an additional 10 min of stirring, the pellet was removed by centrifugation (27, 000 \times g for 30 min, 4 °C). Solid ammonium sulfate (0.243 g/mL, 40%) was added to the supernatant over 10 min at 4 °C. After an additional 30 min of stirring, the protein pellet was recovered by centrifugation (27, 000 \times g for 30 min, 4 °C).

The pellet was dissolved in 4 mL of extraction buffer and loaded directly onto a Phenyl Sepharose 6 Fast flow column (20 mL, 2.5 x 10 cm) that was pre-equilibrated with 200 mL, 25 mM Tris pH 7.6, 10% glycerol, 30% w/v $(\text{NH}_4)_2\text{SO}_4$ (buffer A). The column was washed with buffer A (100 mL) and then 300 mL, 25 mM Tris (pH 7.6), 10% glycerol, 5% w/v $(\text{NH}_4)_2\text{SO}_4$ (buffer B). Finally, β' was eluted with 50 mM Tris pH7.6, 5% glycerol, 1 mM EDTA, 1mM PMSF (buffer C). Fractions (2 mL) containing β' (based on Bradford assay) were collected.

The pooled protein fractions were then loaded onto a Q-Sepharose column (20 mL, 2.5 x 10 cm), which was pre-equilibrated with 100 mL buffer C at 4 °C. The column was washed with 200 mL buffer C and 150 mM KCl. The protein was eluted with a 70 mL x 70 mL linear gradient of 150 – 400 mM KCl in buffer C. Fractions (2 mL) containing β' (based on Bradford assay and 10% SDS PAGE analysis) were collected. The apo β' eluted around 220 mM KCl. A typical yield of 0.4 mg β' /g cells was obtained.

4.2.3 Construction of Y138F- β' , growth, and isolation

The Y138F- β' was generated by site directed mutagenesis using the Quick Change Kit (Stratagene). The β' gene was amplified by PCR using PfuUltra II polymerase (Stratagene) with primers for Y138F mutant (Table 4.1). The sequence of the mutant plasmids was confirmed by sequencing at the MIT biopolymers laboratory. Y138F- β' was expressed and purified as described for β' with similar yields.

Table 4.1: Primers for mutants of β' and α

Name of the mutant	Sequence of the primer (from 5'-3')
Y138F- β' forward	GAATGTTCACTCAGAGATGTTTCAGTTTGCTGATAGACAC
Y138- β' reverse	GTGTCTATCAGCAAACCTGAACATCTCTGAGTGAACATTC
C218S- α forward	CCGCCCACTTTCTAGCTCTTTTCTTCTGAGTATG
C218S- α reverse	CATACTCAG AAGAAAAGAG CTAGAAAGTT GTGGGCGG
C218A- α forward	CCGCCCACTTTCTAGCGCTTTTCTTCTGAGTATG
C218A- α reverse	CATACTCAG AAGAAAAGCGCTAGAAAGTT GTGGGCGG
C429S- α forward	GCAGCAACCTGTCCACAGAAATAGTGGAGTACACC
C429S- α reverse	GGTGTACTCCACTATTTCTGTGGACAGG TTGCTGC
C429A- α forward	CCATCAAATGCAGCAACCTGGCCACAGAAATAGTGGAG
C429A- α reverse	CTCCACTATTTCTGTGGCCAGGTTGCTGCATTTGATGG
C444S- α forward	GAGGTTGCTGTTTCTAATTTGGCTTCCTGGCCC
C444S- α reverse	GGGCCAGGGAAGCCAAATTAGAAACAGCAACCTC
C444A- α	GAGGTTGCTGTTGCTAATTTGGCTTCCTGGCCC

forward	
C444A- α reverse	G GGCCAGGGAAGCCAAATT AG CAACAGCAAC CTC
C787S- α forward	GGAGAATAGAGATGAAT CTCT GATGTGTGGATCCTG
C787S- α reverse	CAGGATCC ACACATCAGAG ATT CATCTC TATTCTCC
C787A- α forward	GCTCTTTGGAGAATAGAGATGA AGCTCT GATGTGTGGATCCTG
C787A- α reverse	CAGGATCC ACACATCAG AGCTT CATCTCTATTCTCCAA AGAG
C790S- α forward	GGAGAATAGAGATGAATGTCTGATGT CT GGATCCTG
C790S- α reverse	CAGGATCC AGAC ATCAGACATTCATCTCTATTCTCC
C790A- α forward	GCTCTTTGGAGAATAGAGATGAATGTCTGAT GGCT GGATCCTG
C790A- α reverse	CAGGATCC AGCC ATCAGACATTCATCTC TATTCTCCAAAGAGC
E431Q- α forward	GCAACCTGTGCACACA AA ATAGTGGAGTACACC
E431Q- α reverse	GGTGTACTCCACTAT TTGT GTGCACAGG TTGC
E431D- α forward	GCAACCTGTGCACAG AC ATAGTGGAGTACACC
E431D- α reverse	GGTGTACT CCACTAT GTCT GTGCACAGG TTGC

The mutation sites are highlighted.

4.2.3 Conversion of apo β' to holo β'

$\beta'2$ (60 μ M) in 500 μ L of 50 mM HEPES, 100 mM KCl, 10% glycerol, pH 7.6 and 2.5 mM ascorbate acid was deoxygenated by 6 cycles of evacuation (for 3 x 10 s) followed by argon flushing (2 min) on a Schlenk line. The deoxygenated $\beta'2$ solution was brought into the glove box (M. Braun, Stratham, NH) and 6 eq. of Fe (II) (deoxygenated ferrous ammonium sulfate in 50 mM Tris, 100 mM KCl, pH 7.6) per $\beta'2$ was added. The resulting mixture was incubated at 4 °C for 30 min. The protein was then removed from

the glove box and 100 μ L of ice cold O₂ saturated 50 mM Tris, 100 mM KCl, pH 7.6 was added. O₂ (g) was also blown over the surface of the protein solution for 1 min. Excess iron was removed by Sephadex G-25 chromatography (40 mL, 2.5 x 30 cm) and the protein fractions pooled to give 3.5 mg/mL. An activity assay was carried out immediately and 250 μ L protein solution was placed in an EPR tube and frozen in liquid N₂ for measurement of the Y•. Typically 0.6 Y•/ β '₂ were observed and the specific activity of this proteins was 420 nmol/min/mg.

4.2.4 Mutants of α : construction of mutant genes, growth, and purification

Mutants of α C218S(A), C429S(A), C444S(A), C787S(A), C790S(A), E431Q(D) were generated by site directed mutagenesis using the Quick Change Kit (Stratagene). For each mutant, the gene was amplified by PCR using PfuUltra II polymerase (Stratagene) with primers (Table 4.1). The sequence of each mutant plasmid was confirmed by the MIT biopolymers laboratory. The mutants were expressed and purified as described below for wt α with similar yields.

4.2.5 Purification of α and α mutants by Ni NTA and dATP affinity chromatography

Cells (15 g) were suspended (5 vol/g) in 50 mM NaH₂PO₄, pH 7.0, 0.1% Triton X-100 and 10 mM 2-mercaptoethanol with the complete protease inhibitor (Roche). The suspension was passed through the French press at 14,000 psi. The cell lysate was centrifuged at 20,000 x g for 30 min. Streptomycin sulfate (10%) was added to the supernatant over 10 min to a final concentration of 1% (w/v) and stirred for additional 10

min. After the pellet was removed by centrifugation, the supernatant was incubated with Ni-NTA agarose resin (1 mL/g of cells, Qiagen) at 4°C for 1 h and then loaded into a column (2.5 × 10 cm). The column was washed with 30 column volumes of 50 mM NaH₂PO₄, 800 mM NaCl, 50 mM imidazole, pH 7.0, 0.1% Triton X-100 and 10 mM 2-mercaptoethanol. The protein was eluted with 50 mM NaH₂PO₄, 300 mM NaCl, 125 mM imidazole, pH 7.0. Fractions containing protein were identified using the Bradford assay. The fractions containing protein were pooled and concentrated to < 10 mL, and then the imidazole was removed by Sephadex G-25 chromatography (200 mL, 2.5 × 50 cm) using 50 mM Tris, pH 7.6, 5% glycerol, 1 mM DTT as eluent. The pooled protein fractions were added to dATP affinity resin (30 mL, equilibrated with 50 mM Tris, pH 7.6, 5% glycerol, 1 mM DTT) (30) and gently mixed for 2 h at 4 °C in a 50 mL falcon tube. The resin was then loaded into a column (2.5 × 10 cm) and washed with 300 mL 50 mM Tris, pH 7.6, 5% glycerol, 300 mM KCl, 1mM DTT. The protein was eluted with 50 mM Tris, pH 7.6, 5% glycerol, 100 mM KCl, 5mM DTT, 10 mM ATP. Fractions containing protein were identified using the Bradford assay. The fractions were pooled and concentrated to < 0.5 mL, and the ATP was removed by Sephadex G-25 chromatography (40 mL, 1.5 × 30 cm). α was stored in 50 mM Tris, 100 mM KCl, 15 mM MgCl₂, 5 mM DTT, pH 7.6, 5% glycerol with a typical yield of 1 mg/g of cells after the Ni affinity column, and 0.2 mg/g of cell pellet after dATP affinity chromatography. Only α used in SEC studies was purified with the dATP chromatography. α in the rest of the experiments and α mutants were purified by Ni affinity chromatography only.

4.2.6 Activity assays:

The reaction mixture contained the following in a final volume of 350 μL : 50 mM Hepes (pH 7.6), 15 mM MgCl_2 , 1 mM EDTA (assay buffer), 0.3 μM (or 3 μM) α , 3 μM (or 0.3 μM) β' , 3 mM ATP, 1 mM [^3H]-CDP (specific activity 5115 cpm/nmol), 100 μM *E. coli* TR, 1.0 μM TR reductase, 2 mM NADPH. The assay mixture was pre-incubated at 37 $^\circ\text{C}$ for 2 min and the reaction was initiated by the addition of [^3H]-CDP. Aliquots of 30 μL were removed over a 15 min time period and quenched in a boiling water bath for 2 min. dCDP production was analyzed, subsequent to removal of the phosphates with alkaline phosphatase as previously described (31) and analyzed by the method of Steeper and Stuart (32).

4.2.7 Time dependent inactivation studies:

The inactivation mixture contained the following in a final volume of 100 μL : 6 μM α , 6 μM β' , 3 mM ATP, 5 mM DTT, and assay buffer. The reaction was initiated by addition of 0.5 or 5 eq. of F_2CDP (3 μM , 30 μM) and incubated at 37 $^\circ\text{C}$. Three types of assays were carried out. In assay 1, aliquots (10 μL) from the reaction mixture were removed at several time points from 30 s to 23 min and diluted 5 fold into 50 μL of assay buffer. dCDP production was measured as described above. A control experiment under identical conditions with the omission of F_2CDP was always carried out to assess the stability of β' . In assays 2 and 3, the activity of each subunit was measured. Aliquots (2.5 μL) of the inactivation mixture were diluted into 50 μL of assay buffer containing 3 μM (10 fold excess) of the second subunit α or β' . dCDP production was measured as described above.

4.2.8 Quantitation of covalent labeling of human $\alpha_n(\beta'2)_m$ with [1'-³H]-F₂CDP and [5-³H]-F₂CDP

A typical reaction mixture contained the following in a final volume of 200 μ L: 8.5 μ M α , β' , with 5 mM DTT, 3 mM ATP in assay buffer. The reaction was initiated with 10.6 μ M of [1'-³H]-F₂CDP (5889 cpm/nmol) or 10.6 μ M of [5-³H]-F₂CDP (6643 cpm/nmol). After 8 min at 37°C, an aliquot of 195 μ L was either directly loaded onto a Sephadex G-50 column (1 cm x 20 cm, 20 mL) that was pre-equilibrated with the assay buffer, or mixed with guanidine-HCl at a final concentration of 6 M, incubated for 5 min, and then loaded onto a Sephadex G-50 column with assay buffer containing 2 M guanidine-HCl. Fractions (1 mL) were collected and assayed for protein by Bradford assay and 500 μ L of each fraction was analyzed by scintillation counting.

4.2.9 Quantitation of cytosine released during the inactivation of human $\alpha_n(\beta'2)_m$ by [5-³H]-F₂CDP

The reaction mixture contained the following in 500 μ L with α , β' each at 1.2 μ M and [5-³H]-F₂CDP (6643 cpm/nmol) at 1.2 μ M (2 eq/ α 2). The reaction was incubated for 15 min at 37 °C. The mixture was then filtered through an YM-30 Centricon device (Millipore) at 4° C. F₂C (60 nmol) and cytosine (120 nmol) were added as carriers before filtration. The flow through was treated with 30 U of alkaline phosphatase (Roche) for 3 h at 37 °C and filtered through a second YM-30 Centricon device. The flow through was analyzed using a Waters 2480 HPLC with an Altech Adsorbosphere Nucleotide Nucleoside C-18 column (250 mm x 4.6 mm) at a flow rate of 1mL/min. The elution buffer contained: Buffer I, 10 mM NH₄OAc, pH 6.8; Buffer II: 100% methanol. A 10

min isocratic elution was followed by a linear gradient to 40% buffer II over 30 min. A linear gradient was then run to 100% buffer II over 5 min. Fractions (1 mL) were collected and 200 μ L of each were analyzed by scintillation counting. The recovery of [5- 3 H]-cytosine and [5- 3 H]-F₂C was calculated based on the UV spectrum (cytosine, $\lambda_{267 \text{ nm}}$, $\epsilon = 6100 \text{ M}^{-1}\text{cm}^{-1}$, F₂C, $\lambda_{268 \text{ nm}}$, $\epsilon = 9360 \text{ M}^{-1}\text{cm}^{-1}$) and normalized for carrier added. The radioactivity recovered with [5- 3 H]-cytosine and [5- 3 H]-F₂C was analyzed by scintillation counting.

4.2.10 SDS PAGE of Inactivation mixture without boiling

The inactivation mixture contained the following in a final volume of 35 μ L: 6 μ M α or C218S- α , 6 μ M β' , 3 mM ATP, with or without 5 mM DTT, and assay buffer. The reaction was initiated by addition of 5 eq. of F₂CDP (30 μ M) and incubated at 37°C for 5 min. Inactivation mixture (8 μ L) was mixed with 8 μ L 2x loading buffer \pm β -mercaptoethanol. The samples were either heated at 90 °C for 2 min or not heated before loading on a 10% SDS-PAGE gel. The proteins were visualized with Coomassie blue staining. The band intensities were quantified using BioRad Quantity One software.

4.2.11 Incubation of [1'- 3 H] F₂CDP and C218S/A-, C429S/A-, C444S/A-, C787S/A-, C790S/A-, E431Q/D- α and β' and analysis for covalent labeling by Sephadex chromatography

A typical reaction mixture contained in a final volume of 200 μ L: 8.5 μ M α mutant and β' , 5 mM DTT, 3 mM ATP in assay buffer. The reaction was initiated with 10.6 μ M of [1'- 3 H]-F₂CDP (5889 cpm /nmol). After 8 min at 37°C, an aliquot of 195 μ L

was loaded onto a Sephadex G-50 column (1 cm x 20 cm, 20 mL) that was pre-equilibrated with the assay buffer. Fractions (1 mL) were collected and assayed for protein presence by Bradford assay and 500 μ L of each fraction was analyzed by scintillation counting.

4.2.12 SEC to examine the quaternary structure of $\alpha_n(\beta'2)_m$ subsequent to inactivation by F_2 CDP:

SEC was performed using a Superdex 200 column (10 x 300 mm, GE healthcare) attached to a Waters 2480 HPLC. Gel filtration molecular weight standards (GE healthcare) were ovalbumin, 43 kDa; conalbumin, 75 kDa; aldolase, 158 kDa; catalase 232 kDa; ferritin, 440 kDa; thyroglobulin, 669 kDa; and blue dextran, 2000 kDa. The elution buffer was 50 mM Hepes (pH 7.6), 15 mM $MgCl_2$, 1 mM EDTA and 0.5 mM ATP. Molecular weight standards were run at the beginning of each experiment. The reaction mixture (400 μ L) contained 15 μ M α and β' (or Y138F- β'), 5 mM DTT, 3 mM ATP, 37.5 μ M F_2 CDP (2.5 eq) in assay buffer. α was purified using Ni affinity- and dATP affinity-chromatography and had a specific activity of 232 nmol/min/mg (measured with β_2). $\beta'2$ contained 0.63 Y• (specific activity 413 nmol/min/mg). After 10 min incubation, 390 μ L was injected onto the column using a 500 μ L loop. The elution rate was 0.5 mL/min and 0.5 mL fractions were collected. If [1 - 3 H]- F_2 CDP was used in the inactivation mixture, 300 μ L aliquots of each fraction were analyzed by scintillation counting.

4.2.13 Quantitative analysis of the subunits of $\alpha_n(\beta'2)_m$ by SDS PAGE

The fractions collected from the SEC analysis above were analyzed directly (8 μ L from each fraction) by 10% SDS- PAGE and compared with concentrations of α and β from *E. coli* RNR (0.05 μ M to 0.4 μ M) as standards. To analyze the peak of protein that eluted first from the SEC studies of the Y138F/ α and the α/β' with ATP control experiment, each fraction through the peak was concentrated before loading on the gel. The proteins were visualized with Coomassie blue staining. The band intensities were quantified using BioRad Quantity One software. The concentrations of α and β' in the complex were determined from standard curves made with *E. coli* subunits as described above.

4.3 Results:

4.3.1 Purification and reconstitution of the $\beta'2$

Growth of $\beta'2$ was carried out in the presence of 1, 10-phenanthroline resulting in apo protein. This procedure gave higher recovery of $Y\bullet$ and activity than standard growth conditions with addition of ferrous ammonium sulfate and ascorbate to the crude lysate prior to purification. $\beta'2$ was purified by addition of Phenyl Sepharose 6 Fast and Q-Sepharose Fast Flow column chromatographies to the procedure of Thelander (27). These steps were required to obtain homogeneous protein by SDS PAGE. A variety of methods to assemble the essential diferric-tyrosyl radical ($Y\bullet$) cluster of $\beta'2$ were examined including use of tagged and non-tagged versions of $\beta'2$ and varying the ratio of Fe^{2+}/β' . The detailed procedure described in Methods gave 0.63 $Y\bullet$ per $\beta'2$ with activity of 420 nmol/min/mg. The procedure reported by the Thelander group gave 1 $Y\bullet$ per $\beta'2$ (non-tagged), but the activity was 95 nmol/min/mg (27). A second purification procedure

reported by Yen and coworkers using a tagged- $\beta'2$ gave $0.8 Y\cdot/\beta'2$ and a specific activity of 50 nmol/min/mg (21). The low activity and high $Y\cdot$ content reported by these groups are at odds with activity being directly proportional to $Y\cdot$ (33, 34). The basis for the discrepancy is not understood. In our hands we have been unable, after many attempts with identical constructs to those used by Thelander and Yen, to obtain higher levels of $Y\cdot/\beta'2$. However, with our previous purification of $h\beta$, our group did obtain the same amount of radical ($1 Y\cdot/\beta'2$) as these groups but with 7-14 fold higher activity. Our ability to only obtain $0.6 Y\cdot/\beta'2$ makes the experiments described subsequently to quantitate products from the F_2CDP reaction more complex as there is always present about $0.4 \beta'2$ and α that have not reacted. In the quantitations reported below we have placed numbers normalized to $1 Y\cdot/\beta'2$ in parentheses.

4.3.2 Time dependent inactivation studies of α , $\beta'2$ by F_2CDP/ATP .

Our previous studies with F_2CDP on human $\alpha_n(\beta'2)_m$ and *E. coli* $\alpha'2\beta'2$ showed that F_2CDP is a sub-stoichiometric mechanism based inhibitor resulting in covalent binding of 1 eq. of the sugar moiety from $[1'-^3H]-F_2CDP$ per $\alpha'2$. To determine if $\beta'2$ behaves in a similar fashion, inactivation studies were carried out with α , β' ($6 \mu\text{M}$ each) and 0.5 or 5 eq. F_2CDP/α in the presence of reductant (either DTT or TR/TRR/NADPH). Three different assays were carried out. In the first assay (Figure 4.1) the enzyme was diluted 5 fold and assayed for dCDP production. Both concentrations of F_2CDP resulted in $> 90\%$ inactivation with the reaction in the presence of 5 fold excess of inhibitor relative to α being complete in four minutes (\blacktriangle). Even under these conditions it is unlikely that the enzyme is saturated with F_2CDP . As with $h\beta$, substoichiometric amounts of inhibitor

result in >90% inactivation (■), although the inactivation is slow and about 60% of the activity is lost in the “fast” phase. The control with $\beta'2$ in the absence of inhibitor reveals that $Y\bullet$ is lost, precluding longer time points (Figure 4.1 ◆). The half life of $Y\bullet$ loss is similar to our observations with $h\beta$ (13).

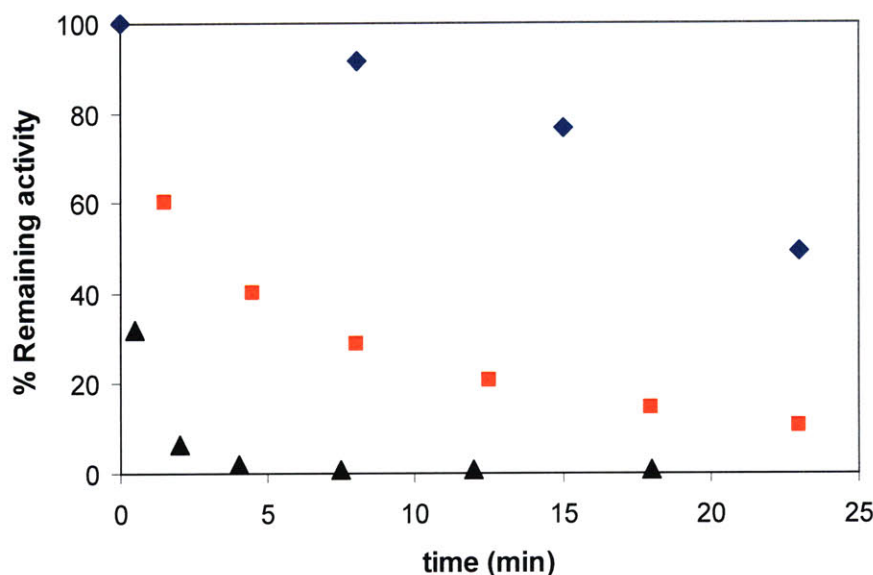


Figure 4.1: A Time dependent inactivation assay of human $\beta'2$ and α by F_2CDP . Inactivation mixture contained final concentrations of α , β' , 6 μM ; F_2CDP , 30 μM (▲), 3 μM (■), 0 μM (◆); ATP, 3mM; DTT, 5mM. Aliquots were removed at various times and diluted 5 fold for determination of RNR activity.

Because of the weak interactions between the two subunits in the class I RNRs, assays of the individual subunits, α (β'), are typically carried out in which a ten fold excess of the second subunit, β' (α), is present in the assay mixture. The result of a typical experiment under these conditions is shown in Figure 4.2. Under these conditions α is 95% inactivated, while β' retained 40% of its activity after correction for β' stability (◆). These results are similar to those for the *E. coli* RNR and the hRNR with β . The

results suggest that excess α can facilitate subunit dissociation and liberate the remaining active β' . The implications of these results will be addressed subsequently.

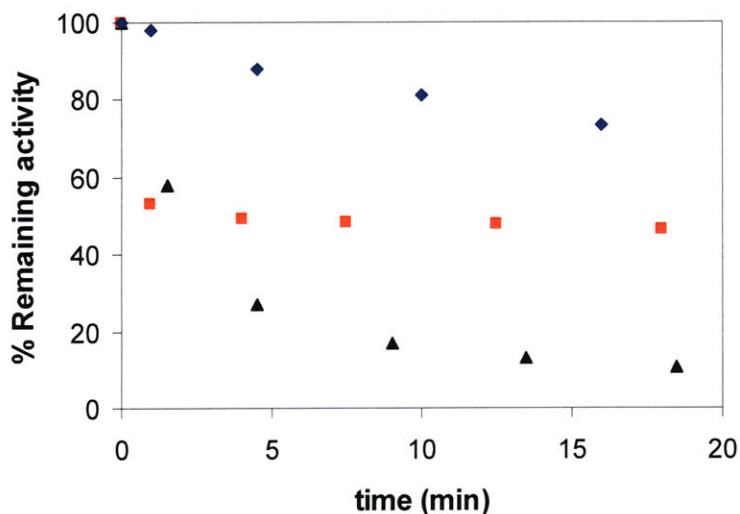


Figure 4.2: Time dependent inactivation assay of human $\beta'2$ and α by F_2CDP in the presence of an excess of the other subunit.

Inactivation mixtures contained final concentrations of α , β' , $6 \mu M$; F_2CDP , $3 \mu M$; ATP, $3mM$; DTT, $5mM$. Aliquots were removed at various times and diluted 20 fold for determination of α (▲) and β' (■) activity in the presence of 10 fold excess of β' or α . The activity of β' (■) was adjusted using results from the control experiment (◆) for β' activity in the absence of inhibitor.

4.3.3 Quantitation of labeled RNR and small molecules generated by inactivation with $[1'-^3H]$ and $[5-^3H]-F_2CDP$

With $[1'-^3H]-F_2CDP$, our previous studies with h $\beta2$ containing 1.2 Y•, identified 0.9 eq./ $\alpha2$ of covalently bound sugar. A similar experiment using α and β' each at $4.2 \mu M$ and 2.5 eq. $[1'-^3H] F_2CDP$ was carried out for 8 min at $37^\circ C$. The reaction mixture was analyzed by Sephadex G50 column chromatography in the presence or absence of denaturant (guanidine-HCl). The results are shown in (Table 4.2) and reveal 0.5 eq./ $\alpha2$

(normalization gives 0.83 eq./ $\alpha 2$). When the experiment was repeated with the [5-³H]-F₂CDP under identical conditions in the absence of denaturant, 0.03 eq./ $\alpha 2$ (0.05) was detected with protein (Table 4.2).

To test if 0.5 eq. sugar/inactivated enzyme is accompanied by 0.5 eq. of cytosine release, two eq. of [5-³H] F₂CDPs (1.2 μ M) were incubated with $\alpha 2\beta'2$ (0.6 μ M) for 15 min at 37 °C. Subsequent to inactivation the nucleotides were recovered by ultrafiltration and analyzed by HPLC. The analysis revealed that 0.65 eq. (1.08) of cytosine were released and 1.35 eq. of F₂C was recovered (Figure 4.3). These results are in agreement with our previous studies on inactivation of human $\alpha_n(\beta'2)_m$ and *E. coli* RNR and reveal that the extent of reaction correlates with the amount of Y• in β or β' .

Table 4.2: Covalent labeling of human $\alpha_n(\beta'2)_m$ with [1'-³H]-F₂CDP and [5-³H]-F₂CDP analyzed by SEC.

Protein	[x- ³ H]-F ₂ CDP where x =	Conditions	[³ H] / $\alpha 2\beta'2$
human	1'	native	0.5
$\beta'2, \alpha$	1'	denaturing	0.5
	5	native	0.03

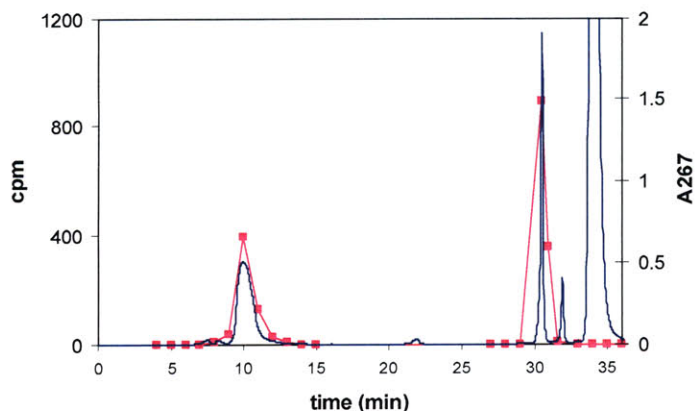


Figure 4.3: Analysis by HPLC of products generated during inactivation of $\alpha_n(\beta'2)_m$ by $[5\text{-}^3\text{H}]\text{-F}_2\text{CDP}$.

The inactivation mixture contained final concentrations of α , β' , 1.2 μM ; $[5\text{-}^3\text{H}]\text{-F}_2\text{CDP}$, 1.2 μM , 3mM ATP, 5mM DTT. Subsequent to removal of the protein from the small molecules by YM3 centricon and removal of the phosphates with alkaline phosphatase, the filtrate was injected into an Altech Adsorbosphere Nucleotide Nucleoside C-18 column at a flow rate of 1mL/min. The elution buffer contained: Buffer A, 10 mM NH_4OAc , pH 6.8; Buffer B: 100% methanol. A 10 min isocratic elution was followed by a linear gradient to 40% B over 30 min. The elution profile monitored by $A_{267\text{nm}}$ (—) and scintillation counting (■). Cytosine (0.65 eq.) was released and 1.35 eq. of F_2C was recovered.

4.3.4 Analysis of the inactivation mixture of wt and C218S- α by SDS PAGE without boiling

Our recent studies with *E. coli* RNR and *L. leichmannii* RNR revealed that when the enzyme inactivated with the inhibitor was analyzed by an SDS PAGE gel without boiling, 30 to 50% of α present migrated as a larger species (~110 kDa for *E. coli* and 110 kDa for *L. leichmannii*) (23, 35). The α with the aberrant migratory properties is likely associated with the covalently bound sugar moiety from F_2CDP . To determine if the substoichiometric labeling of hRNR, both β' and β , was accompanied by production of a modified α , the reaction mixture subsequent to inactivation was analyzed directly without boiling by SDS PAGE (Figure 4.4). It was observed that 24% (40%) and 33% of the α

migrated as a larger species (~120 kDa) with β' and $h\beta$, respectively. This number in each case corresponds roughly to the amount of covalently bound sugar. With all RNRs examined to date, even the monomeric adenosylcobalamin RNR, production of an α with altered migratory properties that is associated with covalent modification by the sugar moiety of $F_2CD(T)P$ occurs.

The same experiment was repeated with C218S of which protein and the results are also shown in Figure 4.4 (Lane 8-13). With this mutant no altered conformation of α is observed suggesting that this residue may play an important role in its production. A proposal for these observations is presented subsequently.

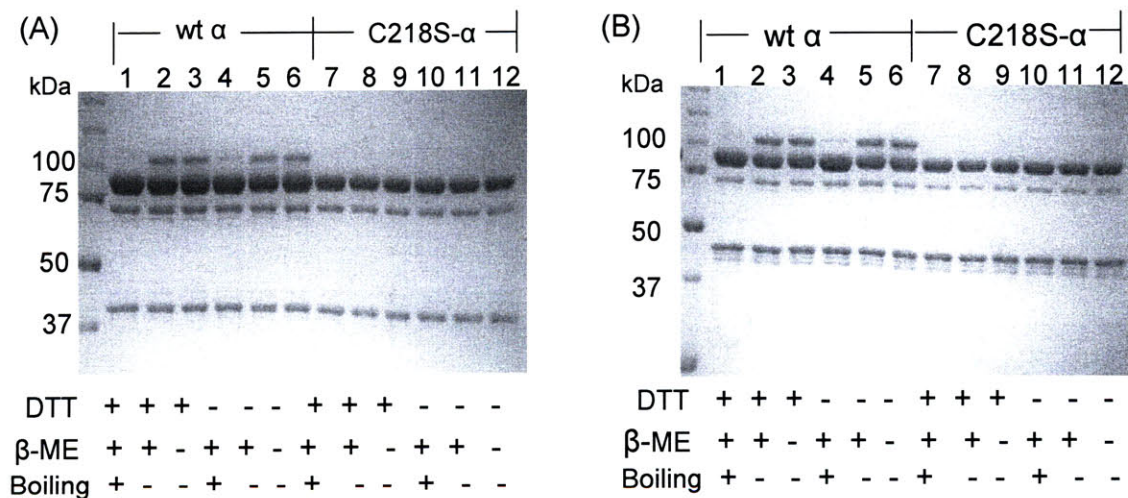


Figure 4.4: SDS-PAGE analysis of the inactivation mixture.

SDS-PAGE analysis of (A) the α/β' (6 μ M) and (B) the α/β (6 μ M), inactivated by F_2CDP (30 μ M) and ATP (3 mM) at 37 $^{\circ}$ C for 5 min. Each sample was mixed with 2x loading buffer \pm β -ME or boiling for 2 min before loading as indicated. A band at 120 kDa is observed in Lanes 2, 3 (inactivation in the presence of DTT, without boiling) and Lanes 5, 6 (inactivation in the absence of DTT, without boiling).

4.3.5 Identification of potential sites of covalent modification of human RNR inactivated by [1'-³H] F₂CDP using site directed mutants of important residues in α involved in catalysis

The recent studies in our lab with *L. leichmannii* RTPR have established that 10% of the label associated with RNR subsequent to inactivation by [1'-³H]-F₂CTP is due to alkylation of the sugar of the nucleotide by both cysteines at the C-terminus of the protein (23). All efforts to identify the major labeled species failed, due to instability and rearrangement, even when NaBH₄ was used to stabilize the alkylated protein. Furthermore, studies with the C225S mutant of *E. coli* RNR, suggested that this residue plays a key role in covalent modification of the enzyme by F₂CDP (35). To identify the site of covalent modification by the sugar derived from F₂CDP, [1'-³H] F₂CDP was incubated with active site mutants of human α : C429S/A, E431Q/D, C787S/A, C790S/A, C444S/A, C218S/A (the equivalent of C225 in *E. coli*) and with β or β' in the presence of DTT. Each mutant was purified as described for wt- α with similar recovery. The extent of covalent labeling measured subsequent to Sephadex G50 chromatography (in the absence of denaturant) was determined by scintillation counting and compared to the labeling of wt-RNR. The results are summarized in Table 4.3.

Table 4.3: Quantitation of sugar label covalently attached to human RNR mutants incubated with [1'-³H]-F₂CDP.

	labeling/ α 2 (with β '2)	labeling/ α 2 (with β 2)
wt α	0.5 (0.8) ^b	0.8-0.9
C429S- α (C439) ^a	0	0.008
C429A- α (C439)	0	0.01
E431Q- α (E441)	0	0.01
E431D- α (E441)	0	0.08
C787S- α (C754)	0.3 (0.5)	0.8
C787A- α (C754)	0.26 (0.4)	0.3
C790S- α (C759)	0.3 (0.5)	0.6
C790A- α (C759)	0	0.1
C444S- α (C462)	0.03 (0.05)	0.4
C444A- α (C462)	0.2 (0.3)	0.7
C218S- α (C225)	0	0.1
C218A- α (C225)	0	0.1
Y138F- β ' (Y122)	0	

a: In parenthesis, the equivalent residues of *E. coli* RNR are given.

b: In parenthesis, the values are normalized to 1 Y•/ β '2.

As expected no label was associated with RNR when the radical initiator on α (C429), essential for removal of the 3'-H for any mechanism based inhibitor, was changed to S or A. Two other mutants E431Q/D- α and C218S/A- α also showed no labeling. The E431 mutant is likely not labeled as this glutamate plays an important role

(although not essential role) in the first two steps of the reduction process by removal of proton from the 3'-OH of F₂CDP. Thus the rate of chemistry on any nucleotide is likely to be greatly reduced when the E is changed to a Q/D. In addition a recent structure of the *S. cerevisiae* α soaked with F₂CDP (Figure 4.5) showed that E431 is 6.2 Å from the 3'-HO of the sugar and that a water molecule intervenes (36). Thus, it is unlikely that this E is the site of labeling.

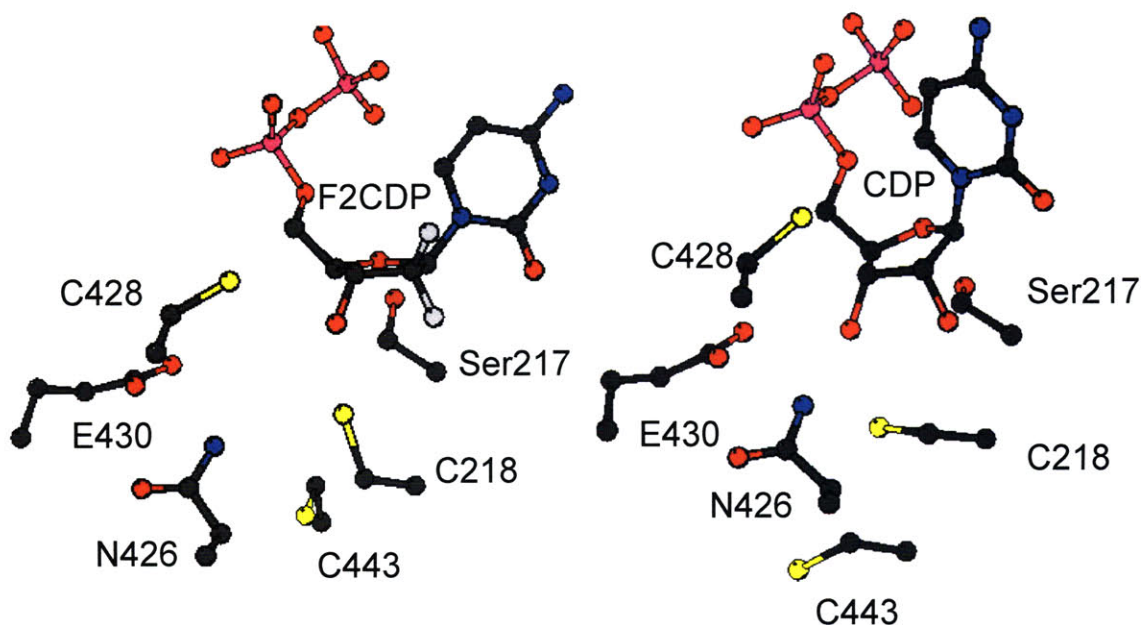


Figure 4.5: The yeast RNR active site structures with F₂CDP (left) or CDP (right) bound.

C225 on *E. coli* α , on the other hand has been implicated as playing a key role in the inactivation pathway involving covalent modification of the *E. coli* RNR (35). Our previous studies with the C225S mutant of *E. coli* have demonstrated that first few steps in catalysis are not impaired by this mutation (37, 38). Thus lack of labeling with C218S/A- α , make this a likely candidate for alkylation. Consistent with this proposal, the *S. cerevisiae* structure (Figure 4.5) shows that this is the only nucleophilic residue

close to the sugar (36). The caveat is however, that the other subunit essential for catalysis is missing in the structure. Thus our favored model is that C218 is covalently modified by a sugar moiety derived from F₂CDP. In line with this proposal, the SDS PAGE gel (Figure 4.4), revealed that with the C218S- α mutant and either h β or β' , that no α with modified migratory properties is observed.

The C-terminal tail mutants of α , C787S/A and C790S/A retain variable amounts of label associated with hRNR (with either β or β'). These cysteines are involved in re-reduction of the active site disulfide generated during the synthesis of dNDP (39). This C terminus must be able to enter the active site to reduce the disulfide between C218 and C444 and then must swing out of the active site to react with the protein reductant thioredoxin. The variability in labeling suggests that one of these cysteines, may be involved in covalent interaction with the sugar moiety as well. Labeling of the active site C218 and a C (787 or 790) in the tail might give rise to the observed conformational change found by SDS PAGE (Figure 4.4).

4.3.6 SEC to examine the quaternary structure of hRNR (with β') inactivated by F₂CDP

Our previous studies have shown that a tight $\alpha_6\beta_6$ complex was generated when human RNR was inactivated by F₂CDP ($\alpha_2\beta_2$ in the case of *E. coli*). The studies presented herein revealed that modification of the enzyme with 0.5 eq. of F₂CDP in the presence of reductants precluded any subsequent turnovers, and left the enzyme in an intermediate state with significantly enhanced interaction between the subunits. To examine the quaternary structure of $\alpha_n(\beta'2)_m$ subsequent to inactivation with [1'-³H]-

F₂CDP, the inactivated complex was examined by SEC with 0.5 mM ATP in the elution buffer. The A_{280nm} revealed protein elution at 18.6 min and at 25.6 min (Figure 4.6). Comparison of the retention times with a standard curve generated with globular proteins of known molecular weight (Figure 4.7) suggested that the peak eluting at 18.6 min exhibits a mass more consistent with $\alpha_6\beta'_6$ than $\alpha_6\beta'_2$ (798 vs 633 kDa). Control experiments with α (88 kDa), α_2 (189 kDa with TTP), β'_2 (116 kDa) (Table 4.4 and Figure 4.8) suggest that the peak eluting at 25.6 min may be composed of β'_2 and α . Each fraction was examined by SDS-PAGE with the amount of α and β' determined from a standard curve made with known concentrations of *E. coli* α and β (Figure 4.9). Analysis of protein in fractions 18, 19 and 20, gave a ratio of α : β' as 1.2, 1.0, 1.0 respectively and respectively 1; an average of 1.06 ± 0.15 (Figure 4.6B, C). This analysis supports the formation of an $\alpha_6\beta'_6$ complex in the presence of F₂CDP and ATP. Each fraction was also analyzed for radioactivity and fractions 18 and 19 contained 0.57 and 0.54 labels/ α_2 respectively.

As discussed above, β'_2 contains only 0.6 Y• and thus gives rise to protein that does not form a complex. The relative amounts of the two peaks support the proposal that the percentage of active quaternary structure correlates with the amount of the Y•. Together with the observations of 0.5 eq. sugar/ α_2 attached, and 0.6 eq. cytosine released after inactivation, these results support a model where 1 eq. of F₂CDP inactivates the two active sites of α_2 by enhancing subunit interactions.

Given the poor resolution of the SEC method, a second control experiment was carried out under identical conditions to those described above in the absence of F₂CDP (Figure 4.6D). The mixture, analyzed by SEC gave two protein peaks: one with a

retention time of 20.9 min and an apparent molecular weight of 543 kDa and the second with a retention time of 26.2 min and an apparent molecular weight of 109 kDa. The SDS-PAGE analysis of the first peak showed only the presence of α , which correspond to α_6 , and the second peak showed the presence of both α and β' corresponding to α_2 and β'_2 based on the apparent MW (Table 4.4).

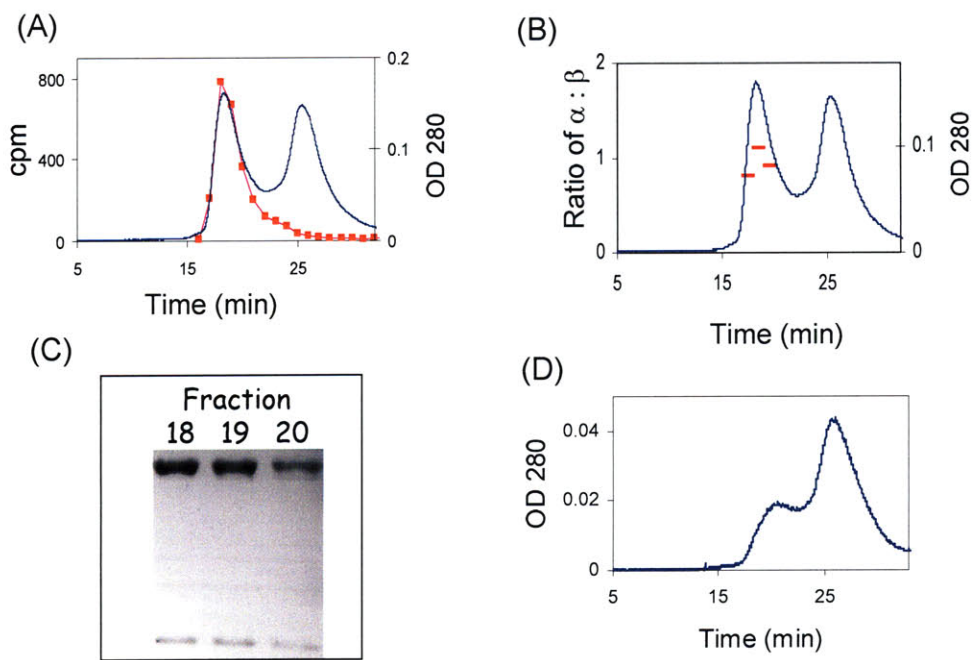


Figure 4.6: SEC on a S200 column to detect complex formation after human p53R2 α is inactivated by [1'- 3 H] F₂CDP.

The inactivation mixture contained final concentrations of α , β' , 15 μ M; [1'- 3 H]-F₂CDP 37.5 μ M; ATP, 3mM; DTT, 5mM. The elution buffer contained 0.5 mM ATP. A, the elution profile monitored by A_{280nm} and scintillation counting (■). The first peak has a retention time of 18.6 min, with apparent molecular weight of 794 kDa; The second peak has a retention time of 25.6min with apparent molecular weight of 116 kDa (α , β'_2 coelute); B, analysis of the ratio of α : β (-), using standard curves generated from known amounts of *E. coli* α and β ; C, SDS PAGE of 8 μ L from fractions 18-20 part A monitored by SDS PAGE; D, A control in the absence of F₂CDP. The first protein peak has a retention time of 20.9 min and an apparent molecular weight of 543 kDa; The second protein peak has a retention time of 26.2 min with apparent molecular weight of 109 kDa.

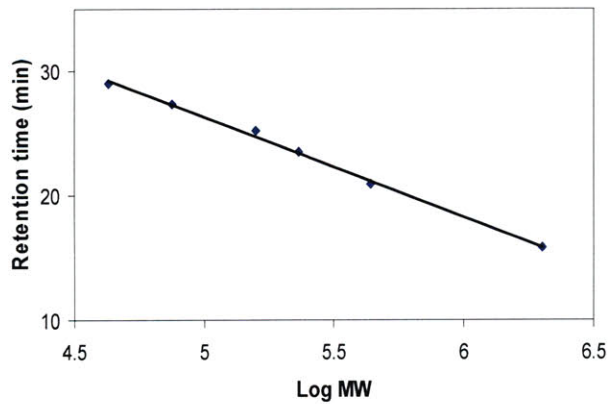


Figure 4.7: Gel filtration molecular weight standards (GE healthcare).
 Ovalbumin, 43 kDa; conalbumin, 75 kDa; aldolase, 158 kDa; catalase 232 kDa; ferritin, 440 kDa; thyroglobulin, 669 kDa; and blue dextran, 2000 kDa (♦ from left to right).

Table 4.4: Molecular weight determination of inactivated hRNR by SEC.

	Protein (effector)	Apparent mass (kDa)	Retention time (min)	Expected mass (kDa)	Oligomeric state
human RNR	β'	116	26	81	$\beta'2$
	α	88	25.6 ^a	92	α
	α (100 μ M TTP)	189	24 ^a	184	$\alpha2$
	α, β' (ATP)	543, 109	20.9, 26.2	552, 184, 81	$\alpha6, \alpha2, \beta'2$
	α, β' inactivated by F_2 CDP	794, 116	18.6, 25.6	798	$\alpha6\beta'6$ complex ^b
	$\alpha, Y138F-\beta'$ inactivated by F_2 CDP	389-712, 88	20-22.5, 26.9	184, 81	$\alpha6\beta'2, \alpha6\alpha2, \beta'2$

- a. Superose 12 column was used.
 b. Un-reacted $\alpha2, \beta'2$ also present.

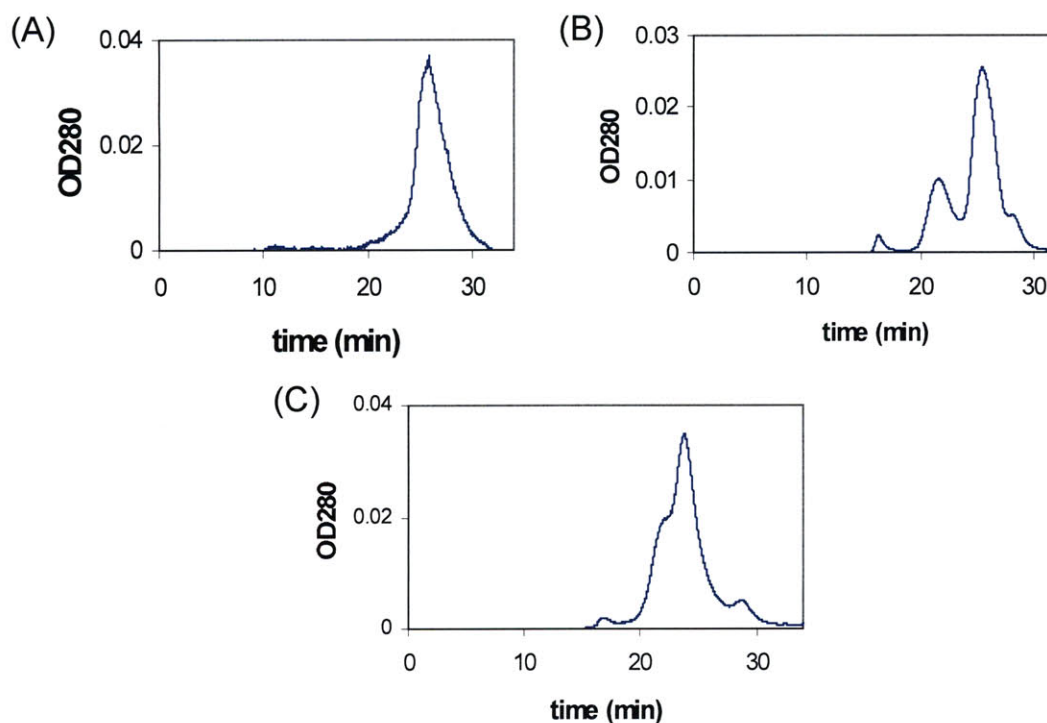


Figure 4.8. SEC of a control with $\beta'2$, α and $\alpha2$ with TTP.

(A) $\beta'2$ (81 kDa) migrates at 26 min with an apparent MW 116 kDa. A S200 column (GE healthcare) was used. (B) α (25 mM DTT). The first peak elutes at 21.7 min is a contaminant that co-purifies with α , the second protein elutes at 25.6 min, with apparent MW 88 kD. (C) $\alpha2$ (100 μ M TTP). The protein peak that elutes at 22 min is the contaminant that co-purifies with α . The second protein elutes at 24 min with an apparent MW 189 kD. Superose 12 column was used in (B) and (C).

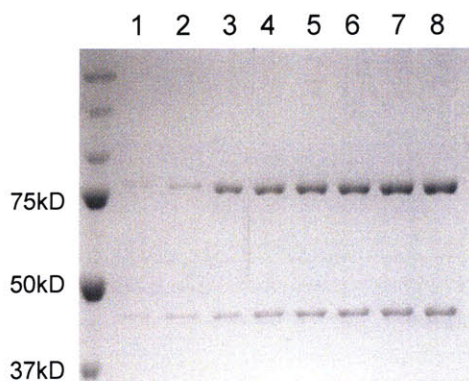


Figure 4.9. *E. coli* α and β (0.05- 0.4 μ M) standards at different concentrations analyzed by SDS-PAGE to determine the ratio of α , β' in Figure 4.6B and Figure 4.10.

4.3.7 An additional control: SEC to examine the quaternary structure of hRNRS with Y138F- β' in the presence of F₂CDP and ATP

To gain further insight into the quaternary structure of hRNR without covalent modification in the presence of F₂CDP, Y138F- β' in which the essential Y• of $\beta'2$ was replaced with an F, was studied. The reaction mixture was identical to that described above except that Y138F- β' replaced wt- β' . Analysis of the reaction mixture by SEC showed that a small portion of protein migrated between 20-22.5 min, with an apparent MW ranging from 389-712 kDa followed by a second protein peak with a retention time at 26.9 min and an apparent MW of 88 kDa (Figure 4.10, Table 4.4). No radioactivity eluted with either peak when [1'-³H] F₂CDP was used. SDS-PAGE analysis revealed that both α and β' were present in the peak that eluted at 20-22.5 min, but the ratio of α : β' is much higher than 1 (within the range 5.8-9.1) by comparison with standards (Figure 4.9). The results suggest a complex equilibrium between nucleotide analog/ATP and subunits, consistent with the existence of $\alpha6\beta2$, $\alpha6$ and other species.

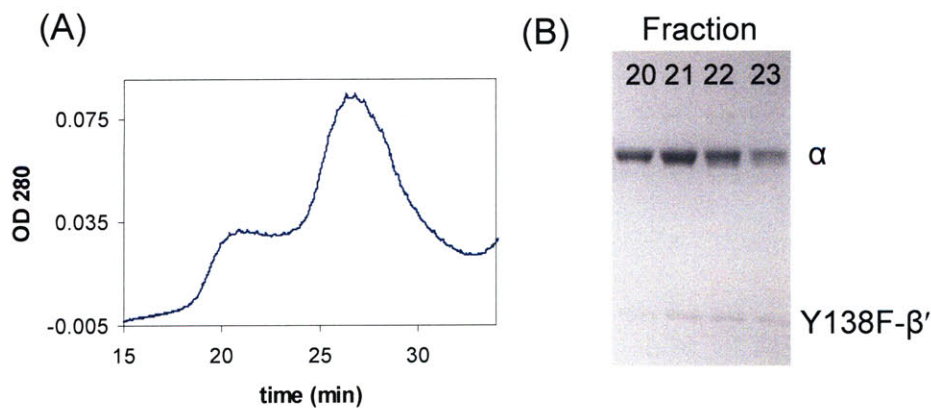


Figure 4.10. SEC on a S200 column to detect complex formation with human Y138F- β' / α incubated with [1'-³H] F₂CDP.

The inactivation mixture contained final concentrations of α , β' , 15 μ M; [1'-³H]-F₂CDP 37.5 μ M; ATP, 3mM; DTT, 5mM. The elution buffer contains 0.5 mM ATP. A, the elution profile monitored by A280nm and scintillation counting. The first peak is very

broad and has a retention time from 20-22.5 min with apparent molecular weights ranging from 389-712 kDa; The second protein peak has a retention time of 26.9 min, with apparent molecular weight of 88 kDa. Neither of these peaks contained radioactivity; B, fractions 20-23 from the first protein peak in A were monitored by 10% SDS PAGE.

4.4 Discussion:

The mechanism of inactivation of RNRs by F₂CDP is obviously very complex. However, despite this complexity, the RNRs from *E. coli*, *L. leichmannii* and the two RNRs from humans share common and mechanistically/structurally informative features. Stoichiometric amounts of inhibitor are sufficient for complete inactivation (13, 40). In the case of the class I RNRs, this inhibition prevents the second α/β pair from reaction because of the tight and unusual subunit interactions (13). In all cases, the protein becomes covalently modified in a chemically fragile state by a sugar moiety generated from F₂CDP and the cofactor (Y• or adenosylcobalamin) is partially inactivated. In all cases, if one waits long enough, two fluoride ions and one cytosine are released, requiring ketone formation at the C3' position of the nucleotide during the inactivation process. Unexpectedly, the α subunit is observed to have two conformations in about an approximately 1:1 ratio on SDS PAGE analysis in the absence of heat. Mutagenesis studies suggest that the second conformation is likely the result of a crosslink between a cysteine in the C-terminus of α and its active site C218, directly involved in water loss in the normal reduction process. The key to the function of RNR is understanding the gymnastics of the structurally floppy, and thus structurally inaccessible, C-termini of β and C-termini of α .

From our present observations information about the subunit architecture/interactions result. The altered α is likely to be formed from an intramolecular crosslink, rather than a cross-link from the C-terminus of the adjacent α in the α_2 dimer. If the crosslink were intermolecular, α should migrate on the SDS PAGE gel as a dimer and would likely be sensitive to β -ME treatment. Re-reduction of the active site disulfide in one α , by the C-terminal tail of the second α in the α_2 complex had previously been suggested by pre-steady state *in vitro* studies on *E. coli* RNR by Ericksson (41) and *in vivo* studies of *S. cerevisiae* RNR by Huang and coworkers (42). Our previous pre-steady state experiments (43) with mutations of the C-terminal cysteines were not inconsistent with the Ericksson proposal. In the Huang studies, the kinetics of re-reduction of the active site disulfide are not measured due to the *in vivo* nature of the experiments. We have previously shown that the two cysteines in the C-terminal tail of *E. coli* RNR can function as a thioredoxin and this observation is also likely to be applicable to the *S. cerevisiae* RNR and could account for their *in vivo* results (39).

A second observation of interest is that the C-terminus of α , must have access to the active site of the same α , while β remains bound. If our interpretation of the altered migratory properties of α is correct, a recent structure of a complex of a class Ib RNR from *Salmonella typhimurium* at 4.5 Å resolution may be informative in the regard (44). In this structure, the two subunits are present with a 360 Å² interface. The interface however, is very informative with respect to the function of the C-termini of each subunit. One can observe the end of β (residue 285), a gap of 20 amino acids and the last eleven amino acids of β bound in a hydrophobic patch formed by 3 helices (α_{10} , α_I and α_D)

within α . One can also locate the C-terminus (residue 699 missing the last 15 amino acids) of α within the structure and its position relative to β . One β is interacting with one α in a fashion that with tightening could align the radical transfer pathway between the two subunits in a chemically competent fashion. In this $\alpha\beta$ the active site cysteines are oxidized and some electron density exists for the ADP substrate. The second α has no substrate bound and no contact with the second β . Examination of the locations of the C-termini of the subunits suggest that the tails of α and β could be intertwined and that complete dissociation of the subunits might require a push from an interaction with a second α_2 interacting with the dangling β_2 . This model would be consistent with the kinetics of inactivation by F_2CDP in all the class I RNRs where a 1:1 complex of subunits is inactive, while assaying for activity of one subunit in the presence of an excess of the other subunit leads to some recovery of β_2 activity as all the $Y\cdot$ has not been destroyed. This type of displacement could account for the biphasic nature of the inactivation process (Figure 1).

Uhlin has suggested that the structure of the class Ib RNR complex is a snapshot of one of the steps during the RNR mediated reduction: either an initial step in subunit interaction or a final step after the reduction process. The unusual conformation of α in the F_2CDP inactivated RNR complex suggests that it might be trapping the enzyme in an asymmetrical configuration as well. The tight interaction between the subunits subsequent to inactivation by F_2CDP suggests that crystallization of the complex may be possible. Recently we have obtained crystals of the *E. coli* RNR that diffract to 6 Å resolution (Stock, Drennan, unpublished work). Obviously higher resolution structures are essential to figure out the key role of the tails of the subunits in the mechanism of

ribonucleotide reduction. Despite the absence of molecular understanding, our studies suggest that both human RNRs can be targeted by F₂CDP, and that the consequences of inactivation may differ depending on growth conditions.

4.5 Reference

- (1) Hertel, L. W., Boder, G. B., Kroin, J. S., Rinzel, S. M., Poore, G. A., Todd, G. C., and Grindey, G. B. (1990) Evaluation of the antitumor-activity of gemcitabine (2',2'-difluoro-2'-deoxycytidine). *Cancer Res.* *50*, 4417-4422.
- (2) Huang, P., Chubb, S., Hertel, L. W., Grindey, G. B., and Plunkett, W. (1991) Action of 2',2'-difluorodeoxycytidine on DNA-synthesis. *Cancer res.* *51*, 6110-6117.
- (3) Plunkett, W., Huang, P., and Gandhi, V. (1997) Gemcitabine: actions and interactions. *Nucleosides & Nucleotides* *16*, 1261-1270.
- (4) Rivera, F., López-Tarruella, S., Vega-Villegas, M. E., and Salcedo, M. (2009) Treatment of advanced pancreatic cancer: from gemcitabine single agent to combinations and targeted therapy. *Cancer Treat Rev.* *35*, 335-339.
- (5) Danesi, R., Altavilla, G., Giovannetti, E., and Rosell, R. (2009) Pharmacogenomics of gemcitabine in non-small-cell lung cancer and other solid tumors. *Pharmacogenomics* *10*, 69-80.
- (6) Bergman, A. M., Pinedo, H. M., and Peters, G. J. (2002) Determinants of resistance to 2',2'-difluorodeoxycytidine (gemcitabine). *Drug Resistance Updates* *5*, 19-33.
- (7) Kashlan, O. B., Cooperman, B. S. (2003) Comprehensive model for allosteric regulation of mammalian ribonucleotide reductase: refinements and consequences. *Biochemistry* *42*, 1696-1706.
- (8) Rofougaran, R., Vodnala, M., and Hofer, A. (2006) Enzymatically active mammalian ribonucleotide reductase exists primarily as an alpha(6)beta(2) octamer. *J. Biol. Chem.* *281*, 27705-27711.
- (9) Stubbe, J., van der Donk WA. (1998) Protein radicals in enzyme catalysis. *Chem. Rev.* *98*, 705-762.
- (10) Larsson, A., and Sjöberg, B. M. (1986) Identification of the stable free-radical tyrosine residue in ribonucleotide reductase. *EMBO J.* *5*, 2037-2040.
- (11) Sjöberg, B. M., Reichard, P. (1977) Nature of Free-Radical in Ribonucleotide Reductase from *Escherichia-Coli*. *J. Biol. Chem.* *252*, 536-541.
- (12) Sjöberg, B. M., Reichard, P., Gräslund, A., Ehrenberg, A. (1978) The tyrosine free radical in ribonucleotide reductase from *Escherichia coli*. *J. Biol.Chem.* *253*, 6863-6865.

- (13) Wang, J., Lohman, G. J., and Stubbe, J. (2007) Enhanced subunit interactions with gemcitabine-5'-diphosphate inhibit ribonucleotide reductases. *Proc. Natl. Acad. Sci. U S A.* 104, 14324-14329.
- (14) Tanaka, H., Arakawa, H., Yamaguchi, T., Shiraishi, K., Fukuda, S., Matsui, K., Takei, Y. and Nakamura, Y. (2000) A ribonucleotide reductase gene involved in a p53-dependent cell-cycle checkpoint for DNA damage. *Nature* 404, 42-49.
- (15) Nakano, K., Balint, E., Ashcroft, M., and Vousden, K.H. (2000) A ribonucleotide reductase gene is a transcriptional target of p53 and p73. *Oncogene* 19, 4283-4289.
- (16) Pontarin, G., Fijolek, A., Pizzo, P., Ferraro, P., Rampazzo, C., Pozzan, T., Thelander, L., Reichard, P. A., and Bianchi, V. (2008) Ribonucleotide reduction is a cytosolic process in mammalian cells independently of DNA damage. *Proc. Natl. Acad. Sci. U.S.A.* 105, 17801-17806.
- (17) Yamaguchi, T., Matsuda, K., Saqiya, Y., Iwate, M., Fujino, M. A., Nakamura, Y., Arakawa, H. (2001) p53R2-dependent pathway for DNA synthesis in a p53-regulated cell cycle checkpoint. *Cancer Res.* 61, 8256-8262.
- (18) Bourdon, A., Minai, L., Serre, V., Jais, J., Sarzi, E., Aubert, S., Chretien, D., Lonlay, P., Paquis-fluckinger, V., Arakawa, H., Nakamura, Y., Munnich, A. and Rötig, A. (2007) Mutation of RRM2B, encoding p53-controlled ribonucleotide reductase (p53R2), causes severe mitochondrial DNA depletion. *Nat. Genet.* 39, 776-780.
- (19) Chang, L., Zhou, B., Hu, S., Guo, R., Liu, X., Jones, SN., and Yen, Y. (2008) ATM-mediated serine 72 phosphorylation stabilizes ribonucleotide reductase small subunit p53R2 protein against MDM2 to DNA damage. *Proc. Natl. Acad. Sci. U.S.A.* 105, 18519-18524.
- (20) Piao, C., Jin, M., Kim, HB., Lee, SM., Amatya, PN., Hyun, JW., Chang, IY., and You, HJ. (2009) Ribonucleotide reductase small subunit p53R2 suppresses MEK-EPK activity by binding to ERK kinase 2. *Oncogene* 28, 2173-2184.
- (21) Shao, J. M., Zhou, B. S., Zhu, L. J., Qiu, W. H., Yuan, Y. C., Xi, B. X., and Yen, Y. (2004) In vitro characterization of enzymatic properties and inhibition of the p53R2 subunit of human ribonucleotide reductase. *Cancer Res.* 64, 1-6.
- (22) Liu, X., Xue, L., and Yen, Y. (2008) Redox property of ribonucleotide reductase small subunit M2 and p53R2. *Methods Mol Biol.* 477, 195-206.
- (23) Lohman, G. J. S., Stubbe, J. (2009) manuscript in preparation.
- (24) Silva, D. J., Stubbe, J., Samano, V., and Robins, M. J. (1998) Gemcitabine 5'-triphosphate is a stoichiometric mechanism-based inhibitor of *Lactobacillus leichmannii* ribonucleoside triphosphate reductase: Evidence for thiyl radical-mediated nucleotide radical formation. *Biochemistry* 37, 5528-5535.
- (25) Stubbe, J., van der Donk WA. (1995) Ribonucleotide reductases: radical enzymes with suicidal tendencies. *Chem. Biol.* 12, 793-801.
- (26) Wang, X., Zhenchuk, A., Wiman, K. G., and Albertioni, F. (2009) Regulation of p53R2 and its role as potential target for cancer therapy. *Cancer Lett.* 276, 1-7.
- (27) Guittet, O., Håkansson, P., Voevodskaya, N., Fridd, S., Gräslund, A., Arakawa, H., Nakamura, Y., Thelander, L. (2001) Mammalian p53R2 protein forms an active ribonucleotide reductase in vitro with the R1 protein, which is expressed both in resting cells in response to DNA damage and in proliferating cells. *J. Biol. Chem.* 276, 40647-40651.

- (28) Lunn, C. A., Kathju, S., Wallace, B. J., Kushner, S. R., Pigiet, V. (1984) Amplification and purification of plasmid-encoded thioredoxin from *Escherichia-Coli*-K12. *J. Biol. Chem.* 259, 469-474.
- (29) Russel, M., and Model, P. (1985) Direct Cloning of the Trxb Gene That Encodes Thioredoxin Reductase. *J. Bacteriol.* 163, 238-242.
- (30) Berglund, O., and Eckstein, F. (1974) ATP- and dATP-substituted agaroses and the purification of ribonucleotide reductases. *Methods Enzymol.* 34, 253-261.
- (31) Perlstein, D. L., Ge, J., Ortigosa, A. D., Robblee, J. H., Zhang, Z., Huang, M., and Stubbe, J. (2005) The active form of the *Saccharomyces cerevisiae* ribonucleotide reductase small subunit is a heterodimer in vitro and in vivo. *Biochemistry* 44, 15366-15377.
- (32) Steeper, J. R., Steuart, C.C. (1970) A rapid assay for CDP reductase activity in mammalian cell extracts. *Anal. Biochem.* 34, 123-130.
- (33) Ortigosa, A. D., Hristova, D., Perlstein, D. L., Zhang, Z., Huang, M. X., and Stubbe, J. (2006) Determination of the in vivo stoichiometry of tyrosyl radical per beta beta ' in *Saccharomyces cerevisiae* ribonucleotide reductase. *Biochemistry* 45, 12282-12294.
- (34) Hristova, D., Wu, C. H., Jiang, W., Krebs, C., and Stubbe, J. (2008) Importance of the maintenance pathway in the regulation of the activity of *Escherichia coli* ribonucleotide reductase. *Biochemistry* 47, 3989-3999.
- (35) Artin, E., Wang, J., Lohman, G., Yu, G., Griffin, G., Barr, G., and Stubbe, J. (2009) Insight into the mechanism of inactivation of ribonucleotide reductase by gemcitabine 5'-diphosphate in the presence and absence of reductant. *submitted to Biochemistry*.
- (36) Xu H, F., C., Uchiki, T., Racca, J. & Dealwis, C. (2006) Structures of eukaryotic ribonucleotide reductase I define gemcitabine diphosphate binding and subunit assembly. *Proc. Natl. Acad. Sci. U.S.A.* 103, 4028-4033.
- (37) Mao, S. S., Johnston, M. I., Bollinger, J. M., and Stubbe, J. (1989) Mechanism-based inhibition of a mutant *escherichia-coli* ribonucleotide reductase (cysteine-225-serine) by its substrate CDP. *Proc. Natl. Acad. Sci. U.S.A.* 86, 1485-1489.
- (38) Mao, S. S., Holler, T. P., Bollinger, J. M. Jr, Yu, G. X., Johnston, M. I., and Stubbe, J. (1992) Interaction of C225SR1 mutant subunit of ribonucleotide reductase with R2 and nucleoside diphosphates: tales of a suicidal enzyme. *Biochemistry* 31, 9744-9751.
- (39) Mao, S. S., Holler, T. P., Yu, G. X., Bollinger, J. M., Booker, S., Johnston, M. I., and Stubbe, J. (1992) A Model for the role of multiple cysteine residues involved in ribonucleotide reduction - amazing and still confusing. *Biochemistry* 31, 9733-9743.
- (40) van der Donk, W. A., Yu, G. X., Perez, L., Sanchez, R. J., Stubbe, J., Samano, V., and Robins, M. J. (1998) Detection of a new substrate-derived radical during inactivation of ribonucleotide reductase from *Escherichia coli* by gemcitabine 5'-diphosphate. *Biochemistry* 37, 6419-6426.
- (41) Eriksson, H. K. (2001) Kinetics in the pre-steady state of the formation of cystines in ribonucleoside diphosphate reductase: evidence for an asymmetric complex. *Biochemistry* 40, 9631-9637.

- (42) Zhang, Z., Yang, K., Chen, C., Feser, J., and Huang, M. (2007) Role of the C terminus of the ribonucleotide reductase large subunit in enzyme regeneration and its inhibition by Sml1. *Proc. Natl. Acad. Sci. U.S.A.* 104, 2217-2222.
- (43) Ge, J., Yu, G. X., Ator, M.A., and Stubbe, J. (2003) Pre-steady-state and steady-state kinetic analysis of E-coli class I ribonucleotide reductase. *Biochemistry* 42, 10071-10083.
- (44) Uppsten, M., Färnegårdh, M., Domkin, V., and Uhlin, U. (2006) The first holocomplex structure of ribonucleotide reductase gives new insight into its mechanism of action. *J. Mol. Biol.* 359, 365-377.
- (45) Lawrence, C. C., Bennati, M., Obias, H. V., Bar, G., Griffin, R. G., Stubbe, J. (1999) High-field EPR detection of a disulfide radical anion in the reduction of cytidine 5'-diphosphate by the E441Q R1 mutant of Escherichia coli ribonucleotide reductase. *Proc. Natl. Acad. Sci. U S A.* 96, 8979-8984.

Chapter 5

Efforts to Understand Sml1 Inhibition of *S. cerevisiae* RNR

5.1 Introduction:

Sml1, a suppressor of *MEC1* lethality, was discovered by Rothstein and coworkers from a genetic screen as an inhibitor of ribonucleotide reductase (RNR) in *S. cerevisiae* (1). The deletion of Sml1 displayed a similar phenotype as over-expression of the RNR large subunit *RNR1* (α), and could restore cell viability in the Mec1 and Rad53 deletion strains. RNR catalyzes the reduction of all four ribonucleotides to the corresponding deoxyribonucleotides and is essential in DNA biosynthesis and DNA repair in all organisms (2-4). It is tightly regulated in cells to keep balanced dNTP pools for DNA replication and repair. Yeast two-hybrid assays, co-immunoprecipitation experiments, and biochemical studies revealed that Sml1 regulates RNR by binding directly to α to repress RNR activity, rather than by controlling its transcription (1). The binding of Sml1 to α is proposed to block the reduction of the active site disulfide formed concomitant with dNTP production, leaving α in the oxidized, inactive state (5). In this study, fluorescent probes were incorporated site-specifically into several positions in Sml1. The resulting Sml1 mutants were used to investigate the model proposed for Sml1's inhibition of *S. cerevisiae* RNR.

Sml1 is a small, dimeric protein composed of 104 amino acids. No crystal structure of Sml1 has been solved thus far. The 2D NMR studies however have revealed that Sml1 contains a loosely folded structure with two α helices located between residues 4-14 and residues 61-80 (Figure 5.1) (6-8). The N-terminal (residues 8-20) of Sml1 are proposed to be responsible for its dimerization (9), while the C-terminal Sml1 mutants (R72G/R72A, L73P/L73A, S75P, I76T, S87P, F94S and F104L) were found to disrupt the interaction of Sml1 and α (7). All of these mutations are found in the last 33 amino

acids residing in the C-terminus, suggesting that the C-terminal tail of Sml1 is a key region for binding to α (10). The Sml1- α interaction has been demonstrated by *in vitro* surface plasmon resonance method to have a K_d equal to 0.4 μ M (11). A second method used to examine α -Sml1 interaction was sucrose gradient centrifugation. Using this method, α was found to sediment as $\alpha 2$ and $\alpha 4$. SDS-PAGE analysis revealed that Sml1 sedimented with $\alpha 2$ but not with $\alpha 4$. Chabes *et al* further demonstrated that Sml1 binding does not affect α binding to $\beta\beta'$ (11). The expression level of Sml1 is regulated by Dun1 phosphorylation via *MEC1/RAD53* checkpoint pathway in response to both cell cycle and DNA damage. Phosphorylation of Sml1 results in its rapid degradation. Thus the concentration of Sml1 is at its lowest level during the S phase of the cell cycle and is almost undetectable after DNA damage (12, 13). The phosphorylation sites were determined to be Ser56, Ser58, and Ser60 on the linker region between the two helices by Mass spectrometry and mutagenesis analysis *in vitro* (6).

From extensive mutagenesis and two-hybrid assay screens, only one α mutant (W688G) was identified that could not only bind to wt Sml1, but also restore interactions with Sml1 mutants which previously failed to bind wt α (10). W688 and E689 of α are highly conserved from bacteria to human RNR. *In vivo* studies carried out by Zhang, *et al* revealed that α -W688A E689D could increase the affinity of α to Sml1 and cause *Sml1*-dependent lethality (5, 10). Moreover, α truncated from 779-888 and including W688/E689D has demonstrated an enhanced binding with Sml1, and reduced interaction to the tail region of the α C-terminal domain (CTD, residues 765-888).

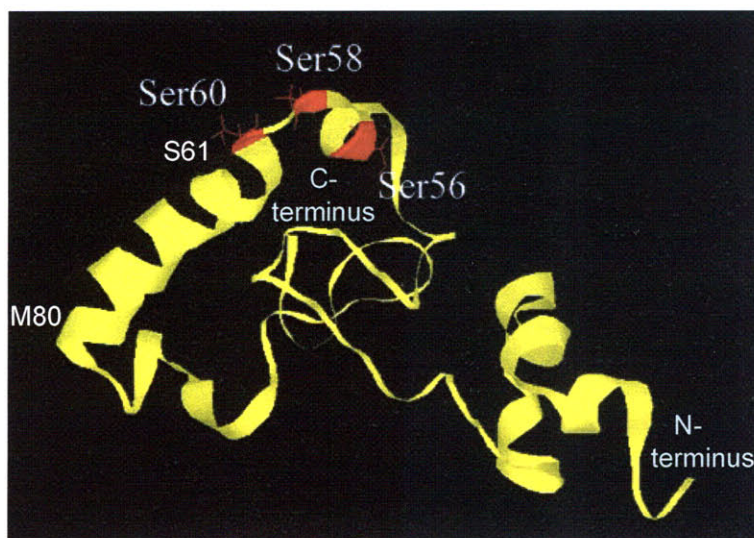
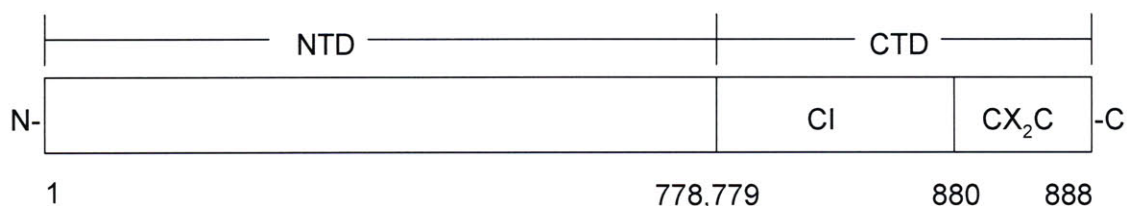


Figure 5.1: A molecular model of yeast Sml1 (6).

The model was constructed based on 2D-NMR analysis. The overall structure of Sml1 is unfolded with two α helices at the N- and C-terminus oriented in anti-parallel fashion. The model shows the proposed phosphorylation sites of Sml1 are Ser 56, Ser 58 and Ser 60, which are solvent exposed. S61 and M80 are the sites to which and DAN is attached.



Scheme 5.1: Substitution and deletions constructs of *S. cerevisiae* RNRI.

Based on studies of *E. coli* RNR, the pair of redox active cysteines (C218/C443 of *S. cerevisiae*) in the active site of α are oxidized concomitant with substrate reduction (14). Another pair of cysteines (C883/C886) on the C-terminal tail of α is required to regenerate the active site cysteines via disulfide exchange (14-16). With yeast, this role of the C-terminal cysteines has not been demonstrated. Recently, *in vivo* studies in *S. cerevisiae* have revealed that the tail of one α can enter into the active site of its

neighboring α and re-reduce the active site disulfide (Figure 5.2 a-d) (5). Evidence led to the model that Sml1 inactivates α by preventing the C-terminal tail of α to access the active site (Figure 5.2 e) is supported by the observations that Sml1 displayed stronger interaction with the N-terminal domain of α (residues 1-778), than the full length α by yeast two-hybrid assays. Thus Sml1 was proposed to behave as an uncompetitive inhibitor relative to the substrate, that is, it binds to the oxidized form in preference to the reduced form.

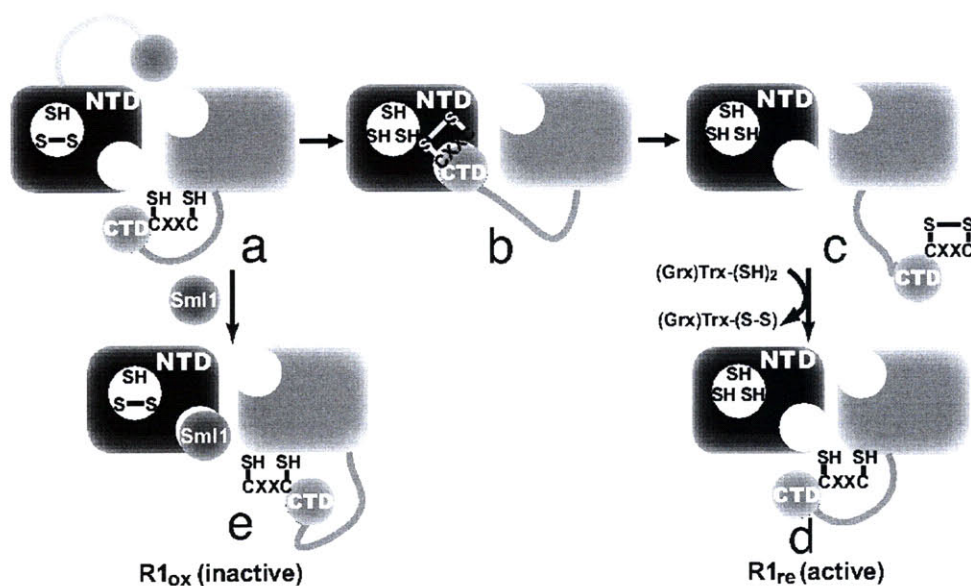


Figure 5.2: A model for the role of the α C-terminal tail in regeneration of the reduced form of α and inhibition by Sml1 (5).

(a) α is oxidized concomitant with substrate reduction. (b) The C-terminal tail of one α enters into the active site of the neighboring α and reduces the active site disulfide by disulfide interchange. (c) A reduced form of α is generated. The active site cysteine pair is reduced while the CX2C motif at the C-terminus tail forms a disulfide (d) The disulfide on the tail is reduced by thioredoxin or glutaredoxin (e) Sml1 competes with the C-terminal tail of α to prevent regeneration of active cysteines (Adapted from reference(5)).

In our study, an environmental sensitive fluorescence probe, BADAN was attached site-specifically to Sml1 and used to measure and compare the affinities between Sml1 to the oxidized and the reduced forms of α . With DAN modification at residue 61, we obtained a similar K_d value to that determined by Thelander using surface plasmon resonance method (SPR), and demonstrated that Sml1 has a stronger interaction with oxidized α than reduced α . Inhibition studies of CDP reduction by Sml1 have also been carried out in an effort to obtain evidence for Sml1 binding to oxidized and/or reduced α .

The detailed mechanism of inactivation of α and its stoichiometry of interaction still remain unresolved. Based on 2D NMR studies and the genetic studies, we proposed that a hydrophobic patch on the C-terminal tail of Sml1 is the binding site to α . The data from our inactivation assays and fluorescence measurements with four DAN modified Sml1s agree with our hydrophobic binding model, and support the proposal that the C-terminal tail of Sml1 plays a key role in the Sml1- α interaction. We have also isolated W688A- α , E689D- α , and W688A E689D- α mutants, and verified their increased interaction with Sml1. However, activity assays revealed significant loss of activity associated with the W mutation, suggesting that low activity of α part of the reason for the *Sml1*-dependent lethality in previous studies.

5.2 Methods

5.2.1 Materials

Competent *E. coli* BL 21 (DE3) RIL codon plus cells were purchased from Stratagene. Complete EDTA-free protease inhibitor tablets and calf alkaline phosphatase (20 U/ μ L) were purchased from Roche Biochemicals (Indianapolis, IN). 6-Bromoacetyl-

2-dimethylaminonaphthalene (BADAN) was purchased from Molecular Probes (Eugene, OR). 5, 5'-Dithio-bis(2-nitrobenzoic acid) (DTNB) was purchased from Sigma (St. Louis, MO). Isopropyl-1-thio- β -D-galactopyranoside (IPTG) and 1, 4-dithiothreitol (DTT) were from Promega (Madison, WI). Ultrafiltration membranes (YM30) were from Millipore (Bedford, MA). The dATP-Sepharose resin was synthesized by members of the Stubbe group (17). Protein concentrations were determined using extinction coefficients ($\epsilon_{280\text{ nm}}$) per monomer [$52,800\text{ M}^{-1}\text{ cm}^{-1}$ for (His)- β , $47,000\text{ M}^{-1}\text{ cm}^{-1}$ for β' , $119,945\text{ M}^{-1}\text{ cm}^{-1}$ for α] and for $\beta\beta'$ heterodimer, $99,800\text{ M}^{-1}\text{ cm}^{-1}$. The plasmid containing W688A E689D *rnr1* double mutant was provided by Prof. M. Huang (University of Colorado Health Sciences Center). The W688A, E689D *rnr1* single mutants were constructed by site directed mutagenesis using a Quick Change Kit by Stratagene. The plasmid sequences were confirmed at the MIT Biopolymer lab. *E. coli* TR (specific activity of 40 U/mg) (18) and TR reductase (specific activity of 1320 U/mg) (19) were isolated as previously described.

5.2.2 Expression and purification of wt α , W688A- α , E689D- α single mutants, and W688A E689D- α double mutants

The plasmids containing the genes for *rnr1* and mutants were transformed into BL21 (DE3) CodonPlus RIL cells and plated on LB agar plates with 30 $\mu\text{g/L}$ chloramphenicol (CM), 75 $\mu\text{g/L}$ kanamycin (Kan). A single colony was selected to inoculate a 5 mL LB culture with 30 $\mu\text{g/L}$ CM and 75 $\mu\text{g/L}$ Kan. Overnight to saturation. The culture was grown at 37 °C and then added to 2 L LB in 6 L flasks and grown until OD_{600} reaches 0.6-0.8. The temperature was then cooled to 15 °C, and IPTG (final

concentration 0.5 mM) was added to induce expression of *rnr1* and cells were grown for an additional 16 h. Typically 5 g of cell paste/L culture were obtained.

The purification was carried out at 4 °C. The procedures for α and α mutants were identical. Ten g of cells were suspended in 50 mL 50 mM Tris-HCl, pH 7.6, 1 mM EDTA, 5% (v/v) glycerol, 1 mM PMSF, and 1 mM DTT, pH 7.6 (PB buffer). One complete protease inhibitor tablet per mL of PB buffer was added. Cells were disrupted by one pass through the French press cell at 14,000 psi. The cell debris was removed by centrifugation at 20,000 g for 20 min. DNA was precipitated by addition of 10% (w/v) streptomycin sulfate stock in PB buffer to a final concentration of 1%, and stirred for an additional 10 min. The precipitated DNA was removed by centrifugation at 20,000 g for 20 min. Solid ammonium sulfate was added to the supernatant (55 mL) over 20 min to a final concentration of 50% saturation (0.31 g/mL) and the mixture was stirred for additional 30 min. The protein pellet was collected by centrifugation at 20,000 g for 20 min and re-dissolved in 1 mL PB buffer. The protein was desalted by passage through a Sephadex G25 column (1.5x30 cm, 40 mL) column. The eluted protein (~30 mL) was loaded on a dATP-Sepharose column (4.5x6.5 cm, 20 mL) at 4 °C for 1 h. The column was washed with 800 mL of 50 mM Tris-HCl, pH7.6, 1mM EDTA, 5% (v/v) glycerol, 1 mM PMSF, 1 mM DTT, 50 mM NaCl, and α was eluted with 50 mM Tris-HCl, 1mM EDTA, 5% (v/v) glycerol, 1 mM PMSF, 1 mM DTT, 10 mM ATP, pH 7.6. Fractions containing α as determined by Bradford assay were combined and concentrated to 0.5 mL by ultrafiltration using a YM30 membrane. ATP was removed by passage through a Sephadex G25 chromatography (4x30 cm, 200 mL). The protein containing fractions were pooled and concentrated by ultrafiltration with a YM30 membrane to 10 mg/mL. α

was stored in 50 mM Tris-HCl, pH 7.6, 100 mM KCl, 15 mM MgCl₂, 5 mM DTT, and 5% (w/v) glycerol. A total of 110 mg (specific activity of wt is 350 nmol/min/mg) was typically obtained from 10 g of cell paste.

5.2.3 Expression and purification of Sml1 and Sml1-E71C, W65C, S61C, M80C

mutants

The Sml1 cysteine mutants were constructed using a Stratagene Quick Change site-directed mutagenesis method with primers shown in Table 1. The Sml1 or Sml1 mutant gene in pET-24a was transformed into *E. coli* BL21-CodonPlus (DE3)-RIL cells and plated on LB agar plates with 30 µg/L CM, 75 µg/L Kan. A single colony was used to inoculate a 5 mL LB which was grown overnight at 37°C with 30 mg/L CM and 75 mg/L Kan. The 5 mL culture was then added to 2 L LB in a 6 L flask and grown at 37°C until an OD₆₀₀ of ~0.8. The culture was then cooled to 30°C, and IPTG (final concentration 0.5 mM) was added to induce Sml1. The cells were grown for an additional 4 h. The cells were harvested at 7,500 rpm with a typical yield of ~ 3 g/L of culture.

Table 5.1: Sml1 mutants primers:

C14S forward	C GCT CAA AAT CGC TCC CAA CAA CAA CAA GCC CC
C14S reverse	GG GGC TTG TTG TTG TTG GGA GCG ATT TTG AGC G
S61C forward	GCT TCT GCC TCC GCT TGT TCA TTA GAA ATG TGG G
S61C reverse	CCC ACA TTT CTA ATG AAC AAG CGG AGG CAG AAG C
W65C forward	CCG CTT CTT CAT TAG AAA TGT GCG AAA AGG ATT TGG AGG
W65C reverse	CCT CCA AAT CCT TTT CGC ACA TTT CTA ATG AAG AAG CGG
E71C forward	GTG GGA AAA GGA TTT GGA GTG CAG ACT CAA CTC TAT CGA TCA TG
E71C reverse	CAT GAT CGA TAG AGT TGA GTC TGC ACT CCA AAT CCT TTT CCC AC
M80C forward	CAA CTC TAT CGA TCA TGA CTG CAA CAA CAA CAA ATT TGG TTC TGG CG
M80C reverse	CGC CAG AAC CAA ATT TGT TGT TGT TGC AGT CAT GAT CGA TAG AGT TG

All the purification steps were performed at 4°C. The cell pellet was resuspended in 50 mM TrisHCl, pH 7.4, 1 mM EDTA and 5 mM DTT (1 g/7-10 mL) containing one Complete protease inhibitor tablet per 10 mL suspension. The cells were lysed by flash freezing in a 50 mL falcon tube with liquid nitrogen and then allowing the frozen cells to thaw at room temperature until the lysate returned to a liquid state. The falcon tube then was placed at 4°C. One freeze-thaw cycle was used. This method was used instead of the French press, because it decreased the amount of clipped Sml1 (11). Once the lysate was thawed, another Complete protease inhibitor tablet per 10 mL suspension was added and the cells were spun in an ultracentrifuge at 150,000 ×g for approximately 1 h and 15 min (Model Beckman L7-55 ultracentrifuge; 45Ti rotor at 36,000 rpm). 10% (w/v) streptomycin sulfate stock solution was added to the supernatant to a final volume of 1%

(w/v). After stirring for 10 min at 4°C, the DNA was pelleted at 40,000 ×g for 20 min. (NH₄)₂SO₄ was then added to 23% saturation (0.136 mg/ml) and stirred at 4°C for 20 min. The precipitated protein was collected by centrifugation at 40,000 ×g for 20 min. The pellet was dissolved into 50 mM TrisHCl (pH 7.4), 1 mM EDTA, 15 mM MgCl₂, 120 mM NaCl, 5% (w/v) glycerol and 5 mM DTT and the (NH₄)₂SO₄ was removed using Sephadex G-25 chromatography (1.5 cm x 25 cm, 20 mL). The protein containing fractions were pooled and concentrated using a YM-3 membrane. The protein concentration was determined using $\epsilon_{280} = 8250 \text{ M}^{-1} \text{ cm}^{-1}$ (11). Protein purity was assessed using SDS-PAGE analysis via a 10-20% TRIS-Tricine gradient gel (Invitrogen). A total of 3 mg was typically obtained from 1 g of cell paste.

5.2.4 Labeling of Sml1 mutants by BADAN

The Sml1-E71C, W65C, S61C, M80C (500 μL, 40 μM) mutants were pre-reduced with 10 mM DTT for 30 min on ice. DTT was then removed by a Sephadex G-25 column (1.5 cm x 25 cm, 40 mL). The column was equilibrated with 50 mM Tris, pH 7.4, 1 mM EDTA, and 15 mM MgCl₂. The Sml1 mutants were then assayed using DTNB to determine the amount of free thiol. The background spectrum of both DTNB (250 μM) and Sml1 (25 μM) in 50 mM Tris, pH 7.4, 1 mM EDTA, and 15 mM MgCl₂ were individually taken at 410 nm. DTNB was added into the cuvette containing Sml1 (500 μL, 25 μM) to a final concentration of 250 μM. The UV/vis spectrum was recorded every min until the reaction was complete. The concentration of TNB (2-nitro-5-benzoate) was determined as follows: $[\text{TNB}]_{\text{mM}} = (A_{410, \text{final}} - A_{410, \text{Sml1 background}} - A_{410, \text{DTNB background}}) / 13.6 \text{ mM}^{-1} \text{ cm}^{-1}$. The Sml1 concentration was determined using $\epsilon_{280} = 8250 \text{ M}^{-1}$

cm^{-1} . The percentage of free thiol per molecule was then calculated by $[\text{TNB}]/[\text{Sml1}]$.

The DTNB assay typically resulted in 90-98% of one thiol.

BADAN (final concentration 400 μM from a 15 mM freshly prepared solution in DMF) was added slowly to the pre-reduced Sml1 mutant (500 μL , 40 μM final concentration) and was gently stirred at 4 $^{\circ}\text{C}$ for 3 h. The solution was covered with foil to protect the reaction from light. The labeling reaction was quenched with 1 μL of β -mercaptoethanol for 30 min at 4 $^{\circ}\text{C}$. To remove excess DAN-mercaptoethanol, the solution was centrifuged at 3400 rpm for 10 min. The supernatant then was placed into a slide-A-lyzer dialysis cassette, MWCO 3500 (Pierce) and dialyzed in 6 x 1 L 50 mM Tris, pH 7.4, 1 mM EDTA, and 15 mM MgCl_2 .

To calculate the extent of labeling, the UV/vis spectrum of each mutant was recorded. Assuming that extinction coefficient for DAN attached to the protein is the same as free DAN, its concentration was determined using $\epsilon_{390} = 21 \text{ mM}^{-1} \text{ cm}^{-1}$ and $\epsilon_{280} = 19.8 \text{ mM}^{-1} \text{ cm}^{-1}$ in H_2O (pH 7.6) (Molecular Probes, Invitrogen). The concentration of Sml1 was determined as above. The stoichiometry of labeling was calculated by $[\text{DAN}]/[\text{Sml1}]$. Each DAN-Sml1 was also analyzed by Sciex triplequadrupole mass spectrometer (model API 365) at Biopolymers, MIT to determine the extent of labeling.

5.2.5 Activity assays:

The reaction mixture contained the following in a final volume of 180 μL : 100 mM Hepes, pH 7.6, 15 mM MgCl_2 , 0.6 μM α (wt or mutants, specific activity of wt is 319 nmol/min/mg), 3 μM $\beta\beta'$ (0.3 $\text{Y}\cdot$, specific activity of 2410 nmol/min/mg), 3 mM ATP, 1 mM $[\text{}^3\text{H}]\text{-CDP}$ (specific activity of 4290 cpm /nmol), 100 μM *E.coli* TR, 1.0 μM

TRR, 2 mM NADPH. In the assay of W688A- α , E689D- α , and W688A E689D- α , at 2 μ M was mixed with Flag- $\beta\beta'$ (7 μ M, 0.3 Y \bullet) and the reaction was carried out for 30 min at 30°C. For assays with C883S C886S- α , 20 mM DTT replaced TR, TRR, and NADPH. Each reaction mixture was pre-incubated at 30 °C for 3 min and the reaction was initiated by addition of α or α mutant. Aliquots of 30 μ L were removed over a 20 min period and the reaction was quenched in a boiling water bath for 2 min. dCDP production was analyzed by the method of Steeper and Steuart (20).

5.2.6 Inactivation assay of wt α and α -C883S C886S by Sml1:

The reaction mixture contained the following in a final volume of 150 μ L: 100 mM Hepes, pH 7.6, 15 mM MgCl₂, 1.6 μ M α (wt, specific activity of 319 nmol/min/mg or mutants), 0.8 μ M $\beta\beta'$ (0.3 Y \bullet , specific activity of 2410 nmol/min/mg), Sml1 (0, 1 μ M, 2 μ M, 4 μ M), 3 mM ATP, 1 mM [³H]-CDP (specific activity 4290 cpm /nmol), 100 μ M *E.coli* TR, 1.0 μ M TRR, 2 mM NADPH. The C883S C886S- α was assayed with 20 mM DTT instead of TR, TRR, NADPH. The reaction was initiated by the addition of [³H]-CDP at 30°C. Aliquots of 30 μ L of were removed at various time points over a 10 min period and the reaction was quenched in a boiling water bath for 2 min. dCDP production was analyzed by the method of Steeper and Steuart.

5.2.7 Determination of K_d for DAN-Sml1 to α :

Fluorescence measurements were performed on a QM-4-SE fluorimeter in from Photon Technology International (Montreal, Quebec) using FELIX software and 2 nm excitation and 6 nm emission bandwidth slits. The excitation was at 390 nm, and the

emission was monitored from 410 nm to 625 nm at 1 nm per sec. The temperature was controlled at 30 °C. Each sample of 400 μL was placed in a 500 μL microcuvette that contained 50 mM HEPES, pH 7.6, 15 mM MgSO₄ and 100 μM TTP, and was scanned from 410 nm to 625 nm at 1 nm per sec before the start of the titration. The titration was started by addition of DAN-Sml1 (1 μL, 19.8 μM) into 400 μL buffer to a final concentration of 0.04 μM. Titration was carried out with pre-reduced α (156 μM) incubated with 100 μM TTP. The pre-reduced α was added in 0.5 μL aliquots with a P2 pipette. The emission spectrum was recorded after 10 min incubation as controls revealed no further changes occurred subsequent to 10 min. The K_d was calculated using Eq 1:

$$K_d = [\alpha 2]_{\text{free}}[\text{DAN-Sml1}]_{\text{free}} / [\alpha 2 - \text{DAN-Sml1}] \quad (1)$$

where [DAN-Sml1]_{free} and [α2]_{free} are the free concentrations of DAN-Sml1 and α2. The above equation for K_d assumes a 1:1 interaction between Dan-Sml1 and α2 where Sml1 is assumed to be a dimer and Eq 1 can be reformulated as

$$F = [\alpha 2]_{\text{free}} / (K_d + [\alpha 2]_{\text{free}}) \quad (2)$$

where F is the fraction of [DAN-Sml1-α2] to the total [DAN-Sml1].

For the sigmoidal dose-response model assume cooperative binding,

$K_d = [\alpha 2]_{\text{free}}^n [\text{DAN-Sml1}] / [(\text{DAN-Sml1})-\alpha 2_n]$, it can be reformulated as

$$F = [\alpha 2]_{\text{free}}^n / (K_d + [\alpha 2]_{\text{free}}^n), \text{ n is hill coefficient} \quad (3)$$

where F is the fraction of [DAN-Sml1-α2_n] to the total [DAN-Sml1].

$$[\alpha 2]_{\text{free}} = [\alpha 2]_{\text{total}} - F[\text{DAN-Sml1}]_{\text{total}}$$

The fraction of bound α2 for both Eq 2 and 3 was determined using Eq 4 where:

$$F = (I - I_0) / (I_{\text{max}} - I_0) \quad (4)$$

where I is the emission intensity, and I_0 is the emission intensity of DAN-Sml1 before addition of $\alpha 2$. K_d was determined by fitting F vs $[\alpha 2]_{\text{free}}$ curve assuming 1:1 binding model or a sigmoidal dose-response model with non-linear least-squares global analysis using Origin 6.1 software. The error bars represent the standard deviation of 2-3 independent experiments.

5.2.8 Preparation of oxidized α :

α (156 μM , 500 μL) was pre-reduced with 25 mM DTT on ice for 1 h and DTT was removed on a Sephadex G-50 column (1 cm x 20 cm, 20 mL) in 50 mM Tris-HCl, pH 7.4, and 5% (v/v) glycerol at 4 °C. In a final volume of 200 μL , pre-reduced α (80 μM) was mixed with His- $\beta\beta'$ (80 μM , 0.3 Y \bullet), 3 mM ATP, 1 mM CDP, 50 mM Hepes, pH 7.6, 15 mM MgCl_2 , and 1 mM EDTA. The oxidation was carried out at 30 °C for 20 min. The reaction mixture was mixed with 500 μL cobalt resin at 4 °C for 1 h then loaded into a 2 mL spin column. The resin was washed with 5 x 1 mL 50 mM Hepes, pH 7.4, 1mM EDTA, 100 mM NaCl, and 10% glycerol until $A_{280\text{nm}} < 0.05$. Fractions of 500 μL were collected and each fraction was checked for α purity by 10% SDS-PAGE. The fractions containing pure oxidized α were combined and concentrated with a YM30 membrane to about 400 μL . To remove ATP and CDP, the concentrated protein was repeatedly diluted to 5 mL using 50 mM Hepes, pH 7.4, 1mM EDTA, 100 mM NaCl, and 10% glycerol buffer, and concentrated to 400 μL three times. The concentration of oxidized α was determined by Bradford assay using reduced α as standard. If $\beta\beta'$ was not completely removed from oxidized α , the concentration of oxidized α was also determined by comparing the band intensities of a standard curve generated by reduced α (0.5 μM to 5

μM) by 10% SDS-PAGE. The band intensities were quantified using Bio-Rads Quantity One software.

5.2.9 Surface plasmon resonance by BIAcore to determine K_d for Sml1 to α :

A Biacore 3000 (GE healthcare) was used to measure the binding of Sml1 to α . The binding was characterized following a modification of the procedure of Thelander (11, 21). Sml1 (200 μM) was diluted in 10 mM sodium acetate, pH 5.2 to 30 μM right before the immobilization process. Sml1 was immobilized onto the dextran layer of the CM5 sensor chip (GE healthcare) using the amine coupling method described by the manufacturer (22). The amine coupling kit containing EDC (N-ethyl-N-(diaminopropyl) carbodiimide), NHS (N-hydroxysuccinimide) and ethanolaminehydrochloride, pH 8.5 was obtained from GE healthcare. The matrix of CM5 is carboxymethylated dextran covalently attached to a gold surface. The carboxylic acid group of the dextran was activated with 30 μL of 0.2 M EDC and 0.05 M NHS. Sml1 (35 μL , 20 μM) was flowed at a rate of 5 $\mu\text{L}/\text{min}$ over the channel. Afterward, 30 μL of 1 M ethanolaminehydrochloride pH 8.5 was injected to convert the remaining activated esters to amides. The immobilization level of Sml1 was 2000 resonance unit (RU), which corresponds to 2000 pg/mm^2 . The RU is proportional to the mass, that is, 1 RU corresponds to 1 pg/mm^2 of the 100 nm thick dextran layer. With a surface of 0.8 mm^2 , 1600 pg, or 16 fmol of protein is immobilized. The low degree of immobilization avoids multiple attachment sites for a single Sml1 molecule. All studies were carried out at 22 $^{\circ}\text{C}$ with a flow rate of 30 $\mu\text{L}/\text{min}$. The ligand (α or $\beta\beta'$) was pre-equilibrated with running buffer (PBS buffer), pH 7.2. The binding of Sml1 and α was studied by allowing the

immobilized Sml1 to interact with the increasing concentrations of α (0.16 μM to 20 μM) in 100 μM TTP. The surface was regenerated between each α injection with 10 μL of 0.5 M KCl in PBS buffer. The complex formed is detected by a change in RU over time. The affinity of Sml1 for α was analyzed using BIAcore Evaluation 3.2 software.

5.2.10 Inhibition on studies with Sml1 using CDP as the variable substrate:

The reaction mixture contained in a final volume of 135 μL : 50 mM Hepes (pH 7.6), 15 mM MgCl_2 , 3 mM ATP, 2 mM NADPH, 100 μM TR, 1 μM TRR and 0.3 μM α_2 (319 nmol/min/mg), 3 μM His $\beta\beta'$ (2400 nmol/min/mg). The concentration of [^3H]-CDP (specific activity is 5860 cpm / nmol) was varied: 0.044 mM, 0.067 mM, 0.1 mM, 0.2 mM, 1 mM. The concentration of Sml1 varied from 0 μM , 0.25 μM , 0.5 μM , 1 μM , 1.5 μM , 2 μM . Aliquots of 30 μL were taken out of the reaction mixture at 1 min intervals at the beginning and 5 min intervals at the end over a 22 min course, and followed up as described above.

5.3 Results:

5.3.1 Alkylation of Sml1, site specifically, with BADAN:

Based on 2D NMR data and biochemical studies (23), Ortigosa in the Stubbe lab generated a helical wheel for residues 61-80 in Sml1 known to play a role in the interaction with α (Figure 5. 3A, B). The model shows an acidic patch (pink, Figure 5.3A) and hydrophobic patch (orange, Figure 5.3A). Moreover, the residues R72, L73 and I76 which were identified earlier in the mutagenesis studies as key residues for Sml1 inhibition and binding to α are close or within the hydrophobic patch (7, 24). To identify the binding site and measure the affinity of Sml1 for α_n , we have attached DAN, an

environmentally sensitive fluorescence probe, to single cysteines within Sml1 generated by site directed mutagenesis. Previous studies of Dealwis and coworkers established that Sml1 forms a dimer through intermolecular disulfide bond formation via C14 (7, 24). A C14S-Sml1 retains its biological activity and its ability to form a dimer. To simplify the strategy for attachment of DAN via cysteine alkylation by BADANs (Figure 5.4), we carried out all of our studies in a C14S-Sml1 background.

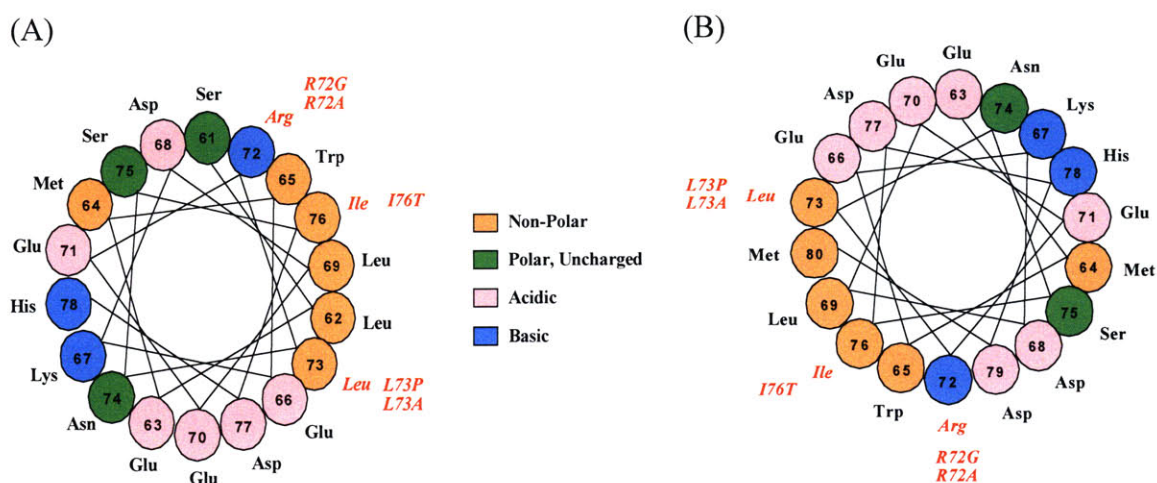


Figure 5.3: Model for the Sml1-Y1 binding.

The alpha helix within the C-terminal tail of Sml1 is shown. The residues (R72, I76, L73) which were found essential for α inhibition from previous genetic studies are indicated in red. A hydrophobic patch (orange ■) and an acidic patch (pink ■) which are composed of hydrophobic residues or acidic residues on the C-terminal tail of Sml1 are proposed as the binding site to α . The polar residues are shown in green (■), and the basic residues are shown in blue (■). (A) Helical wheel projection of residues 61-78. (B) Helical wheel projection of residues 63-80. (Adapted from Dr. Allison Ortigosa's final report)

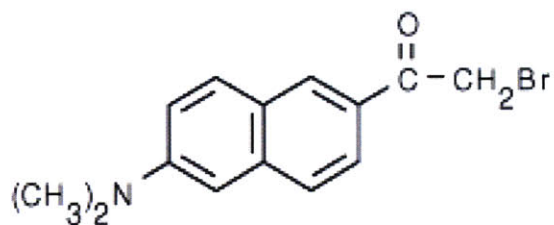


Figure 5.4: Structure of BADAN (6-bromoacetyl-2-dimethylamino-naphthalene).

Four sites for probe attachment were chosen: W65, M80, S61, E71. As shown in Figure 5.3, W65 resides within the hydrophobic patch, M80 is located at the edge of the hydrophobic patch and at the C-terminus of the α helix; S61 is at the N-terminus of the α helix. DAN labeling at S61 or M80 may allow for the detection of changes on the binding DAN-Sml1 to α with the minimal perturbation of binding if the model is correct. E71 which is located outside the hydrophobic patch in the helix was chosen as a control.

5.3.2 Labeling Sml1 mutants with BADAN

Each Sml1 mutant was alkylated with BADAN. Subsequent to its pre-reduction with 10 mM DTT, the DTNB assay demonstrated in each case a single thiol/Sml1. The labeling was carried out for 3h at 4 °C and was quenched with β -mercaptoethanol. The excess DAN-mercaptoethanol was removed by dialysis and each DAN-Sml1 was analyzed by ESI-MS. The results are shown in Table 5.2 with a typical spectrum shown (Figure 5.5). The unlabeled material appeared to be a small portion of total Sml1. In addition, it should be noted that a little amount of doubly labeled Sml1 might exist. Incubation for longer time periods leads to alkylation of histidines and lysines and complicates the fluorescence titration analysis.

Table 5.2: Determine the amount of DAN labeling with mass spectrometry

	Unlabeled (Calculated Mass)	Unlabeled (from Mass spec)	Singly Labeled (Calculated Mass)	Singly Labeled (from Mass spec)
S61C	11834.1	11833.6	12045.4	12045.5
M80C	11790.0	11787.3	12001.3	12000.2
E71C	11792.1	11789.0	12003.4	12000.6
W65C	11735.0	11732.3	11946.3	11944.1

as the non-alkylated Sml1 mutants. DAN-M80 gained potency subsequent to alkylation of the cysteine 80.

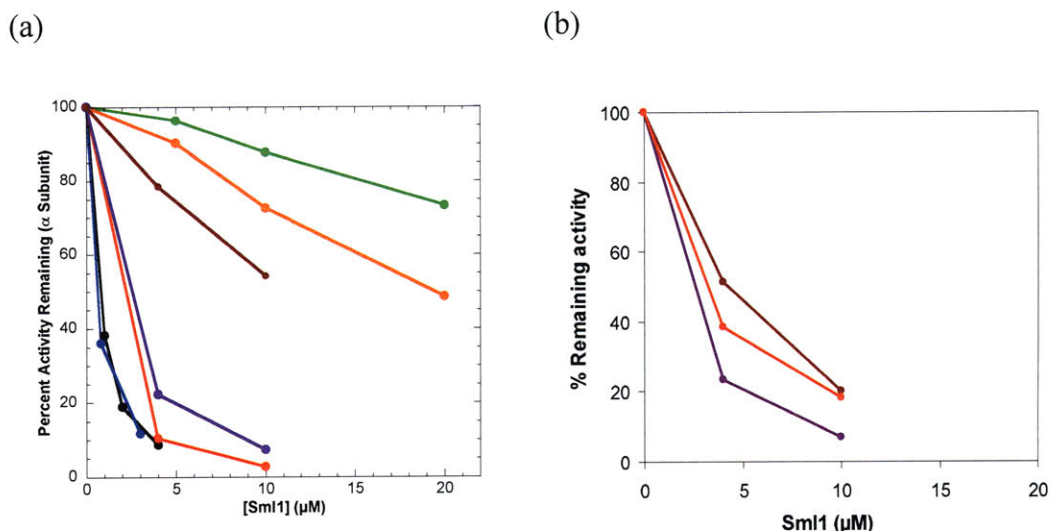


Figure 5.6: α inactivation by the Sml1 cysteine mutants.

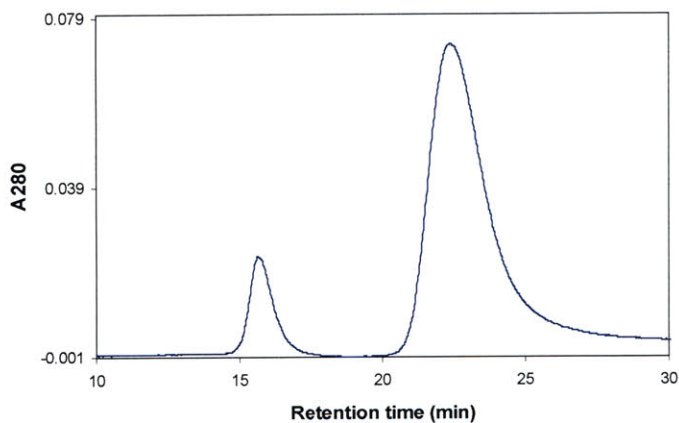
The cysteine mutants (a) and DAN-labeled cysteine mutants (b) of Sml1 were tested for their ability to inhibit RNR activity. The inactivation mixture contained final concentrations of α, 0.6 μM, His-ββ', 3.0 μM. Percent of remaining α activity are shown at varying concentrations of wt Sml1 (•), C14S (•), S61C (•), E71C (•), M80C (•), W65F (•) and W65C (•).

5.3.4 Measurement of the K_d for DAN-Sml1 relative to α

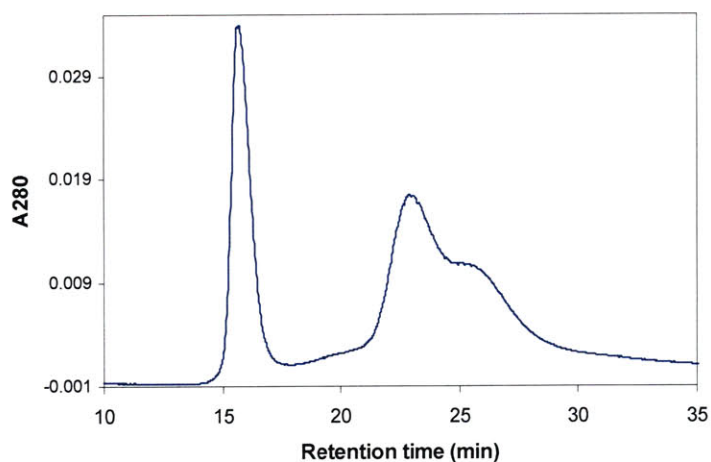
To study the interaction of Sml1-Dan with α, we wished to identify conditions in which α exists in a homogeneous quaternary state. Although the quaternary structure of class Ia RNR in *E. coli* and mouse have been extensively studied, little information is available about the quaternary structure of *S. cerevisiae* α. Chabes *et al* using SEC under 5 mM DTT and 100 μM TTP conditions reported that α is a dimer in equilibrium with a tetramer (11). Dimerization of α is known to occur in the presence of dNTPs which bind to the specificity site within the 4 helix bundle at the subunit interface. We examined the MW of α in the presence of various of dNTPs by SEC (S200), with dNTP in the elution

buffer (Table 5.3). With dGTP (40 μ M), multiple species (α_2 , α) were detected. With TTP (100 μ M), 80% of α appears as a dimer, while 20% appears as a monomer (Figure 5.7 A). With DTT (25 mM), α is predominantly a monomer (90%). The studies above suggested that the best conditions for measurement of Sml1 binding to α was to pre-reduce α and incubate it with 100 μ M TTP. Unlike that reported by Chabes *et al*, tetramer was not detected in our experiment with TTP. Instead, in all of our SEC experiments various amount of high MW aggregates were observed, which complicated our fluorescence titrations. The aggregation might result from the dATP-Sepharose chromatography purification.

(a)



(b)



(c)

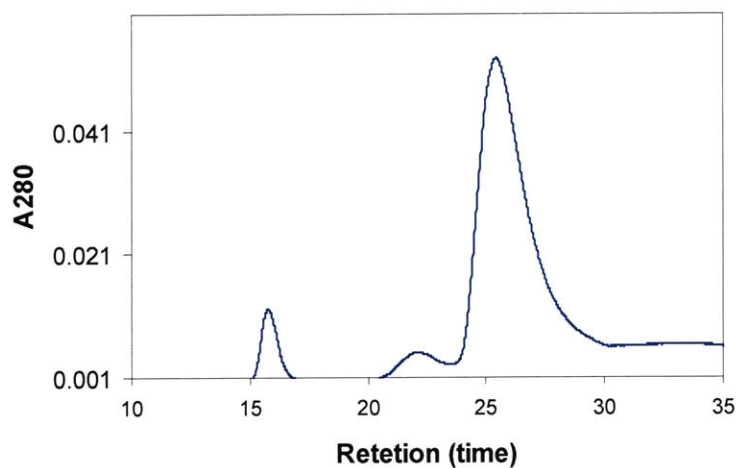


Figure 5.7: SEC spectra of α in the presence of TTP.

α (44 μ M) was pre-reduced with 30 mM DTT for 30 min and the excess DTT was removed by Sephadex G25 column. The α was then incubated (a) with 100 μ M TTP or (b) with 40 μ M dGTP for 30 min or (c) without nucleotide, and injected onto a S200 column (GE heathcare). A_{280nm} was monitored. Peak 1 eluted in the void volume (16 min) is likely aggregate of α . (a) With TTP, the peak 2 eluted at 22.6 min with the apparent MW of 244 kDa. (b) With dGTP, the peak 2 eluted at 23.1 min with the apparent MW of 212 kDa, Peak 3 (shoulder) eluted at 25.9 min, with the apparent MW of 110 kDa (c) Peak 2 eluted at 25.6 min with the apparent MW of 118 kDa The S200 column was equilibrated in 100 mM HEPES pH 7.6, 20 mM MgSO₄ at a flow rate of 0.5 mL/min.

Table 5.3: Molecular Weight Determination of *S. cerevisiae* α in the presence of effectors by SEC.

Protein (effector)	Apparent mass (kDa)	Expected mass (kDa)	Oligomeric state	Retention time (min)
α (100 μ M TTP)	244	199	α_2	22.6
α (40 μ M dGTP)	212, 110	199,100	α_2, α	23.1, 25.9
α (25 mM DTT)	118	100	α	25.6

Having established a quaternary homogeneous state for α_n , DAN-Sml1-S61C was placed in a cuvette with 100 μ M TTP and titrated with increasing concentrations of α_2 (100 μ M TTP). Two control experiments in which DAN-Sml1-E71C, and DAN-Sml1-W65C were used revealed no significant fluorescence intensity changes during titrations; alkylation of W65 with a bulky group inhibited binding while modification of E71 with the label failed to reveal Sml1- α interactions. Thus, results from the control experiments further support our model of the putative binding helix.

DAN-Sml1-S61C was expected to be most informative probe because it is located adjacent to the proposed site of binding and showed the most potent inhibition of nucleotide reduction. The results of a typical titration are shown in Figure 5.8. To determine the time required for establishing equilibrium subsequent to each addition of α_2 , spectra was recorded every min until no further fluorescence change was observed. Ten min was chosen as the standard time interval between additions. For titration of DAN-Sml1-S61C with α_2 in the presence of TTP, the emission intensity increased and was blue shifted by 20 nm, suggesting a change to a more hydrophobic environment (25), in agreement with our binding model. The K_d (0.47 μ M) for DAN-Sml1-S61C and α_2 (TTP) at 30 $^{\circ}$ C was obtained by fitting the fraction bound vs $[\alpha_2]_{\text{free}}$ curve with Eq 2 (Figure 5.8 a, b). In the presence of both CDP and TTP, the binding of DAN-Sml1-S61C

and $\alpha 2$ was significantly increased, given a much lower K_d of $0.17 \mu\text{M}$. The emission was blue shifted by 10 nm, indicating a conformational change of the Sml1 binding site upon addition of the substrate. The enhanced binding of Sml1 to α in the presence of CDP suggests that Sml1 binds to the ES form with increased affinity compared to the E form, which displays a mixed or uncompetitive binding character.

Only the intensity changes were considered in the data analysis, and the dimer concentrations of both α and Sml1 were used to compare the K_d values to Thelander's value. The K_d reported by Thelander using Biacore method was $0.4 \mu\text{M}$ in the absence of TTP at $22 \text{ }^\circ\text{C}$ (11). The running buffer was 10 mM HEPES, pH 7.4, 200 mM potassium acetate, 1 mM EDTA, 5 mM magnesium acetate, and 0.05% surfactant P20.

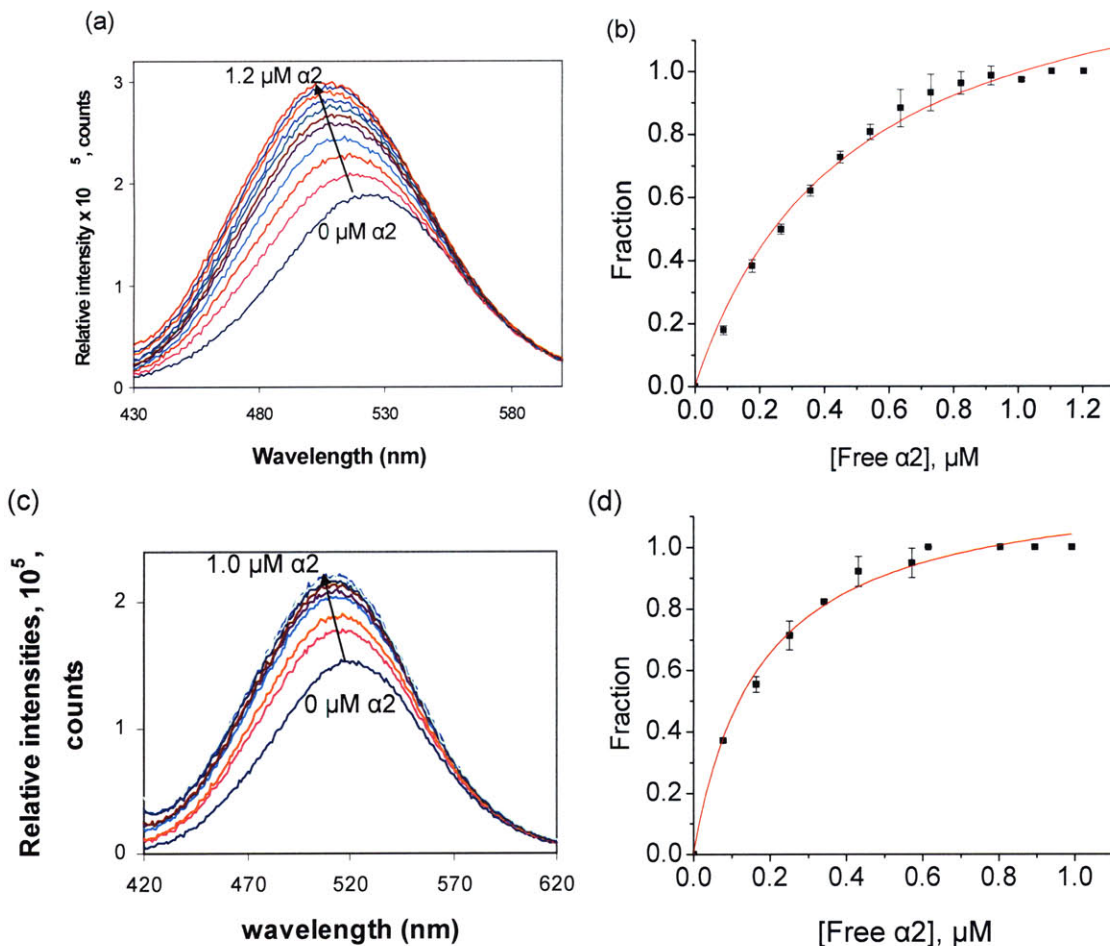


Figure 5.8: Titration of DAN-Sml1-S61C with α_n .

(a) HEPES 50 mM, pH 7.6, 15 mM MgSO_4 , 100 μM TTP in 400 μL with DAN-Sml1-S61C (0.04 μM , dimer) was titrated with α_2 (78 μM) with TTP from 0 to 1.2 μM . Each emission curve was taken after 10 min incubation at 30 $^\circ\text{C}$. The emission wavelength was blue shifted by 20 nm during the titration. (b) $K_d = 0.47 \mu\text{M}$ was obtained by fitting with Eq. 2. (c) The titration condition is identical to (a), except that α_2 was incubated with 1 mM CDP, which was also added in the titration buffer. The emission wavelength was blue shifted by 10 nm. (d) $K_d = 0.17 \mu\text{M}$ was obtained by fitting with Eq. 2.

In an effort to determine if probe placement effects K_d , a second DAN-Sml1 was used. Titrations of DAN-Sml1-M80C with α were carried out in the presence of TTP \pm CDP. Eq. 3 with sigmoid shape binding model was used to fit the binding data, from which K_d obtained was 1.1 μM (hill coefficient $n=1.3$) in the absence of CDP, and 0.46 μM ($n=1.4$) in the presence of CDP. The emission wavelength blue shifted 20 and 25 nm

in the absence of CDP and in the presence of CDP respectively (Figure 5.9). DAN-Sml1-M80C shows again that Sml1 binds the ES form with increased affinity than the E form. Comparison of these K_d values to the values for S61C to α_2 , suggest that weaker binding of M80C to α_2 (TTP) might possibly result from a partial impairment of the α -Sml1 binding site by substitution at M80 as indicated by the inhibition assays (Figure 5.6).

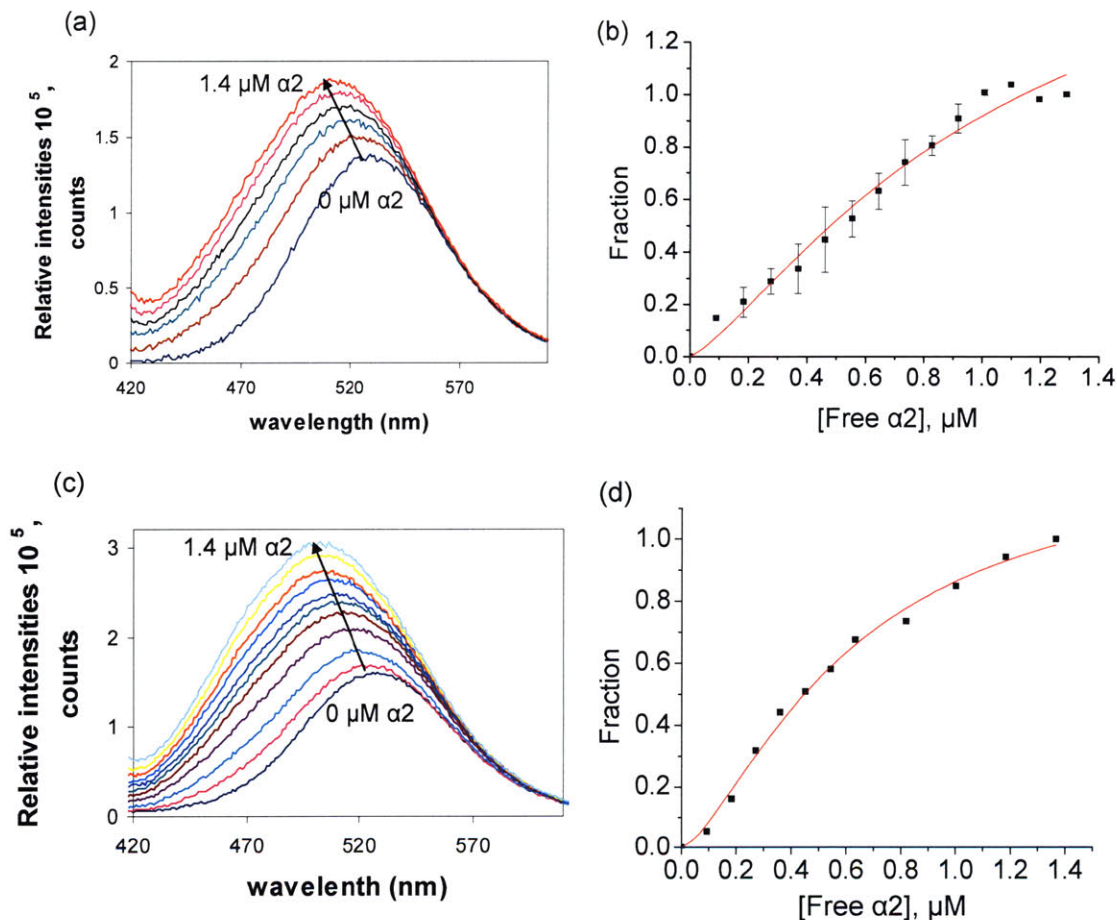


Figure 5.9: Titration of DAN- Sml1-M80C by α_2 .

(a) HEPES 50 mM pH 7.6, 15 mM $MgSO_4$, 100 μM TTP in 400 μL with DAN-Sml1-M80C (0.04 μM , dimer) was titrated with α_2 (78 μM) with TTP from 0 to 1.4 μM . Each emission curve was taken after 10 min incubation at 30 $^{\circ}C$. The emission wavelength was blue shifted by 20 nm during the titration. (b) $K_d = 1.1 \mu M$, $n=1.3$ was obtained by fitting with Eq. 3, (c) The titration condition is identical to (a), except that α_2 was incubated with 1 mM CDP, which was also added in the titration buffer. The emission wavelength was blue shifted by 10 nm. The emission wavelength was blue shifted by 25 nm.(d) $K_d = 0.46 \mu M$, $n=1.4$ was obtained by fitting with Eq. 3.

As a 2nd method, surface plasmon resonance method via BIAcore has been carried out using the procedure which Thelander (26) applied to measure α/β subunit interaction in mouse RNR. The wt Sml1 was immobilized onto a CM5 sensor chip via the amine coupling method. The ligand (α 2 (TTP) or $\beta\beta'$) was equilibrated in the running buffer (PBS buffer, pH 7.2) at 22 °C. Interaction with α (0.156 μ M to 20 μ M) 100 μ M TTP at 30 μ L/min gave rise to a typical chromatograph (Figure 5.10a). The TTP was present to ensure α was predominantly a dimer. A $K_d = 0.6 \mu$ M in the presence of TTP was obtained from our preliminary data by fitting with 1:1 binding model using Eq 2 (Figure 5.10c). The results of a similar experiment using 5 μ M $\beta\beta'$ are shown in Figure 5.10b. No binding to $\beta\beta'$ was observed as previously reported by Thelander.

The results from two independent methods are similar with the caveat being that the quaternary state of α in neither set of experiment is known. A K_d of 0.6 μ M relates to the physiologically reported concentrations of Sml1 and α ($0.76 \pm 0.23 \mu$ M) (27) and is thus likely to be interesting.

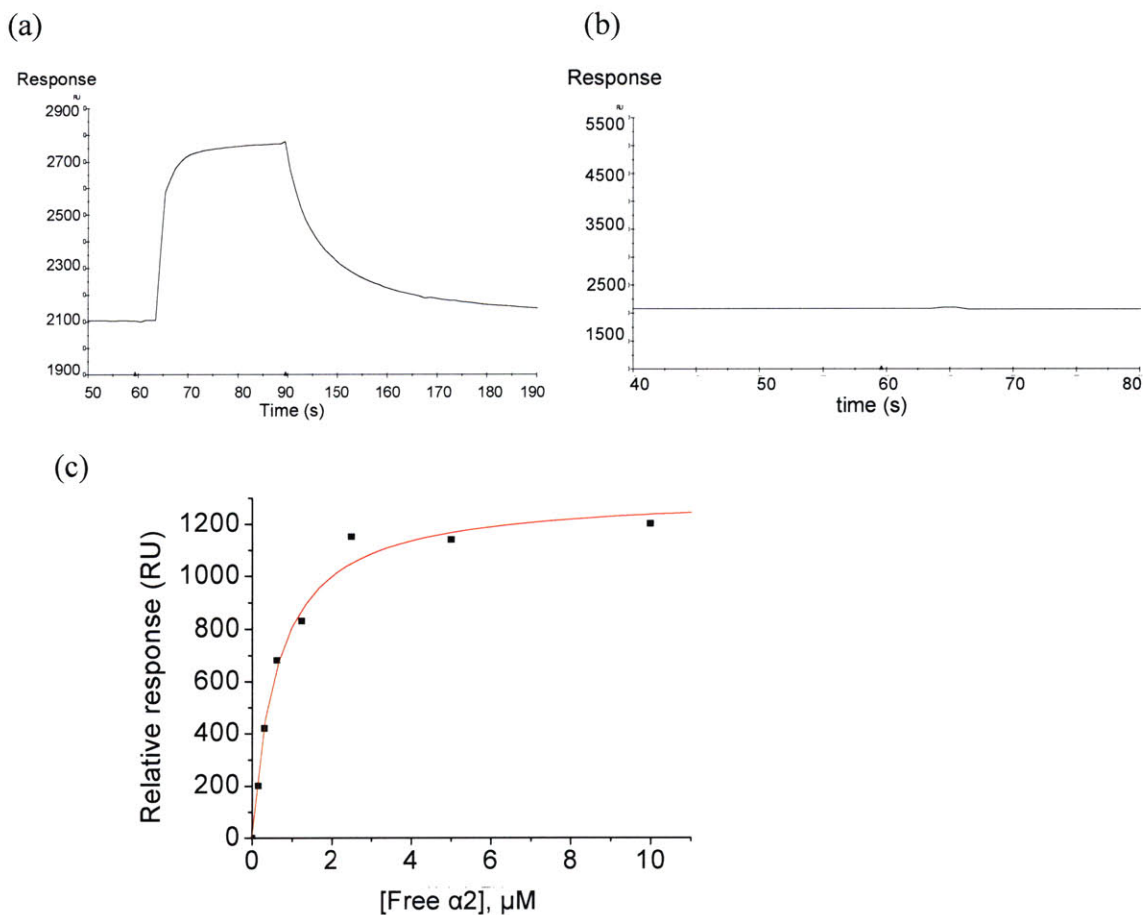


Figure 5.10: Determine the K_d of wtSml1 with α with surface plasmon resonance method using a Biacore.

Sml1 was immobilized on the CM5 sensor chip surface, $\alpha 2$ (5 μM) incubated with 100 μM TTP was passed through the sensor chip surface to interact with Sml1. (a) The plot showed Sml1 could bind $\alpha 2$. (b) Sml1 was immobilized on the CM5 sensor chip surface, 5 μM $\beta\beta'$ (0.4 $\text{Y}\bullet$) was passed through the sensor chip surface to interact with Sml1. (c) Sml1 was immobilized on the surface and titrated with $\alpha 2$ (TTP) at increasing concentrations.

5.3.5 Purification and activity assays of W688A- α , E689D- α , W688A, E689D- α :

Yeast two-hybrid studies by the Rothstein's group suggested that Sml1 interacted strongly with α -W688G. This mutation partially restored interactions between α and seven Sml1 mutants (R72, L73, S75, I76, S87, F94, F104) which have significantly reduced binding affinity to α (10). In addition, Zhang *et al* performed yeast two hybrid

assays and showed that W688A, E689D- α could increase the α -Sml1 affinity. W688 and E689 in α are highly conserved from bacteria to human. Both mutations are located at an α helical region on the outside surface of *E. coli* and yeast α structure (Figure 5.20). The Huang lab also demonstrated that the W688A E689D mutations were lethal to a *rnr3* Δ strain in the presence of Sml1. Removal of Sml1 from the strain restored cell viability (5). The hypothesis to account for this result was that increased affinity between α and Sml1 maintained inhibition of α resulting in insufficient concentrations of dNDPs for cell viability. To test this proposal, W688A- α , E689D- α , and W688A E689D- α were purified following the established protocol for α purification, using dATP affinity chromatography (Figure 5.11).

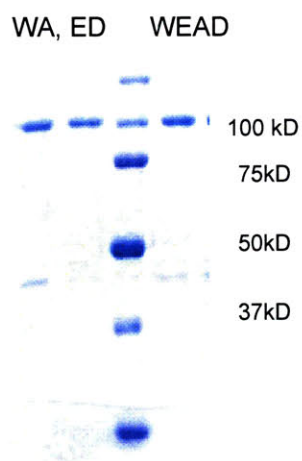


Figure 5.11: SDS-PAGE gel (10%) of purified W688A- α , E689D- α single mutants (left), and W688A E689D- α double mutants (right).

10 μ M α mutants were loaded. The band at 100 kD is the α mutant, and the lower band between 37-50 kD is impurities.

The activity of each mutant (1 μ M) in the presence of 7 μ M Flag- $\beta\beta'$ (0.3 Y \bullet), and [3 H]-CDP (specific activity of 5307 cpm/nmol), 3mM ATP, TR, TRR, NADPH was carried out for 30 min at 30 $^{\circ}$ C. The activity of wt- α control was 245 nmol/min/mg.

E689D- α retained 79% of the wt α activity (Table 5.4 and Figure 5.12), while activities for W688A- α and W688A E689D- α were 1% that of wt. Assays were performed in triplicate (Table 5.4 and Figure 5.12 a, b). Thus the mutation of W688 is mainly responsible for the loss of RNR activity.

Previous studies of Huang and coworkers reported that the W688A E689D- α exhibited a slower growth phenotype relative to the wt α . The results shown above suggest that the slower growth phenotype could also be associated with the low activity of the mutant α .

To more quantitatively evaluate the slower growth phenotype, Huang's group examined the effect of these mutations on wt growth rate in the absence of Sml1 (Figure 5.13). The data show that W688A or W688G- α , as well as W689A E689D- α display a prolonged S-phase (30-40 min) relative to wt α and a small portion of mutant cells showed S-phase arrest. E689D- α has a similar growth rate to wt α . Western blot in Figure 5.14 shows that the level of the mutants are the same as wt α . These results agree well with our in vitro assays that the W688 mutation affects cell viability by losing RNR activity, rather than affecting the protein expression.

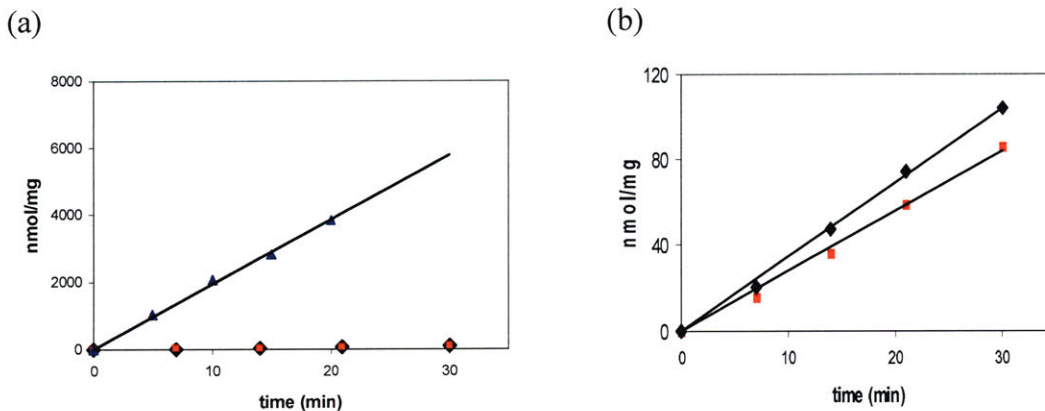


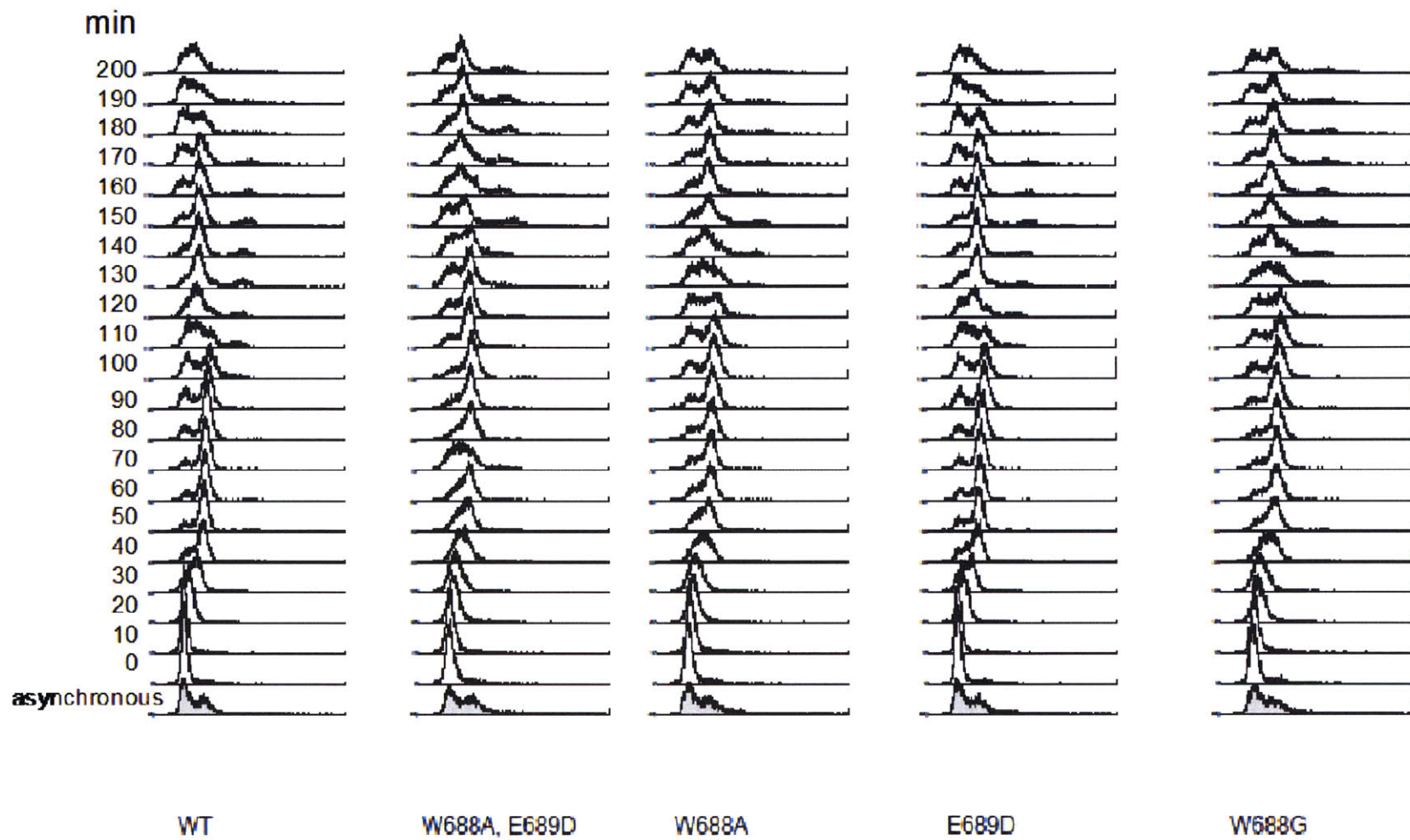
Figure 5.12: Activity assay of W688A- α , E689D- α , W688A E689D - α mutants. The W688A- α (\blacklozenge), E689D- α (\blacktriangle), and W688A, E689D- α (\blacksquare) (a) were assayed at 1 μ M with 7 eq. of Flag- $\beta\beta'$ (7 μ M, 0.3 Y \bullet), in the presence of 1mM [3 H]-CDP (5307 cpm/nmol), 3mM ATP and TR, TRR, NADPH. The assays were carried out over a 30 min time period at 30 $^{\circ}$ C. (b) Expansion of the data in (a) for W688A E689D double mutant (\blacksquare) and W688A mutant (\blacklozenge) assays (b) are repeated 3 times. Data is shown in table 5.2 below.

Table 5.4: Summary of W688A, E689D α single mutants and W688A E689D α double mutant.

	Activity (nmol/min/mg)	Activity %
W688A	3.3 \pm 0.25	1%
E689D	193	79%
W688A E689D	2.8 \pm 0.7	1%
wt α	245	100%

Figure 5.13: FACS analysis by Huang's group.

All strains were of *rrn1:: HIS3, rrn3:: Kan, Sml1:: Kan* background. The *rrn1* mutants were on a TRP1CEN plasmid (1 to 3 copies per cell). All strains were grown in YPD to early log phase, synchronized in G1 phase by alpha factor mediated arrest, and released back into the cell cycle by washing off the pheromone-containing medium. Cells were collected at 10 minutes intervals up to 200 min post release and processed for FACS analyses. For wt, the 1st S phase between 20-30 min, the first G2 phase 50-60 min, and the second S phase is ~110 min. For the WE-to-AD mutant, the first S phase is between 20' and 70' (greatly prolonged by 30 to 40 min), G2 is at 80'-90', and the second S phase is hard to tell because the cells are out of synchrony. W688A and W688G are similar as the double mutant, the first S phase is between 20' – 50 min (prolonged by 20 to 30 min), the second S is around 120 to 150 min. E689D is similar to WT in cell cycle progression.



AXY743 = MATa, mrl::HIS3, mr3::Kan, sml1::Kan

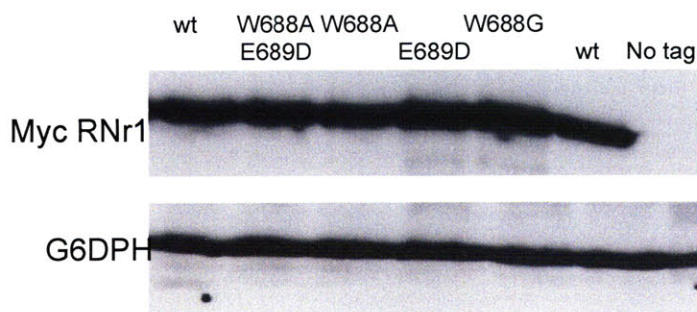


Figure 5.14: Western blot showing the protein levels of wt- α , W688A E689D- α , W688A- α , E689D- α , W688G- α mutants (Left to Right) (From Huang group).

5.3.6 Measurement of the affinity of Sml1 for W688A, E689D- α

The slow growth phenotype could also be the result of tighter binding of Sml1 to the α mutants as originally proposed (28, 29). To test this model, W688A was titrated with DAN-Sml1-S61C. The results of a typical experiment with the W688A E689D- α double mutant in the absence of CDP are shown in Figure 5.15 a. Analysis of the data with Eq. 3 gave a $K_d=0.004 \mu\text{M}$ (Figure 5.15 b). Cooperative binding appeared and the emission wavelength was blue shifted 14 nm. Thus the W688A E689D- α has significantly higher affinity for Sml1 as suggested by the two hybrid studies, as well as significantly lower catalytic activity (5). The mechanism of this tight cooperative binding needs further analysis.

The binding studies are difficult to interpret for several reasons. First analysis by SEC of W688A E689D- α in the presence of TTP reveals that it is $\sim 40\%$ aggregation and 60% dimer (Figure 5.16). The effect of the aggregates on the fluorescence titration thus makes a molecular picture of the interaction between Sml1 and α impossible to describe. The aggregate state of W688A E689D- α is double that (40%) of wt (20%). Further

analysis could be carried out if aggregation could be separated from wt $\alpha 2$ and can be shown not to re-equilibrate.

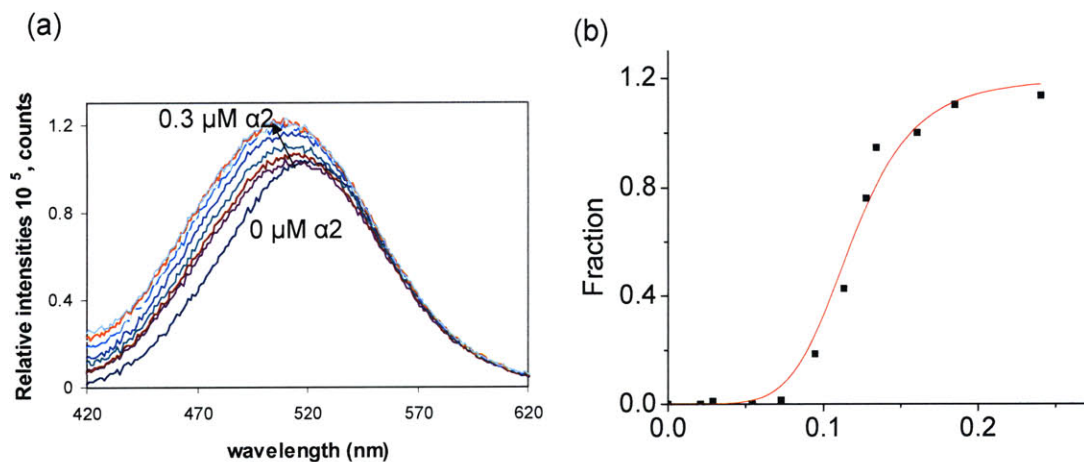


Figure 5.15: Titration of DAN- Sml1-S61C with W688A E689D- α double mutant. HEPES 50 mM, pH 7.6, 15 mM MgSO_4 , 100 μM TTP in 400 μL with DAN-Sml1-S61C (0.04 μM , dimer) was titrated with (a) W688A E689D- $\alpha 2$ (24 μM) from 0 to 0.3 μM with TTP. The emission wavelength was blue shifted 15 nm. (b) $K_d = 0.004$ μM , $n=6$ was obtained by fitting with Eq. 3.

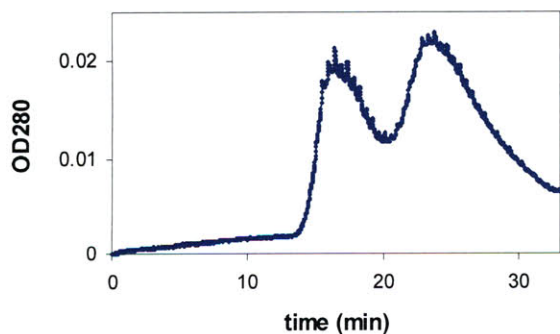


Figure 5.16: SEC spectra of W688A E689D- α in the presence of TTP. W688A E689D- α (24 μM) was pre-reduced with 30 mM DTT for 30 min, then incubated with 100 μM TTP, before injection onto a S200 column (GE heathcare). $A_{280\text{nm}}$ was monitored. Peak 1 eluted at void volume (16 min) is likely an aggregate of α . Peak 2 eluted at 23.7 min, with apparent MW 214 kDa. The calculated $\alpha 2$ is 200 kDa. S200 column was equilibrated in 100 mM HEPES pH 7.6, 20 mM MgSO_4 , 100 μM TTP at a flow rate of 0.5 mL/min.

5.3.7 Purification and activity assays of C883S C886S- α :

The hypothesis for the mechanism of inhibition of RNR α by Sml1 is that Sml1 prevents the C-terminus of α from entering the α active site to re-reduce the active site disulfide produced concomitant with dNDP production. As a test of this model, mutations of the C-terminal cysteines (C883S, C886S) postulated to be involved in this re-reduction were prepared. The hypothesis was that these mutants would still be active with DTT as a reductant, inactive with TR/TRR, NADPH as reductant, and that by using C883S C886S- α , DTT would be able to enter directly into the active site in the presence of Sml1 and re-reduce the active site disulfide.

The double mutant was generated, expressed and purified following the protocol for wt- α . Activity assays of C883S, C886S- α with 20 mM DTT gave an activity of 46 nmol/min/mg, 50% of the wt activity. Note that the wt activity, 92 nmol/min/mg with DTT, is 50% of that obtained when using TR/TRR/NADPH as reductant. When the assay was carried out on the double mutant using TR/TRR, no activity was detected. Thus the C-terminal cysteines of eukaryotic RNR appear to play a similar role to that for prokaryotic systems despite differences in the cysteine motif (CXXC vs CX4C).

The inhibition of RNR activity by Sml1 using DTT as a reductant was then examined with the mutant and wt α and the results are shown in Figure 5.17. No difference in inhibition was observed, suggesting that the hypothesis of Huang is correct for Sml1 inhibition, and DTT is unable to access the active site. To test this model further, a CTD (residues 765-888) shown in yeast two hybrid assays to compete with Sml1 binding would need to be constructed and characterized. It could potentially compete with Sml1 for binding to α and in fact could potentially re-reduce the active site disulfide.

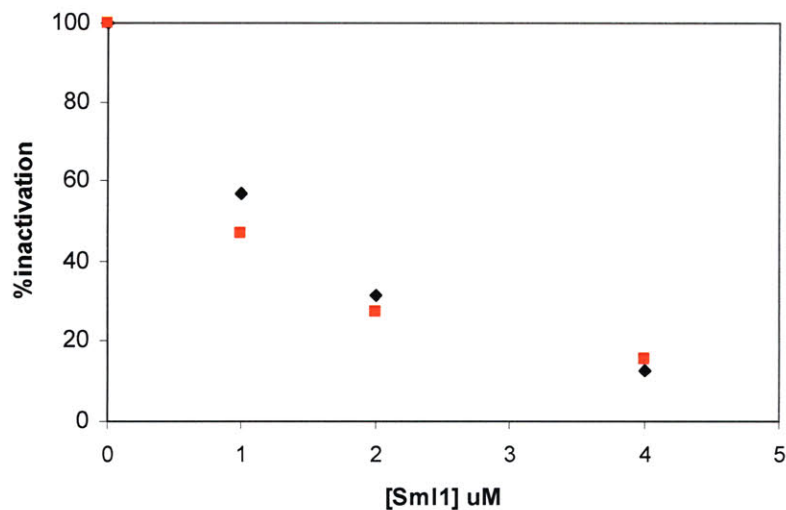


Figure 5.17: Inactivation assay of wt- α and C883SC886S- α by Sml1.

Inactivation mixture contained final concentrations of 1.6 μ M wt α (♦) (specific activity of 319 nmol/min/mg) or 1.6 μ M C883SC886S α mutants (■), in the presence of 0.8 μ M $\beta\beta'$ (0.3 Y•, specific activity of 2410 nmol/min/mg), 3 mM ATP, [Sml1] = 0, 1, 2, 4 μ M. The wt α was assayed with TR, TRR, NADPH. And the C883SC886S- α mutant was assayed with 20 mM DTT. Assays were carried out at 30 °C. The percentage of the activities remained of wt α (♦) and C883SC886S- α (■) at varying concentrations of wt Sml1 are shown.

5.3.8 Measurement of the affinity of Sml1 to oxidized α

The model of Huang *et al* further suggests that Sml1 may preferentially bind to the oxidized form of α rather than the reduced form. Therefore, oxidized α was prepared by incubating pre-reduced α with excess His- $\beta\beta'$ (0.3 Y•), in the presence of 3 mM ATP, 1 mM CDP at 30 °C for 20 min. The His- $\beta\beta'$ was removed from the resulting oxidized α by use of cobalt resin. Unfortunately the recovery of oxidized α using this procedure was 20% and the protein appeared to be even less soluble than reduced α . Attempts to concentrate oxidized α to facilitate fluorescence titrations resulted in its precipitation.

Given these caveats, the K_d of the DAN-Sml1-S61C for the oxidized α in the presence and absence of dCDP were measured (Figure 5.18a, b). The emission wavelength blue shifted 10 nm (Figure 5.18a) and the binding curve exhibited

cooperative behavior as shown in Figure 5.18b. The fit to the data using Eq. 3 in the absence of dCDP is shown, giving a $K_d=0.05 \mu\text{M}$ ($n=3$). The titration in the presence of dCDP showed very small changes relative to that in the absence of dCDP. The fit as a consequence is poor. Furthermore, no blue shift was observed in contrast with all other titrations. The basis for these observations are unknown, but could be related to aggregation of α . Our preliminary SEC data has revealed that the quaternary structure of oxidized α in the absence of dCDP, but in the presence of TTP is predominantly a monomer, while the reduced α is predominantly a dimer under the same conditions. In the analysis of the data in Figure 5.18b, dimer concentrations of both Sml1 and α were used. The binding of one monomer of the Sml1 to oxidized α may promote the binding of the second monomer to an additional oxidized α . Characterizations of oxidized α and the number of oxidized α interactions with Sml1 dimer requires further investigation.

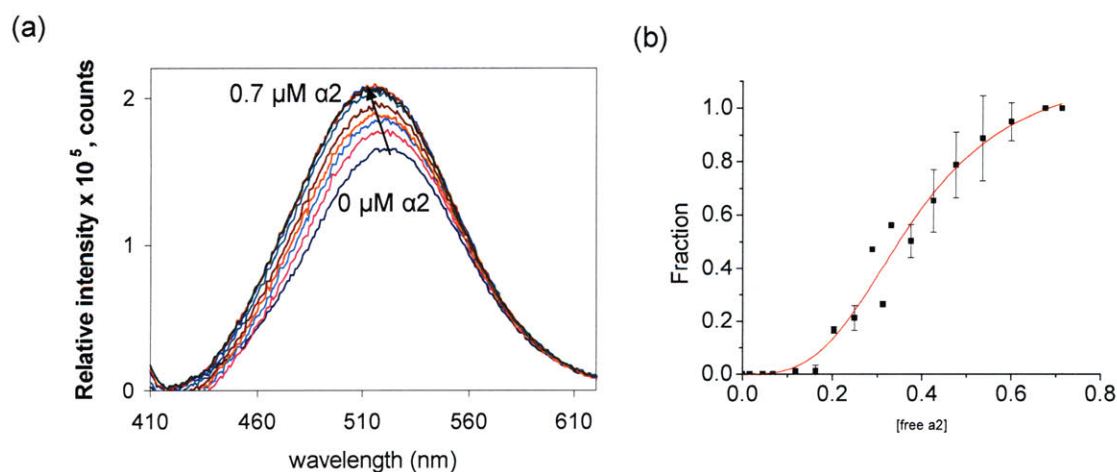
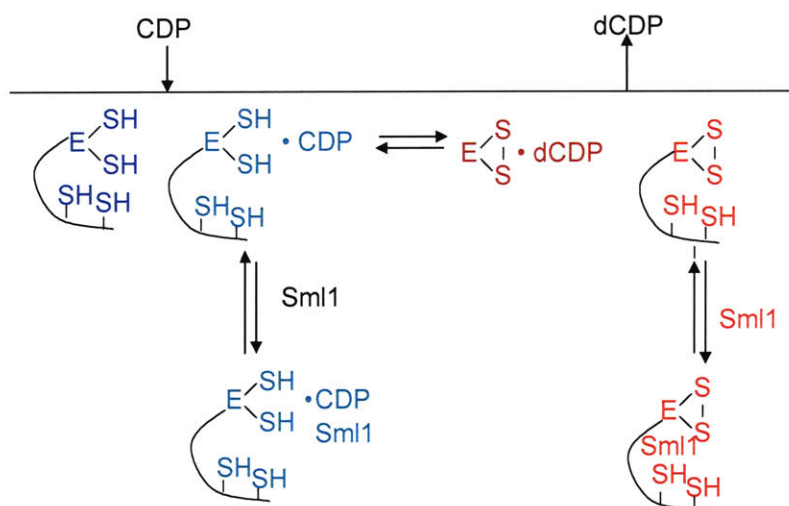


Figure 5.18: Titration of DAN-S61C-Sml1 with oxidized α (100 μM TTP).

HEPES 50 mM pH 7.6, 15 mM MgSO_4 , 100 μM TTP in 400 μL buffer with DAN-Sml1-S61C (0.04 μM , dimer) was titrated with (a) isolated oxidized α in the absence of dCDP, in the presence of TTP from 0 μM (blue) to 0.7 μM (red). The emission wavelength was blue shifted 10 nm. (b) $K_d = 0.05 \mu\text{M}$ ($n=3.2$) was obtained. The titration was carried out at 30 $^\circ\text{C}$.

5.3.9 Mechanism of inhibition of Sml1 relative to CDP:

The model of Huang further suggests that Sml1 could bind to either the reduced form of α (α_{SH}) in the presence of CDP or the oxidized form (α_{S}). A simple kinetic model is shown in scheme 5.2. Binding to either form could potentially inhibit re-reduction of the active site disulfide by the C-terminal tail. If Sml1 bound only to oxidized α , then its inhibition should be uncompetitive with CDP as it binds to a different form of the E, than CDP and the forms are irreversibly connected. On the other hand, if Sml1 binds to both the oxidized and reduced form, then the inhibition would be noncompetitive.



Scheme 5.2: The kinetic model of Sml1 binding to different forms of α .

The inhibition kinetic analysis was carried out using the TR/TRR/NADPH radioactive assay. The concentrations of CDP were varied between 0.044 mM and 1 mM, while the concentrations of Sml1 were varied between 0 and 2 μM . The result of the analysis as a Lineweaver Burk plot is shown in Figure 5.19. The data suggests that the inhibition pattern changes as [Sml1] increases. The data were fit to either equations for

competitive, $v=V_{\max}[S]/(\alpha K_m+[S])$; noncompetitive, $v=V_{\max}[S]/[\alpha(K_m+ [S])]$; or uncompetitive $v=V_{\max}[S]/(K_m+ \alpha'[S])$ binding, where $\alpha=1+[I]/K_i$, $\alpha'=1+[I]/K_i'$. In the fitting, K_m and V_{\max} are fixed with the values obtained at $[Sml1]=0$. For $[Sml1]=0.5, 1, 1.5, 2 \mu M$, the data fits the best with the uncompetitive model (Table 5.5). For $[Sml1]=0, 0.5 \mu M$, the uncompetitive inhibition still fits better than the noncompetitive and competitive inhibition models.

From our studies, Sml1 binds to the reduced form ($K_d = 0.47 \mu M$) and to the oxidized form ($0.05 \mu M$) of α . In the presence of CDP, Sml1 binds with increased affinity to the reduced form of α ($K_d = 0.17 \mu M$). Sml1 binding would require CDP to put the enzyme into the correct state, the oxidized form, which may explain the higher affinity observed in this case.

Table 5.5: Fitting v vs [CDP] data to distinguish competitive and uncompetitive inhibition model.

[Sml1](μM)		Competitive	Uncompetitive	Noncompetitive
0.5	R^2	0.9	0.98	0.96
	Chi^2	886	150	386
1	R^2	0.8	0.99	0.98
	Chi^2	1047	52	118
1.5	R^2	0.38	0.99	0.89
	Chi^2	1462	28	259
2	R^2	-0.18	0.99	0.7
	Chi^2	1408	8.9	342

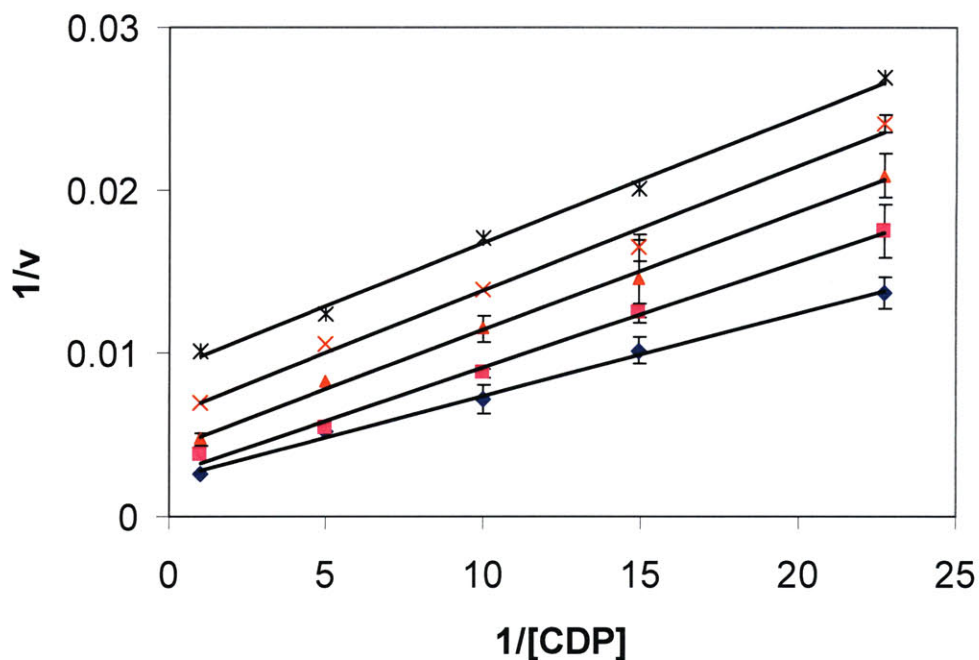


Figure 5.19: CDP vs Sml1 competition assay.

0.3 μM Y1 ($\alpha 2$, 330 nmol/min/mg) was assayed in the presence of 3 μM Flag- $\beta\beta'$ (0.3 Y•) with 3 mM ATP and TR, TRR, NADPH. [Sml1] = 0 μM (\blacklozenge), 0.5 μM (\blacksquare), 1 μM (\blacktriangle), 1.5 μM (\times), 2 μM (\times), (from bottom to top), [^3H]-CDP = 0 mM, 0.044 mM, 0.067 mM, 0.1 mM, 0.2 mM, 1 mM, with specific activity 5860 cpm/nmol. The assays were carried out at 30 $^\circ\text{C}$ for 20 min. Double-reciprocal plot (1/v vs 1/[CDP]) are displayed. The equations which used to fit the plots are as follows,
 $y = 0.0005x + 0.0023$, $R^2 = 0.995$, [Sml1] = 0 μM ,
 $y = 0.0007x + 0.0026$, $R^2 = 0.995$, [Sml1] = 0.5 μM ,
 $y = 0.0007x + 0.0042$, $R^2 = 0.997$, [Sml1] = 1 μM ,
 $y = 0.0008x + 0.0062$, $R^2 = 0.997$, [Sml1] = 1.5 μM ,
 $y = 0.0008x + 0.009$, $R^2 = 0.996$, [Sml1] = 2 μM .

5.4 Discussion:

The proposal based on biochemical and yeast two hybrid studies is that Sml1 binds to $\alpha 2$ and prevents re-reduction of the active site disulfide generated concomitant with dNDP production (29). Sml1 is proposed to interact with a helical surface of α

including W688 (28, 29) and prevent access of the C-terminal insertion and C-terminal tail region of α (scheme 5.1).

Several experiments have been described to test the model. While 2D NMR methods revealed that the structure of Sml1 is predominantly unfolded, an α -helix within its C-terminus was identified. The C-terminus of Sml1 has been demonstrated by deletion studies to interact with α . Generation of an α helical wheel from this region revealed an amphipathic helix with both an acidic patch and a hydrophobic patch (Figure 5.3). In addition, the *S. cerevisiae* α structure revealed that W688 is located at the entrance of a tunnel into the active site (Figure 5.20). Interestingly, the structure also shows a hydrophobic region (cyan circle) and a basic region (pink circle) adjacent to W688, which can adapt the binding of the hydrophobic patch and acid patch of the helical wheel of Sml1. Unfortunately the C-terminus of yeast α , shown *in vivo* to be essential for reduction of the disulfide in the active site, is not visible in any structures. Thus based on this model, cysteine mutants of Sml1 were generated adjacent to the helix and on different faces of the helix.

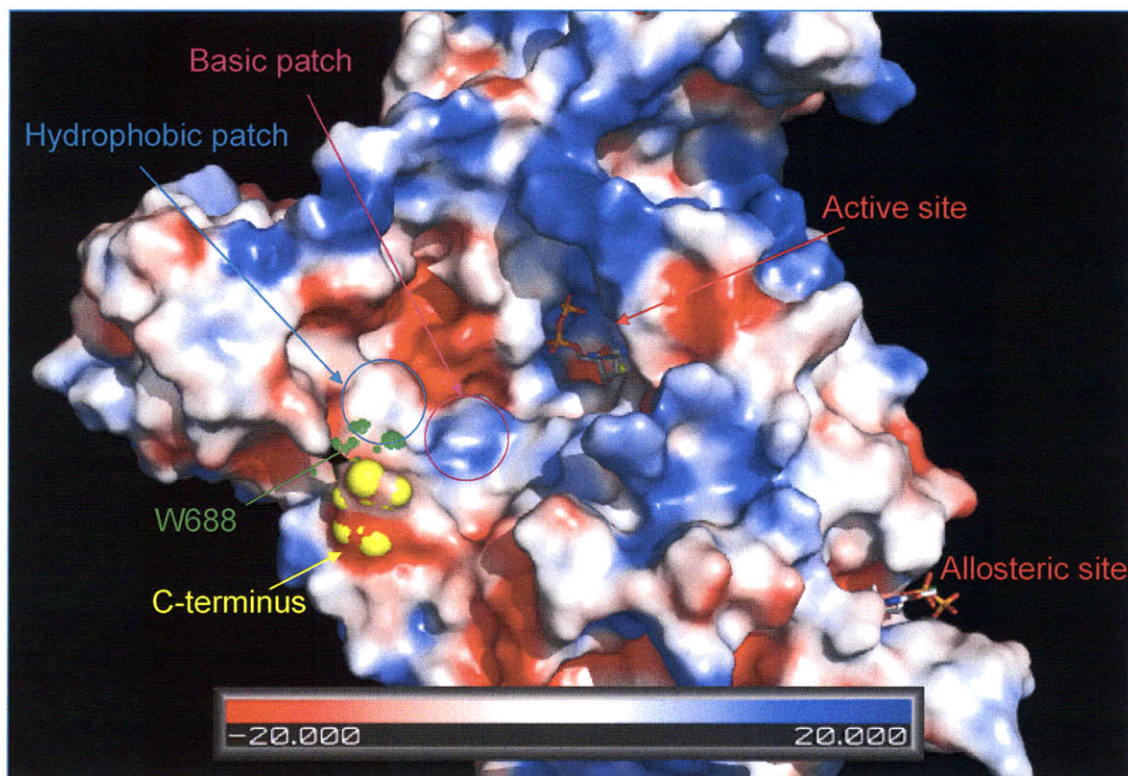


Figure 5.20: Structure of *S. cerevisiae* α showing the position of W688 GDP in the active site, and TTP in the allosteric site are shown in stick. The position of W688 (green) and the last visible residue Q746 (yellow) in this structure at the C-terminus are highlighted. The charge on the surface is displayed from positive charge or basic (blue) to negative charge or acidic (red) and the hydrophobic region is in white color. A hydrophobic region (cyan) and a basic region (pink) around W688 are identified which could potentially bind the hydrophobic patch and acid patch of Sml1.

Attachment of the fluorescent probe DAN through alkylation generated several DAN-Sml1 that were examined for interactions with α . We have found a site (S61 of Sml1) to attach DAN that minimally perturbed binding to α and exhibited a moderate change in fluorescence binding. The binding partner α , unfortunately is not as well behaved and complicates analysis of both binding and kinetic studies. Previous studies by Thelander measured Sml1 binding to α via SPR (surface plasmon resonance). In their

studies, Sml1 was attached to the chip. They reported that the K_d for interaction in the presence or absence with TTP was 0.4 μM . In the same paper, they analyzed α (TTP) by SEC and sucrose gradient AUC and found that α was a dimer in equilibrium with a tetramer. No comment was made about the heterogeneity of α and how it could potentially complicate their data interpretation. We studied the oligomerization state of α using SEC method with nucleotide in the running buffer, in an attempt to find a set of conditions with a single complex of α . From previous studies on *E. coli* and mouse α (30, 31), TTP binds to the specificity site and enhance α dimerization. In our studies on *S. cerevisiae* α in the presence of TTP, 20% of α was aggregate and 80% of α was a dimer (Figure 5.7). This condition was chosen for our binding studies, because of the higher percentage of homogeneity.

We determined the K_d of Sml1 for α using fluorescence titrations. However, with our initial titration of α (TTP) with Sml1, the data was not well fit to a hyperbolic binding curve (Figure 5.8). Addition of CDP gave enhanced binding with better fits, and a K_d of 0.17 μM . We additionally reproduced the SPR experiments of Thelander, attaching Sml1 to the chip and using α (TTP) as elute. The apparent K_d was 0.6 μM , similar to the 0.4 μM reported. Thus the K_d of Sml1 to α is 0.4 to 0.6 μM , with CDP increasing Sml1 affinity for α .

The Huang model is that Sml1 prevents re-reduction of the active site disulfide by the CXXC motif in the C-terminal tail of α . Thus, we conducted experiments using oxidized α and DAN-Sml1-S61C to test this hypothesis. Oxidized α was generated by incubation with CDP/ATP and $\beta\beta'$ in the absence of reductant. The oxidized α was then separated from tagged $\beta\beta'$ by affinity chromatography. However, the oxidized form of α

is not well behaved and resisted concentration. Preliminary SEC analysis revealed oxidized α is predominately a monomer. Previous studies by Thelander on *E. coli* enzyme suggested that α in its oxidized state is a monomer as well (30). Further study of the oligomeric state of oxidized α is warranted to shed insight into its nature. A fluorescence titration of oxidized α with DAN-Sml1-S61 was carried out in the presence and absence of dCDP. In the presence of dCDP, fluorescence changes were very small and not blue shifted as all other titrations. This data was not analyzed further due to small total changes. In the absence of dCDP, binding was cooperative with an apparent K_d of 0.05 μ M. An understanding of the quaternary structure of oxidized α is required to think about a molecular model to explain this behavior.

Further analysis of interaction between Sml1 and α was thus carried out to test the effect of the W688A (G) mutation in α . By two independent methods, Rothstein and Huang demonstrated increased affinity of Sml1 for W688A (G)- α mutants. The single and double mutants of α at residues W688 and E689 were purified. Surprisingly, given the location of the mutants (Figure 5.20), the W688-single mutant and the double mutant had 1% the activity of wt RNR. The mutant at residue 689 had little effect on activity. This mutant was then analyzed by fluorescence titration with DAN-Sml1-S61C and by SEC chromatography. The binding curve exhibited very steep sigmoidicity with an apparent K_d of 0.004 μ M. The low K_d from fits demonstrates that we actually carry out a stoichiometric titration. However, SEC revealed 45% of the protein was aggregated.

The activities of the mutant and their apparent tight binding to Sml1 could account for their observed biological “slow growth” phenotype and 30 min increase in progression through the cell cycle relative to wt α . We thought that we might be able to

get a further handle on the mode of inhibition by Sml1 using a kinetic analysis with CDP as the variable substrate. The uncompetitive inhibition pattern suggests Sml1 binds to a different form of α , than CDP, but the complicity of the assay, including potential competition of Sml1 and Trx for binding to α , has made interpretation a challenge. Obviously more studies are essential to understand the nature of Sml1 inhibition, including studies to determine the quaternary structure of α in its reduced and oxidized states in the presence of nucleotides.

The main conclusion from this work is thus that Sml1 binds to oxidized and reduced α and binds more tightly to the W688A- α mutant than the wt α . The cooperativity in binding is intriguing and likely relates to the effect of Sml1 on altering the quaternary structure of α . Finally the results with CXXC to SXXS mutants of the α -C-terminal tail demonstrate that these residues are involved in active site disulfide re-reduction. This behavior suggests this mechanistic aspect has been evolutionary conserved; *E. coli* RNR also demonstrates this behavior although it has a different C-terminal motif (CX4C).

Summary:

Sml1 binds to α , inhibiting dNDP production by a mechanism that involves its C-terminal helix (likely the hydrophobic face) and a region of α that includes W688. Sml1 can bind to multiple states of α , but detailed inhibition mechanism requires further analysis.

5.5 Reference

- (1) Zhao, X., Muller, E. G. and Rothstein, R. . (1998) A suppressor of two essential checkpoint genes identifies a novel protein that negatively affects dNTP pools. *Mol. Cell.* 2, 329-340.
- (2) Stubbe, J. (1990) Ribonucleotide reductases. *Adv Enzymol Relat Areas Mol Biol.* 63, 349-419.
- (3) Jordan, A., and Reichard, P. (1998) Ribonucleotide reductases. *Annu Rev Biochem.* 67, 71-98.
- (4) Kolberg, M., Strand, K. R., Graff, P., and Andersson, K. K. (2004) Structure, function, and mechanism of ribonucleotide reductases. *Biochim. Biophys. Acta.* 1699, 1-34.
- (5) Zhang, Z., Yang, K., Chen, C., Feser, J., and Huang, M. (2007) Role of the C terminus of the ribonucleotide reductase large subunit in enzyme regeneration and its inhibition by Sml1. *Proc. Natl. Acad. Sci. U.S.A.* 104, 2217-2222.
- (6) Uchiki, T., Dice, L. T. Hettich, R. L., and Dealwis, C. (2004) Identification of phosphorylation sites on the yeast ribonucleotide reductase inhibitor Sml1. *J. Biol. Chem.* 279, 11293-11303.
- (7) Zhao, X., Georgieva, B., Chabes, A., Domkin, V., Ippel, J. H., Schleucher, J., Wijmenga, S., Thelander L., and Rothstein, R. (2000) Mutational and structural analyses of the ribonucleotide reductase inhibitor Sml1 define its Rnr1 interaction domain whose inactivation allows suppression of Mec1 and Rad53 lethality. *Mol. Cell. Biol.* 20, 9076-9083.
- (8) Danielsson, J., Liljedahl, L., Bárány-Wallje, E., Sonderby, P., Kristensen, L. H., Martinez-Yamout, M. A., Dyson, H. J., Wright, P. E., Poulsen, F. M., Maler, L., Gräslund, A., and Kragelund, B. B. . (2008) The intrinsically disordered RNR inhibitor Sml1 is a dynamic dimer. *Biochemistry* 47, 13428-13437.
- (9) Gupta, V., Peterson, C. B., Dice, L. T., Uchiki, T., Racca, J., Guo, J. T., Ying, X., Hettich, R., Zhao, X. L., Rothstein, R., and Dealwis, C. G. (2004) Sml1p is a dimer in solution: characterization of denaturation and renaturation of recombinant Sml1p. *Biochemistry* 43, 8568-8578.
- (10) Georgieva, B., Zhao, X., and Rothstein, R. (2000) Damage response and dNTP regulation: the interaction between ribonucleotide reductase and its inhibitor, Sml1. *Cold spring harbor Symp Quant Biol* 65, 343-346.
- (11) Chabes, A., V. Domkin and Thelander, L.,. (1999) Yeast Sml1, a protein inhibitor of ribonucleotide reductase. *J. Biol. Chem.* 274, 36679-36683.
- (12) Zhao, X., and Rothstein, R. (2002) The Dun1 checkpoint kinase phosphorylates and regulates the ribonucleotide reductase inhibitor Sml1. *Proc. Natl. Acad. Sci. U.S.A.* 99, 3746-3751.
- (13) Zhao, X., Chabes, A., Domkin, V., Thelander, L., and Rothstein, R. (2001) The ribonucleotide reductase inhibitor Sml1 is a new target of the Mec1/Rad53 kinase cascade during growth and in response to DNA damage. *EMBO J* 20, 3544-3553.
- (14) Mao, S. S., Holler, T. P., Yu, G. X., Bollinger, J. M., Booker, S., Johnston, M. I., and Stubbe, J. (1992) A Model for the role of multiple cysteine residues involved in ribonucleotide reduction - amazing and still confusing. *Biochemistry* 31, 9733-9743.

- (15) Aberg, A., Hahne, S., Karlsson, M., Larsson, A., Ormo, M., Ahgren, A., and Sjoberg, B.M. . (1989) Evidence for two different classes of redox-active cysteines in ribonucleotide reductase of escherichia coli. *J Biol Chem* 264, 12249-12252.
- (16) Lin, A. N. I., Ashley, G. W., and Stubbe, J. (1987) Location of the redox-active thiols of ribonucleotide reductase - sequence similarity between the escherichia-coli and lactobacillus-leichmannii enzymes. *Biochemistry* 26, 6905-6909.
- (17) Berglund, O., and Eckstein, F. (1974) ATP- and dATP-substituted agaroses and the purification of ribonucleotide reductases. *Methods in Enzymology* 34, 253-261.
- (18) Russel, M., and Model, P. (1985) Direct Cloning of the Trxb Gene That Encodes Thioredoxin Reductase. *J. Bacteriol.* 163, 238-242.
- (19) Lunn, C. A., Kathju, S., Wallace, B. J., Kushner, S. R., Pigiet, V. (1984) Amplification and purification of plasmid-encoded thioredoxin from *Escherichia-Coli*-K12. *J Biol Chem* 259, 469-474.
- (20) Steeper, J. R., Steuart, C.C. (1970) A rapid assay for CDP reductase activity in mammalian cell extracts. *Anal. Biochem.* 34, 123-130.
- (21) Rova, U., Goodtzova, K., Ingemarson, R., Behravan, G., Graslund, A., Thelander, L. (1995) Evidence by site-directed mutagenesis supports long-range electron transfer in mouse ribonucleotide reductase. *Biochemistry* 34, 4267-4275.
- (22) Johnsson, B., Lofas, S., and Lindquist, G. (1991) *Anal. Biochem.* 198, 268-277.
- (23) Zhao, X., Georgieva, B., Chabes, A., Domkin, V., Ippel, J. H., Schleucher, J., Wijmenga, S., Thelander, L., and Rothstein, R. (2000) Mutational and structural analyses of the ribonucleotide reductase inhibitor Sml1 define its Rnr1 interaction domain whose inactivation allows suppression of mec1 and rad53 lethality. *Mol. Cell. Biol.* 20, 9076-9083.
- (24) Gupta, V., Peterson, C. B., Dice, L. T., Uchiki, T., Racca, J., Guo, J. T., Ying, X., Hettich, R., Zhao, X. L., Rothstein, R., and Dealwis, C. G. (2004) Sml1 1p is a dimer in solution: Characterization of denaturation and of recombinant Sml1 1p. *Biochemistry* 43, 8568-8578.
- (25) Koehorst, R. B., Spruijt, R. B., and Hemminga, M. A. (2008) Site-directed fluorescence labeling of a membrane protein with BADAN: probing protein topology and local environment. *Biophys J.* 94, 3945-3955.
- (26) Rova, U., Goodtzova, K., Ingemarson, R., Behravan, G., Graslund, A., Thelander, L. (1995) Evidence by site-directed mutagenesis supports long-range electron transfer in mouse ribonucleotide reductase. *Biochemistry* 34, 4267-4275.
- (27) Perlstein, D. L. (2005) Defining the active form of ribonucleotide reductase from *Saccharomyces Cerevisiae* in vitro and in vivo. *PH. D thesis Massachusetts Institute of Technology.*
- (28) Georgieva, B., Zhao, X., and Rothstein, R. (2000) Damage response and dNTP regulation: the interaction between ribonucleotide reductase and its inhibitor, Sml1. *Cold Spring Harb Symp Quant Biol.* 65, 343-346.
- (29) Zhang, Z., Yang, K., Chen, C., Feser, J., and Huang, M. (2007) Role of the C terminus of the ribonucleotide reductase large subunit in enzyme regeneration and its inhibition by Sml1. *Proc. Natl. Acad. Sci. U S A.* 104, 2217-2222.
- (30) Thelander, L. (1973) Physicochemical Characterization of Ribonucleoside Diphosphate Reductase from *Escherichia-Coli*. *Journal of Biological Chemistry* 248, 4591-4601.

- (31) Ingemarson, R., and Thelander, L. (1996) A kinetic study on the influence of nucleoside triphosphate effectors on subunit interaction in mouse ribonucleotide reductase. *Biochemistry* 35, 8603-8609.

Jun Wang

Mailing Address:
7 University Houses, APT B
Madison, WI 53705

Contact Information:
E-mail: junw@mit.edu
Phone: (617) 230-1205

Education

Massachusetts Institute of Technology (MIT)

Cambridge, MA

Ph.D., Biochemistry (expected August, 2009)

University of Wisconsin

Madison, WI

M.S., Analytical Chemistry (2000)

Peking University

Beijing, China

B.S., Chemistry (1997)

Professional Experience

MIT

Cambridge, MA

Graduate Research Associate (directed by Prof. Stubbe)

2004-2009

- Investigation of anti-cancer mechanism of Gemcitabine as a human ribonucleotide reductase inhibitor
- Investigation of the regulation mechanism of yeast ribonucleotide reductase

Sunesis Pharmaceutical Inc.

South San Francisco, CA

Staff Research Associate in the Department of New Technology Development

2000-2004

- Involved in the development of novel drug discovery strategies
- Conducted studies of small molecule-protein and protein-protein interactions using mass spectroscopy (QSTAR LC/MS/MS)
- Performed research on characterization of protein dynamics and protein-small molecule interactions using peptide mapping, H/D exchange and nanospray analyses.

University of Wisconsin

Madison, WI

Graduate Research Associate (directed by Prof. Schwartz)

1998-2000

- Conducted studies of whole genome shotgun mapping of the *Trypanosoma brucei* Genomes

Awards

David Koch Graduate Fellowship of MIT Center for Cancer Research

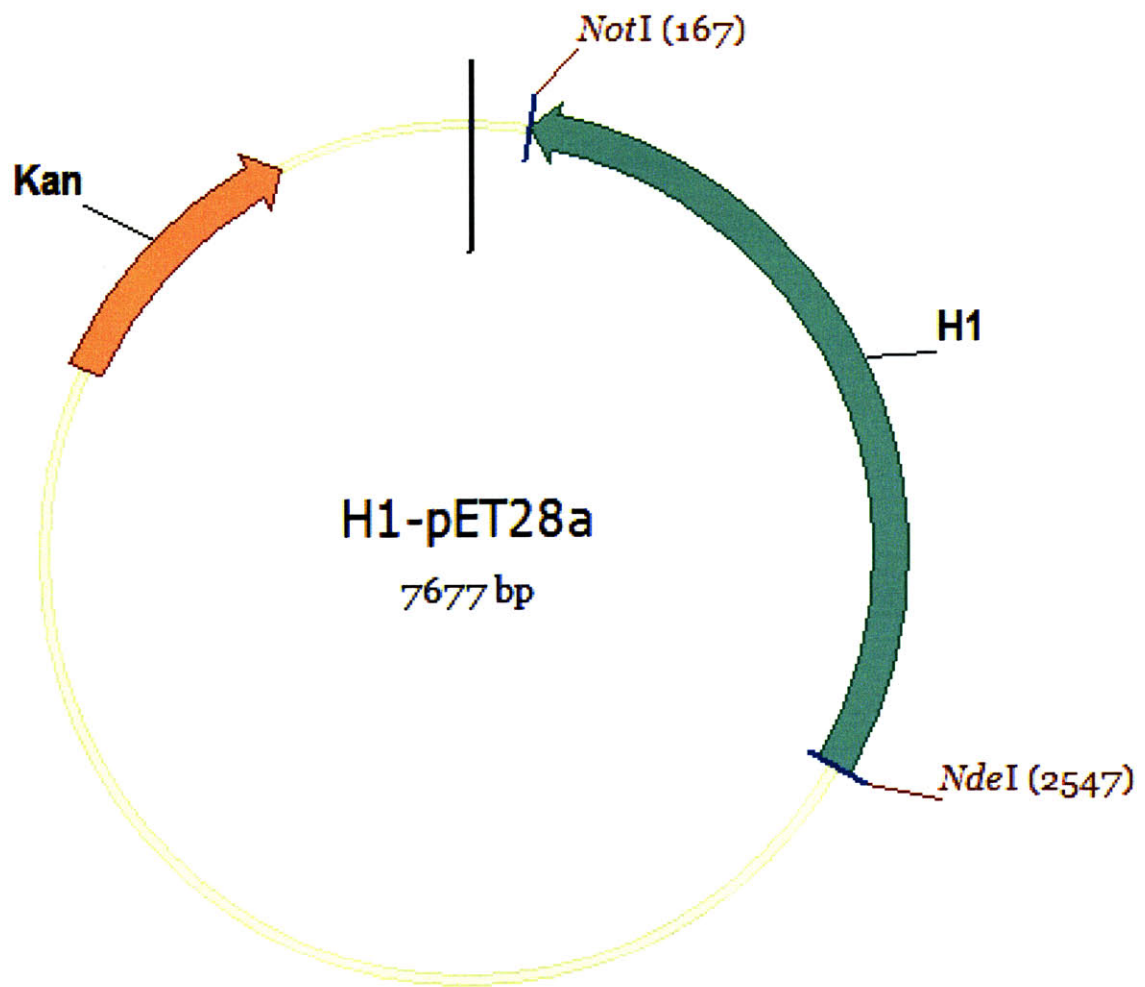
2006-2007

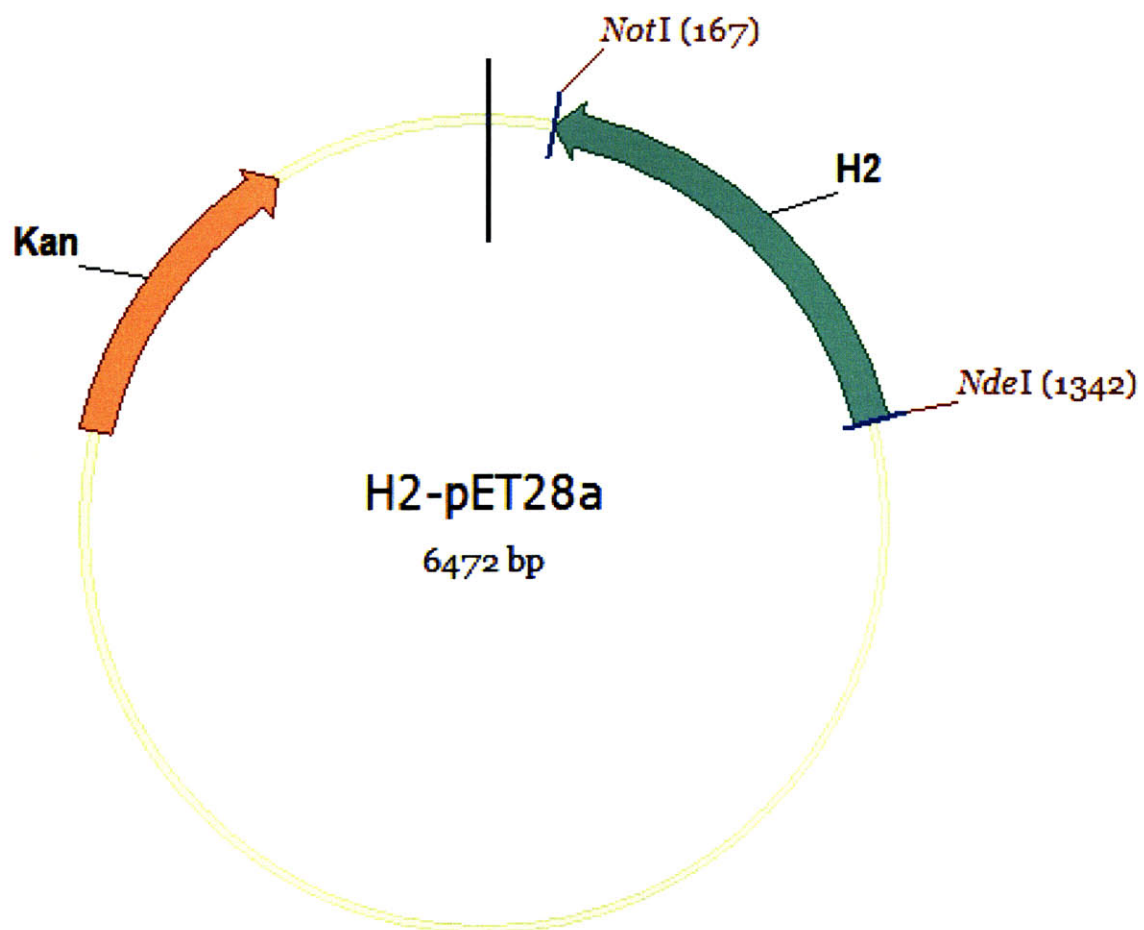
Publications

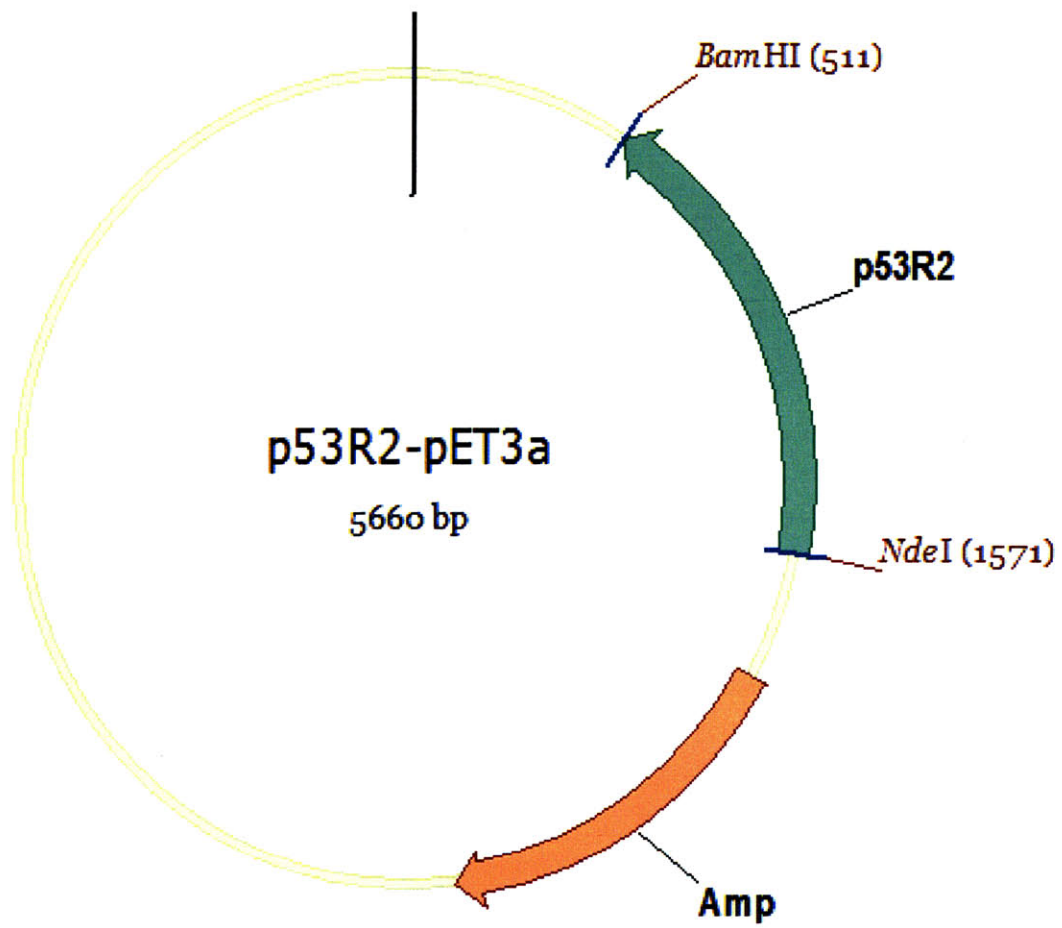
1. Lee, Y. D.; **Wang, J.**; Stubbe, J., Elledge, S. J. "Dif1 is a DNA-damage-regulated facilitator of nuclear import for ribonucleotide reductase" *Mol. Cell* **2008**, *32*, 70-80.
2. **Wang, J.**; Lohman, G. J.; Stubbe, J. "Enhanced subunit interactions with gemcitabine-5'-diphosphate inhibit ribonucleotide reductases" *Proc. Natl. Acad. Sci. U. S. A.* **2007**, *104*, 14324-14329.
3. He, M. M.; Smith, A. S.; Oslob, J. D.; Flanagan, W. M.; Braisted, A. C.; Whitty, A.; Cancilla, M. T.; **Wang, J.**; Lugovskoy, A. A.; Yoburn, J. C.; Fung, A. D.; Farrington, G.; Eldredge, J. K.; Day, E. S.; Cruz, L. A.; Cachero, T. G.; Miller, S. K.; Friedman, J. E.; Choong, I. C.; Cunningham, B. C. "Small-Molecule inhibition of TNF- α " *Science* **2005**, *310*, 1022-1025.
4. Arkin, M. R.; Randal, M.; DeLano, W. L.; Hyde, J.; Luong, T. N.; Oslob, J. D.; Raphael, D. R.; Taylor, L.; **Wang, J.**; McDowell, R. S.; Wells, J. A.; Braisted, A. C. "Binding of small molecules to an adaptive protein-protein interface" *Proc. Natl. Acad. Sci. U. S. A.* **2003**, *100*, 1603-1608.
5. Zhou, S. G.; Deng, W.; Anantharaman, T. S.; Lim, A.; Dimalanta, E. T.; **Wang, J.**; Wu, T.; Tao, C.; Creighton, R.; Kile, A.; Kvikstad, E.; Bechner, M.; Yen, G.; Garic-Stankovic, A.; Severin, J.; Forrest, D.; Runnheim, R.; Churas, C.; Lamers, C.; Perna, N. T.; Burland, V.; Blattner, F. R.; Mishra, B.; Schwartz, D.C. "A whole-genome shotgun optical map of *Yersinia pestis* strain KIM" *Appl. Environ. Microbiol.* **2002**, *68*, 6321-6331.
6. Huang, J. B.; Zhu, B. Y.; Mao, M.; He, P.; **Wang, J.**; He, X. "Vesicle Formation of 1:1 Cationic and Anionic Surfactant Mixtures in Nonaqueous Polar Solvents" *Colloid Polym. Sci.* **1999**, *277*, 354.

Appendix I

Plasmid Maps







Dif1 Is a DNA-Damage-Regulated Facilitator of Nuclear Import for Ribonucleotide Reductase

Yang David Lee,¹ Jun Wang,^{2,3} JoAnne Stubbe,^{2,3} and Stephen J. Elledge^{1,*}

¹Harvard Medical School, Department of Genetics, Brigham and Women's Hospital, Center for Genetics and Genomics, Howard Hughes Medical Institute, Boston, MA 02115, USA

²Department of Chemistry

³Department of Biology

Massachusetts Institute of Technology, Cambridge, MA 02139, USA

*Correspondence: selledge@genetics.med.harvard.edu

DOI 10.1016/j.molcel.2008.08.018

SUMMARY

The control of dNTP concentrations is critical to the fidelity of DNA synthesis and repair. One level of regulation is through subcellular localization of ribonucleotide reductase. In *Saccharomyces cerevisiae*, the small subunit Rnr2-Rnr4 is nuclear, whereas the large subunit Rnr1 is cytoplasmic. In response to S phase or DNA damage, Rnr2-Rnr4 enters the cytoplasm to bind Rnr1, forming an active complex. We previously reported that Wtm1 anchors Rnr2-Rnr4 in the nucleus. Here, we identify *DIF1*, which regulates localization of Rnr2-Rnr4. Dif1 binds directly to the Rnr2-Rnr4 complex through a conserved Hug domain to drive nuclear import. Dif1 is both cell-cycle and DNA-damage regulated, the latter of which occurs via the Mec1-Dun1 pathway. In response to DNA damage, Dun1 directly phosphorylates Dif1, which both inactivates and degrades Dif1 and allows Rnr2-Rnr4 to become cytoplasmic. We propose that Rnr2-Rnr4 nuclear localization is achieved by a dynamic combination of Wtm1-mediated nuclear retention to limit export and regulated nuclear import through Dif1.

INTRODUCTION

In response to DNA replication blocks, cells activate the DNA-damage and replication stress-response pathway, the DDR, which includes the *MEC1-RAD53-DUN1-CHK1* kinase cascade in budding yeast and the *rad3-cds1-chk1* pathway in fission yeast. The downstream effects include cell-cycle arrest, stabilization of replication forks, inhibition of late origin firing, and the initiation of DNA repair (Harper and Elledge, 2007). Part of this process involves activation of the ribonucleotide reductase (RNR) pathway—the rate-limiting step in the conversion of rNDPs to dNDPs. *Saccharomyces cerevisiae* has a Class Ia RNR and is composed of homodimers of Rnr1 (α_2) and heterodimers of structurally homologous Rnr2 and Rnr4 ($\beta\beta'$) (Voegtli et al., 2001). The intimate relationship between the DDR pathway and RNR function is demonstrated by the fact that the lethality of the *mec1Δ* or *rad53Δ* mutants can be rescued by the activation of the RNR pathway

(Desany et al., 1998; Vallen and Cross, 1999; Huang et al., 1998; Zhao et al., 1998).

Adjusting the intracellular concentration of dNTPs to meet demands under different conditions is critical, as both elevated or insufficient levels of dNTP can lead to increased mutagenesis rates (Chabes et al., 2003; Holmberg et al., 2005). Thus, cells have devised multiple strategies to regulate Rnr (Nordlund and Reichard, 2006). For example, transcriptional induction of the RNR genes in *S. cerevisiae* involves Dun1 phosphorylation and inactivation of the Crt1-Ssn6-Tup1 repressor complex (Huang et al., 1998; Zhou and Elledge, 1992). In addition, effectors binding the large subunit can alter the rate of catalysis or change the specificity of the enzyme toward particular ribonucleotide substrates (Reichard, 2002). Posttranslational regulation in *S. cerevisiae* involves the Sml1 inhibitor, which can bind to the large subunit Rnr1 through its C-terminal tail (Chabes et al., 1999; Zhao et al., 2000) and interfere with the regeneration of the catalytic site on Rnr1 (Zhang et al., 2007). Dun1 is required for Sml1 degradation in response to DNA damage. Dun1 can phosphorylate Sml1 in vitro, but the consequences of this phosphorylation have not been examined in vivo (Zhao and Rothstein, 2002).

Rnr subcellular localization is an additional layer of control (Lincker et al., 2004; Liu et al., 2003; Xue et al., 2003; Yao et al., 2003). The Rnr small subunits of both *Schizosaccharomyces pombe* and *S. cerevisiae* are sequestered in the nucleus. S phase and DNA damage can independently control the translocation of nuclear Rnr small subunits out to the cytoplasm, presumably to form active complexes with cytoplasmic Rnr1. We previously identified *WTM1* as a regulator of Rnr2-Rnr4 localization (Lee and Elledge, 2006; Zhang et al., 2006). Wtm1 is a nuclear protein that binds to Rnr2-Rnr4. Their physical association is reduced after DNA damage and replication stress, coincident with the release of Rnr2-Rnr4 from the nucleus. Deletion of *WTM1* causes a significant nuclear-to-cytoplasmic shift of Rnr2-Rnr4. Forced localization of Wtm1 to the nucleolus recruits Rnr2-Rnr4 to the nucleolus, suggesting that Wtm1 functions as a nuclear anchor. How DNA damage regulates this association is unknown. In *S. pombe*, deletion of the *spd1* gene causes mislocalization of the nuclear RNR small subunit Suc22 (SpRnr2). In vitro experiments have demonstrated that Spd1 binds to the RNR large subunit Cdc22 (SpRnr1), but not to the small subunit SpRnr2 (Hakansson et al., 2006). Whether and how this binding between Spd1 and the large RNR subunit results in nuclear localization of the small subunit is unknown.

Here, we describe the discovery of the *S. cerevisiae* *Damage-regulated Import Facilitator 1 (DIF1)*, which mediates the localization of Rnr small subunits in response to DNA damage. Dif1 shares elements of different Rnr regulators and provides a unified view of Rnr localization regulation.

RESULTS

Dif1 Has a Conserved Domain Present among Rnr-Inhibitor Homologs in Yeasts

Wtm1 binding to Rnr2-Rnr4 is disrupted in response to DNA damage, resulting in their cytoplasmic localization. We sought to understand how this regulation was accomplished. As the upstream regulators are protein kinases, we identified three phosphorylation sites on Rnr2: S15, S22, and S41. However, mutation of these sites did not alter the nuclear localization. Therefore, we initiated a search for additional regulators.

S. cerevisiae Sml1 and *S. pombe* Spd1 proteins are small inhibitors of the RNR pathway that both bind the Rnr large subunit (Hakansson et al., 2006; Liu et al., 2003; Zhao et al., 1998). However, Spd1 and Sml1 appear unrelated. Furthermore, whereas Spd1 is essential for the nuclear localization of the Rnr small subunit Suc22 (Liu et al., 2003), Sml1 plays no such role in *S. cerevisiae* (Yao et al., 2003). It was thought that there was no Spd1 ortholog in budding yeast. However, using the N-terminal half of the Spd1 sequence as a query, we identified two proteins with sequence similarity. One was Hug1, a 7.5 kD protein that is highly induced after DNA damage and is thought to play a role in feedback inhibition of the RNR pathway through an unknown mechanism (Basrai et al., 1999). Its genomic sequence is located immediately 5' of *SML1*. The second candidate is a novel uncharacterized protein, *YLR437c* (hereafter referred to as *DIF1*). BLAST analysis with Dif1 identified similarity to Sml1. Alignment of Dif1, Spd1, Sml1, Hug1, and Aer122c (a Dif1/Sml1 ortholog in *Ashbya gossypii*) revealed a conserved domain that we named the Hug domain, which is present in all homologs except for Sml1 (Figures 1A and 1B). We also observed a second domain conserved in Dif1, Aer122c, and Sml1, which we call the Sml domain. Aer122c, Sml1, and, to a lesser extent, Spd1 share yet a third domain in their C termini that we call the Rnr1-binding (R1B) domain because it contains residues required for Sml1 binding to Rnr1 (Zhao et al., 2000).

The relationship between Dif1 and Sml1 suggests evolution from a common ancestral gene. As *S. cerevisiae* underwent a genome duplication during its evolution, we searched for synteny surrounding *HUG1*, *SML1*, and *DIF1*. As shown in Figure 1C, Dif1 and Hug1-Sml1 are paralogs derived from an ancestral gene duplication event that included multiple adjacent genes (Dietrich et al., 2004; Kellis et al., 2004). We assume that the ancestral gene is most similar to the ortholog from *A. gossypii*, as it contains only one gene that shares homology to Dif1, Hug1, and Sml1. Duplication and divergence would allow for the splitting of the ancestral gene into three genes—*DIF1* on chromosome XII, and *HUG1* and *SML1* on chromosome XIII.

DIF1 Dosage Regulates the Viability of *mec1Δ* Mutants

To test whether Dif1 is a negative regulator of the RNR pathway, we overexpressed *DIF1* under *GAL1* control in *mec1Δ sml1Δ* and *sml1Δ* strains. Dif1 overexpression slowed growth in *sml1Δ*

cells, but was lethal to the *mec1Δ sml1Δ* cells (Figure 1D). Dif1 overexpression also rendered *dun1Δ* mutants more hydroxyurea (HU) sensitive (data not shown). Strains were switched from glucose to galactose to induce Dif1 expression and were analyzed for DNA content by FACS. *mec1Δ sml1Δ* cells overexpressing Dif1 arrested in S phase (Figure 1E), consistent with a role in the negative regulation of RNR.

Upregulation of RNR activity can suppress the lethality of the *MEC1* deletion (Desany et al., 1998; Zhao et al., 1998). Whereas tetrad dissection of a *MEC1/mec1Δ* diploid always resulted in only two viable spores, dissection of the *MEC1/mec1Δ::his5⁺*; *DIF1/dif1Δ::TRP1* tetrads yielded many viable three- or four-spore tetrads. In these, one or two colonies were significantly smaller and were *mec1Δ::his5⁺ dif1Δ::TRP1* (data not shown) (Figure 1F).

Dif1 Is Required for Rnr2-Rnr4 Nuclear Localization

DIF1 is nonessential, and its deletion has no effect on Rnr protein levels (data not shown). However, *dif1Δ* mutants show cytoplasmic localization of Rnr2 independent of cell-cycle stage (Figure 2A). Since Rnr2-Rnr4 is released from the nucleus in response to DNA damage or replication stress, the cytoplasmic localization in *dif1Δ* mutants could be indirect. To examine this, we generated *dun1Δ dif1Δ* mutants that still showed cytoplasmic Rnr2 (Figure 2B), indicating that Dif1 does not mislocalize Rnr2 by mimicking DNA damage.

Whereas Rnr2 mislocalization in *dif1Δ* mutants is cell-cycle independent, α factor-arrested *dif1Δ* mutants showed significant residual nuclear Rnr2. We have previously shown that the protein Wtm1 is required for the nuclear localization of Rnr2-Rnr4 through an anchoring mechanism (Lee and Elledge, 2006; Zhang et al., 2006). We examined the localization phenotype of *wtm1Δ* and *dif1Δ* mutants. Both mutants showed very similar defects in Rnr2 nuclear localization with some residual nuclear Rnr2, especially in G1 (Figure 2C), suggesting that they may work in the same pathway.

Dif1 Is the Regulated Component of the Rnr2-Rnr4 Localization Switch

A key question with respect to control of Rnr subcellular localization has been the identity of the molecule that imparts cell-cycle and DNA-damage regulation on the switch. To examine whether Dif1 might be that molecule, we generated Dif1 antibodies. Western blot analysis showed that Dif1 levels peaked at ~70 min after the release from α factor arrest with an inverse relationship to the levels of Clb5, an S phase marker (Figure 3A). The low levels of Dif1 during S phase coincided with Rnr2-Rnr4 release from the nucleus. A significant decrease in Dif1 abundance was also observed when log phase cells were treated with HU or methylmethane sulfonate (MMS), also coinciding with Rnr2-Rnr4 release. This damage-induced reduction in Dif1 levels is *DUN1* dependent (Figure 3B). To separate the cell-cycle-induced reduction of Dif1 from the DNA-damage-induced reduction of Dif1, cells were first arrested in G2/M phase by nocodazole, and then treated with phleomycin or ionizing radiation (IR) while maintaining G2/M arrest. Under these conditions, phleomycin and IR also reduced the abundance of Dif1 in a *DUN1*-dependent manner (Figure 3C).

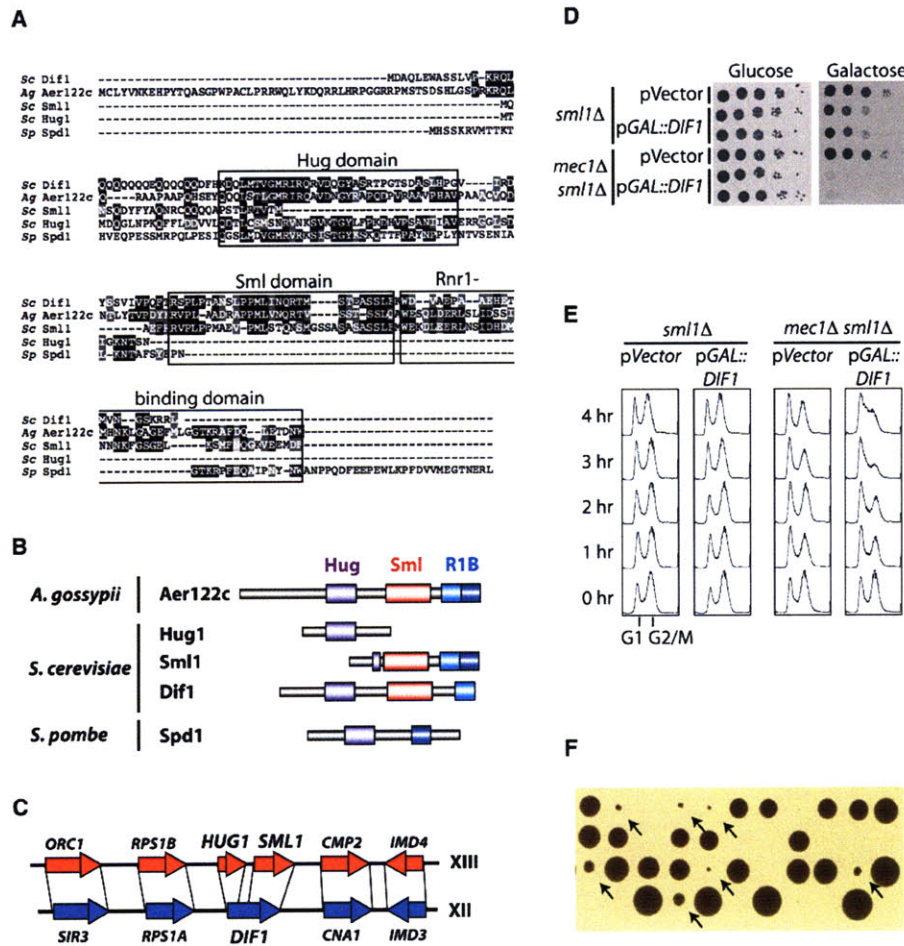


Figure 1. Dif1 Is an Inhibitor of S Phase Cell-Cycle Progression and a Paralog of Sml1

(A) Sequence alignment between *S. cerevisiae* (Sc) Dif1, Sml1, and Hug1; *S. pombe* (Sp) Spd1; and *A. gossypii* (Ag) Aer122c. The three conserved domains, the Hug domain, the Sml domain, and the Rnr1-binding domain, are boxed.

(B) Simplified diagrams showing the three different domains of the orthologs of Dif1. The Rnr1-binding domain (R1B), which has been characterized through mutational analysis, was further divided into an N-terminal (cyan) and a C-terminal (blue) subdomain.

(C) Synteny in the proximity of the *HUG1/SML1* loci on chromosome XIII and the *DIF1* (*YLR437c*) locus on chromosome XII in *S. cerevisiae*.

(D) *sml1Δ* and *mec1Δ sml1Δ* strains containing vector alone or a galactose-inducible *DIF1* plasmid (*pGAL::DIF1*) were serially diluted and spotted on glucose and galactose media.

(E) Cell-cycle profiles of *sml1Δ* and *mec1Δ sml1Δ* strains overexpressing *DIF1*. Cells were grown to log phase in glucose before being switched to galactose. Samples were taken from 0 to 4 hr after the galactose switch for FACS analysis of DNA content.

(F) Tetrad dissection of the *MEC1/mec1Δ::his5+ DIF1/dif1Δ::TRP1* diploid. Arrows mark small colonies, which are HU sensitive and tryptophan and histidine prototrophic (data not shown).

Dif1 Is Phosphorylated after Hydroxyurea Treatment

We observed that N-terminal tagging of endogenous Dif1 with 3Myc led to an increase of the abundance of Dif1 protein. As early as 20 min after the release of the *sml1Δ* strain from G1 into HU, 3Myc-Dif1 was observed to migrate as a doublet (Figure 3D). However, in the *mec1Δ sml1Δ* mutant, the shift of 3Myc-Dif1 from lower to higher mobility was delayed by as much as 40–60 min and never reached completion even after 2 hr, compared with 40 min for wild-type (WT). HU treatment does not reduce the 3Myc-Dif1 levels, indicating that WT Dif1 is destroyed in response to HU, but that 3Myc-Dif1 is stabilized.

The mobility shift of 3Myc-Dif1 in response to DNA damage suggested possible phosphorylation. Phosphatase (PPase) treatment of 3Myc-Dif1 from HU-treated cells confirmed that the mobility shift was due to phosphorylation (Figure 3E).

The delayed phosphorylation of 3Myc-Dif1 in the *mec1Δ sml1Δ* mutant is most likely due to the redundant function of the Tel1 kinase, as the phosphorylation of Rad53 still occurs, although with slower kinetics (data not shown). This Dif1 phosphorylation is not observed in *dun1Δ* mutants (Figure 3F), suggesting that Dun1 may directly phosphorylate Dif1.

To assess if 3Myc-Dif1 is inactivated after phosphorylation independent of degradation, G1-arrested 3Myc-DIF1 cells

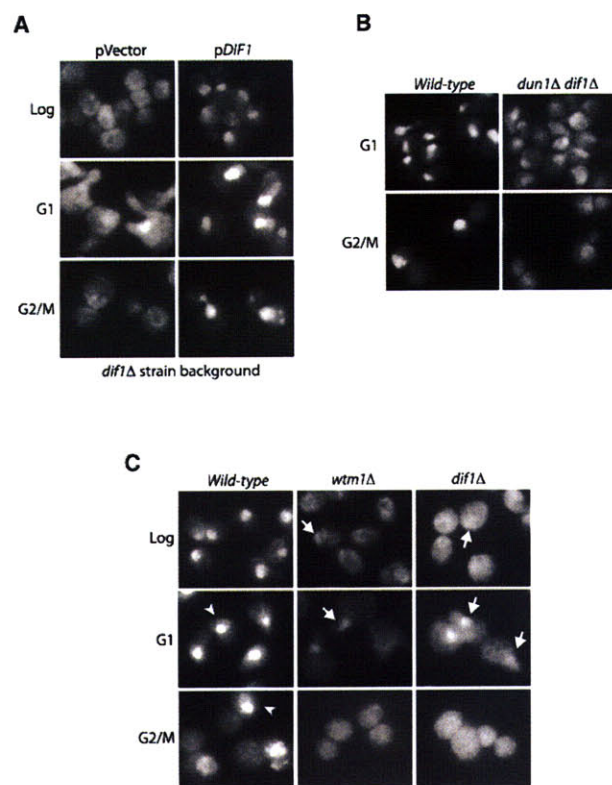


Figure 2. Dif1 Is Required for the Nuclear Localization of Rnr Small Subunits

(A) *dif1Δ* strains complemented with either vector alone or with a plasmid containing the wild-type (WT) *DIF1* gene were grown to log phase, or arrested in G1 with α factor, or arrested in G2/M with nocodazole. Cells were processed for Rnr2 visualization by indirect immunofluorescence.

(B) G1- or G2/M-arrested WT and *dun1Δ dif1Δ* strains were processed for Rnr2 visualization by indirect immunofluorescence.

(C) Comparison of Rnr2 localization in WT and *wtm1Δ* and *dif1Δ* mutants. Cells were either grown to log phase, arrested in G1, or arrested in G2/M. Samples were processed for Rnr2 visualization by indirect immunofluorescence. Examples of cells with strong nuclear Rnr2 staining are marked with white arrowheads, and cells with partially nuclear Rnr2 staining are marked with white arrows.

were released into 150 mM HU and examined for Rnr2 localization. The 3Myc-*DIF1* strain showed a degree of nuclear Rnr2 release that was comparable to WT (Figure 3G), although the phosphorylated 3Myc-Dif1 protein is not efficiently degraded even after 2 hr of HU treatment (Figures 3D and 3F). Thus, degradation is not absolutely required for Rnr2 regulation and suggests that phosphorylation may be sufficient to inhibit Dif1 function.

The Sml Domain of Dif1 Is a Phospho-Degron

To identify potential phosphorylation sites on Dif1, a large-scale immunoprecipitation and mass spectrometry analysis was carried out with lysates from HU-treated 3Myc-*DIF1* cells. Phosphomapping detected phosphorylation on S103 or T104 of the Sml domain (Figure 3H).

Sml1 can be phosphorylated by the Dun1 kinase in vitro, and its degradation during S phase and after DNA damage requires

Dun1 (Uchiki et al., 2004; Zhao and Rothstein, 2002). To link Dif1 phosphorylation to its degradation, we mutated several of the mapped and conserved serine and threonine residues in the Sml domain to alanine. Dif1 carrying these single mutations showed no increase in protein stability after DNA damage or replication stress (data not shown). Therefore, we made a mutant Dif1 (*DIF1-4A*) consisting of the two residues mapped by mass spectrometry (S103 and T104) along with two highly conserved serine residues (S107 and S108) that are conserved in Sml1 and were shown to be phosphorylated by Dun1 in vitro (Uchiki et al., 2004). Dif1-4A was not degraded when G2/M-arrested cells were treated with phleomycin (Figure 4A) or when G1 cells were released into the cell cycle in the presence of HU (Figure 4B), and Dif1-4A mutants were significantly impaired with regard to the release of Rnr2-Rnr4 in both circumstances (Figures 4C–4E).

Since the degree of conservation is high throughout the Sml domain in addition to the serines and threonines mutated in Dif1-4A, we reasoned that a larger part of this domain may be required for the degron function. Therefore, we changed the most conserved residues, PPMLINQRT, in this domain to alanines while preserving the four phosphoserine/threonine residues and tested this mutant protein (Dif1-sml) for its stability during DNA-damage response. As shown in Figures 4F and 4G, the Dif1-sml mutant protein failed to display a comparable mobility shift or reduction in protein level after HU or phleomycin treatment compared to WT Dif1, but maintained the ability to localize Rnr2-Rnr4 inside the nucleus (Figure 4H). Therefore, the Sml domain is required for the phosphorylation and degradation of Dif1 after DNA damage or replication stress.

Dif1 Is Directly Phosphorylated by the Dun1 Kinase

To determine whether Dun1 can directly phosphorylate Dif1, we purified GST-Dun1 from Baculovirus-infected SF9 insect cells and incubated it with different mutant Dif1 proteins in the presence of [γ - 32 P]ATP. As shown in Figure 4I, incubation of GST-Dun1 with WT Dif1 (Dif1-WT) and a Dif1 mutant altered in the Hug domain (Dif1-hug, see Figure 7 for details), but not phospho mutant Dif1 (Dif1-4A), results in incorporation of 32 P. This, together with the phosphomapping data by mass spectrometry (Figure 3H), indicates that the Dun1 kinase can directly phosphorylate Dif1 on residues, which leads to its inactivation and degradation.

Dif1 Is Much Less Abundant than Rnr2

One model for the role of Dif1 in Rnr2-Rnr4 localization is as an adaptor that enhances the association of Rnr2-Rnr4 with Wtm1. If this model is correct, Dif1 and Rnr2-Rnr4 should be present in roughly equal amounts. Thus, we carefully determined the absolute abundance of Rnr1, Rnr2, Rnr4, and Dif1. Rnr1 and Rnr2-Rnr4 were purified as previously described (Ge et al., 2001; Nguyen et al., 1999), and Dif1 was purified from *E. coli* as a His₆-tagged protein. We estimated the concentration of purified Rnr1, Rnr2, Rnr4, and Dif1 proteins with Coomassie staining by using known BSA standards (Figures 5A–5D, left panels). Serial dilutions of these protein samples were loaded alongside cell lysates from asynchronous cultures of WT cells in log phase or cell lysates from samples after release from a G1 block (Figures 5A–5D, right panels). Cib5 serves as a marker of cell-cycle progression

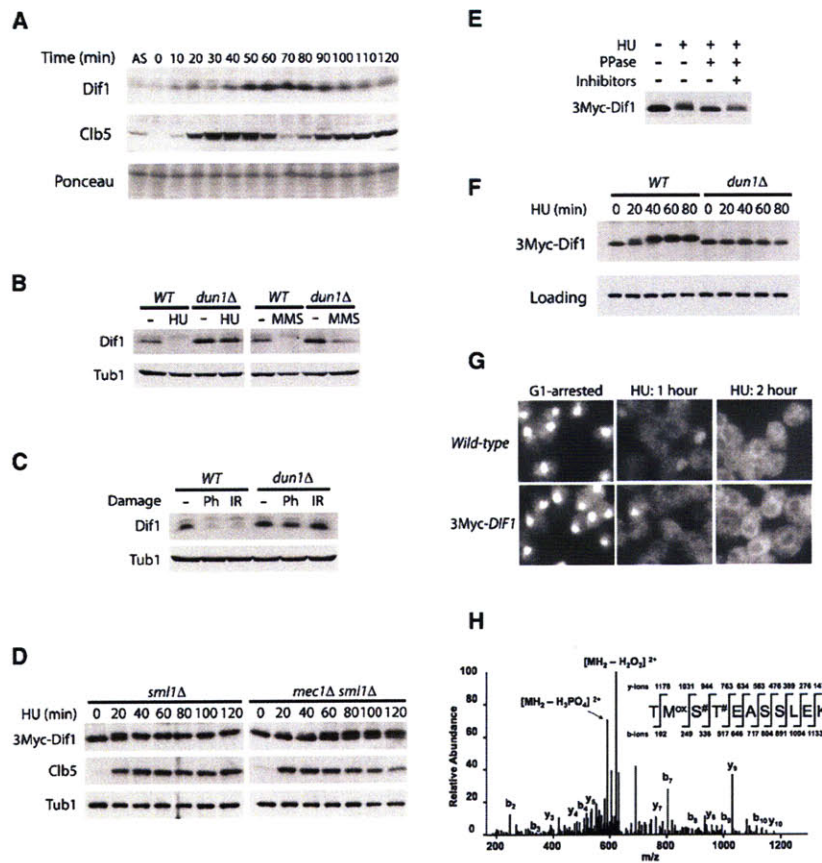


Figure 3. Dif1 Is Regulated during the Cell-Cycle and DNA-Damage Responses

(A) Cell-cycle analysis of Dif1 abundance. Cells arrested in G1 by α factor were released into the cell cycle. Samples were collected at 10 min intervals for western blotting of Dif1. Clb5 was used to monitor cell-cycle progression. Ponceau staining served as a loading control. A log phase sample from an asynchronous (AS) population of cells was loaded in the first lane for comparison.

(B) Western blot analysis of Dif1 from log phase wild-type (WT) and *dun1Δ* cells treated with HU (150 mM, 1.5 hr) or MMS (0.1%, 1.5 hr). Tubulin (Tub1) serves as a loading control.

(C) Western blot analysis of Dif1 from WT and *dun1Δ* cells treated with phleomycin (Ph, 50 ng/ml, 1 hr) or ionizing radiation (IR, 20 kRad, 1 hr) while maintained in G2/M arrest.

(D) Mec1-dependent posttranslational modification of 3Myc-Dif1 in *sm1Δ* and *mec1Δ sm1Δ* cells. Cells with a single copy of 3Myc-DIF1 integrated at the endogenous locus were arrested in G1 by α factor, and then released into the cell cycle in the presence of HU (150 mM). Samples were collected at 20 min intervals for western analysis of 3Myc-Dif1 mobility and abundance. Clb5 was used to monitor cell-cycle progression.

(E) Phosphatase (PPase) treatment of 3Myc-Dif1. Log phase yeast cells carrying integrated 3Myc-DIF1 were treated with HU (150 mM, 1.5 hr). 3Myc-Dif1 was immunoprecipitated from the lysate and subjected to PPase treatment, with or without PPase inhibitors.

(F) Dun1-dependent Dif1 phosphorylation after HU treatment. WT and *dun1Δ* strains with

integrated 3Myc-DIF1 were arrested in G1 by α factor, and then released into HU media (150 mM). Samples were collected at 20 min intervals for western analysis of 3Myc-Dif1 mobility and abundance.

(G) Rnr2 visualization by indirect immunofluorescence of WT or a 3Myc-DIF1-integrated strain arrested in G1 phase with α factor, and then released into HU media (150 mM) for 1 and 2 hr.

(H) Phosphomapping of 3Myc-Dif1. Log phase cells with integrated 3Myc-DIF1 were treated with HU (150 mM, 1.5 hr). 3Myc-Dif1 was immunoprecipitated with anti-Myc antibodies, resolved and silver stained on SDS-PAGE, and excised for phosphomapping by mass spectrometry. The “#” signs indicate two potential sites for phosphorylation.

(Figure 5E). We estimate that during log phase, the number of molecules per cell for Dif1, Rnr1, Rnr2, and Rnr4 is 1,300, 16,000, 190,000, and 130,000, respectively. The molecular ratio of Dif1:Rnr1 is ~1:12, and that of Dif1:Rnr2 is ~1:140. At 80 min after G1 release, when cells are in G2 and the abundance of Dif1 is maximal, the ratio of Dif1:Rnr1 is 1:8.3, whereas that of Dif1:Rnr2 is 1:110. Thus, the number of Rnr2 molecules greatly exceeds that of the Dif1 molecules. This indicates that Dif1 cannot act as a stoichiometric adaptor that facilitates binding to Wtm1, and instead suggests that Dif1 functions catalytically to maintain nuclear Rnr2-Rnr4.

DIF1 and WTM1 Regulate Rnr2-Rnr4 Localization through Mechanistically Distinct Pathways

The elimination of the Wtm1 adaptor role for Dif1 opened up the possibility that it might work in a separate pathway from Wtm1 even though their null phenotypes are very similar (Figure 2C). Thus, we examined Rnr2 localization in the *dif1Δ wtm1Δ* mutants

compared to the single mutants. Whereas each mutant displayed residual nuclear accumulation, *dif1Δ wtm1Δ* double mutants lost this residual nuclear Rnr2 staining and often displayed significant Rnr2 nuclear exclusion (Figure 6A, black arrows). The above-mentioned observation suggests that Wtm1 and Dif1 can function through separate mechanisms and may be involved in different pathways.

If Dif1 functions through a mechanism independent of Wtm1, hyperactivation of either the Dif1 or Wtm1 pathway might suppress the defective Rnr2-Rnr4 anchoring phenotype of the other mutants. Thus, we overproduced Dif1 in the *wtm1Δ* background, or Wtm1 in the *dif1Δ* background. Dif1 overproduction significantly rescued the Rnr2 localization defect in *wtm1Δ* mutants (Figure 6B), whereas overproduction of Wtm1 in *dif1Δ* mutants had no effect (data not shown). Together, the enhanced defect of the double mutants and the suppression of *wtm1Δ* mutants by DIF1 overproduction suggest that Wtm1 and Dif1 operate in two independent branches of the Rnr2 localization pathway.

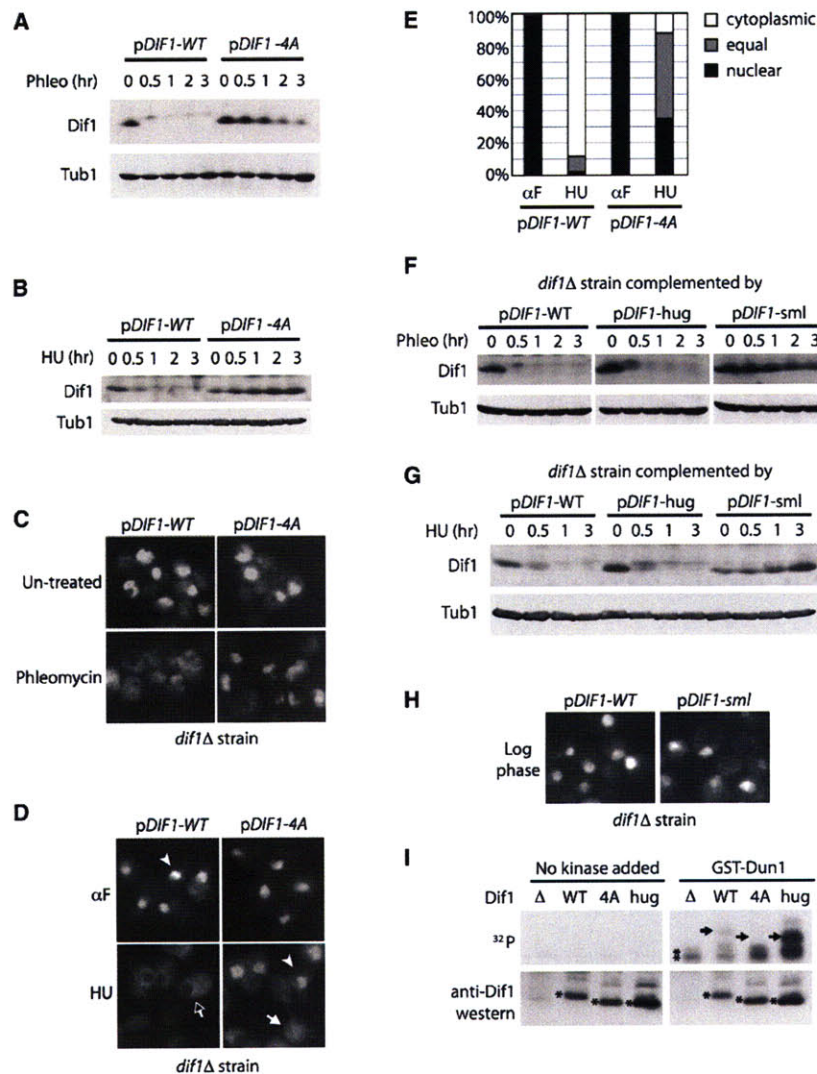


Figure 4. The Sml and Hug Domains Have Distinct Roles in Dif1 Regulation

(A) Western blot analysis of wild-type (WT) and phospho mutant Dif1 after phleomycin treatment. *dif1Δ* strains containing a WT *DIF1* plasmid (pDIF1-WT) or the phospho mutant plasmid (pDIF1-4A) were treated with phleomycin (50 ng/ml) for the indicated times during G2/M arrest by nocodazole. Tubulin (Tub1) served as a loading control.

(B) Western blot analysis of WT and phospho mutant Dif1 from cells arrested in G1 by α factor, and then released into HU media (150 mM) for the indicated times.

(C) G2/M-arrested WT and phospho mutant Dif1 strains were treated with phleomycin for 2 hr and processed for Rnr2 visualization by indirect immunofluorescence.

(D) WT or phospho mutant Dif1 cells were arrested in G1 by α factor (α F) or released from G1 into HU (150 mM) for 1 hr and processed for Rnr2 visualization by indirect immunofluorescence. Examples of cells with Rnr2 staining that is predominately nuclear (white arrowhead), predominately cytoplasmic (black arrow), or equal in distribution (white arrow) are indicated.

(E) Quantification of (D). For each treatment, more than 160 cells were counted (range: 161–200 cells).

(F) Western blot analysis of WT, hug-domain mutant, or sml-domain mutant Dif1 after phleomycin treatment. *dif1Δ* strains complemented by plasmids containing WT (pDIF1-WT), hug-domain mutant (pDIF1-hug), or sml-domain mutant (pDIF1-sml) versions of *DIF1* were treated with phleomycin (50 ng/ml) for the indicated times while maintained in G2/M. Tubulin (Tub1) served as the loading control.

(G) Western blot analysis of Dif1, Dif1-hug, and Dif1-sml mutants after HU treatment. *dif1Δ* strains complemented by plasmids containing WT (pDIF1-WT), hug-domain mutant (pDIF1-hug), or sml-domain mutant (pDIF1-sml) versions of *DIF1* were arrested in G1 by α factor, and then released into HU media (150 mM) for the indicated times.

(H) Rnr2 visualization by indirect immunofluorescence from log phase cultures of *dif1Δ* strains carrying pDIF1-WT or pDIF1-sml plasmids.

(I) Dun1 in vitro kinase assay. Polyclonal anti-Dif1 antibodies were used to immunoprecipitate Dif1 from *dif1Δ* yeast strain complemented by plasmid alone (Δ), wild-type (WT), phospho mutant (4A), and hug-domain mutant (hug) Dif1, and then incubated with or without recombinant GST-Dun1 purified from insect cells in the presence of [γ - 32 P]ATP. The bottom panel shows a western blot with anti-Dif1 antibodies. The predominant Dif1 bands are marked with single asterisks. The difference in their size is due to site-directed mutagenesis. The top panel shows an autoradiograph; the expected position of each Dif1 from the western blot is marked by arrows. The nonspecific bands present even in the *dif1Δ* sample are marked by double asterisks.

DIF1 Is Required for the Nuclear Import of Rnr2-Rnr4

The inability of *dif1Δ* mutants to localize Rnr2-Rnr4 could be due either to a defective import or to a problem in retaining Rnr2-Rnr4 inside the nucleus once imported (i.e., enhanced export or failed anchoring). If this is a nuclear retention defect, blocking nuclear export should accumulate Rnr2-Rnr4 inside the nucleus. Alternatively, if the defect occurs prior to nuclear import, blocking the nuclear export would have a minimal effect on nuclear accumulation. Therefore, we used leptomycin B (LMB) to inhibit the Crm1 exportin pathway (Kudo et al., 1998), which is essential for the release of nuclear Rnr after DNA damage in *S. pombe* (Liu et al., 2003). We confirmed that release of Rnr2 from the nucleus after HU treatment is inhibited by LMB, by using a strain

carrying the LMB-sensitive *CRM1-T439C* allele (Neville and Rosbash, 1999) (data not shown).

We first examined the effects of blocking nuclear export in the *wtm1Δ* mutant. A *GAL1::GFP-RNR4* reporter plasmid was introduced into different strains, induced for 3 hr, then repressed by the addition of glucose to prevent further synthesis of the reporter during the analysis (Figure 6C). LMB was then added for an additional hour prior to visualization. LMB treatment led to the nuclear accumulation of GFP-Rnr4 in the *wtm1Δ*, LMB-sensitive background (Figures 6D and 6E), consistent with a role for Wtm1 in nuclear retention rather than import. In contrast, LMB treatment of the *dif1Δ* or *dif1Δ wtm1Δ* double mutants did not cause nuclear accumulation of the GFP-Rnr4 reporter

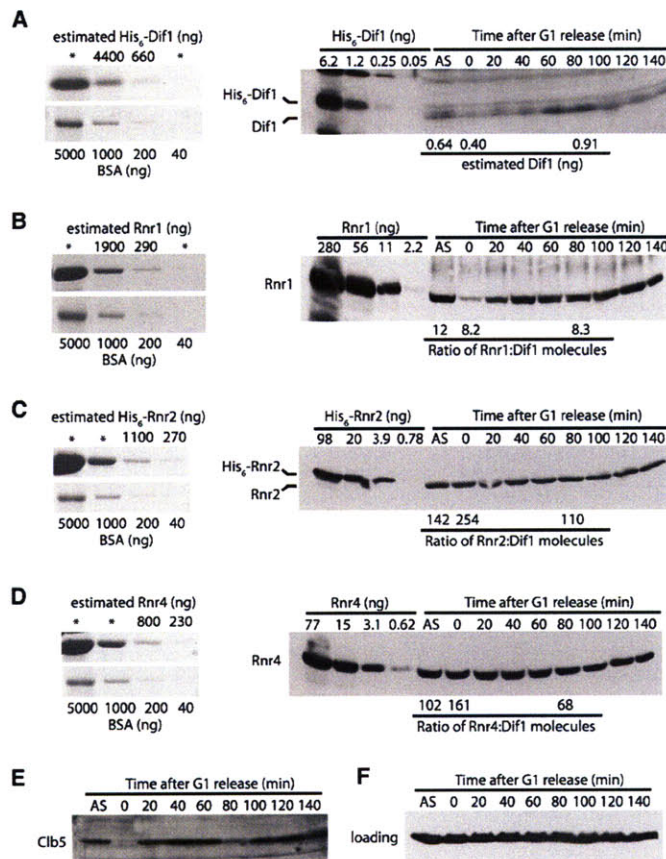


Figure 5. Dif1 Is Much Less Abundant than the Rnr2-Rnr4 Heterodimer

(A) Left panel: known standards of bovine serum albumin (BSA) were resolved on SDS-PAGE alongside of five-fold serial dilutions of purified recombinant His₆-Dif1 to estimate the concentration of the original Dif1 sample in nanograms. Dif1 serial dilutions that are beyond the range of the BSA standard were not used for estimation of protein concentration and were marked by asterisks (*). Right panel: known quantities of His₆-Dif1 were resolved on SDS-PAGE alongside of lysates from asynchronous (AS) and synchronized WT cells released from a G1 block and taken at 20 min intervals. The membrane was probed with anti-Dif1 antibodies.

(B) As in (A), except measuring Rnr1. Right panel: estimated Rnr1:Dif1 ratios are indicated below the western blot for the asynchronous, 0 min, and 80 min time points.

(C) As in (A), except measuring Rnr2.

(D) As in (A), except measuring Rnr4.

(E) Clb5 western blot to show progression of S phase in the synchronized culture.

(F) Tubulin western blot serves as a loading control.

(Figures 6D and 6E), indicating that the defect of the *dif1Δ* mutant occurs prior to nuclear import. To rule out potential cell-cycle artifacts, α factor was used to arrest cells in G1 before LMB treatment and provided similar results (Figure 6F). These results indicate that Dif1 is a regulator of nuclear import of Rnr2-Rnr4.

Dif1 Directly Binds to Rnr2-Rnr4 Complexes

Dif1 may affect nuclear import of Rnr2-Rnr4 directly or indirectly. However, a strong prediction of the direct importer model is that Dif1 will directly bind Rnr2-Rnr4 complexes. Consistent with that possibility, during the course of our investigation we found that purified recombinant Dif1 had a mild but reproducible inhibitory effect on RNR enzymatic activity in vitro (data not shown). We therefore examined binding between purified Dif1 and RNR subunits by using surface plasmon resonance. Rnr2-Rnr4 immobilized on the surface of the sensor chip could bind to Dif1 in a dose-dependent manner (Figure 7A). We calculated the K_D of this binding to be 0.6 μ M. Conversely, Dif1 immobilized on the surface of the sensor chip also bound to Rnr2-Rnr4 heterodimers (data not shown). No detectable binding to the Rnr1 homodimer was observed (data not shown). To examine what portion of Dif1 might mediate this interaction, we generated mutations in the conserved Hug domain (Dif1-hug) (Figure 7B). The binding of Dif1 to Rnr2-Rnr4 required an intact Hug domain (Figure 7A). Importantly, the Dif1-hug mutant was also defective for the proper nuclear localization of Rnr2-Rnr4 (Figure 7C), even though it

maintained similar kinetics of phosphorylation and degradation as Dif1-WT (Figures 4F and 4G). We have consistently observed higher levels of endogenous Dif1-hug compare to WT Dif1 for unknown reasons. These data suggest that Dif1 facilitates the nuclear import of Rnr2-Rnr4 via direct binding through its Hug domain.

DISCUSSION

The precise control of intracellular dNTP pools is critical to the maintenance of genomic integrity. Therefore, organisms have evolved multilayered controls to regulate the RNR pathway. In yeast, RNR is regulated by the cell-cycle and DNA-damage response pathways through gene expression, inhibitor destruction, and subcellular localization—the focus of this study. Our previous studies demonstrated that the nuclear protein Wtm1 secures Rnr2-Rnr4 inside the nucleus through an anchoring mechanism. However, how localization responded to DNA damage was not understood. Our current study identifies a DNA-damage-regulated protein, Dif1, that controls the nuclear localization of Rnr2-Rnr4 by regulated nuclear import.

Dif1 and Wtm1 Form Distinct Branches of the RNR Nuclear Localization Pathway

Initially, the similarities in the phenotypes of *dif1Δ* and *wtm1Δ* mutants suggested that they might function in the same pathway, possibly by forming a complex with Wtm1 and Rnr2-Rnr4. However, careful analysis of the relative abundance of Dif1 and the Rnr proteins showed that Dif1 was much less abundant than Rnr2 and Rnr4, eliminating the co-tether model. Instead, we find that *DIF1* and *WTM1* function in different branches of the Rnr localization pathway based on several pieces of data. First, *dif1Δ wtm1Δ* double mutants display enhanced cytoplasmic localization of Rnr2-Rnr4 relative to the single mutants. Second, overexpression of Dif1 suppresses the defect in Rnr2-Rnr4 nuclear localization in *wtm1Δ* mutants. Finally, blocking nuclear export by using LMB in *wtm1Δ* mutants caused accumulation of nuclear

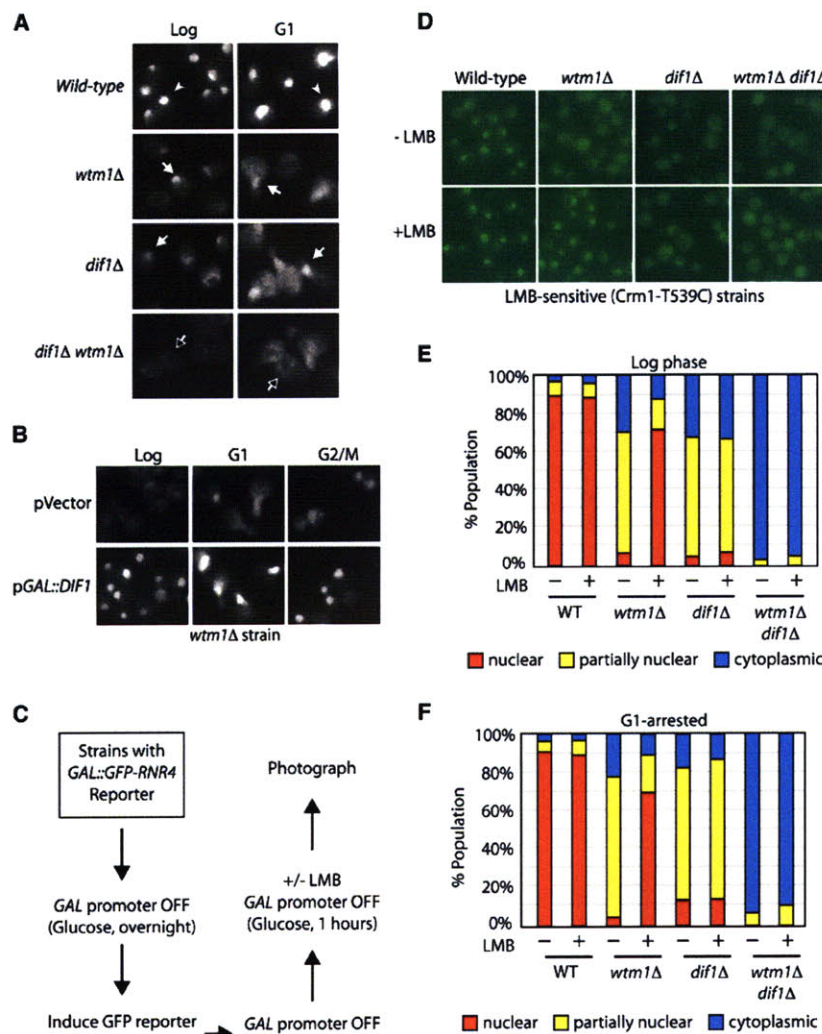


Figure 6. Dif1 Controls the Nuclear Import of Rnr2-Rnr4

(A) The nuclear localization of Rnr2 in the *dif1Δ wtm1Δ* double mutant was compared to wild-type (WT), *wtm1Δ*, and *dif1Δ* single mutants. Log phase and G1-arrested cells were processed for visualization of Rnr2 by indirect immunofluorescence. Cells with strong nuclear Rnr2 staining (white arrowhead), residual nuclear Rnr2 staining (white arrow), and Rnr2 nuclear exclusion staining (black arrow) are indicated.

(B) *wtm1Δ* strains containing vector alone or a galactose-inducible *DIF1* plasmid (pGAL::DIF1) were grown to log phase in glucose media. Cells were then switched to galactose media for 3 hr, while either being kept in log phase or arrested in G1 or G2/M. Samples were processed for Rnr2 visualization by indirect immunofluorescence.

(C) A schematic of the experiment used to examine nuclear import of Rnr2-Rnr4. Cells were grown to log phase in raffinose-glucose media, then switched to raffinose-galactose media for 3 hr to turn on the transcription of the *GAL1-GFP-RNR4* reporter. The promoter was shut off by switching back to glucose media for 3 hr, before leptomyacin B was added for an additional hour (LMB, 200 ng/ml). For the analysis of G1-arrested cells, the last two steps (4 hr) were carried out in the presence of α factor. Cells were photographed for GFP-Rnr4 localization.

(D) GFP-Rnr4 localization in WT, *wtm1Δ*, *dif1Δ*, and *wtm1Δ dif1Δ* mutants in the LMB-sensitive (Crm1-T539C) background were treated with or without LMB during log phase.

(E) Quantification of GFP-Rnr4 localization in (D). (F) Quantification of GFP-Rnr4 localization in G1-arrested cells, treated with or without LMB.

Rnr2-Rnr4, and this accumulation was prevented in the *wtm1Δ dif1Δ* double mutants. This observation is consistent with the role of Wtm1 as a nuclear anchor to limit nuclear export, whereas Dif1 facilitates the nuclear import of Rnr2-Rnr4 and leads to the model shown in Figure 7D. In this model, Wtm1 acts to limit the nucleoplasmic levels of Rnr2-Rnr4 complexes that are available for nuclear export. This reduces the rate of flux out of the nucleus and makes the system more responsive to the rate of nuclear import.

Regulation of this localization switch is accomplished largely through modulation of the rate of nuclear import through Dif1. Dif1 is controlled at three levels. First it is cell-cycle regulated, with its abundance peaking at the end of S phase, when Rnr2-Rnr4 returns to the nucleus. There are likely to be additional aspects to this regulation induced by α factor, as Dif1 levels are lower in α factor-arrested cells, yet they are sufficient to localize Rnr2-Rnr4 into the nucleus. The rates of nuclear export could be regulated by α factor. Consistent with this, *wtm1Δ* mutants show more nuclear localization in α factor-arrested cells. Second, Dif1 is regulated by proteolysis through direct phosphorylation by the

Dun1 kinase on the Sml domain, which constitutes a phosphodegron. The four serine and threonine residues near the end of the Sml domain are essential for the phosphorylation, inhibition, and destruction of Dif1 in response to DNA damage. Mutation of the phosphorylation sites results in stabilization of Dif1 and defective release of nuclear Rnr2-Rnr4 in response to DNA damage. Finally, phosphorylation of the Sml domain is sufficient to abolish the function of Dif1 prior to its degradation. This, to our knowledge, is the first example of a phosphorylation event that both inactivates a protein and separately targets it for degradation.

Although regulatory information flows through the Dif1 branch of the pathway, there are additional regulatory inputs into the system, because the residual nuclear localization seen in *dif1Δ* mutants can be relieved by treatment with HU to generate a nuclear halo or empty nucleus phenotype seen in *wtm1Δ dif1Δ* double mutants. Whether this works through regulation of Wtm1-Rnr2-Rnr4 affinity, the rate of nuclear export via regulation on the exportin Crm1, or the residual *DIF1*-independent Rnr2-Rnr4 nuclear import pathway remains to be determined.

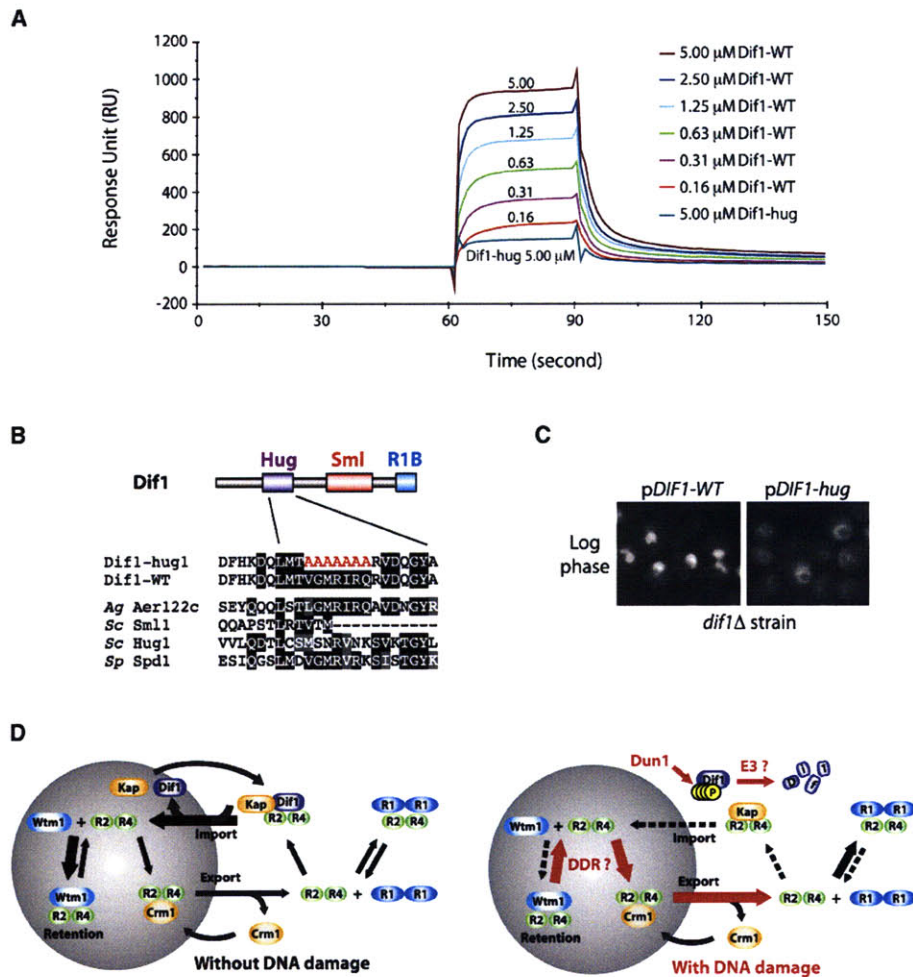


Figure 7. Dif1 Directly Interacts with Rnr2-Rnr4

(A) Binding between Dif1 and Rnr2-Rnr4 was detected with BIAcore. Purified Rnr2-Rnr4 was immobilized on the sensor surface. Recombinant wild-type (WT) Dif1 protein (Dif1-WT) flowed over the immobilized Rnr2-Rnr4 at the indicated concentrations. Recombinant Dif1-hug (Dif1-hug) protein flowed over the same sensor surface at a concentration of 5.0 μ M (turquoise line). Binding between Rnr2-Rnr4 and Dif1 was measured in response units (RU).

(B) Diagram of the amino acid changes in the Dif1-hug mutant.

(C) Rnr2 visualization by indirect immunofluorescence from log phase cultures of *dif1* Δ strains carrying pDIF1-WT or pDIF1-hug plasmids.

(D) Model demonstrating nuclear import and retention of Rnr2-Rnr4 in response to DNA damage. (Left) Dif1 facilitates the nuclear import of Rnr2-Rnr4, whereas Wtm1 functions as a nuclear anchor for Rnr2-Rnr4. In the absence of DNA damage, the net contribution of these two pathways leads to a net accumulation of Rnr2-Rnr4 inside the nucleus. (Right) Activation of the DNA-damage response (DDR) leads to the phosphorylation, inactivation, and degradation of Dif1, reducing the nuclear import of Rnr2-Rnr4. DNA damage also releases the pool of nuclear Rnr2-Rnr4, either by decreasing the affinity between the Wtm1-Rnr2-Rnr4 interactions, or through an increased rate of Crm1-mediated Rnr2-Rnr4 nuclear export.

The key mechanistic insight into Dif1 function comes from the direct binding of Dif1 with Rnr2-Rnr4 through the Hug domain. Dif1-hug mutants retain the ability to be phosphorylated and degraded in response to DNA damage, but fail to properly localize Rnr2-Rnr4. Given the inability of the *dif1* Δ mutant to import Rnr2-Rnr4, the simplest model is that Dif1 binds the Rnr2-Rnr4 complex through its Hug domain and activates import by serving as an adaptor or by activating a latent nuclear localization signal on the Rnr2-Rnr4 complex. In unpublished work, we have identified candidate importins/karyopherins with defective Rnr2-Rnr4 nuclear localization. The mechanism of how Dif1 influences

the interaction between Rnr2-Rnr4 and its importin(s) remains an important area to be elucidated.

A Unifying Theory for Functions of the Spd1, Dif1, and Sml1 Families of Rnr Regulators

The *DIF1* and the *HUG1/SML1* loci are syntenic and arose from a genome duplication in an ancestor of *S. cerevisiae* (Dietrich et al., 2004; Kellis et al., 2004) that further diverged into three separate genes. The likely structure of the original protein is best illustrated by their ortholog, *Aer122c*, in *Ashbya gossypii*, a species closely related to *S. cerevisiae* but which did not

undergo the genome duplication. Aer122c is also related to *S. pombe* Spd1, the first demonstrated regulator of Rnr small subunit localization. Spd1 has been shown to maintain spRnr2 (Suc22) of *S. pombe* in the nucleus (Liu et al., 2003). However, recent experiments have suggested that it acts as an inhibitor of RNR activity by binding to *S. pombe* spRnr1 (Cdc22), the large RNR subunit, casting doubt on the suggested spRnr2 nuclear retention mechanism. Our work proposes an explanation for these seeming discrepancies. We propose that Spd1, Dif1, Sml1, and Hug1 all evolved from a common ancestral gene related to Aer122c that had three basic domains. The first domain, which we call the Hug domain, is required for the physical binding and nuclear import of Rnr2 family members. The second domain, the Sml domain, is a degron/phosphodegron that confers DNA-damage and cell-cycle regulation on the activities of the proteins. The third domain is the R1B domain that binds the Rnr1 subunit to act as an RNR enzymatic inhibitor. Thus, this ancestral gene employed two different mechanisms through which to negatively regulate RNR function and a regulatory region that allowed those functions to be modulated. We propose that Spd1 is closely related to this ancestral gene and retains all three functions, although its degradation is likely regulated at the level of ubiquitin ligase activation rather than through phosphorylation of the degron (Liu et al., 2005). This explains what had on the surface appeared to be an inconsistency with the ability of Spd1 to bind spRnr1 but at the same time localize spRnr2. In budding yeast, these functions have been split between Dif1 and Sml1. Both proteins retain a phosphodegron that confers cell-cycle and DNA-damage regulation through an as yet unknown ubiquitin ligase. However, Dif1 lacks the C-terminal Rnr1-interacting domain, whereas Sml1 lacks the Rnr2-binding Hug domain. The biochemical role of the damage-inducible Hug1 protein remains to be elucidated, although our model would predict that it should be able to bind Rnr2-Rnr4, and possibly compete with or negatively regulate Dif1 activity.

Our discovery of Dif1 has illuminated part of the mechanism cells use to regulate localization of RNR small subunits. To our knowledge, the combination of a nuclear anchor limiting nuclear export and a regulated importer to coordinate subcellular localization appears to be unique. This is yet another example of a dynamic switch in which two antagonistic processes, here export and import, are coordinately regulated to produce an outcome, much like Cdk1 phosphorylation and dephosphorylation (Harper and Elledge, 2007) and Cdc20 ubiquitination and deubiquitination (Stegmeier et al., 2007). This is likely to be a strategy that will be found to regulate the localization of many other proteins in the future.

EXPERIMENTAL PROCEDURES

Media and Growth Conditions

α factor and nocodazole arrest were carried out as previously described (Desany et al., 1998). DNA-damage agents were used at the following concentrations: phleomycin, 25–100 ng/ml; MMS, 0.1%; HU, 150 mM; and ionizing radiation, 20 kRad. Leptomycin B (LC laboratories) was used at 100–200 ng/ml.

Polyclonal Antibody for Dif1

Recombinant full-length GST-Dif1 was purified from *E. coli* and was used to generate a rabbit antibodies (Bethyl Laboratories). For western blot analysis, a 1:1000 dilution was used.

Protein Sample Preparation and Phosphatase Treatment

TCA precipitation was performed as previously described (Longhese et al., 1997). Phosphatase treatment of protein sample was carried out as described (Vialard et al., 1998), except that calf intestinal phosphatase (New England Biolab) was used as the phosphatase, and 10 mM Na_2VO_4 and 50 mM EDTA were used as the phosphatase inhibitors.

Indirect Immunofluorescence and Visualization of GFP

Indirect immunofluorescence was performed as previously described (Lee and Elledge, 2006). Both anti-Rnr2 and anti-Rnr4 antibodies were used at 1:10,000 (Yao et al., 2003).

Phosphomapping of Dif1 and Rnr2

Strains carrying 3HA-Rnr2 and 3Myc-Dif1 were HU treated. 3HA-Rnr2 and 3Myc-Dif1 were immunoprecipitated and resolved by SDS-PAGE. The gel with the 3HA-Rnr2 sample was Coomassie stained, whereas that with 3Myc-Dif1 was silver stained by SilverQuest (Invitrogen). The bands were excised for phosphomapping analysis.

In Vitro Dun1 Kinase Assay

Wild-type, phosphoserine/threonine-mutated, or Hug-domain-mutated Dif1 strains were used for immunoprecipitation by anti-Dif1 polyclonal antibodies. The Dif1 proteins were left on 15 μl protein A beads and washed twice with kinase buffer (50 mM Tris-HCl [pH 7.5], 10 mM MgCl_2 , 1 mM DTT, 0.1 mM NaVO_4). GST-Dun1 purified from Baculovirus-infected SF9 insect cells was incubated with the protein A beads containing Dif1 in 100 μl kinase buffer, with 2 μM cold ATP, and 5 μCi [γ - ^{32}P]ATP at 30°C for 45 min.

Protein Expression and Purification

Rnr1 and Rnr2-Rnr4 were purified from yeast as described (Ge et al., 2001; Nguyen et al., 1999). His₆-tagged *DIF1* plasmid (based on the pET15b vector) in BL21(DE3) pLysS cells were grown to an OD_{600} of 0.6 and were induced overnight with IPTG (0.2 mM) at 18°C. Cells were washed, resuspended in binding buffer (30 mM Tris [pH 7.5], 150 mM NaCl, 1 mM DTT, 0.1% Triton, 1 mM PMSF, Roche Complete Protease Inhibitor Cocktail), and sonicated to disrupt the cells. The crude lysate was spun at 10,000 \times g for 15 min. Dif1 protein in the supernatant was purified by using Ni-NTA beads according to the Qiaexpressionist manual (QIAGEN), with 5 mM imidazole added to the binding and washing steps to increase the stringency of purification. His₆-Dif1 was eluted by 200 mM imidazole and dialyzed into the appropriate buffers.

Quantification of Protein Abundance

Coomassie-stained SDS-PAGE or exposed films from western blots were scanned digitally, and the intensity of protein bands was quantified by using the gel analysis function of ImageJ software (NIH). For the western blot quantification of Dif1, Rnr1, Rnr2, and Rnr4, each lane was loaded with 170, 17, 3.4, and 3.4 ng protein from cell lysate, respectively. The total number of cells used for protein extraction was determined by colony plating and optical density (OD_{600}) and is used for the calculation of molecules per cell.

BIAcore Analysis

Purified Rnr2-Rnr4 was immobilized on a CM5 chip by amine coupling at a level of 9945 response units (RU). All analytes were dialyzed in PBS buffer, which also serves as the running buffer. The binding assay was carried out at 25°C with a flow rate of 30 $\mu\text{l}/\text{min}$ on a Biacore 3000. Data were analyzed by using BIAevaluation 3.2 software, and reference was subtracted and corrected for the bulk effect. Binding affinity was calculated by steady-state fit by using a 1:1 binding model.

Strains and Plasmids

For a complete list of yeast strains and plasmids used for this work, see Table S1 (available online).

SUPPLEMENTAL DATA

The Supplemental Data include a table listing the strains and plasmids used and are available at <http://www.molecule.org/cgi/content/full/32/1/70/DC1/>.

ACKNOWLEDGMENTS

We thank M. Rosbash for strains, P. Silver and A. Amon for helpful suggestions, and J. Li for assistance with the preparation of GST-Dun1 kinase. We thank T. Tomaino for assistance with data analysis. We are grateful to Minxia Huang for communicating results prior to publication. This work was supported by National Institutes of Health grants to S.J.E. and J.S. S.J.E. is an Investigator with the Howard Hughes Medical Institute.

Received: March 9, 2008

Revised: July 28, 2008

Accepted: August 20, 2008

Published: October 9, 2008

REFERENCES

- Basrai, M.A., Velculescu, V.E., Kinzler, K.W., and Hieter, P. (1999). NORF5/HUG1 is a component of the MEC1-mediated checkpoint response to DNA damage and replication arrest in *Saccharomyces cerevisiae*. *Mol. Cell. Biol.* **19**, 7041–7049.
- Chabes, A., Domkin, V., and Thelander, L. (1999). Yeast Sml1, a protein inhibitor of ribonucleotide reductase. *J. Biol. Chem.* **274**, 36679–36683.
- Chabes, A., Georgieva, B., Domkin, V., Zhao, X., Rothstein, R., and Thelander, L. (2003). Survival of DNA damage in yeast directly depends on increased dNTP levels allowed by relaxed feedback inhibition of ribonucleotide reductase. *Cell* **112**, 391–401.
- Desany, B.A., Alcasabas, A.A., Bachant, J.B., and Elledge, S.J. (1998). Recovery from DNA replicational stress is the essential function of the S-phase checkpoint pathway. *Genes Dev.* **12**, 2956–2970.
- Dietrich, F.S., Voegeli, S., Brachat, S., Lerch, A., Gates, K., Steiner, S., Mohr, C., Pohlmann, R., Luedi, P., Choi, S., et al. (2004). The *Ashbya gossypii* genome as a tool for mapping the ancient *Saccharomyces cerevisiae* genome. *Science* **304**, 304–307.
- Ge, J., Perlstein, D.L., Nguyen, H.H., Bar, G., Griffin, R.G., and Stubbe, J. (2001). Why multiple small subunits (Y2 and Y4) for yeast ribonucleotide reductase? Toward understanding the role of Y4. *Proc. Natl. Acad. Sci. USA* **98**, 10067–10072.
- Hakansson, P., Dahl, L., Chilkova, O., Domkin, V., and Thelander, L. (2006). The *Schizosaccharomyces pombe* replication inhibitor Spd1 regulates ribonucleotide reductase activity and dNTPs by binding to the large Cdc22 subunit. *J. Biol. Chem.* **281**, 1778–1783.
- Harper, J.W., and Elledge, S.J. (2007). The DNA damage response: ten years after. *Mol. Cell* **28**, 739–745.
- Holmberg, C., Fleck, O., Hansen, H.A., Liu, C., Slaaby, R., Carr, A.M., and Nielsen, O. (2005). Ddb1 controls genome stability and meiosis in fission yeast. *Genes Dev.* **19**, 853–862.
- Huang, M., Zhou, Z., and Elledge, S.J. (1998). The DNA replication and damage checkpoint pathways induce transcription by inhibition of the Crt1 repressor. *Cell* **94**, 595–605.
- Kellis, M., Birren, B.W., and Lander, E.S. (2004). Proof and evolutionary analysis of ancient genome duplication in the yeast *Saccharomyces cerevisiae*. *Nature* **428**, 617–624.
- Kudo, N., Wolff, B., Sekimoto, T., Schreiner, E.P., Yoneda, Y., Yanagida, M., Horinouchi, S., and Yoshida, M. (1998). Leptomycin B inhibition of signal-mediated nuclear export by direct binding to CRM1. *Exp. Cell Res.* **242**, 540–547.
- Lee, Y.D., and Elledge, S.J. (2006). Control of ribonucleotide reductase localization through an anchoring mechanism involving Wtm1. *Genes Dev.* **20**, 334–344.
- Lincker, F., Philipps, G., and Chaboute, M.E. (2004). UV-C response of the ribonucleotide reductase large subunit involves both E2F-mediated gene transcriptional regulation and protein subcellular relocalization in tobacco cells. *Nucleic Acids Res.* **32**, 1430–1438.
- Liu, C., Powell, K.A., Mundt, K., Wu, L., Carr, A.M., and Caspari, T. (2003). Cop9/signalosome subunits and Pcu4 regulate ribonucleotide reductase by both checkpoint-dependent and -independent mechanisms. *Genes Dev.* **17**, 1130–1140.
- Liu, C., Poitelea, M., Watson, A., Yoshida, S.H., Shimoda, C., Holmberg, C., Nielsen, O., and Carr, A.M. (2005). Transactivation of *Schizosaccharomyces pombe* *cdt2+* stimulates a Pcu4-Ddb1-CSN ubiquitin ligase. *EMBO J.* **24**, 3940–3951.
- Longhese, M.P., Paciotti, V., Fraschini, R., Zaccarini, R., Plevani, P., and Lucchini, G. (1997). The novel DNA damage checkpoint protein *ddc1p* is phosphorylated periodically during the cell cycle and in response to DNA damage in budding yeast. *EMBO J.* **16**, 5216–5226.
- Neville, M., and Rosbash, M. (1999). The NES-Crm1p export pathway is not a major mRNA export route in *Saccharomyces cerevisiae*. *EMBO J.* **18**, 3746–3756.
- Nguyen, H.H., Ge, J., Perlstein, D.L., and Stubbe, J. (1999). Purification of ribonucleotide reductase subunits Y1, Y2, Y3, and Y4 from yeast: Y4 plays a key role in diiron cluster assembly. *Proc. Natl. Acad. Sci. USA* **96**, 12339–12344.
- Nordlund, P., and Reichard, P. (2006). Ribonucleotide reductases. *Annu. Rev. Biochem.* **75**, 681–706.
- Reichard, P. (2002). Ribonucleotide reductases: the evolution of allosteric regulation. *Arch. Biochem. Biophys.* **397**, 149–155.
- Stegmeier, F., Rape, M., Draviam, V.M., Nalepa, G., Sowa, M.E., Ang, X.L., McDonald, E.R., III, Li, M.Z., Hannon, G.J., Sorger, P.K., et al. (2007). Anaphase initiation is regulated by antagonistic ubiquitination and deubiquitination activities. *Nature* **446**, 876–881.
- Uchiki, T., Dice, L.T., Hettich, R.L., and Dealwis, C. (2004). Identification of phosphorylation sites on the yeast ribonucleotide reductase inhibitor Sml1. *J. Biol. Chem.* **279**, 11293–11303.
- Vallen, E.A., and Cross, F.R. (1999). Interaction between the MEC1-dependent DNA synthesis checkpoint and G1 cyclin function in *Saccharomyces cerevisiae*. *Genetics* **151**, 459–471.
- Vialard, J.E., Gilbert, C.S., Green, C.M., and Lowndes, N.F. (1998). The budding yeast Rad9 checkpoint protein is subjected to Mec1/Tel1-dependent hyperphosphorylation and interacts with Rad53 after DNA damage. *EMBO J.* **17**, 5679–5688.
- Voegtli, W.C., Ge, J., Perlstein, D.L., Stubbe, J., and Rosenzweig, A.C. (2001). Structure of the yeast ribonucleotide reductase Y2Y4 heterodimer. *Proc. Natl. Acad. Sci. USA* **98**, 10073–10078.
- Xue, L., Zhou, B., Liu, X., Qiu, W., Jin, Z., and Yen, Y. (2003). Wild-type p53 regulates human ribonucleotide reductase by protein-protein interaction with p53R2 as well as hRRM2 subunits. *Cancer Res.* **63**, 980–986.
- Yao, R., Zhang, Z., An, X., Bucci, B., Perlstein, D.L., Stubbe, J., and Huang, M. (2003). Subcellular localization of yeast ribonucleotide reductase regulated by the DNA replication and damage checkpoint pathways. *Proc. Natl. Acad. Sci. USA* **100**, 6628–6633.
- Zhang, Z., An, X., Yang, K., Perlstein, D.L., Hicks, L., Kelleher, N., Stubbe, J., and Huang, M. (2006). Nuclear localization of the *Saccharomyces cerevisiae* ribonucleotide reductase small subunit requires a karyopherin and a WD40 repeat protein. *Proc. Natl. Acad. Sci. USA* **103**, 1422–1427.
- Zhang, Z., Yang, K., Chen, C.C., Feser, J., and Huang, M. (2007). Role of the C terminus of the ribonucleotide reductase large subunit in enzyme regeneration and its inhibition by Sml1. *Proc. Natl. Acad. Sci. USA* **104**, 2217–2222.
- Zhao, X., and Rothstein, R. (2002). The Dun1 checkpoint kinase phosphorylates and regulates the ribonucleotide reductase inhibitor Sml1. *Proc. Natl. Acad. Sci. USA* **99**, 3746–3751.
- Zhao, X., Muller, E.G., and Rothstein, R. (1998). A suppressor of two essential checkpoint genes identifies a novel protein that negatively affects dNTP pools. *Mol. Cell* **2**, 329–340.
- Zhao, X., Georgieva, B., Chabes, A., Domkin, V., Ippel, J.H., Schleucher, J., Wijmenga, S., Thelander, L., and Rothstein, R. (2000). Mutational and structural analyses of the ribonucleotide reductase inhibitor Sml1 define its Rnr1 interaction domain whose inactivation allows suppression of *mec1* and *rad53* lethality. *Mol. Cell. Biol.* **20**, 9076–9083.
- Zhou, Z., and Elledge, S.J. (1992). Isolation of *crt* mutants constitutive for transcription of the DNA damage inducible gene *RNR3* in *Saccharomyces cerevisiae*. *Genetics* **131**, 851–866.

Enhanced subunit interactions with gemcitabine-5'-diphosphate inhibit ribonucleotide reductases

Jun Wang[†], Gregory J. S. Lohman^{†‡}, and JoAnne Stubbe^{†§¶}

Departments of [†]Chemistry and [§]Biology, Massachusetts Institute of Technology, Cambridge, MA 02139

Contributed by JoAnne Stubbe, July 23, 2007 (sent for review June 20, 2007)

Ribonucleotide reductases (RNRs) catalyze the conversion of nucleotides to deoxynucleotides in all organisms. The class I RNRs are composed of two subunits, α and β , with proposed quaternary structures of $\alpha_2\beta_2$, $\alpha_6\beta_2$, or $\alpha_6\beta_6$, depending on the organism. The α subunits bind the nucleoside diphosphate substrates and the dNTP/ATP allosteric effectors that govern specificity and turnover. The β_2 subunit houses the diferric Y^* (1 radical per β_2) cofactor that is required to initiate nucleotide reduction. 2',2'-Difluoro-2'-deoxycytidine (F_2C) is presently used clinically in a variety of cancer treatments and the 5'-diphosphorylated F_2C (F_2CDP) is a potent inhibitor of RNRs. The studies with [$1\text{'-}^3\text{H}$]- F_2CDP and [$5\text{'-}^3\text{H}$]- F_2CDP have established that F_2CDP is a substoichiometric mechanism based inhibitor (0.5 eq F_2CDP/α) of both the *Escherichia coli* and the human RNRs in the presence of reductant. Inactivation is caused by covalent labeling of RNR by the sugar of F_2CDP (0.5 eq/ α) and is accompanied by release of 0.5 eq cytosine/ α . Inactivation also results in loss of 40% of β_2 activity. Studies using size exclusion chromatography reveal that in the *E. coli* RNR, an $\alpha_2\beta_2$ tight complex is generated subsequent to enzyme inactivation by F_2CDP , whereas in the human RNR, an $\alpha_6\beta_6$ tight complex is generated. Isolation of these complexes establishes that the weak interactions of the subunits in the absence of nucleotides are substantially increased in the presence of F_2CDP and ATP. This information and the proposed asymmetry between the interactions of $\alpha n\beta n$ provide an explanation for complete inactivation of RNR with substoichiometric amounts of F_2CDP .

Gemcitabine, or 2',2'-difluoro-2'-deoxycytidine (F_2C), is a drug that is used clinically in the treatment of advanced pancreatic cancer and non-small cell lung carcinomas (1–3). In humans, F_2C enters the cell via CNT-type or ENT-type transporters (4–6) and must be phosphorylated to exhibit its cytotoxicity. The monophosphate of F_2C (F_2CMP) is generated by deoxycytidine kinase (7) and is rapidly phosphorylated to the di- and triphosphates (F_2CDP and F_2CTP) (8, 9). Diphosphorylated F_2C (F_2CDP) is an irreversible inhibitor of ribonucleotide reductase (RNR) (10–13), and F_2CTP functions as a chain terminator in the DNA polymerase reaction (14, 15). Differentially phosphorylated states of gemzar can also interfere with other enzymes involved in nucleotide metabolism. The mechanisms of cytotoxicity of F_2C depend on the phosphorylated state of the inhibitor and are likely to be cell specific and multifactorial. Our recent synthesis of [$1\text{'-}^3\text{H}$]- F_2CDP has provided the required tool to investigate the mechanism by which this molecule inactivates RNRs. Studies reported herein provide a previously unrecognized approach for RNR inhibition, one in which the mechanism based inhibitor (F_2CDP) enhances the interactions between the two subunits of RNR preventing nucleotide reduction despite substoichiometric labeling.

RNRs catalyze the conversion on nucleoside di(tri)phosphates to deoxynucleoside di(tri)phosphates in all organisms and are the predominant control point for abundance and ratios of dNTPs pools required for the initiation and elongation processes catalyzed by DNA polymerases (16, 17). The class I RNRs are composed of two types of subunits, α and β . The quaternary structure of α is nucleotide- and organism-dependent. It can be a monomer, dimer, tetramer, or hexamer (16, 18). β is a homodimer that houses the diferric-tyrosyl radical (Y^*) required for initiating nucleotide re-

duction on α . Current evidence suggests that there is one Y^* and 2 di-iron clusters/ β_2 (19, 20). The interactions between α and β are weak (K_d of 0.2 μM) in the absence of nucleotide (21). In prokaryotic systems α and β are both homodimers. The active *Escherichia coli* RNR is thought to be an $\alpha_2\beta_2$ complex (22, 23). The α oligomeric state of the mouse RNR has been the best characterized eukaryotic RNR to date. In the absence of nucleotides, α is a monomer. It dimerizes in the presence of allosteric effectors (dATP, TTP, dGTP, and ATP) (18). In addition, the millimolar levels of ATP found intracellularly cause α to oligomerize to a hexamer (α_6). β is a homodimer (β_2). The quaternary structure of eukaryotic RNRs is still being actively investigated. The complex responsible for RNR activity has been proposed by Cooperman and coworkers (18) to be $\alpha_2\beta_2$, $\alpha_6\beta_2$, or $\alpha_6\beta_6$ on the basis of a variety of physical biochemical and kinetic studies. Recent gas-phase electrophoretic-mobility macromolecule analysis studies have suggested that the mouse quaternary structure is $\alpha_6\beta_2$ (24). Studying subunit interactions has been difficult by conventional methods because of α 's nucleotide-dependent aggregation state and the weak binding of α and β , which is also nucleotide-dependent (21). Determination of apparent molecular masses of the active RNR complexes requires nucleotides in the analysis buffer, and thus protein detection by UV spectroscopy is obscured (18, 23).

A number of years ago, we reported on the inactivation of *E. coli* RNR by F_2CDP (11, 12). We showed that 1 eq of F_2CDP per *E. coli* RNR, presumably $\alpha_2\beta_2$, in the presence of reductants, thioredoxin (TR) and TR reductase or DTT, is sufficient for enzyme inactivation and that the inactivation is accompanied by release of 2 fluoride ions and one cytosine (12). We also demonstrated that the mode of inhibition changed in the absence of reductants. Thus, as with all nucleotide mechanism based inhibitors of RNRs studied in detail, multiple modes of inactivation are involved in the inhibition process (Scheme 1). The details of the inhibition by F_2CDP have remained largely unexplored because of the unavailability of sugar and base radiolabeled F_2CDP . We have recently developed a method to synthesize [$1\text{'-}^3\text{H}$]- F_2CDP and [$5\text{'-}^3\text{H}$]- F_2CDP (9). These compounds have allowed us to reinvestigate the mechanism of inhibition of the *E. coli* RNR and to report for the first time on the details of the inhibition of the human RNR. The present communication shows that incubation of human and *E. coli* RNRs with [$1\text{'-}^3\text{H}$] or [$5\text{'-}^3\text{H}$] F_2CDP results in 1 eq of sugar covalently bound per α_2 , which is sufficient for RNR inactivation. Size exclusion chromatography (SEC) of the inactivated RNRs reveals that this modification of α dramatically alters $\alpha n/\beta n$ subunit interactions,

Author contributions: J.S. designed research; J.W. and G.J.S.L. performed research; J.W., G.J.S.L., and J.S. analyzed data; and J.S. wrote the paper.

The authors declare no conflict of interest.

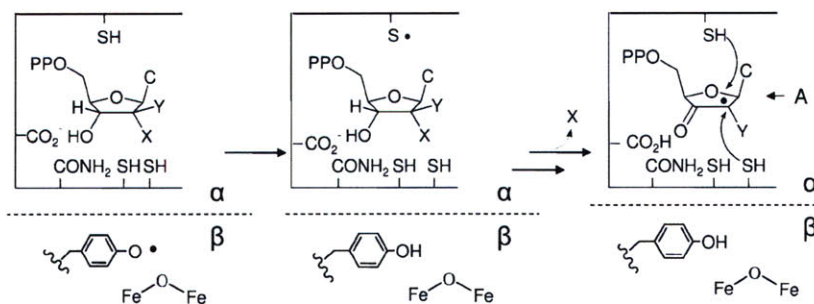
Abbreviations: F_2C , 2',2'-difluoro-2'-deoxycytidine; F_2CDP , diphosphorylated F_2C ; RNR, ribonucleotide reductase; TR, thioredoxin; SEC, size exclusion chromatography.

[†]Present address: Momenta Pharmaceuticals, 675 West Kendall Street, Cambridge, MA 02142.

[¶]To whom correspondence should be addressed. E-mail: stubbe@mit.edu.

This article contains supporting information online at www.pnas.org/cgi/content/full/0706803104/DC1.

© 2007 by The National Academy of Sciences of the USA



Scheme 1.

forming a tight complex, which is ultimately responsible for complete RNR inhibition.

Results

Synthesis of [1'-³H]-F₂CDP and [5-³H]-F₂CDP. Synthesis of [1'-³H]-F₂C involved modification of previously published procedures (25, 26). The 2-deoxy-3,5-di-*O*-benzoyl-3,3-difluororibonolactone was reduced with [³H]-disiamylborane made from NaB³H₄ and 2-methyl-2-butene. The lactol formed was converted without purification to 2-deoxy-3,5-di-*O*-benzoyl-3,3-difluoro-1-*O*-methanesulfonyl- β -D-ribofuranoside which was then coupled with bis(trimethylsilyl)-cytosine to give, subsequent to deblocking, an α,β mixture (60:40) of [1'-³H]-F₂C. Phosphorylation to the monophosphate (F₂CMP) was effected by using human deoxycytidine kinase (7). Because only the β isomer of the nucleoside is a substrate, this step allowed removal of α F₂C. F₂CMP was then phosphorylated to the diphosphate with human UMP/CMP kinase (8). The details of these syntheses will be reported elsewhere (9).

Purification of the α and β Subunits of Human RNR. The clones for α and β were obtained from the Y. Yen laboratory (City of Hope National Medical Center, Duarte, CA). Mutations in the genes were corrected to the sequence reported in the National Center for Biotechnology Information (NCBI) database (27, 28), and the N terminus of each protein was reengineered to maintain the (His)₆ tag and to reduce the length of the intervening linker before the start of the gene to 10 aa. The proteins were purified to \approx 90% homogeneity based on SDS/PAGE, using Ni affinity chromatography.

β 2 as isolated is a dimer in the apo form and was reconstituted by following the protocol we have developed for reconstitution of the *E. coli* β 2 (29). The resulting protein had 0.8 tyrosyl radicals/ β 2 and a specific activity of 1,089 nmol/min/mg in the presence of a 7-fold excess of α . α was difficult to work with because of its low solubility. However, its specific activity in the presence of a 7-fold excess of β was 462 nmol/min/mg. These results contrast with previous reports in the literature of 75 nmol/min/mg and 158 nmol/min/mg for β and 6.8 nmol/min/mg for α (30, 31). The basis for the activity differences are not understood, but are likely related to the complexity of the assay as we articulated in detail in ref. 32.

Table 1. Covalent labeling of *E. coli* and human RNR with [1'-³H]-F₂CDP and [5-³H]-F₂CDP analyzed by SEC

Protein	[³ H]-F ₂ CDP	Conditions	[³ H]/ α 2
<i>E. coli</i> RNR	1'	Native	0.9
	1'	Denaturing	1.11
	5	Native	0.19
	5	Denaturing	0.08
Human RNR	1'	Native	0.85
	1'	Denaturing	0.8
	5	Native	0.1
	5	Denaturing	0.1

Time-Dependent Inactivation of Human and *E. coli* RNRs. Our previous studies of the mechanism of F₂CDP inactivation of RNR were carried out on the *E. coli* enzyme, by using unlabeled inhibitor. Our results were provocative in that 1 mol of F₂CDP inactivated 1 mol of α 2 β 2, which has two active sites. The experiments have been repeated by using [1'-³H]-F₂CDP and [5-³H]-F₂CDP. Incubation of 15 μ M α 2 and 15 μ M β 2 with 15 or 30 μ M of [1'-³H]-F₂CDP resulted in recovery of 0.9 (1.1) mol of radiolabel/RNR (α 2 β 2) from analysis of the reaction mixture that was passed through a Sephadex G50 column in the absence or presence of denaturant (Table 1). With the [5-³H]-F₂CDP, 0.19 and 0.08 eq were detected in the absence or presence of denaturant, respectively. These results establish that there is 1 eq of the sugar from F₂CDP covalently bound to the enzyme and that most of the cytosine has been released. In addition, under these conditions, 40% of the tyrosyl radical is lost similar to our previous studies (12). These results, in conjunction with the time-dependent inactivation studies, establish that substoichiometric amounts of F₂CDP completely inactivate the *E. coli* RNR.

A similar set of experiments has been carried out on the human RNR. Time-dependent inactivation studies in which the inactivation mixture contained 0.5, 1.0, or 5.0 eq of F₂CDP/ α reveal that 0.5 eq of F₂CDP/ α results in complete loss of RNR activity (Fig. 1). The instability of the β 2 radical requires that a control in the absence of F₂CDP be carried out and used to correct the data observed in its presence. The weak interaction between α and β of RNR allow assays of the subunit activity individually (21, 32). Thus, the inactivation mixture was assayed for activity of α (β) in the presence of a 7-fold excess of β (α). Under these conditions, α is 100% inactive. In contrast to expectations, β retained 60–70% of its activity [supporting information (SI) Fig. 4], suggesting that the excess α is capable of facilitating subunit dissociation. The results of these experiments have interesting implications in recovering RNR activity *in vivo* subsequent to its inactivation by F₂CDP and will be discussed subsequently.

Studies using [1'-³H]-F₂CDP and [5-³H]-F₂CDP were carried out

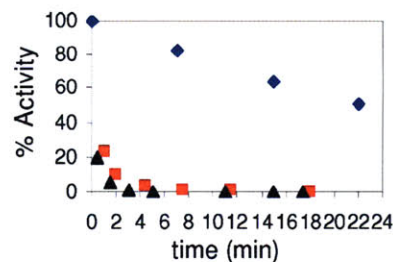


Fig. 1. Time-dependent inactivation of human RNR by F₂CDP. Inactivation mixture contained final concentrations of α , β , 1.2 μ M; F₂CDP, 0.6 μ M (■), and 6 μ M (▲); ATP, 3 mM; and DTT, 5 mM. Aliquots were removed at various times and diluted 4-fold for determination of RNR activity. Control experiment (◆) is identical to the experiment except that F₂CDP was omitted.

to determine whether the label was attached covalently. Incubation of [$1'$ - 3 H] or [5 - 3 H]-F₂CDP with human RNR followed by Sephadex G50 chromatography under native and denaturing conditions gave the results summarized in Table 1. With the [$1'$ - 3 H] F₂CDP 0.8–0.85 labels were bound per α 2, whereas with the [5 - 3 H] only 0.1 labels were covalently bound. The results are very similar to those observed with the *E. coli* RNR, with the unusual stoichiometry of 1 F₂CDP per α 2 observed.

Cytosine Release by Human RNR. The inactivation studies suggested that covalent modification is accompanied by cytosine release. To test this hypothesis, 2 eq of [5 - 3 H] F₂CDPs were incubated with α 2 β 2. Subsequent to inactivation the nucleotides were recovered by ultrafiltration and analyzed by HPLC. The analysis revealed 1 eq of cytosine and 1 eq of F₂CDP. These results parallel those reported for inactivation of *E. coli* RNR (12) and support the model that inactivation can be achieved with substoichiometric amounts of F₂CDP.

Subunit Interactions of *E. coli* RNR in the Presence of F₂CDP. The active form of *E. coli* RNR is thought to be a 1:1 mixture of α 2 and β 2, although there is only one Y* per β 2, suggesting the active RNR complex is asymmetric. One way to achieve complete inactivation of α 2 β 2 with 1 F₂CDP is that once chemistry has occurred in the active site of the first α , it precludes chemistry from occurring in the active site of the second α . This chemistry further leads to a tight complex between the two subunits preventing recycling of the unmodified α . To test this model, the inactivation mixture and a number of controls (including one with a mixture of α , β , and ATP) were examined by using SEC on a Superose 12 FPLC column. All elution buffers contained either 0.5 mM ATP or 100 μ M TTP previously shown to enhance α 2 formation and more recently to enhance α 2 β 2 interactions.

The results of SEC analysis of RNR inactivated with F₂CDP/ATP, with ATP in the elution buffer, are summarized in Fig. 2A–C and Table 2. Fig. 2A reveals a single protein peak. Fractions collected through the protein peak were analyzed by scintillation counting and by SDS/PAGE. The former revealed 0.9 labels per α 2 β 2 (Fig. 2A). The SDS/PAGE analysis (Fig. 2B) revealed the presence of α and β . Their relative ratios were determined in each fraction by comparison with standard curves made with known concentrations of α and β (Fig. 2B, standard curves not shown) and found to be \approx 1:1 (Fig. 2C).

A control SEC analysis in the absence of F₂CDP, with ATP in the elution buffer reveals separation of α 2 and β 2 (Fig. 2D and E). Analysis of the ratio of α : β supports this conclusion (Fig. 2F). The analysis in Fig. 2 suggests that a tight complex between subunits is unique to the presence of F₂CDP.

Further experiments were carried out to assess the resolution of the SEC method and to obtain information about the relative molecular masses of the observed protein peaks. The behavior of the individual subunits and complex were examined. In the absence of nucleotides, α migrates as a mixture of monomer and dimer with apparent molecular masses of 105 and 143 kDa (Table 2), respectively. The apparent molecular masses are obtained by comparison of the retention times of the eluting proteins with retention times of known molecular mass standards (SI Fig. 5). With ATP or TTP in the running buffer, α now migrates as a dimer (α 2) of 174 kDa (Table 2 and SI Fig. 5). When RNR is inactivated by [$1'$ - 3 H] F₂CDP/ATP and chromatographed with ATP in the running buffer, the protein has an apparent molecular mass of 277 kDa (Fig. 2A and SI Fig. 5). The SEC analysis presented in Fig. 2A–C, the stability of the complex during the inactivation reaction and the subsequent 25 min chromatography, and the apparent molecular mass suggests that the active form of RNR is α 2 β 2 and that the interaction between the subunits has dramatically increased relative to the non-nucleotide bound forms (Table 2).

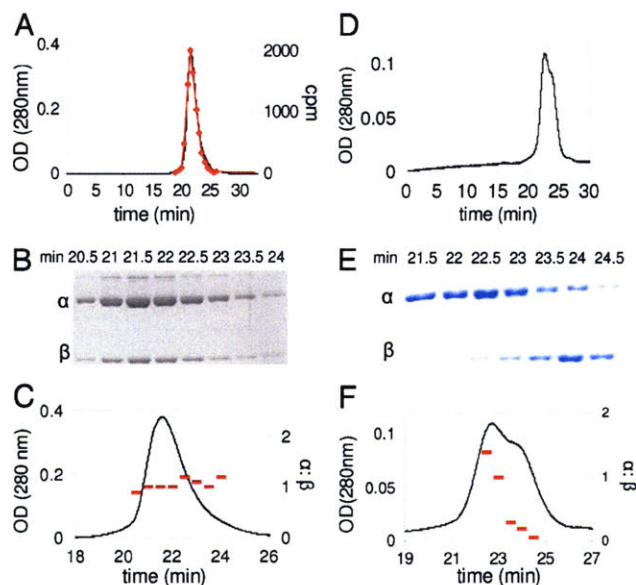


Fig. 2. SEC on a Superose 12 column to detect complex formation (α 2 β 2) in *E. coli* RNR incubated with ATP in the presence or absence of [$1'$ - 3 H] F₂CDP. Elution buffer contains 0.5 mM ATP. (A–C) Presence of F₂CDP. (A) Elution profile monitored by A_{280 nm} and scintillation counting (\blacklozenge). (B) Fractions through the protein peak in A monitored by SDS/PAGE. Note the slower migrating band (5% of the protein) is an altered conformation of α . (C) Analysis of the ratio of α : β (–), using standard curves generated from known amounts of α and β . (D–F) Absence of F₂CDP. (D) Elution profile. (E) Fractions through the protein peak in D monitored by SDS/PAGE. (F) Analysis of the ratio of α : β , using standard curves generated from known amounts of α and β .

Subunit Interactions of Human RNR in the Presence of F₂CDP. A similar set of experiments has been carried out with the human RNR. The Cooperman laboratory has demonstrated that in contrast with the prokaryotic RNRs, the active mouse RNR can be α 2 β 2, α 6 β 2, and α 6 β 6 depending on the concentration of ATP (18). Recent studies using gas phase electrophoretic mobility macromolecule analysis have suggested that the active form of hRNR is α 6 β 2 (24). Biacore studies and kinetic studies demonstrate that the interactions between α and β in the absence of nucleotides, as in the prokaryotic case, are weak ($K_d = 0.2 \mu$ M) (21). Anticipated differences in the aggregation state of active RNR relative to the *E. coli* RNR caused us to switch to a Superdex 200 column for molecular mass analysis in the presence and absence of F₂CDP in addition to ATP. The results of incubation of either 0.5 or 1 eq of [$1'$ - 3 H] F₂CDP/ATP by SEC with ATP in the elution buffer are shown in Fig. 3A and B and are summarized in Table 2. Fractions were collected through the protein peak and analyzed by scintillation counting and by SDS/PAGE (Fig. 3B). In the former case, analysis gave 0.8 radiolabels/ α 2. SDS/PAGE revealed the presence of both α and β . The relative ratio of α : β of 1:1 was established by using standard curves made from α and β (SI Fig. 6).

Experiments were also carried out to assess the resolution of the SEC method and to obtain information about the relative molecular masses of the observed protein peaks. β 2 migrates with an apparent molecular mass of 108 kDa (calculated 94.1 kDa; SI Fig. 7). α in the absence of nucleotides migrates as the expected monomer, whereas in the presence of TTP, it migrates as a dimer of 189 kDa (SI Fig. 7). The retention time of the protein peak eluted from the RNR inactivated with F₂CDP/ATP and with ATP in the elution buffer, relative to molecular mass standards reveals an apparent molecular mass of 872 kDa (SI Fig. 7). The 1:1 ratio of α : β , the radiolabeling of the complex, and the apparent molecular mass in comparison with the expected mass of 834 kDa for α 6 β 6, 646 kDa for α 6 β 2, and 278 kDa for α 2 β 2, suggest that the active form of the

Table 2. Molecular mass determination of *E. coli* and human RNR and their subunits by SEC

Protein	Protein (effector)	Apparent mass, kDa	Expected mass, kDa	Oligomeric state
<i>E. coli</i> RNR	β	96	87	β_2
	α^*	143, 105	172, 86	α_2, α
	α (100 μ M TTP)	174	172	α_2
	α (0.5 mM ATP)	174	172	α_2
	α, β^*	156, 108	172, 87	α_2, β_2
	α, β (ATP) [†]	167, 109	172, 87	α_2, β_2
	α, β inactivated by F ₂ CDP [†]	277	259	$\alpha_2\beta_2$ complex
Human RNR	β	108	94	β_2
	α	88	92	α
	α (100 μ M TTP)	189	184	α_2
	α, β (ATP)	589, 94	553, 94	α_6, β_2
	α, β inactivated by F ₂ CDP ^{††}	872	834	$\alpha_6\beta_6$ complex

*The HPLC trace indicates multiple species. Gaussian fits to the peak shape, using Origin software, Version 6.1, gave the peak retention times.

[†]Elution buffer contains 0.5 mM ATP. Fractions were collected through the protein peak and were analyzed by 10% SDS/PAGE as summarized in Fig. 2 A–F and Fig. 3.

^{††}Peak I, apparent mass 872 kDa ($\alpha_6\beta_6$, 834 kDa) based on standard curve (SI Fig. 6); Peak II: ArnA, apparent mass 484 kDa (hexamer of ArnA is 446 kDa); Peak III, subunit molecular mass 65 kDa based on SDS/PAGE.

human RNR is $\alpha_6\beta_6$ and that the subunits are tightly interacting. The results, as in the case of the *E. coli* RNR, provide an explanation for complete RNR inactivation with substoichiometric amounts of F₂CDP. Inactivation of class I RNRs by F₂CDP thus provides another paradigm for inhibitor design of this protein: increasing the subunit affinity.

A number of additional features in the chromatogram in Fig. 3A, peaks II and III, require comment. Two proteins copurify with α and can be seen on SDS/PAGE with subunit molecular masses of 74 kDa and 65 kDa. The protein from peak II was isolated, sequenced and identified as an *E. coli* protein ArnA, which exists as a hexamer in its native state (33). The identity of peak III has not been determined, but SDS/PAGE analysis reveals it is not associated with RNR. Efforts to further purify α via peptide and dATP affinity chromatography and several different anion exchange methods failed, because α is not very soluble and is prone to aggregation. Recovery of α and radiolabel from the column was 82%. The difference in the intensity of proteins in peak II and III (Fig. 3A) relative to SDS/PAGE is not understood.

Discussion

Many 2'-substituted-2'-deoxynucleotides have been shown to be potent mechanism based inhibitors of RNRs because the initial experiments in 1976 (34). Detailed studies on 2'-fluoro, 2'-chloro and 2'-azido derivatives have provided the basis for a general mechanism of inhibition by these substrate analogs (Scheme 1) (35, 36). The Y* in β is reduced and generates a transient thiyl radical

in α that initiates nucleotide reduction by 3'-hydrogen atom abstraction. Loss of the 2' substituent (HO⁻, F⁻, Cl⁻, N₃⁻, or their conjugate acids) results in formation of intermediate A, which then partitions into two pathways depending on whether the 2'-radical is reduced by the top face thiol or a bottom face thiol. In the former case, the inactivation is caused by formation of a 3'-ketodeoxynucleotide which dissociates from the active site and decomposes to generate the nucleic acid base, pyrophosphate, and a furanone. The furanone then alkylates α resulting in its inactivation. In the case of bottom face reduction, in addition to generating the 3'-ketodeoxynucleotide that eventually inactivates α from solution through the furanone, the Y* in β remains reduced, thus β also becomes inactivated. Most 2'-substituted deoxynucleotides inhibit class I RNRs by a combination of these pathways.

Studies presented herein suggest an additional mechanism by which 2'-substituted nucleotides may inactivate RNR. Gemzar has two fluorines at C2'. Both are lost during inactivation, at least in the case of the *E. coli* and *Lactobacillus leichmannii* RNRs, which have thus far been examined (12, 13). In addition, with [1'-³H] F₂CDP inactivation is accompanied by 0.5 eq of sugar labeling from F₂C/ α , \approx 20–40% of tyrosyl radical loss and 100% loss of RNR activity. The mechanisms by which F₂CDP inactivate the *E. coli* and human RNRs, thus, must occur by multiple pathways as previously observed with other 2'-substituted nucleotides. Furthermore, all pathways result in covalent labeling with the sugar of F₂CDP and loss of cytosine. The details of the inactivation mechanism are complex and are not yet understood.

The observation of substoichiometric amounts of nucleotide resulting in complete RNR inactivation, at face value, seems difficult to understand. An explanation for the unusual stoichiometry is provided by the analysis of the RNR quaternary structure. In the case of the *E. coli* RNR, SEC reveals a tight $\alpha_2\beta_2$ complex (Fig. 2 A–C) when it is inactivated by F₂CDP. A control in the absence of F₂CDP reveals that α_2 separates from β_2 by the same chromatographic analysis (Fig. 2 D–F). In retrospect, we have previously seen this type of behavior with another substoichiometric mechanism based inhibitor: 2'-azido-2'-deoxynucleotides, N₃NDP (19, 37, 38). During a 2-min incubation of RNR with [5'-³H] N₃NDPs, >90% of RNR activity is lost, 50% of Y* is lost, and 0.7 eq radiolabel are associated with RNR. Protein denaturation, however, resulted in radiolabel release suggesting it is non-covalently bound or covalently bound in an unstable structure. In contrast with F₂CDP, activity of α with N₃UDP is recovered to 50% and complete inactivation over 30 min is associated with 100% loss of Y*. Thus, although the subunits must be tightly associated initially to account for >90% loss of activity with just 50% loss of

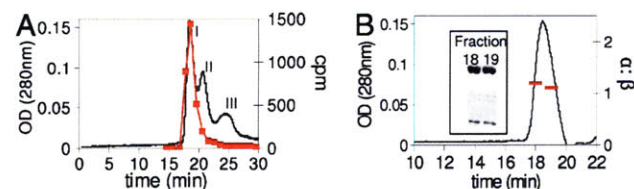


Fig. 3. SEC on a Superdex 200 column to detect the complex formation ($\alpha\beta$) in human RNR upon inactivation by F₂CDP/ATP. (A) The elution profile monitored by A₂₁₄ and scintillation counting (■). (B) Fractions through the protein peak in A monitored by SDS/PAGE and analysis of the ratio of α : β using standard curves generated from known amounts of α and β . Peak I contains α and β ; Peak II contains ArnA; and Peak III contains no α or β , but an unidentified protein of monomer molecular mass 65 kDa. We have repeated this experiment with homogeneous α (provided by the C. G. Dealwis laboratory, University of Tennessee, Knoxville, TN). The results are identical, but look cleaner, because the *E. coli* contaminating protein has been removed.

Y*, further chemistry associated with nucleotide allows subunit weakening and dissociation. An SEC experiment similar to the one described in Fig. 2 provides no evidence for an $\alpha\beta_2$ complex (SI Fig. 8). The unique chemistry associated with the different inhibitors thus can dramatically effect subunit interactions.

Inactivation of the human RNR, at least in the presence of reductant, mirrors the observations made with the *E. coli* RNR. One major difference, however, involves the quaternary structure of the human RNR. Our SEC studies have provided direct evidence in support of an active $\alpha\beta_6\beta_6$ complex. This result contrasts with previous proposals of active $\alpha_2\beta_2$ and with the recent mass spectrometric studies suggesting that $\alpha\beta_2$ is the active form of RNR (24). Our results support the importance of the α_6 form of the large subunit, first proposed by Cooperman's laboratory (18). The SEC results also suggest that inactivation is the result of tight complex formation between the subunits that can occur even in the presence of substoichiometric amounts of nucleotide. At odds with this interpretation are the activity assays for each subunit in the presence of an excess of the second subunit. If a tight complex were present subsequent to inactivation, one would have expected that α and β would be 100% inactive. Although this was the case for α (SI Fig. 4), β_2 retains 60% of its activity. These results are very intriguing and provide us with additional insight about subunit interaction. The recovery of β_2 activity requires that excess α can form a transient ternary complex with $\alpha\beta_6\beta_6$ and liberate β_2 , which has retained some of its Y* and is thus active. This proposal is supported by a recent structure of a complex of the $\alpha_2\beta_2$ from *E. coli* where only one of the two β s interacts with α (39). Thus, one could propose that binding of α to the unattached β of β_2 could facilitate α_2 release. In the case of the inactivated $\alpha\alpha^*\beta_2$ complex assayed with excess α (α^* = covalently labeled α), this mechanism would result in release of $\alpha\alpha^*$ and formation of active $\alpha_2\beta_2$. Because there is only one [^3H]-label per α_2 , one would have expected the unlabeled monomer to be also active in the presence of excess β , but this is not the case. Thus, this result provides strong support for asymmetry within the α_2 (α_6); that is, modification of one α precludes activity of the other. The results suggest that if the cell was able to increase the amount of α , then active RNR could be recovered. Interestingly resistance in a number of cell lines has identified elevated α levels (40–42). F_2CDP is unique with respect to the well characterized 2'-substituted nucleotide mechanism based inhibitors, in that in addition to labeling α and loss of Y* on β , inactivation is the result of tight subunit association.

Summary. RNR is inactivated by 0.5 eq of $\text{F}_2\text{CDP}/\alpha$, as a consequence of altering the affinity of its two subunits and generating an asymmetric interaction within this complex. Recent studies using α and β substituted site specifically with unnatural amino acids have also been interpreted to suggest an asymmetry within the active RNR complex (19, 20). Our results suggest that the paradigm of a 1:1 symmetrical complex between the two subunits of RNR must be re-evaluated. They further suggest a novel mode of inactivation of RNR.

Materials and Methods

[^3H] F_2C and 2-deoxy-3,5-di-*O*-benzoyl-3,3-difluororibonolactone were kind gifts of Eli Lilly (Indianapolis, IN). Competent *E. coli* BL 21 (DE3) cells were purchased from Stratagene (La Jolla, CA). Complete EDTA-free protease inhibitor tablets and calf alkaline phosphatase (20 units/ μl) were purchased from Roche Biochemicals (Indianapolis, IN). Plasmids containing the genes for α (formerly called H1) and β (formerly called H2), phRRM1, and phRRM2, were generous gifts from Y. Yen (City of Hope National Medical Center). Protein concentrations were determined by using extinction coefficients ($\epsilon_{280\text{ nm}}$) per monomer [45,900 $\text{M}^{-1}\text{ cm}^{-1}$ for (His) $_6$ - β and 119,160 $\text{M}^{-1}\text{ cm}^{-1}$ for α]. *E. coli* TR (specific activity of 40 units/mg) and TR reductase (specific activity of 1,320 units/mg) were isolated as described in refs. 43 and 44.

Expression Plasmids for Human α and β in *E. coli*. Sequencing of the α and β genes in phRRM1 and phRRM2, respectively, revealed a number of mutations relative to the sequences reported in the NCBI database (27, 28). In the α gene, nucleotide C521 was mutated to a T, resulting in a Val to Ala substitution. At residue 1763, C was changed to T, resulting in an Ile to Thr substitution. In the gene for β , A650 was changed to G, resulting in the conversion of a Lys to Arg. These mutations were corrected by site-directed mutagenesis, using the QuikChange Kit by Stratagene. In addition the N-terminal tags of each protein were reengineered to minimize the number of additional residues. The NdeI digestion site in α was silenced. Both α and β genes were digested with NdeI and NotI and ligated into the NdeI–NotI sites of pET-28a (Novagen) to produce (His) $_6$ - α and (His) $_6$ - β containing a MGSSHHHHHS-SGLVPRGSH-N terminus. All constructs were verified by sequencing at the MIT biopolymers laboratory.

Expression and Purification of Human α and β . phRRM1 and phRRM2 were transformed into *E. coli* BL21 (DE3) (Stratagene) and plated on LB agar plates with 50 $\mu\text{g}/\text{ml}$ kanamycin, and a single colony was chosen for growth. For isolation of β , an overnight culture (40 ml) grown to saturation was diluted into 2 liters of LB containing 50 $\mu\text{g}/\text{ml}$ kanamycin and grown at 37°C to an OD $_{600}$ of 0.7–0.9. Isopropyl-1-thio- β -D-galactopyranoside (1 mM) was then added, and the cells were grown for an additional 6 h at 30°C. For growth of α , an overnight culture (40 ml) was grown from a single colony at 37°C and transferred to 2 liters of LB and grown at 37°C. Isopropyl-1-thio- β -D-galactopyranoside (1 mM) was added at an OD $_{600}$ of 0.7–0.9, and the cells were grown overnight at 25°C. The isolation of β_2 and α were carried out by the following general procedure: The cells were harvested and typically yielded 4 g/liter. The cell pellets were suspended (5 vol/g) in 50 mM NaH_2PO_4 , pH 7.0, 0.1% Triton X-100, and 10 mM 2-mercaptoethanol. The suspension was passed through the French press at 14,000 psi. The cell lysate was centrifuged at 20,000 $\times g$ for 30 min. The supernatant was treated with streptomycin sulfate to a final concentration of 1% (wt/vol), and the pellet was removed by centrifugation. The supernatant was incubated with Ni-NTA agarose resin (1 ml/g of cells; Qiagen, Valencia, CA) at 4°C for 1 h and then loaded into a column (2.5 \times 10 cm). The column was subsequently washed with 40 column vol of 50 mM NaH_2PO_4 /800 mM NaCl/50 mM imidazole, pH 7.0/0.1% Triton X-100/10 mM 2-mercaptoethanol. The protein was eluted with 50 mM NaH_2PO_4 /300 mM NaCl/125 mM imidazole, pH 7.0. Fractions containing protein were identified by using the Bradford assay. The fractions were pooled and concentrated to <10 ml, and then the imidazole was removed by Sephadex G-25 chromatography (200 ml, 2.5 \times 50 cm). β_2 was stored in 50 mM Tris, 100 mM KCl, pH 7.6, 5% glycerol. α was stored in 50 mM Tris, 100 mM KCl, 15 mM MgCl_2 , 5 mM DTT, pH 7.6, 5% glycerol. Protein yields of α and β were \approx 2 mg and 15 mg/liter culture, respectively. The purity of α and β were analyzed on 10% SDS/PAGE. Two more rapidly migrating bands detected by SDS/PAGE copurified with α . One of these impurities, identified by sequencing, is Arna, a hexameric *E. coli* protein with a subunit molecular mass of 74 kDa. The second impurity has not been identified.

Conversion of Human apo β_2 to Holo β_2 . Stock solutions of (His) $_6$ - β_2 (2 ml, 2.5 mg/ml) were deoxygenated by 6 cycles of evacuation (for 3 \times 10 s) followed by argon flushing (2 min) on a Schlenk line. The deoxygenated β_2 solution was brought into the glovebox (MBraun, Stratham, NH) and 5 eq of Fe(II) per β_2 was added from a FeNH_4SO_4 solution in buffer A (50 mM Tris/100 mM KCl, pH 7.6/5% glycerol). The resulting mixture was incubated at 4°C for 15 min. The protein was then removed from the glovebox, and 1 ml of O_2 saturated buffer A (50 mM Tris/100 mM KCl, pH 7.6, 5%) was added. Excess iron was removed by Sephadex G-25 chromatography (40 ml, 2.5 \times 20 cm).

Activity Assays. A reaction mixture contained, in a final volume of 350 μ l, 50 mM Hepes (pH 7.6), 15 mM MgCl₂, 1 mM EDTA, 0.3 μ M (or 2.1 μ M) α , 2.1 μ M (or 0.3 μ M) β , 3 mM ATP, 1 mM [³H]-CDP (specific activity 3,400 cpm/nmol), 100 μ M *E. coli* TR, 1.0 μ M TR reductase, and 2 mM NADPH. The assay mixture was preincubated at 37°C for 3 min, and the reaction was initiated by the addition of CDP. Aliquots (50 μ l) were removed over a 15-min time period and quenched in a boiling water bath. dCDP production was analyzed by the method of Steeper and Stuart (45).

Time-Dependent Inactivation Studies. The inactivation mixture contained in a final volume of 100 μ l: 1.2 μ M α /1.2 μ M β /3 mM ATP/1 mM [³H]-CDP (specific activity 3,400 cpm/nmol)/5 mM DTT/50 mM Hepes (pH 7.6)/15 mM MgCl₂/1 mM EDTA. The reaction was initiated by addition of F₂CDP (0.6 μ M, 1.2 μ M and 6 μ M, final concentrations) and incubated at 37°C. Aliquots (12.5 μ l) were removed from 30 s to 17 min and assayed for dCDP production as described above. Control experiments were carried out in which the F₂CDP was omitted.

Quantitation of Covalent Labeling of *E. coli* RNR and Human RNR with [1'-³H]-F₂CDP and [5-³H]-F₂CDP. A typical reaction mixture (5.5 μ M α , β in 300 μ l) was identical to that described above, except that F₂CDP was replaced by either [1'-³H]-F₂CDP (5,889 cpm/nmol) or [5-³H]-F₂CDP (6,643 cpm/nmol). After 10 min at 37°C, a 270- μ l aliquot was loaded onto a Sephadex G-50 column (1 \times 20 cm, 20 ml) that was pre-equilibrated with the assay buffer (50 mM Hepes/15 mM MgCl₂/1 mM EDTA, pH 7.6) or made 6 M in guanidine-HCl and loaded onto a Sephadex G-50 column with assay buffer containing 2 M guanidine-HCl. Fractions (1 ml) were collected and assayed for A₂₈₀ and A₂₆₀, and 500 μ l of each fraction was analyzed by scintillation counting.

Quantification of Cytosine Released During the Inactivation of *E. coli* and Human RNR by [5-³H]-F₂CDP. The reaction mixture was as described in *Time-Dependent Inactivation Studies* (1.2 μ M human RNR α , β in 500 μ l). The reaction was initiated by addition of 1.2 μ M [5-³H]-F₂CDP (6643 cpm/nmol). After 20 min, the inactivation mixture was filtered through an YM-30 Centricon device (Millipore, Billerica, MA) at 4°C. F₂C (120 nmol) and cytosine (120 nmol) were added as carriers before filtration. The flow-through was treated with 30 units of alkaline phosphatase (Roche) for 3 h at 37°C and filtered through a second YM-30 Centricon device. The flow through was analyzed by using a Waters (Milford, MA) 2480 HPLC with an Altech Adsorbosphere Nucleotide Nucleoside C-18

column (250 mm \times 4.6 mm) at a flow rate of 1 ml/min. The elution buffer contained buffer A (10 mM NH₄OAc, pH 6.8) and buffer B (100% methanol). A 10-min isocratic elution was followed by a linear gradient to 40% B over 30 min. A linear gradient was then run to 100% B over 5 min. Fractions (1 ml) were collected, and 200 μ l of each were analyzed by scintillation counting. Standards were as follows: retention times are: cytosine, 5.7 min; cytidine, 12.6 min; ara-C, 17.4 min; dC, 19.0 min and F₂C, 23.2 min. The recovery of cytosine and F₂C was calculated based on the UV spectrum (cytosine, λ_{267} , ϵ = 6100 M⁻¹ cm⁻¹, F₂C, λ_{268} , ϵ = 9360 M⁻¹ cm⁻¹). The radioactivity recovered with cytosine and F₂C was analyzed by scintillation counting.

SEC to Examine the Quaternary Structure of RNRs Subsequent to Inactivation by F₂CDP. SEC was performed by using a Superose 12 column (10 \times 300 mm, GE Healthcare, Little Chalfont, U.K.) for *E. coli* RNR or a Superdex 200 column (10 \times 300 mm, GE Healthcare) for human RNR attached to a Waters 2480 HPLC. Gel filtration molecular mass standards (GE Healthcare) were ovalbumin, 43 kDa; conalbumin, 75 kDa; aldolase, 158 kDa; pyruvate kinase, 232 kDa or catalase 232 kDa; ferritin, 440 kDa; thyroglobulin, 669 kDa; and blue dextran, 2,000 kDa. The elution buffer was 50 mM Hepes (pH 7.6)/15 mM MgCl₂/0.5 mM ATP, with or without 150 mM KCl. Molecular mass standards were run at the beginning of each experiment. The reaction mixture was prepared as described above (15 μ M α , β in 300 μ l or 30 μ M α , β in 150 μ l). After 10 min of incubation, 150 μ l or 300 μ l was injected onto the column. The elution rate was 0.5 ml/min and 0.5 ml fractions were collected. If [1'-³H]-F₂CDP was used in the inactivation, 100- μ l aliquots of each fraction was analyzed by scintillation counting.

Quantitative Analysis of the Subunits of *E. coli* and Human RNRs by SDS/PAGE. The fractions collected from the SEC analysis were analyzed by 10% SDS/PAGE and compared with concentrations of α and β from *E. coli* RNR (0.4 μ M to 3.2 μ M) or human RNR (0.2 μ M to 1.6 μ M) as standards. The proteins were visualized with Coomassie blue staining. The band intensities were quantified by using Quantity One software (Bio-Rad, Hercules, CA). The concentrations of α and β in the complex were determined from the standard curves.

We thank Dr. Yun Yen for providing pRRM1 and pRRM2 plasmids, Eli Lilly for providing F₂C, the Chris G. Dealwis group laboratory for supplying us with homogeneous α . This work was supported by National Institutes of Health Grant GM 29595 and David Koch funds from The Massachusetts Institute of Technology Center for Cancer Research.

- Hertel LW, Boder GB, Kroin JS, Rinzel SM, Poore GA, Todd GC, Grindey GB (1990) *Cancer Res* 50:4417-4422.
- Huang P, Chubb S, Hertel LW, Grindey GB, Plunkett W (1991) *Cancer Res* 51:6110-6117.
- Plunkett W, Huang P, Gandhi V (1997) *Nucleosides Nucleotides* 16:1261-1270.
- Mackey JR, Mani RS, Selner M, Mowles D, Young JD, Belt JA, Crawford CR, Cass CE (1998) *Cancer Res* 58:4349-4357.
- Bergman AM, Pinedo HM, Peters GJ (2002) *Drug Resist Updat* 5:19-33.
- Garcia-Manteiga J, Molina-Arcas M, Casado FJ, Mazo A, Pastor-Anglada M (2003) *Clin Cancer Res* 9:5000-5008.
- Usova EV, Eriksson S (1997) *Eur J Biochem* 248:762-766.
- Van Rompay AR, Johansson M, Karlsson A (1999) *Mol Pharmacol* 56:562-569.
- Lohman GJS (2006) PhD Thesis (MIT, Cambridge, MA).
- Heinemann V, Xu YZ, Chubb S, Sen A, Hertel LW, Grindey GB, Plunkett W (1990) *Mol Pharmacol* 38:567-572.
- Baker CH, Banzon J, Bollinger JM, Stubbe J, Samano V, Robins MJ, Lippert B, Jarvi E, Resvick R (1991) *J Med Chem* 34:1879-1884.
- van der Donk WA, Yu GX, Perez L, Sanchez RJ, Stubbe J, Samano V, Robins MJ (1998) *Biochemistry* 37:6419-6426.
- Silva DJ, Stubbe J, Samano V, Robins MJ (1998) *Biochemistry* 37:5528-5535.
- Gandhi V, Legha J, Chen F, Hertel LW, Plunkett W (1996) *Cancer Res* 56:4453-4459.
- Miura S, Izuta S (2004) *Curr Drug Targets* 5:191-195.
- Nordlund N, Reichard P (2006) *Annu Rev Biochem* 75:681-706.
- Kolberg M, Strand KR, Graff P, Andersson KK (2004) *Biochim Biophys Acta* 1699:1-34.
- Kashlan OB, Scott CP, Lear JD, Cooperman BS (2002) *Biochemistry* 41:462-474.
- Fritscher J, Artin E, Wnuk S, Bar G, Robblee JH, Kacprzak S, Kaupp M, Griffin RG, Bennati M, Stubbe J (2005) *J Am Chem Soc* 127:7729-7738.
- Seyedsayamdost MR, Stubbe J (2006) *J Am Chem Soc* 128:2522-2523.
- Ingemarson R, Thelander L (1996) *Biochemistry* 35:8603-8609.
- Thelander L (1973) *J Biol Chem* 248:4591-4601.
- Brown NC, Reichard P (1969) *J Mol Biol* 46:39-55.
- Rofougaran R, Vodnala M, Hofer A (2006) *J Biol Chem* 281:27705-27711.
- Kohn P, Samaritano RH, Lerner LM (1965) *J Am Chem Soc* 87:5475-5480.
- Chou TS, Heath PC, Patterson LE, Poteet LM, Lakin RE, Hunt AH (1992) *Synthesis* 565-570.
- Parker NJ, Begley CG, Fox RM (1991) *Nucleic Acids Res* 19:3741.
- Pavloff N, Rivard D, Masson S, Shen, SH, MesMasson AM (1992) *DNA Sequence* 2:227-234.
- Bollinger JM, Tong WH, Ravi N, Huynh BH, Edmondson DE, Stubbe J (1995) *Methods Enzymol* 258:8-303.
- Guittet O, Hakansson P, Voevodskaya N, Fridt S, Graslund A, Arakawa H, Nakamura Y, Thelander L (2001) *J Biol Chem* 276:40647-40651.
- Shao JM, Zhou BS, Zhu LJ, Qiu WH, Yuan YC, Xi BX, Yen Y (2004) *Cancer Res* 64:1-6.
- Ortigosa AD, Hristova D, Perlstein DL, Zhang Z, Huang MX, Stubbe J (2006) *Biochemistry* 45:12282-12294.
- Gatzeva-Topalova PZ, May AP, Sousa MC (2005) *Structure (London)* 13:929-942.
- Thelander L, Larsson B (1976) *J Biol Chem* 251:1398-1405.
- Licht S, Stubbe J (1999) in *Mechanistic Investigations of Ribonucleotide Reductases*, ed Poulter CD (Elsevier, Amsterdam), pp 163-203.
- Stubbe JA, van der Donk WA (1995) *Chem Biol* 2:793-801.
- Salowe S, Bollinger JM, Ator M, Stubbe J, McCracken J, Peisach J, Samano MC, Robins MJ (1993) *Biochemistry* 32:12749-12760.
- Salowe SP, Ator MA, Stubbe J (1987) *Biochemistry* 26:3408-3416.
- Uppsten M, Farnegårdh M, Domkin V, Uhlin U (2006) *J Mol Biol* 359:365-377.
- Davidson JD, Ma LD, Flagella M, Geeganage S, Gelbert LM, Slapak CA (2004) *Cancer Res* 64:3761-3766.
- Bergman AM, Eijk PP, van Haperen V, Smid K, Veerman G, Hubeek I, van Ijssel P, Ylstra B, Peters GJ (2005) *Cancer Res* 65:9510-9516.
- Jordheim LP, G. O., Lepoivre M, Galmarini CM, Dumontet C (2005) *Mol Cancer Ther* 4:1268-1276.
- Russel M, Model P (1985) *J Bacteriol* 163:238-242.
- Lunn CA, Kathju S, Wallace BJ, Kushner SR, Pigiet V (1984) *J Biol Chem* 259:469-474.
- Steeper JR, Steuart CC (1970) *Anal Biochem* 34:123-130.